Ernst Schering Research Foundation
Workshop 49

Molecular Imaging

An Essential Tool in Preclinical Research, Diagnostic Imaging, and Therapy

A. A. Bogdanov Jr.
K. Licha
(Editors)

Springer

Ernst Schering Research Foundation Workshop 49
Molecular Imaging

Ernst Schering Research Foundation
Workshop 49

Molecular Imaging

An Essential Tool in Preclinical Research, Diagnostic Imaging, and Therapy

A. A. Bogdanov Jr., K. Licha
Editors

With 79 Figures

Springer

Series Editors: G. Stock and M. Lessl

Library of Congress Control Number: 2004103454

ISSN 0947-6075

ISBN 3-540-21021-0 Springer Berlin Heidelberg New York

Springer is a part of Springer Science+Business Media
springeronline.com

Printed in Germany

Editor: Dr. Ute Heilmann, Heidelberg
Desk editor: Wilma McHugh, Heidelberg
Production editor: Andreas Gösling, Heidelberg
Cover design: design & production GmbH, Heidelberg
Typesetting: K+V Fotosatz GmbH, Beerfelden

Printed on acid-free paper – 21/3150/AG-5 4 3 2 1 0

Preface

"Molecular imaging" has been previously defined as "the in vivo characterization and measurement of biologic processes at the cellular and molecular level." This broad definition emerged during the last few years as a consequence of the convergence of molecular and cell biology with imaging science, including medical physics and technology. One of the major goals of molecular imaging has become the development of noninvasive strategies of "molecular profiling" in living subjects, i.e., the acquisition and analysis of maps reflecting the spatial and temporal distribution of a given molecular target at a precise anatomical location without biopsies. The mapping of disease-relevant gene expression profiles in vivo would be especially important for individualizing established therapy regimens in clinical practice and selecting patients for novel experimental therapies.

The 49th Ernst Schering Foundation Workshop, "Molecular Imaging; An Essential Tool in Preclinical Research, Diagnostic Imaging, and Therapy," is the second in the history of the foundation devoted to this topic. The purpose of the workshop was to discuss and overview multiple applications and emerging technologies in the area of diagnostic imaging including its fundamental capabilities in preclinical research, the opportunities for medical care, and the options involving therapeutic concepts. The contributions from leading clinical and basic researchers included in this book clearly demonstrate the large strides that are being taken in recent years toward attaining the scientific goals of molecular imaging, and toward translating new ideas in this exciting and rapidly evolving field into practical bene-

fit. Scientific disciplines covered in the workshop were molecular and cell biology, synthetic chemistry and radiochemistry, spectroscopic and magnetic analytics, and imaging techniques. From the perspective of application, the workshop included topics in the area of magnetic resonance imaging, radiodiagnostics (PET and SPECT), radiotherapy, ultrasound imaging, optical imaging, and photodynamic therapy.

Feedback from the participants led to the conclusion that the interdisciplinary nature and scientific diversity of this area of science was well reflected during the workshop, attracted great interest, and led to a better understanding of each other's expertise and knowledge.

We wish to express our sincere gratitude to all participants for their contributions to the workshop and to this book. We also thank the Ernst Schering Research Foundation for the generous support in making the workshop a great success.

Contents

List of Editors and Contributors

Editors

Bogdanov, A. A. Jr.
Center for Molecular Imaging Research, Building 149,
Massachusetts General Hospital, 13th Street, Charleston,
MA 02129, USA
e-mail: abogdanov@helix.mgh.harvard.edu

Licha, K.
Medicinal Chemistry 6, Schering AG, Müllerstr. 170–178,
13342 Berlin, Germany
e-mail: kai.licha@schering.de

Contributors

Aime, S.
Dipartimento di Chimica I.F.M. e Centro per il Molecular Imaging,
Università di Torino, Via P. Giuria 7, 10125 Turin, Italy
e-mail: silvio.aime@junito.it

Barge, A.
Dipartimento di Chimica I.F.M. e Centro per il Molecular Imaging,
Università di Torino, Via P. Giuria 7, 10125 Turin, Italy
e-mail: alessandro.barge@unito.it

Bremer, C.
Westfälische Wilhelms-Universität, Münster Institut für Klinische
Radiologie, Albert-Schweitzer-Straße 33, 48129 Münster, Germany
e-mail: bremerc@uni-muenster.de

Bretonnière, Y.
University of Durham Department of Chemistry, South Road, Durham DH1 3LE, UK
e-mail: yann.bretonniere@durham.ac.uk

Cecchini, M. G.
Urology Research Laboratory, Department of Urology and Department of Clinical Research, University of Bern, MEM C813, Murtenstr. 35, 3010 Bern, Switzerland
e-mail: marco.ceccini@dkf6.unibe.ch

Chen, J. W.
Massachusetts General Hospital, Center for Molecular Imaging Research, Building 149, 13th Street, Charleston, MA 02129, USA

Gianolio, E.
Dipartimento di Chimica I.F.M. e Centro per il Molecular Imaging, Università di Torino, Via P. Giuria 7, 10125 Turin, Italy
e-mail: eliana.gianolio@unito.it

Hany, T. F.
University Hospital Zurich Dept. of Medical Radiology/Division of Nuclear Medicine, Rämistraße 100, 8091 Zurich, Switzerland
e-mail: Thomas.hany@dmr.usz.ch

Hasan, T.
Wellmann Laboratories of Photomedicine, Harvard Medical School Massachusetts General Hospital, 540 Blossom Street, Bartlett 314, Boston, MA 02114, USA
e-mail: edqvist@partners.org

Kang, H. W.
Massachusetts General Hospital, Center for Molecular Imaging Research, Building 149, 13th Street, Charleston, MA 02129, USA

Klibanov, A. L.
University of Virginia Medical Center, Cardiovascular Division, Box 100158, Charlottesville, VA 22908, USA
e-mail: alk6n@virginia.edu

Lowik, C.
Department of Endocrinology, Building 1, C4-R86 Leiden University Medical Center, Albinusdreet 2, 2333 ZA Leiden, The Netherlands
e-mail: c.w.g.m.lowik@lumc.nl

Luker, K.E.
Molecular Imaging Center, Mallinckrodt Institute of Radiology, and Department of Molecular Biology and Pharmacology, Washington University Medical School, Box 8225, 510 S. Kingshighway Blvd, St. Louis, MO 63110, USA

Maecke, H.R.
Institute of Nuclear Medicine, Division of Radiological Chemistry, University Hospital Basel, 4031 Basel, Switzerland
e-mail: hmaecke@uhbs.ch

Maggi, A.
Department of Pharmacological Sciences and Center of Excellence on Neurogenerative Disease, University of Milan, Italy

Ortel, B.
Wellman Laboratories of Photomedicine, Department of Dermatology, Massachusetts General Hospital, Harvard Medical School, Boston, MA 02114, USA
e-mail: ortel@helix.mgh.havard.edu

Paganelli, G.
European Institute of Oncology, Division of Nuclear Medicine, 20141 Milan, Italy
e-mail: direzione.mnu@ieo.it

Pagliarin, R.
Dipartimento di Chimica Organica e Industriale,
Università di Milano, Viale Venezian 21, 20133 Milan, Italy

Parker, D.
University of Durham Department of Chemistry, South Road, Durham DH1 3LE, UK
e-mail: david.parker@durham.ac.uk

Piwnica-Worms, D.
Washington University School of Medicine Molecular Imaging Center, 510 S. Kingshighway Blvd, Box 8225 St. Louis, MO 63110, USA
e-mail: Piwnica-WormsD@mir.wustl.edu

van der Pluijm, G.
Department of Endocrinology, Building 1, C4-R86 Leiden University Medical Center, Albinusdreet 2, 2333 ZA Leiden, The Netherlands

Pogue, B.
Wellman Laboratories of Photomedicine, Department of Dermatology, Massachusetts General Hospital, Harvard Medical School, Boston, MA, 02114, USA
Thayer School of Engineering, Dartmouth College, Hanover, NH 03755, USA

von Schulthess, G. K.
Clinic and Policlinic of Nuclear Medicine, University Hospital Zürich, Rämistrasse 100, 8091 Zurich, Switzerland

Silengo, L.
Dipartimento di Genetica, Biologia e Biochimica, Università di Torino, Via Santona 5-bis, 10126 Turin, Italy

Solban, N.
Wellman Laboratories of Photomedicine, Department of Dermatology, Massachusetts General Hospital, Harvard Medical School, Boston, MA 02114, USA

Tavitian, B.
INSERM ERM 103 Service Hospitalier, Frédéric Joliot CEA Direction des Sciences du Vivant Direction de la Recherche Medicale, 4 place du General Leclerc, 91401 Orsay Cedex, France
e-mail: tavitian@shfj.cea.fr

Tei, L.
Dipartimento di Medicina Interna, Università di Torino, C. so Dogliotti 14, 10125 Turin, Italy

Weissleder, R.
Massachusetts General Hospital, Center for Molecular Imaging Research, Building 149, 13th Street, Charleston, MA 02129, USA
e-mail: weissleder@helix.mgh.havard.edu

1 Oligonucleotides as Radiopharmaceuticals

B. Tavitian

If medicine is molecular, then imaging should become molecular.
Henry Wagner Jr.

In a general sense, molecular imaging is a term used to define in vivo imaging of molecules and stands in contrast to anatomical or physiological imaging. In that sense, any type of imaging that uses molecules as indicators or addresses molecules as targets is molecular, e.g., fluorodeoxyglucose (FDG), positron emission tomography (PET) scanning or octreotide single photon emission computed tomography (SPECT) are molecular imaging techniques. In a more restrictive sense however, the field of molecular imaging stands in respect to imaging just as molecular biology stands in respect to biological chemistry, i.e., it deals with nucleic acids and genetics. This part of molecular imaging, also referred to as *genetic* molecular imaging (Blasberg 2002) is booming thanks to the reporter gene imaging technologies developed in the 1990s in the United States, which have progressed to the point that they can be applied in humans (Jacobs et al. 2001).

The parallel between molecular biology and molecular imaging is representative of where the imaging science stands today, that is, at the point where molecular biology was twenty years ago. Both fields of research have the capacity to introduce and detect reporter genes in biological tissues, e.g., β-galactosidase for molecular biology and thymidine kinase for molecular imaging. However, molecular imaging is still far from the achievements of molecular biology that started it as an "industry" working at a very large scale: the ability to analyze *specifically any* given gene. This was made possible by two inventions: the detection of specific sequences among DNA fragments separated by gel electrophoresis (Southern 1975) and the phosphoramidite chemistry allowing to synthesize ad libitum small pieces of nucleic acids (Caruthers and Beaucage 1980).

Oligonucleotides were the key molecular tools for both inventions. Oligo (Greek for "few") nucleotides are short polymers of nucleotides, the building blocks of nucleic acids consisting in a 5-carbon sugar, a phosphate group, and any one of four different nucleobases (Fig. 1). Being small pieces of nucleic acids endows oligonu-

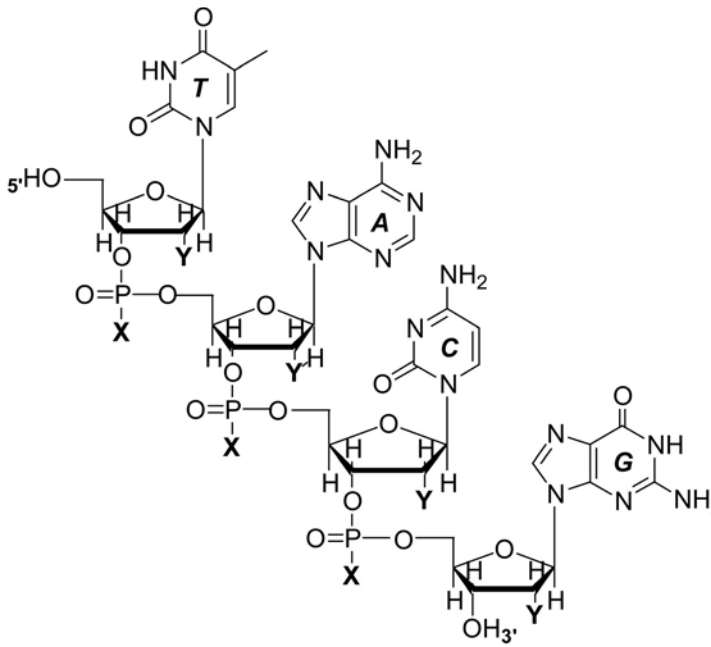

Fig. 1. Structure of oligonucleotides. *T*, thymine; *A*, adenine; *C*, cytosine; *G*, guanine. X is O in phosphodiester, S in phosphorothioate, and CH_3 in methylphosphonate. Y is H in deoxyribonucleotides, OH in ribonucleotides, and O-CH_3 in 2′-O-methyl ribonucleotides

cleotides with the biological properties of these nucleic acids, i.e., the capacity to stock and transmit genetic information (Fig. 2). Oligonucleotides are exquisitely precise molecular gene tools with in vitro usages that are growing exponentially, notably the major molecular biology methods of detecting specific gene expressions such as PCR, biochip arrays, in situ hybridization, etc. In addition, oligonucleotides have demonstrated the capacity to control gene expression in many different ways, some of which, such as siRNA (small interfering double-stranded RNA), have been unveiled only recently (Table 1). Interestingly, many mechanisms by which oligonucleotides control gene expression have been the subject of intense, sometimes excessive speculations for biomedical applications, often before

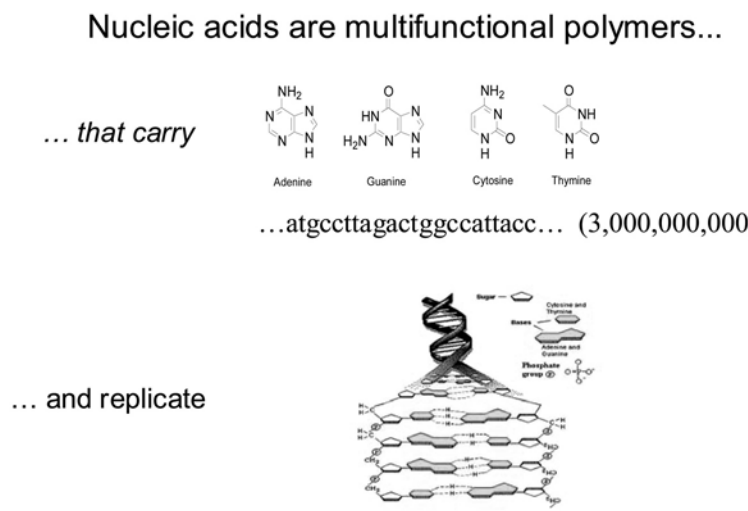

Fig. 2. Oligonucleotides and biological information

Table 1. Oligonucleotides are modulators of gene expression

Oligo-nucleotide	Target	Mechanism of activity		
		Base pairing	Molecular recognition	
Antisense	RNA	+	–	Double helix ± enzymatic
Ribozyme	RNA	±	–	Enzymatic
Antigene	DNA	+	–	Triple helix
Tweezer	RNA	+	–	Triple helix
Sense	DNA/RNA Binding Protein	–	+	Binding
Aptamer	Any	–	+	Binding
SiRNA, μRNA	RNA	+	–	Recognition + enzymatic

these mechanisms were demonstrated to exist in living organisms (Lavorgna et al. 2003).

Molecular imaging lags behind molecular biology, and the methods that would allow the specific detection of any given gene by noninvasive imaging techniques are still sky-high. A major challenge of molecular imaging is to turn molecular biology tools such as oligonucleotides into in vivo imaging agents, just as reporter genes and probes have been recently. Naturally, the difficulties of the task should not be underestimated including, among those apparent at first sight, the fact that all organisms have developed efficient strategies to avoid invasion by foreign nucleic acids. Efficient delivery is the key to oligonucleotide imaging, as it is to molecular medicine in general (Jain 1998).

This chapter inventories the present use of oligonucleotides as radiopharmaceuticals. It exposes first the applications of imaging to oligonucleotides, viz. imaging *of* oligonucleotides, and then the applications of oligonucleotides to imaging, viz. imaging *with* oligonucleotides. Based on the present state-of-the-art conditions, I hope to convince the reader that imaging *of* oligonucleotides is a reality with numerous applications, while imaging *with* oligonucleotides, still in its infancy, is a major avenue for the exploration of gene expression.

1.1 Imaging of Oligonucleotides

1.1.1 Radiolabeling of Oligonucleotides

Methods to radiolabel oligonucleotides with iodine-125, iodine-123, indium-111, technetium-99m, carbon-11, fluorine-18, bromine-76, and gallium-68 for imaging studies have been described (Table 2; reviewed in Younes et al. 2002). All these methods modify the oligonucleotide, either by covalent attachment of labeled groups or by addition of isotope chelating groups. Several studies have reported that the hybridization capacity of the oligonucleotide is maintained unchanged after labeling (Hnatowich et al. 1995; Tavitian et al. 1998; Roivanen et al. 2004). In contrast, the labeling is not without consequences on the pharmacokinetics. For instance, technetium-99m chelating groups modify the accumulation and efflux of octodecanucleo-

Table 2. Oligonucleotide radiolabeling methods for imaging

Isotope	Labeling group	Labeling method
Iodine-125	*p*-Methoxyphenyl isothiocyanate (PMPITC)	5′ Aminohexyl group
Iodine-125	Iodo-tyramine	5′ Amido
Iodine-125	4-Iodobenzamide	5′ Tributylstannylbenzamide
Iodine-125	Iodobenzoacetamide	5′ Thiophosphate
Iodine-125	Iodo dCTP	Primer extension with DNA pol I
Iodine-123	Iodovinyl analog of 2′-deoxy-U	5′ End incorporation of stannyl U derivative
Indium-111	Diethylenetriaminepentaacetate (DTPA)	Isothiocyanate
Indium-111	Isothiocyanobenzyl-EDTA	Amino-dU
Technetium-99m	Hydrazino nicotinamide	*N*-hydroxysuccinimide derivative
Technetium-99m	MAG3 (benzoylmercaptoglycylglycylglycine)	Amine derivative
Technetium-99m	MAG3 (benzoylmercaptoglycylglycylglycine)	3′ Hexylamine
Technetium-99m	MAG2	Amino
Carbon-11	Butyrate from ethylketene	Hexylamine
Fluorine-18	4-([^{18}F]Fluoromethyl)phenyl isothiocyanate	5′-Hexylamine derivative
Fluorine-18	*N*-succimidyl 4-[^{18}F]fluorobenzoate	5′-Hexylamine derivative
Fluorine-18	[^{18}F]fluorobenzylbromoacetamide	3′-Thiophosphate
Fluorine-18	5′-Deoxy-5′-fluoro-O_4-methylthymidine	5′-Phosphoramidite
Fluorine-18	[^{18}F]fluorobenzylbromoacetamide	Cysteine (PNA)
Bromine-76	*N*-Succinimidyl 4-[^{76}Br]Bromobenzoate	5′-Hexylamine derivative
Gallium-68	DOTA (1,4,7,10-tetraazacyclododecane-*N*,*N*′,*N*″,*N*‴-tetraacetic acid)	5′-Aminohexyl

tide antisense DNA against the Ria subunit of PKA in the kidney cancer cell line ACHN (Zhang et al. 2001). The biodistribution in normal mice is also heavily influenced by the labeling method: 4 h following the injection of ^{99m}Tc-labeled DNA, the percentage of injected dose per gram (ID/g) varied from 2.5 to 30.1 in kidney and 3.3 to 24 in liver for MAG3 and HYNIC chelators, respectively. From these studies, Hnatowich and his group concluded that biodistribution of intravenously administered oligonucleotides depends on the method for radiolabeling the antisense oligonucleotide, and that this method should be adapted to the organ localization of the target gene (Zhang et al. 2001).

In this respect, positron emitters such as carbon-11 and fluorine-18 have the advantage over metal γ-emitters that they can be incorporated into small molecular structures leading to limited chemical modification of the oligonucleotide. Our laboratory has developed generic methods to label oligonucleotides with fluorine-18 (Fig. 3). Radiolabeling is performed in two steps, (a) radiolabeling of a synthon designed for high reactivity and stable incorporation of halogens, and (b) regioselective conjugation of the synthon to the oligonucleotide. Performing the radiosynthesis of the synthon separately from the synthesis of the oligonucleotide allows (a) high yield incor-

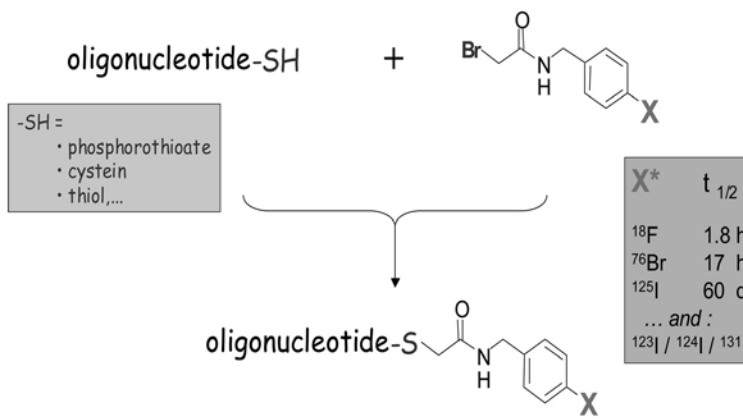

Fig. 3. Fluorine-18 labeling of oligonucleotides as described in Dollé et al. 1997; Kühnast et al. 2000 a, b, 2002, 2003 a, b

poration in an activated C6 aromatic ring of the halogen through the use of harsh conditions that would not be compatible with the stability of the oligonucleotides, (b) HPLC purification of the synthon from other radioactive by-products, and (c) its coupling to any oligonucleotide obtained in-house or commercially, without tedious unblocking steps to protect the oligonucleotides from unwanted reactions. The coupling reaction itself is designed to be rapid and efficient in conditions compatible with the chemical stability of the oligonucleotides and the half-life of isotopes.

The method is workable with short and long oligonucleotides and is independent of both the base sequence and the chemistry of the backbone. It has been applied to phosphodiester (Dollé et al. 1997), phosphorothioate, methylphosphonate, carbon 2′-modified ribose ribonucleotides (Kühnast et al. 2000a, b), peptide nucleic acids (Kühnast et al. 2002; Hamzavi et al. 2003), and enantiomeric ribo- and deoxyribo-nucleotides (Kühnast et al 2003a). The label can be conjugated either at the 3′ end or at the 5′ end of the oligonucleotide (Kühnast et al 2003b). The same procedure can be used to label oligonucleotides with iodine-125 (Kühnast et al. 2000b).

1.2 Imaging In Vivo Pharmacokinetics and Biodistribution of Oligonucleotides

A generic labeling method for oligonucleotides opens the possibility of imaging the pharmacodistribution of virtually any present or future modification aimed at improving the bioavailability of oligonucleotides. Together with metabolic analysis, it allows direct evaluation of the characteristics of labeled oligonucleotides as in vivo tracers and is most useful for drug and radiotracer design and development of oligonucleotides.

Systematically administered oligonucleotides must escape plasmatic and tissular nucleases and cross various biological membranes in order to reach their cellular target. Many technological tricks have been explored in order to circumvent the efficient mechanisms by which living organisms protect themselves from an invasion by exogenously administered nucleic acids, such as modifications of the natural oligonucleotides' backbones that enhance their stability with-

out being deleterious to their activity. Another line of research is to incorporate oligonucleotides into synthetic vectors acting as Trojan horses (Prochiantz 1998) able to simultaneously protect them against nucleic attack and direct them inside cells. In vivo imaging of oligonucleotides is a powerful technique to evaluate the outcome of both these strategies.

1.3 Comparative Pharmaco-Imaging of Oligonucleotides

1.3.1 Effect of Length

Most oligonucleotides tested for in vivo applications range between 8 and 25 nucleotides, a compromise between specificity which increases with length, and bioavailability which decreases with size. Langström et al. reported the pharmacodistribution of [^{76}Br]-labeled oligonucleotides of different lengths (6, 12, 20, and 30 bases) targeting the rat Chromogranin A mRNA (Wu et al. 2000). Distribution was clearly dependent on length, with the highest uptake in the kidney cortex for the shortest, and in the liver and spleen for the longest oligonucleotides. Significant uptake in the adrenals remained at modest values and was observed only with the 20- and 30-mer oligonucleotides.

1.3.2 Influence of Chemistry

Few studies have explored the general pharmacological profile of oligonucleotides in the absence of a defined target. Hnatowich et al. imaged (^{99m}Tc)-labeled phosphodiester and phosphorothioate 22-mer oligonucleotides in normal mice (Hnatowich et al. 1996). Both compounds showed low molecular weight metabolites, demonstrating that phosphorothioate is not totally stable in vivo and shows high levels of protein binding. Whole body clearance was much slower for the phosphorothioate than for the phosphodiester (PO) due to a high hepatic uptake of the phosphorothioate (PS). The authors concluded the phosphodiester DNA may be the preferred ^{99m}Tc-labeled

oligonucleotide to avoid the high and persistent liver uptake observed with the phosphorothioate DNA.

Our laboratory performed imaging studies with 3′-end [^{18}F])-labeled oligonucleotides, concentrating on the pharmacodistribution differences between phosphodiester, phosphorothioate, and 2′-*O*-methyl RNA (34). The same sequence, negative for any endogenous complementary sequence match, was constructed with these 3 chemistries, [^{18}F]-labeled at its 3′ end, and imaged in nonhuman primates (Tavitian et al. 1998). Metabolic analysis in plasma sampled at regular time intervals after injection showed a rapid degradation of the phosphodiester (half-life in the plasma 3–5 min) and comparison with the unlabeled ODN indicated that metabolism was not significantly modified by labeling. In contrast, labeled phosphorothioate and 2′-*O*-methyl RNA remained intact in plasma during the 2 h following injection. Pharmacodistribution of the radioactivity showed that the phosphodiester was eliminated both through the renal and the digestive system, while the phosphorothioate and 2′-*O*-methyl RNA showed only renal excretion. The phosphorothioate showed persistent accumulation in the liver (0.1% of injected dose per ml of tissue between 20 and 80 min after injection) while the 2′-*O*-methyl RNA accumulated in the kidney (0.03% at 80 min after injection). The data reported in this study showed (a) that the radiolabeling method has no detrimental effect on the capacity of the antisense oligonucleotide to hybridize to its target complementary sequence; (b) that after i.v. injection of the [^{18}F]oligonucleotide it is possible to quantitatively evaluate by PET the kinetics of [^{18}F] radioactivity in any selected tissue or organ; (c) that these kinetics are highly variable with the nature of the oligonucleotide backbone; and (d) that it is possible to measure the concentration of ^{18}F-labeled metabolites in the plasma during the PET measurements, opening the way to the quantitative evaluation of the tissular concentrations of [^{18}F]oligonucleotide. Overall it demonstrated that this approach was relevant for the comparative evaluation of oligonucleotides in vivo (Tavitian et al. 1998).

In a study published just recently, Roivanen and coworkers repeated the comparison of phosphodiester, phosphorothioate and 2′-*O*-methyl RNA labeled with the positron emitter gallium-68, in rats. Surprisingly, they found high uptake of the phosphorothioate in kid-

neys, and low plasmatic stability of the 2′-*O*-methyl RNA (Roivanen et al. 2004). The difference between these results and those obtained in our laboratory may be explained by the different species and/or labeling methods used in the two studies and call for further pharmacokinetics studies of oligonucleotides.

1.4 Evaluation of Delivery Vectors for Oligonucleotides

Chemical modifications may decrease sequence specificity and/or activity of oligonucleotides, and have little or no effect or may even be deleterious for membrane passage. In contrast, even nuclease-sensitive oligonucleotides can be protected by synthetic vectors manmade on the basis of their known physico-chemical properties. Many attempts have been made to include oligonucleotides into vectors such as cationic lipids or polyamines in order to improve cellular uptake and internalization, and also to ensure protection against nucleases. Among the difficulties most commonly encountered with synthetic vectors are the capture of particulate material by cells of the reticulo-endothelial system, immunogenicity or toxicity of the delivery vehicle for certain cell types (Azzazy et al. 1995; Kaesh et al. 1996; Maus et al. 1999) and segregation in the endocytosis vesicles. Cationic lipids and polyethylenimine are taken up by endocytosis, with the limitation that efficient release from the endosomes must then occur intracellularly, through lipid fusion or endosome destabilization.

Chemical conjugation or physical association of antisense oligonucleotide to various cationic lipid formulations (Zelphati and Szoka 1996) or to polyethylenimine (Boussif et al. 1995) has been reported to support efficient delivery in many cell types in vitro. Incorporation into liposomes (Thierry and Dritschilo 1992; Wang et al. 1995) or nanoparticles (Schwab et al. 1994; Lambert et al. 2001) or coupling to hydrophobic ligands (Chow et al. 1994) increased their membrane passage. Anchoring of VEGF aptamer in liposomes improved the anti-VEGF activity (by decreasing plasma clearance of the aptamer) in in vitro inhibition assays of endothelial cells proliferation, and reduced vascular permeability and angiogenesis in vivo (Willis et al. 1998). The intracellular distribution of a fluorescein-la-

beled phosphoramidate coupled to streptolysine-O demonstrated the permeability of lymphoid cell lines, and the confocal microscopy images demonstrated a nuclear fluorescent signal which was correlated with the expected antisense activity (Faria et al. 2001). The encapsulation of oligonucleotide in antibody-targeted liposomes has been proposed to circumvent extracellular degradation by nucleases and address these molecules more efficiently to target cells. For example, delivery of anti-myb oligonucleotide to human leukemia cells has been improved by using anti-CD32 or anti-CD2 immunoliposomes (Ma and Wei 1996). In another targeting approach, an elegant study demonstrated that an oligonucleotide coupled covalently to mitochondria-targeted peptide and incorporated into a cationic liposome entered the cytoplasm of human fibroblasts and, following dissociation, reached the inner compartment of mitochondria (Geromel et al. 2001).

Particularly challenging is the targeting of oligonucleotides into the brain, a topic which has been addressed by Pardridge and coworkers. A strategy which their group found successful was to couple the oligonucleotide to a monoclonal antibody (mAb) against transferrin, which undergoes receptor-mediated transcytosis through the rat blood brain barrier in vivo (Pardridge 1997). In a recent study, the coupling of an iodine-labeled biotinylated peptide nucleic acid (PNA) targeting the luciferase mRNA to an avidin-linked mAb against the rat transferrin receptor allowed imaging of the gene expression in the brain (Shi et al. 2000). Brain sections clearly showed an accumulation of the iodinated PNA in brain tumors. This study suggests that gene brain imaging can be realized with an adapted oligonucleotide carrier by-passing the blood brain barrier and undergoing endocytosis.

Complexes of DNA with cationic lipids (lipoplex; Felgner et al. 1997) result in the respective condensation of both entities by way of electrostatic interactions. Unfortunately, oligonucleotides or DNA transfer with lipoplex exhibiting a positive global charge is inefficient due to nonspecific binding with anionic serum proteins. In a recent study, an oligonucleotide was encaged in a unique formulation process which allowed preparation of stable and homogenous lipoplex exhibiting a negative global charge (Lavigne and Thierry 1997). We then applied the PET technology to whole body quantita-

tive imaging of the oligonucleotide-vector complex (Tavitian et al. 2002). We showed (a) that PET imaging yields in vivo quantitative pharmacokinetics information that is ideal for evaluating the modifications induced by vectors in the biodistribution and organ bioavailability of the oligonucleotide; (b) that competitive hybridization pictures the capacity of synthetic vectors to enhance in vivo stability; and (c) that the combination of these two techniques is able to demonstrate that carefully tailored anionic vectors dramatically improve the in vivo delivery of an oligonucleotide (Tavitian et al. 2002).

Imaging studies could answer many of the questions raised about vector efficiency and specificity and, in combination with examination of the in vivo stability of the vector-oligonucleotide conjugate, and the fate of the conjugate after membrane passage, help greatly to evaluate their clinical as well as imaging applications. Strictly from the imaging point of view however, one drawback of oligonucleotide vectorization is that biodistribution becomes predominantly dependent on the vector's distribution, and may not reflect anymore the oligonucleotide's target distribution.

1.5 Imaging with Oligonucleotides

Among the wide number of effects that have been assigned to oligonucleotides (Table 1), the potential for imaging of antisense and aptamer oligonucleotides will be considered here.

1.5.1 Antisense Oligonucleotides

Based on the formation of a Watson-Crick hybrid between an oligonucleotide and an RNA, the antisense technology provides a simple and elegant approach to inhibit the expression of a target gene. An antisense is an oligonucleotide, usually 12–25 bases long, which sequence is complementary and can bind to its target RNA (viral RNA or mRNA), thereby inhibiting its translation. The mechanism of inhibition is either through a steric blockage of the pre-mRNA splicing or of the initiation of translation, or through ribonuclease H-mediated recognition of the mRNA oligonucleotide duplex fol-

lowed by degradation of the mRNA. Antisense oligonucleotides complementary to a target region of a candidate mRNA have been successfully used to inhibit protein synthesis in a number of biological systems (Zamecnik and Stephenson 1978; Crooke 1999). This method of gene regulation, based on the hybridization of two nucleic acids strands through Watson-Crick base pair formation, is extremely simple to design and has many potential therapeutic applications in cancer, viral infections, and in inflammatory disorders (Zamecnik and Stephenson 1978; Crooke 1999).

1.6 Antisense Oligonucleotides for Gene-Related Disease Therapy

Antisense for therapy is an active field of drug development (reviews in Agrawal 1996b; Hogrefe 1999). Tens of oligonucleotides are currently tested in clinical trials, mostly in Phase II, but so far, only one has been approved by the FDA, Vitravene for cytomegalovirus retinitis. About one half of the oligonucleotides in clinical trials are built with the phosphorothioate chemistry, 50% target cancer-related genes, 25% target viral infections including hepatitis C, and three target chronic inflammatory diseases such as Crohn and hemorrhagic rectocolitis.

Many of these candidate antisense drugs address hematological disorders such as chronic myeloid leukemia (for review see Agarwal and Gewirtz 1999), by targeting specific proto-oncogenes involved in cell proliferation and neoplasic transformation: Bcr/ab1 (deFabritiis 1998), c-myb (Ratjczak et al. 1992), c-myc or the tumor suppressor gene p53 (Bishop et al. 1996). Other antisense strategies are based on the chemosensitization of tumor cells by depressing antiapoptotic genes such as Bcl-2 expression (Miyashita and Reed 1993). The antisense drug Genasense (Genta, Inc., Berkeley Heights, NJ) is an anti Bcl2 antisense now in Phase 3 clinical trials in lymphoma (Cotter et al. 1994), and is also assayed as a chemosensitizer for dacarbazine treatment of human melanoma (Janssen et al. 1998, 2000). In another approach, glioma cells collected at surgery are treated ex vivo with an antisense oligonucleotide against the type I

insulin-like growth factor receptor and reimplanted into the patient, inducing apoptosis and a host response (Andrews et al. 2001).

Although there are now a number of reports of antisense inhibition of human tumors, it should be stressed that only for a very little number of patients has complete remission been observed. Many antisense oligonucleotides have been found to induce a variety of biological effects not related to their specific hybridization to the target mRNA, including immune stimulation and other activities by oligonucleotide-containing CpG motifs, release of pharmacologically active concentration of deoxyribonucleosides, or aptameric binding to proteins. In some cases, side-effects of antisense drugs that are not based on an antisense effect could be therapeutically useful, as suggested by a recent report showing that oligonucleotides with CpG motifs can reduce prion toxicity in mice (Sethi et al. 2002). Clinical efficacy of antisense on tumor growth and development is difficult to evaluate (Crooke 2000) and could certainly benefit from in vivo imaging evaluation methods.

1.7 Improving Antisense for In Vivo Applications

Generic molecular tools that have the capacity to adapt to any possible target or at least a large number of different targets, such as antibodies or oligonucleotides, are often difficult to handle in vivo. This is especially true for antisense oligonucleotides which, although they have been sometimes presented as "magic bullets," suffer
from a number of major drawbacks that complicate their use in vivo, essentially (a) in vivo stability; (b) access to target sequences; and (c) nonspecific interactions (Piwnica-Worms 1994; Tavitian 2000).

To hit intracellular RNA target sequences, oligonucleotides should cross cellular membranes, which they do poorly because of their low lipid solubility. In addition, RNAs are highly structured molecules exhibiting double-stranded secondary structures such as stem-loops, hairpins, pseudoknots, etc., leaving relatively little access to hybrid formation by the oligonucleotides in vivo. It has been demonstrated that, at best, no more than 6%–12% of oligonucleotides targeting an RNA sequence are efficient at forming the duplex necessary for the

antisense effect (Stein 1999). Another concern is that cellular concentration of mRNA may not be high enough to allow for its imaging by antisense hybridization. This concentration can be relatively high for viral RNA in infected cells, but as a rule, the mRNA coding for a given protein is less abundant than the protein itself. Abundant mRNAs such as the one coding for tyrosine hydroxylase in catecholaminergic cells, about 1,800 molecules per cell (Kedzierski and Porter 1990) are in principle detectable, while low abundance mRNAs in less than ten copies per cell might not be.

Binding of oligonucleotides to undesired sequences may pose little problem, because dissociation constants of oligonucleotides are in the nanomolar range and depend strictly on the complementarity of the two strands of the duplex. In contrast, nonspecific binding to proteins has been reported, especially for the phosphorothioate derivatives (Benimetskaya et al. 1995), and can induce toxic effects in some cases (Henry et al. 1997). Studies using photoactivatable crosslinking of a phosphodiester oligonucleotide added to a cell culture showed that up to 90% was bound to a cell membrane protein of 75–79 kDa (Yabukov et al. 1989; Geselowitz and Neckers 1992). In the presence of serum, bovine serum albumin binds oligonucleotides with a K_m in the 10^{-5}-M range (Geselowitz and Neckers 1995), predominantly on site I of the protein, and this is found also with human serum albumin (Srinivasan et al. 1995). Several other proteins also bind oligonucleotides, and the physiological state of the cell influences binding patterns (Hawley and Gibson 1996).

1.8 In Vivo Imaging Studies with Antisense Oligonucleotides

A small number of imaging studies with oligonucleotides have been reported. The first report by Dewanjee et al. (1994) showed tumor imaging in mice with an antisense directed against the c-myc oncogene. The uptake of the antisense in the tumor was 10% at 30 min after IV injection, compared to less than 1% with control oligonucleotides. These very promising results have not been replicated by subsequent studies. Hjelstuen et al. labeled with ^{99m}Tc a 20-mer phosphodiester ODN targeted against the mRNA for CAPL, a cancer-related gene (Hjelstuen et al. 1998). A sequence with the same

bases in a random order was used as control. Biodistribution in normal mice demonstrated that the radiolabeled oligonucleotides were distributed in an unspecific manner. In contrast, an ex vivo imaging study of rat glioma with a 25-mer [^{11}C]-labeled phosphorothioate ODN targeted to glial fibrillary acidic protein (GFAP) mRNA reported prominent radioactivity uptake in the glioma, which contrasted with the adjacent cerebral tissue in autoradiograms (Kobori et al. 1999). None of the two control sequences, a sense sequence and a sequence with 20% mismatch, showed differences of uptake between the glioma and the rest of the brain. This suggests that accumulation in the glioma was correlated with recognition by the antisense probe of the GFAP mRNA overexpressed in tumoral tissue. Finally, Langström and co-workers reported the pharmacodistribution of [^{76}Br]-labeled PS oligonucleotides of different lengths (6, 12, 20, and 30 bases) targeting the rat Chromogranin A mRNA (Wu et al. 2000). Distribution was clearly dependent on length, with the highest uptake in the kidney cortex for the shortest, and in the liver and spleen for the longest oligonucleotides. Significant uptake in the adrenals, the organ targeted by the Chromogranin A antisense, was observed only with the 20- and 30-mer oligonucleotides, and remained at modest values.

All in all, the feasibility of antisense imaging is still questionable. Nevertheless, a proof of in vivo hybridization of two complementary sequences was provided by a study in which a [^{99m}Tc]-labeled 15-base PNA was shown to target its complementary PNA (cPNA) sequence coupled to polystyrene beads implanted intramuscularly in the thigh of a mouse (Mardirossian et al. 1997). A tenfold difference in the binding to the cPNA-coupled vs. uncoupled beads was reached during the first hour, and was maintained for at least 24 h, yielding a sufficient contrast for detection on a gamma camera.

Based on these results, the group of Hnatowich has developed a PNA-based pretargeting strategy taking advantage of PNA's in vivo stability and high affinity for complementary sequences. A ligand linked to a PNA sequence is administered and allowed to bind to its target for a few hours, after which the [^{99m}Tc]-labeled complementary PNA is injected to reveal the localization of the initial complex (Ruckowski et al. 1997; Wang et al. 2001). The very poor membrane passage of PNA limits this method, which is similar in its

principle to the avidin-biotin system developed for proteins, to accessible targets. Its expected advantages are the insensitivity to plasma biotinase degradation, and the absence of avidin immunogenicity and of the side effects of biotin administration.

In a recently published study by the groups at universities in Turku, Finland and Uppsala, Sweden, imaging with an H-ras antisense dodecanucleotide labeled with gallium-68 and its targeting to tumors xenografted in nude rats were reported (Roivanen et al. 2004). The biodistribution and pharmacokinetics varied considerably with the nature of the oligonucleotide backbone. One hour after IV injection, the best tumor-to-muscle ratio was reached with the phosphorothioate antisense, where it raised to 5.8 in the tumors carrying the target mRNA, while it was 4.9 in control tumors without the target. For both types of tumors and all oligonucleotides tested, the tumor-to-blood ratio was always below unity, again pointing to the difficulty in achieving significant uptake in tumors.

1.9 Aptamer Oligonucleotides

Combinatorial approaches are a modern alternative to the rational conception of ligands. Very large libraries of candidate molecules can be randomly synthesized and screened simultaneously to identify those with the wanted property. Combinatorial libraries of oligonucleotides may thus yield selective ligands for specific targets called *aptamers* ("adaptable oligomers"; Ellington and Szostak 1990; Tuerk and Gold 1990). Aptamers are selected by a generic method termed SELEX (*S*ytematic *E*volution of *L*igands by *EX*ponential enrichment), which combines the use of three basic properties of oligonucleotides:

1. *The possibility of creating very large families of combinatorial molecules*. The number of different molecules in a library of oligonucleotides with a window of randomized sequence *n* residues in length [i.e., in which any of the four bases (A, T, G, C) is introduced randomly at any position] is 4^n. Under 1 μm scale solid-phase DNA synthesis it is possible to obtain ca. 10^{14} to 10^{15} individual sequences.

2. *The possibility of binding to small molecules and protein motifs.* Like any biopolymer, oligonucleotides fall in a three-dimensional arrangement which can make contact with other molecules. The binding of an aptamer to its target molecule is based on the complementarity of their respective 3-D structure and not on the formation of a Watson-Crick duplex between complementary sequences. Nevertheless, the 3-D structures of oligonucleotides depend on their sequence of bases rather than on the sugar phosphate backbone. Aptamers can achieve high target selectivity with dissociation constants in the micromolar to low picomolar range (Osborne and Ellington 1997; Wilson and Szostak 1999) comparable to antibody-antigen interactions.
3. *The capacity to be readily multiplied unchanged.* Amplification of libraries of oligonucleotides is achieved by flanking the window of random sequence with known fixed sequences that are complementary to the primers used for PCR. This allows for easy handling and amplification of libraries containing up to 1,015 different molecules.

The SELEX strategy was designed to select, from a random library of oligonucleotides, those molecules with the desired binding property for a designed target (Ellington and Szostak 1990, Tuerk and Gold 1990). Single-stranded DNA oligonucleotides, or RNA oligonucleotides with an additional transcription step may be used. SELEX is basically an iterative cycle of the following actions in sequential order: (a) incubation of the random sequence oligonucleotide library with a decoy, i.e., a system in which all the elements of the true target binding system (support, linkers, buffer, etc.), *except* the specific target aimed at, are present; (b) separation of unbound oligonucleotides from those bound to the decoy, which are discarded; (c) incubation of the unbound pool with the true target; (d) separation of oligonucleotides bound to the target from those unbound, which are discarded, and recovery of the bound pool; (e) amplification of the bound pool, yielding a library enriched in sequences binding to the target but not to the decoy. This pool is then submitted to the next selection/amplification cycle. Once affinity saturation of binding to the target is achieved, usually after 5–20 cycles of selection/amplification, the enriched library is cloned and se-

quenced. Isolated, individual oligonucleotides are then screened for sequences of potential binding sites and tested individually for their ability to bind specifically to the target molecule.

The difficulties in adapting oligonucleotides to the in vivo context differ somewhat for aptamers and for antisense. Target accessibility is much less of a problem for aptamers than for antisense. Many aptamer targets are extracellular proteins readily accessible in vivo and relatively abundant in regard to the low concentrations of intracellular RNA targets for antisense. However, in vivo stability of oligonucleotides is an issue for the aptamers, because the modifications introduced in the sugar-phosphate backbone in order to improve oligonucleotide stability are generally not compatible with the polymerases used during the amplification steps of the SELEX procedure. Modifications that increase resistance to nucleases may be introduced after selection of the aptamer sequence, but then there is great risk that the folding pattern and the binding properties of the aptamer will be altered (Usman and Blatt 2000; Aurup et al. 1992). Hence, post-selection modifications require a tedious systematic testing of the influence of every modified residue in the sequence both on stability and binding. A limited number of modifications of the 2′ carbon of ribose confer increased resistance to the oligonucleotides and are compatible with the T7 RNA polymerase, allowing the use of 2′-Fluoro- and 2′-amino-2′-deoxynucleoside oligonucleotides directly during the SELEX process (Aurup et al. 1992; Ruckman et al. 1998).

Another approach is to substitute natural D-ribose with L-ribose to create totally stable aptamers in a mirror-image configuration termed Spiegelmers. While L-ribose is not accepted by T7 polymerase, the selection of natural D-ribose aptamers binding to the mirror-image of the target, such as, for instance, a D-amino acid peptide, followed by the chemical synthesis of the mirror-image of the selected sequence, yields by virtue of molecular symmetry a Spiegelmer that binds to the natural target molecule (i.e., the L-amino acid). Spiegelmers that bind to GnRH I have been recently isolated and characterized with this *mirror-image* SELEX (Wlotzka et al. 2002), and the method for labeling with fluorine-18 has been extended to Spiegelmers (Kühnast et al. 2003 a).

1.10 Applications and Therapeutic Aptamers

SELEX has proven successful against a variety of targets, such as proteins, small molecules, and RNA, and has high potential in the fields of therapy (Osborne et al. 1997), diagnosis (Jayasena 1999), and biotechnology (Famulok and Jenne 1998). Aptamers rival antibodies in terms of affinity for their biological target, with the advantage that they are smaller, cheaper, and easier to engineer (Table 3). Hence, they have quickly become valuable research tools (Gold 1995) and many therapeutic and diagnostic applications have been envisaged (Gold 1995; Jayasena 1999; White et al. 2000; Cerchia et al. 2003). In contrast to antibody production, aptamers can be generated against any small molecule or protein target using a completely synthetic method, and their binding characteristics depend on the experimental system used during the selection process. The selectivity of aptamers can thus be oriented through the choice of pertinent counter-selection/selection targets, as shown by reports of aptamers capable of discriminating between isoforms of protein kinase C (Conrad et al. 1994), or of interfering with Ras binding to Raf-1 but not to B-Raf, a Raf-1-related protein (Kimoto et al. 2002). Conversely, the discrimination capacity can be reduced and aptamers have been obtained that recognize ERK-2 both in its native and denatured forms (Bianchini et al. 2001).

Moreover, the SELEX process is not limited to the use of purified proteins as targets but can be applied to complex heterogeneous targets such as cells, organelles, or even tissues (Morris et al. 1998). Using a combination of proteic and cellular targets (*blended*

Table 3. Comparison between antibodies and aptamers

	Aptamers	Antibodies
Size	9–15 kDa	>150 kDa
Discrimination (theophylline vs. caffeine)	+++	+/++
Affinity	5–100 nM	0.1–100 nM
Design	Synthetic	Animal
Price	–	–

SELEX), RNA aptamers were selected against tenascin-C, an extracellular matrix protein overexpressed during tumor growth (Hicke et al. 2001). This approach may also help to identify molecular hallmarks of cell surfaces, as shown with human red blood cell membranes (Morris et al. 1998), or to differentiate between quiescent and proliferating states of the same endothelial cells (Blank et al. 2001). In this latter study, *deconvolution* SELEX was carried out to identify the membrane protein that was one of the targets of the aptamers in the selected binding pool, and was found to be specifically expressed during endothelial cell proliferation (Blank et al. 2001). Selecting aptamers in a physiological context in which cell surface proteins are displayed in their native state paves the way to in vivo applications of aptamers. Until now only limited studies have been realized in vivo, but it is remarkable that aptamers have entered in therapeutic trials in such a short time after their invention was conceived (Cerchia et al. 2003).

Effective aptamer strategies have been developed for in vivo therapeutics. Aptamers can compete with the natural ligands of their target proteins and thus antagonize their biological function. Antagonistic aptamers to the platelet-derived growth factor β chain (PDGF-B) induced a significant reduction of mesangioproliferative changes in rats with progressive glomerulonephritis (Ostendorf et al. 2001). Injection of antagonistic aptamers against PDGF-B in rats with PROb colon carcinomas decreased interstitial hypertension in the tumors (Pietras et al. 2001). Aptamer NX 1838 significantly reduced vascular endothelial growth factor (VEGF)-induced vascular permeability in vivo (Miyashita and Reed 1993) and is currently in phase-I clinical trials in humans (Sun 2000).

1.11 Aptamers as Contrast Agents for Diagnosis

The molecular weight of aptamers (10–15 kDa) is one order of magnitude lower than that of antibodies (150 kDa); hence, they exhibit higher tissue penetration and faster blood clearance, two critical parameters for imaging agents. In the first aptamer imaging study published, the ability of an aptamer binding to human neutrophil elastase to image inflammation was compared to the reference antibody

in vivo in a rat reverse-passive Arthus reaction model (Charlton et al. 1997). The aptamer performed better than the reference antibody to achieve a peak target-to-background ratio. The conclusion of that pioneer study was that aptamer ligands were useful in diagnostic imaging, and could offer significant advantages over monoclonal antibodies.

Recently, DNA aptamers directed against human alpha-thrombin were evaluated for thrombus-imaging potential. However, in a rabbit jugular vein thrombus model in vivo, the rapid clearance from circulation, and slow mass transfer in the clot, did not permit thrombin-dependent imaging (Dougan et al. 2003).

The use of aptamers for in vivo imaging is especially promising due to the very wide range of possibilities available to introduce changes in their structure through defined chemical modifications that will modify their pharmacokinetics properties (Cerchia et al. 2003). For instance, the clearance rates of aptamers can be altered to keep them in circulation by anchoring them to liposome bilayers, and by coupling them to inert large molecules such as polyethylene glycol or to other hydrophobic groups (Willis et al. 1998). The discrimination and targeting capacities of aptamers are exquisitely suited to be imaging agents for noninvasive diagnostic procedures. In this respect, *escort* aptamers are a budding concept in which the aptamer oligonucleotide may be used to deliver an active drug, radionuclide, toxin, or cytotoxic agent to the desired site for diagnosis and therapy (Jhaveri et al. 2000).

1.12 Future Developments Needed for In Vivo Imaging with Oligonucleotides: Mastering the Nonspecific Interactions and Signal-to-Noise Ratio

What studies with oligonucleotides have demonstrated so far is the feasibility of the imaging approach. Thanks to the ever-increasing sensitivity of imaging techniques and the very high specific activity with which oligonucleotides can be labeled, the capacity to detect even minute concentrations of specific RNA in cells is theoretically feasible (Lewis and Jia 2003).

1.12.1 Sensitivity

Target concentrations is not a real matter of concern for the aptamer oligonucleotides, for which protein targets are in the concentration range and readily accessible to nuclear medicine radiopharmaceuticals, but it is one for antisense oligonucleotides which aim at the RNA, always present in lower concentration than the protein. Available quantitative data report mRNA concentrations in the nanomolar range which are at the lower limit of the detection range for sensitive nuclear medicine techniques such as PET (Kedzierski and Porter 1990; Tavitian 2000). Another matter of concern is the highly variable turnover rate of the RNAs, which can be as low as minutes for some species (Dani et al. 1984). Thus, it is likely that antisense imaging, if successful, will be limited to abundant mRNAs with low turnover rates, or to exogenous RNA from bacteria, viruses, or parasites, usually expressed in high concentrations in the infected organs.

1.12.2 Affinity

The affinity of an oligonucleotide for its target is usually in the nanomolar range, both for antisense oligonucleotides targeting a complementary RNA (Sauer et al. 1999) or for aptamer oligonucleotides targeting proteins (Famulok et al. 2000; Hermann and Patel 2000). While this appears ideal for a radiopharmaceutical, the kinetics of binding is a more critical consideration for oligonucleotides in vivo. For antisense, the binding is a multistep process induced by recognition of a nucleation site followed by hybridization, similar to a zipper mechanism. The hybridization rates of antisense oligonucleotides are low (Freier 1993) and depend on the secondary structure of the target (Monia et al. 1992). Concerning aptamers, it is not clear whether molecular recognition is achieved by the folding of an initially unstructured RNA around its target, or if the processes of RNA folding and binding are uncoupled like in typical protein-ligand complexes (Sussman et al. 2000).

1.12.3 "Nonspecific" Binding

Nonspecific interactions, probably better defined as "nondesired" interactions, are certainly the major pitfall for specific imaging of biological targets with oligonucleotides. This stands in contrast to pharmaceutical applications, where nonspecific binding is of little importance as long as it does not lead to toxic effects and preserves the specific binding responsible for the pharmacological activity. For imaging purposes, the signal-to-noise ratio is given by the relative concentrations of the oligonucleotide's binding to the specific versus the nonspecific binding sites.

Binding to undesired targets is difficult to avoid for oligonucleotides, in part because they are large ligands (5–15 kDa) with multiple functional groups. – Bovine serum albumin (Geselowitz and Neckers 1995) and human serum albumin (Srinivasan et al. 1995) bind oligonucleotides with a K_m in the 10^{-4} to 10^{-5} M range. Several other proteins also bind oligonucleotides (Geselowitz and Neckers 1992; Benimetskaya et al. 1995). Undesired binding may also occur in the case of unmethylated CpG sequences that are recognized by the immune system (Krieg 2001).

Concerning nonspecific binding, the case of antisense is special because, by definition, they have statistically a large number of incomplete targets. Moreover, specificity is an essential parameter for in vivo antisense since they should ideally discriminate point mutations on mRNA. Given the size of mammalian mRNA pools, there is statistically less than one occurrence of a complementary target for a given 13–14-nucleotide-long oligonucleotide. In *Xenopus* oocytes, microinjection of fully matched, partially matched and even random sequence oligonucleotides all led to cleavage of the fibronectin mRNA, and the authors concluded that, at least in this system, it was not possible to target specifically one mRNA without binding to nontargeted mRNAs (Woolf et al. 1992).

In contrast, a study on the possibility of distinguishing between the oncogenic and the wild-type forms of Ha-Ras, which consist of a single-point mutation on codon 12, showed that the best antisense achieved a fivefold discrimination between the two forms, a value that, if maintained in vivo, would be compatible with selective imaging (Monia et al. 1992). Recently, Zhang and co-workers reported

accumulation of a ^{99m}Tc-labeled antisense phosphorothioate against the type I regulatory subunit alpha of cyclic adenosine monophosphate-dependent protein kinase A (RIα) mRNA in tumor cell lines (Zhang et al. 2001). This accumulation was attributed to the specific binding of the antisense to RIα mRNA on the basis of (a) increased accumulation of the antisense versus the control sense sequence; (b) increased accumulation of the antisense in tumor cell lines versus nontumor cells; (c) decreased accumulation of the labeled antisense by competition with unlabeled antisense. Although they pertain solely to in vitro cultured tumor cells, the results are convincing and address a number of pertinent questions. They also support the view that antisense in vivo imaging might become a reality in the future (Urbain 2001).

1.13 Conclusion

Oligonucleotide radiopharmaceuticals is a slowly but steadily progressing field. With a panel of labeling and imaging techniques mastered by several groups, imaging of oligonucleotides is now relatively accessible and will be applied to more and more trials of oligonucleotide pharmacology. Imaging with oligonucleotides is still a few miles farther ahead of us, but the stakes of detecting gene expression noninvasively in vivo are so high that it will certainly become a reality in the near future.

Acknowledgements. I am most grateful to all the personnel at the Service Hospitalier Frédéric Joliot. Supported by EU contract QLG1-CT-2000–00562 and Programme d'Imagerie du Petit Animal. This work is to be considered a contribution from the Network of European Molecular Imaging Laboratories (EMIL).

References

Agarwal N, Gewirtz AM (1999) Oligonucleotide therapeutics for hematologic disorders. Biochim Biophys Acta 1489:85–96

Agrawal S (1996a) Antisense oligonucleotides: towards clinical trials. Trends Biotechnol 14:376–387

Agrawal S (1996b) Antisense therapeutics. Humana Press, Totawa
Akhtar S, Agrawal S (1997) In vivo studies with antisense oligonucleotides. Trends Pharmacol Sci 18:12–18
Andrews DW, Resnicoff M, Flanders AE, Kenyon L, Curtis M, Merli G, Baserga R, Iliakis G, Aiken RD (2001) Results of a pilot study involving the use of an antisense oligodeoxynucleotide directed against the insulin-like growth factor type I receptor in malignant astrocytomas. J Clin Oncol 19:2189–2200
Aurup H, Williams DM, Eckstein F (1992) 2′-Fluoro- and 2′-amino-2′-deoxynucleoside 5′-triphosphates as substrates for T7 RNA polymerase. Biochemistry 31:9636–9641
Azzazy HM, Hong K, Wu MC, Gross GW (1995) Interaction of cationic liposomes with cells of electrically active neuronal networks in culture. Brain Res 695:231–236
Benimetskaya L, Tonkinson JL, Koziolkiewicz M, Karwowski B, Guga P, Zeltser R, Stec W, Stein CA (1995) Binding of phosphorothioate oligodeoxynucleotides to basic fibroblast growth factor, recombinant soluble CD4, laminin and fibronectin is P-chirality independent. Nucleic Acids Res 23:4239–4245
Bianchini M, Radrizzani M, Brocardo MG, Reyes GB, Gonzalez Solveyra C, Santa-Coloma TA (2001) Specific oligobodies against ERK-2 that recognize both the native and the denatured state of the protein. J Immunol Methods 252:191–197
Bishop MR, Iversen PL, Bayever E, Sharp JG, I Greiner TC, Copple BL, Ruddon R, Zon G, Spinolo J, Arneson M, Armitage JO, Kessinger A (1996) Phase trial of an antisense oligonucleotide OL(1)p53 in hematologic malignancies. J Clin Oncol 14:1320–1326
Blank M, Weinschenk T, Priemer M, Schluesener H (2001) Systematic evolution of a DNA aptamer binding to rat brain tumor microvessels selective targeting of endothelial regulatory protein pigpen. J Biol Chem 276: 16464–16468
Blasberg R (2002) PET imaging of gene expression. Eur J Cancer 38:2137–2146
Boussif O, Lezoualc'h F, Zanta MA, Mergny MD, Scherman D, Demeneix B, Behr JP (1995) A versatile vector for gene and oligonucleotide transfer into cells in culture and in vivo: polyethylenimine. Proc Natl Acad Sci USA 92:7297–7301
Brody EN, Gold L (2000) Aptamers as therapeutic and diagnostic agents. J Biotechnol 74:5–13
Caruthers MH, Beaucage SL, Efcavitch JW, Fisher EF, Matteucci MD, Stabinsky Y (1980) New chemical methods for synthesizing polynucleotides. Nucleic Acids Symp Ser 7:215–223
Cerchia L, Hamm J, Libri D, Tavitian B, de Francis V (2002) Nucleic acid aptamers in cancer medicine. FEBS Lett 528:12–16

Charlton J, Sennello J, Smith D (1997) In vivo imaging of inflammation using an aptamer inhibitor of human neutrophil elastase. Chem Biol 4:809–816

Chow TY, Juby C, Brousseau R (1994) Specific targeting of antisense oligonucleotides to neutrophils. Antisense Res Dev 4:81–86

Conrad R, Keranen LM, Ellington AD, Newton AC (1994) Isozyme-specific inhibition of protein kinase C by RNA aptamers. J Biol Chem 269: 32051–32054

Cotter FE, Johnson P, Hall P, Pocock C, al Mahdi N, Cowell JK, Morgan G (1994) Antisense oligonucleotides suppress B-cell lymphoma growth in a SCID-hu mouse model. Oncogene 9:3049–3055

Crooke ST (1998) Antisense research and applications. Springer, Berlin Heidelberg New York

Crooke ST (1999) Molecular mechanisms of action of antisense drugs. Biochim Biophys Acta 1489:31–44

Crooke ST (2000) Evaluating the mechanism of action of antiproliferative antisense drugs. Antisense Nucleic Acid Drug Dev 10:123–127

Dani C, Blanchard JM, Piechaczyk M, Riaad-El-Sabouty S, Marty L, Jeanteur P (1984) Extreme instability of myc mRNA in normal and transformed human cells. Proc Natl Acad Sci USA 81:7046–7050

Dewanjee MK, Ghafouripour AK, Kapadvanjwala M, Dewanjee S, Serafini AN, Lopez DM, Sfakianakis GN (1994) Noninvasive imaging of c-myc oncogene messenger RNA with indium-111-antisense probes in a mammary tumor-bearing mouse model. J Nucl Med 35:1054–1063

de Fabritiis P, Petti MC, Montefusco E, De Propris MS, Sala R, Bellucci R, Mancini M, Lisci A, Bonetto F, Geiser T, Calabretta B, Mandelli F (1998) BCR-ABL antisense oligodeoxynucleotide in vitro purging and autologous bone marrow transplantation for patients with chronic myelogenous leukemia in advanced phase. Blood 91:3156–3162

Dollé F, Hinnen F, Vaufrey F, Tavitian B, Crouzel C (1997) A general method for labeling oligodeoxynucleotides with ^{18}F for in vivo PET imaging. J Label Compounds Radiopharm 34:319–330

Doudna JA, Cech TR, Sullenger BA (1995) Selection of an RNA molecule that mimics a major autoantigenic epitope of human insulin receptor. Proc Natl Acad Sci USA 92:2355–2359

Dougan H, Weitz JI, Stafford AR, Gillespie KD, Klement P, Hobbs JB, Lyster DM (2003) Evaluation of DNA aptamers directed to thrombin as potential thrombus imaging agents. Nucl Med Biol 30:61–72

Ellington AD, Szostak JW (1990) In vitro selection of RNA molecules that bind specific ligands. Nature 346:818–822

Famulok M, Jenne A (1998) Oligonucleotide libraries-variation delectat. Curr Opin Chem Biol 2:320–327

Famulok M, Mayer G, Blind M (2000) Nucleic acid aptamers – from selection in vitro to applications in vivo. Acc Chem Res 33:591–599

Faria M, Spiller DG, Dubertret C, Nelson JS, White MR, Scherman D, Helene C, Giovannangeli C (2001) Phosphoramidate oligonucleotides as potent antisense molecules in cells and in vivo. Nat Biotechnol 19:40–44

Felgner PL, Barenholz Y, Behr JP, Cheng SH, Cullis P, Huang L, Jessee JA, Seymour L, Szoka F, Thierry AR, Wagner E, Wu G (1997) Nomenclature for synthetic gene delivery systems. Hum Gene Ther 8:511–512

Freier S (1993) Hybridization: considerations affecting antisense drugs. In: Crooke ST, Lebleu B (eds) Antisense research and applications. CRC Press, Boca Raton, pp 67–82

Geromel V, Cao A, Briane D, Vassy J, Rotig A, Rustin P, Coudert R, Rigaut JP, Munnich A, Taillandier E (2001) Mitochondria transfection by oligonucleotides containing a signal peptide and vectorized by cationic liposomes. Antisense Nucleic Acid Drug Dev 11:175–180

Geselowitz DA, Neckers LM (1992) Analysis of oligonucleotide binding, internalization, and intracellular trafficking utilizing a novel radiolabeled crosslinker. Antisense Res Dev 2:17–25

Geselowitz DA, Neckers LM (1995) Bovine serum albumin is a major oligonucleotide-binding protein found on the surface of cultured cells. Antisense Res Dev 5:213–217

Gold L (1995) Oligonucleotides as research, diagnostic, and therapeutic agents. J Biol Chem 270:13581–13584

Hamzavi R, Dollé F, Tavitian B, Dahl O, Nielsen P (2003) Modulation of the pharmacokinetic properties of PNA: preparation of galactosyl, mannosyl, fucosyl, *N*-acetyl-galatosaminyl and *N*-acetyl-glycosaminyl derivatives of aminoethylglycin peptide nucleic acid monomers and their incorporation into PNA oligomers. Bioconj Chem 14:941–954

Hawley P, Gibson I (1996) Interaction of oligodeoxynucleotides with mammalian cells. Antisense Nucleic Acid Drug Dev 6:185–195

Henry SP, Novotny W, Leeds J, Auletta C, Kornbrust DJ (1997) Inhibition of coagulation by a phosphorothioate oligonucleotide. Antisense Nucleic Acid Drug Dev 7:503–510

Hermann T, Patel DJ (2000) Adaptive recognition by nucleic acid aptamers. Science 287:820–825

Hicke BJ, Marion C, Chang YF, Gould T, Lynott CK, Parma D, Schmidt PG, Warren S (2001) Tenascin-C aptamers are generated using tumor cells and purified protein. J Biol Chem 276:48644–48654

Hjelstuen OK, Tonnesen HH, Bremer PO, Verbruggen AM (1998) 3′-^{99m}Tc-labeling and biodistribution of a CAPL antisense oligodeoxynucleotide. Nucl Med Biol 25:651–657

Hnatowich DJ, Mardirossian G, Fogarasi M, Sano T, Smith CL, Cantor CR, Rusckowski M, Winnard PJ (1996) Comparative properties of a technetium-99m-labeled single-stranded natural DNA and a phosphorothioate derivative in vitro and in mice. J Pharm Exp Ther 276:326–334

Hnatowich DJ (1999) Changing focus: applying antisense to nuclear medicine imaging. Mol Med Today 5:151

Hogrefe RI (1999) An antisense oligonucleotide primer. Antisense Nucleic Acid Drug Dev 9:351–357

Jacobs A, Voges J, Reszka R, Lercher M, Gossmann A, Kracht L, Kaestle C, Wagner R, Wienhard K, Heiss WD (2001) Positronemission tomography of vector-mediated gene expression in gene therapy for gliomas. Lancet 358:727–729

Jain RK (1998) The next frontier of molecular medicine: delivery of therapeutics. Nat Med 4:655–657

Jansen B, Schlagbauer-Wadl H, Brown BD, Bryan RN, van Elsas A, Muller M, Wolff K, Eichler HG, Pehamberger H (1998) bcl-2 antisense therapy chemosensitizes human melanoma in SCID mice. Nat Med 4:232–234

Jansen B, Wacheck V, Heere-Ress E, Schlagbauer-Wadl H, Hoeller C, Lucas T, Hoermann M, Hollenstein U, Wolff K, Pehamberger H (2000) Chemosensitization of malignant melanoma by BCL2 antisense therapy. Lancet 356:1728–1733

Jayasena SD (1999) Aptamers: an emerging class of molecules that rival antibodies in diagnostics. Clin Chem 45:1628–1650

Jhaveri S, Rajendran M, Ellington AD (2000) In vitro selection of signaling aptamers. Nat Biotechnol 18:1293–1297

Kaesh S, Kim JB, Cariola M, Ralston E (1996) Improved lipid-mediated gene transfer into primary cultures of hippocampal neurons. Mol Brain Res 35:344–348

Kedzierski W, Porter JC (1990) Quantitative study of tyrosine hydroxylase mRNA in catecholaminergic neurons and adrenals during development and aging. Mol Brain Res 7:45–51

Kimoto M, Shirouzu M, Mizutani S, Koide H, Kaziro Y, Hirao I, Yokoyama S (2002) Anti-(Raf-1) RNA aptamers that inhibit Ras-induced Raf-1 activation. Eur J Biochem 269:697–704

Kobori N, Imahori Y, Mineura K, Ueda S, Fujii R (1999) Visualization of mRNA expression in CNS using ^{11}C-labeled phosphorothioate oligodeoxynucleotide. Neuroreport 10:2971–2974

Krieg AM (2001) From bugs to drugs: therapeutic immunomodulation with oligodeoxynucleotides containing CpG sequences from bacterial DNA. Antisense Nucleic Acid Drug Dev 11:181–188

Kühnast B, Dollé F, Tavitian B (2002) Fluorine-18 labeling of peptide nucleic acids. J Label Compounds Radiopharm 45:1–11

Kühnast B, Dollé F, Vaufrey F, Hinnen F, Crouzel C, Tavitian B (2000a) Fluorine-18 labeling of oligonucleotides bearing chemically-modified ribose-phosphate backbones. J Label Compounds Radiopharm 43:837–848

Kühnast B, Dollé F, Terrazzino S, Rousseau B, Loc'h C, Vaufrey F, Hinnen F, Doignon I, Pillon F, David C, Crouzel C, Tavitian B (2000b) A general method to label antisense oligonucleotides with radioactive halogens for pharmacological and imaging studies. Bioconj Chem 11:627–636

Kühnast B, Hinnen F, Boisgard R, Tavitian B, Dollé F (2003b) Fluorine-18 labeling of oligonucleotides: prosthetic labeling at the 5′-end using the

N-(4-[^{18}F]fluorobenzyl)-2-bromoacetamide reagent. J Label Compounds Radiopharm 46:1093–1103

Kühnast B, Klussmann S, Hinnen F, Boisgard R, Rousseau B, Fürste JP, Tavitian B, Dollé F (2003a) Fluorine-18- and iodine-125 labeling of Spiegelmers. J Label Compounds Radiopharm 46:1205–1219

Lambert G, Fattal E, Couvreur P (2001) Nanoparticulate systems for the delivery of antisense oligonucleotides. Adv Drug Deliv Rev 47:99–112

Lavigne C, Thierry AR (1997) Enhanced antisense inhibition of human immunodeficiency virus type 1 in cell cultures by DLS delivery system. Biochem Biophys Res Commun 237:566–571

Lavorgna G, Dahary D, Lehner B, Sorek R, Sanderson CM, Casari G (2004) In search of antisense. Trends Biochem Sci 29:88–94

Lewis MR, Jia F (2003) Antisense imaging: and miles to go before we sleep? J Cell Biochem 90:464–472

Ma DD, Wei AQ (1996) Enhanced delivery of synthetic oligonucleotides to human leukaemic cells by liposomes and immunoliposomes. Leuk Res 20:925–930

Mardirossian G, Lei K, Rusckowski M, Chang F, Qu T, Egholm M, Hnatowich DJ (1997) In vivo hybridization of technetium-99m-labeled peptide nucleic acid (PNA). J Nucl Med 38:907–913

Maus U, Rosseau S, Mandrakas N, Schlingensiepen R, Maus R, Muth H, Grimminger F, Seeger W, Lohmeyer J (1999) Cationic lipids employed for antisense oligodeoxynucleotide transport may inhibit vascular cell adhesion molecule-1 expression in human endothelial cells: a word of caution. Antisense Nucleic Acid Drug Dev 9:71–80

Miyashita T, Reed JC (1993) Bcl-2 oncoprotein blocks chemotherapy-induced apoptosis in a human leukemia cell line. Blood 81:151–157

Monia BP, Johnston JF, Ecker DJ, Zounes MA, Lima WF, Freier SM (1992) Selective inhibition of mutant Ha-ras mRNA expression by antisense oligonucleotides. J Biol Chem 267:19954–19962

Morris KN, Jensen KB, Julin CM, Weil M, Gold L (1998) High affinity ligands from in vitro selection: complex targets. Proc Natl Acad Sci USA 95:2902–2907

Osborne SE, Ellington AD (1997) Nucleic acid selection and the challenge of combinatorial chemistry. Chem Rev 97:349–370

Osborne SE, Matsumura I, Ellington AD (1997) Aptamers as therapeutic and diagnostic reagents: problems and prospects. Curr Opin Chem Biol 1:5–9

Ostendorf T, Kunter U, Grone HJ, Bahlmann F, Kawachi H, Shimizu F, Koch KM, Janjic N, Floege J (2001) Specific antagonism of PDGF prevents renal scarring in experimental glomerulonephritis. J Am Soc Nephrol 12:909–918

Pardridge WM (1997) Drug delivery to the brain. J Cereb Blood Flow Metab 17:713–731

Pietras K, Ostman A, Sjoquist M, Buchdunger E, Reed RK, Heldin CH, Rubin K (2001) Inhibition of platelet-derived growth factor receptors reduces interstitial hypertension and increases transcapillary transport in tumors. Cancer Res 61:2929–2934

Piwnica Worms D (1994) Making sense out of anti-sense: challenges of imaging gene translation with radiolabeled oligonucleotides. J Nucl Med 35:1064–1066

Prochiantz A (1998) Peptide nucleic acid smugglers. Nat Biotechnol 16: 819–820

Ratajczak MZ, Kant JA, Luger SM, Hijiya N, Zhang J, Zon G, Gewirtz AM (1992) In vivo treatment of human leukemia in a scid mouse model with c-myb antisense oligodeoxynucleotides. Proc Natl Acad Sci USA 89: 11823–11827

Roivainen A, Tolvanen T, Salomaki S, Lendvai G, Velikyan I, Numminen P, Valila M, Sipila H, Bergstrom M, Harkonen P, Lonnberg H, Langstrom B (2004) 68Ga-labeled oligonucleotides for in vivo imaging with PET. J Nucl Med 45:347–355

Ruckman J, Green LS, Beeson J, Waugh S, Gillette WL, Henninger DD, Claesson-Welsh L, Janjic N (1998) 2′-Fluoropyrimidine RNA-based aptamers to the 165-amino acid form of vascular endothelial growth factor (VEGF165). Inhibition of receptor binding and VEGF-induced vascular permeability through interactions requiring the exon 7-encoded domain. J Biol Chem 273:20556–20567

Rusckowski M, Qu T, Chang F, Hnatowich DJ (1997) Pretargeting using peptide nucleic acid. Cancer 80:2699–2705

Sauer M, Brecht A, Charisse K, Maier M, Gerster M, Stemmler I, Gauglitz G, Bayer E (1999) Interaction of chemically modified antisense oligonucleotides with sense DNA: a label-free interaction study with reflectometric interference spectroscopy. Anal Chem 71:2850–2857

Schwab G, Chavany C, Duroux I, Goubin G, Lebeau J, Helene C, Saison Behmoaras T (1994) Antisense oligonucleotides adsorbed to polyalkylcyanoacrylate nanoparticles specifically inhibit mutated Haras-mediated cell proliferation and tumorigenicity in nude mice. Proc Natl Acad Sci USA 91:10460–10464

Sethi S, Lipford G, Wagner H, Kretzschmar H (2002) Postexposure prophylaxis against prion disease with a stimulator of innate immunity. Lancet 360:229–230

Shi N, Boado RJ, Pardridge RW (2000) Antisense imaging of gene expression in the brain in vivo. Proc Natl Acad Sci USA 97:14709–14714

Southern EM (1975) Detection of specific sequences among DNA fragments separated by gel electrophoresis. J Mol Biol 598:503–517

Srinivasan SK, Tewary HK, Iversen PL (1995) Characterization of binding sites, extent of binding, and drug interactions of oligonucleotides with albumin. Antisense Res Dev 5:131–139

Stein CA (1999) Keeping the biotechnology of antisense in context. Nat Biotech 17:209
Sun S (2000) Technology evaluation: SELEX, Gilead Sciences Inc. Curr Opin Mol Ther 2:100–105
Sussman D, Nix JC, Wilson C (2000) The structural basis for molecular recognition by the vitamin B 12 RNA aptamer. Nat Struct Biol 7:53–57
Tavitian B, Marzabal S, Boutet V, Kühnast B, Terrazzino S, Moynier M, Dollé F, Deverre JR, Thierry AR (2002) Characterization of a synthetic anionic vector for oligonucleotide delivery using in vivo whole body dynamic imaging. Pharm Res 19:367–376
Tavitian B, Terrazzino S, Kühnast B, Marzabal S, Stettler O, Dollé F, Deverre JR, Jobert A, Hinnen F, Bendriem B, Crouzel C, Di Giamberardino L (1998) In vivo imaging of oligonucleotides with positron emission tomography. Nat Med 4:467–471
Tavitian B (2000) In vivo antisense imaging. Q J Nucl Med 44:236–255
Thierry AR, Dritschilo A (1992) Intracellular availability of unmodified, phosphorothioated and liposomally encapsulated oligodeoxynucleotides for antisense activity. Nucleic Acids Res 20:5691–5698
Tuerk C, Gold L (1990) Systematic evolution of ligands by exponential enrichment: RNA ligands to bacteriophage T4 DNA polymerase. Science 249:505–510
Urbain JL (2001) Sense, antisense, and common sense. J Nucl Med 42: 1670–1672
Usman N, Blatt LM (2000) Nuclease-resistant synthetic ribozymes: developing a new class of therapeutics. J Clin Invest 106:1197–1202
Wang S, Lee RJ, Cauchon G, Gorenstein DG, Low PS (1995) Delivery of antisense oligodeoxyribonucleotides against the human epidermal growth factor receptor into cultured KB cells with liposomes conjugated to folate via polyethylene glycol. Proc Natl Acad Sci USA 92:3318–3322
Wang Y, Chang F, Zhang Y, Liu N, Liu G, Gupta S, Rusckowski M, Hnatowich DJ (2001) Pretargeting with amplification using polymeric peptide nucleic acid. Bioconjug Chem 12:807–816
White RR, Sullenger BA, Rusconi CP (2000) Developing aptamers into therapeutics. J Clin Invest 106:929–934
Wickstrom E (1998) Clinical trials of genetic therapy with antisense DNA and DNA vectors. Marcel Decker, New York
Willis MC, Collins BD, Zhang T, Green LS, Sebesta DP, Bell C, Kellogg E, Gill SC, Magallanez A, Knauer S, Bendele RA, Gill PS, Janjic N, Collins B (1998) Liposome-anchored vascular endothelial growth factor aptamers. Bioconjug Chem 9:573–582
Wilson DS, Szostak JW (1999) In vitro selection of functional nucleic acids. Annu Rev Biochem 68:611–647
Wlotzka B, Leva S, Eschgfaller B, Burmeister J, Kleinjung F, Kaduk C, Muhn P, Hess-Stumpp H, Klussmann S (2002) In vivo properties of an

anti-GnRH Spiegelmer: an example of an oligonucleotide-based therapeutic substance class. Proc Natl Acad Sci USA 99:8898–8902

Woolf TM, Melton DA, Jennings CG (1992) Specificity of antisense oligonucleotides in vivo. Proc Natl Acad Sci USA 89:7305–7309

Wu F, Yngve U, Hedberg E, Honda M, Lu L, Eriksson B, Watanabe Y, Bergstrom M, Langstrom B (2000) Distribution of [^{76}Br]-labeled antisense oligonucleotides of different length determined ex vivo in rats. Eur J Pharm Sci 10:179–186

Yakubov LA, Deeva EA, Zarytova VF, Ivanova EM, Ryte AS, Yurchenko LV, Vlassov VV (1989) Mechanism of oligonucleotide uptake by cells: involvement of specific receptors? Proc Natl Acad Sci USA 86:6454–6458

Younes CK, Boisgard R, Tavitian B (2002) Labeled oligonucleotides as radiopharmaceuticals: pitfalls, problems and perspectives. Curr Pharm Des 8: 1451–1466

Zamecnik PC, Stephenson ML (1978) Inhibition of Rous sarcoma virus replication and cell transformation by a specific oligodeoxynucleotide. Proc Natl Acad Sci USA 75:280–284

Zelphati O, Szoka FC Jr (1996) Mechanism of oligonucleotide release from cationic liposomes. Proc Natl Acad Sci USA 93:11493–11498

Zhang YM, Liu N, Zhu ZH, Rusckowski M, Hnatowich DJ (2000) Influence of different chelators (HYNIC, MAG3 and DTPA) on tumor cell accumulation and mouse biodistribution of technetium-99m-labeled to antisense DNA. Eur J Nucl Med 27:1700–1707

Zhang YM, Wang Y, Liu N, Zhu ZH, Rusckowski M, Hnatowich DJ (2001) In vitro investigations of tumor targeting with [^{99m}]Tc-labeled antisense DNA. J Nucl Med 42:1660–1669

2 Imaging Protein-Protein Interactions in Whole Cells and Living Animals

D. Piwnica-Worms, K. E. Luker

Protein-protein interactions regulate a variety of cellular functions, including cell cycle progression, signal transduction, and metabolic pathways. On a whole organism scale, protein-protein interactions regulate signals that affect overall homeostasis, patterns of development, normal physiology, and disease in living animals (Zhang et al. 1997; Stark et al. 1998; Ogawa et al. 2002). In addition, protein-protein interactions have untapped potential as therapeutic targets (Heldin 2001; Darnell 2002). Evidence is accumulating that pathways of protein interactions in specific tissues produce regional effects that cannot be investigated fully within vitro systems and thus, there is considerable interest in evaluating protein interactions in living animals.

Fundamentally, the detection of physical interaction among two or more proteins can be observed if association between the interactive partners leads to production of a readily observed biological or physical readout (Toby and Golemis 2001). Most strategies for detecting protein-protein interactions in intact cells are based on fusion of the pair of interacting molecules to defined protein elements to

reconstitute a biological or biochemical function. Examples of reconstituted activities include activation of transcription, repression of transcription, activation of signal transduction pathways, and reconstitution of a disrupted enzymatic activity (Toby and Golemis 2001). A variety of these techniques have been established for investigating protein-protein interactions in cultured cells and several are now being validated for use in living animals, including the two-hybrid system and protein fragment complementation. The major features of these two methods and their potential utility for in vivo imaging are described below.

2.1 Two-Hybrid Systems

Two-hybrid systems exploit the modular nature of transcription factors, many of which can be separated into discrete DNA-binding and activation domains (Fields and Song 1989). Proteins of interest are expressed as fusions with either a DNA-binding domain (BD) or activation domain (AD), creating hybrid proteins. If the hybrid proteins bind to each other as a result of interaction between the proteins of interest, then the separate BD and AD of the transcription factor are brought together within the cell nucleus to drive expression of a reporter gene. In the absence of specific interaction between the hybrid proteins, the reporter gene is not expressed because the BD and AD do not associate independently. Two-hybrid assays can detect transient and/or unstable interactions between proteins, and this technique is reported to be independent of expression of endogenous proteins (von Mering et al. 2002). Although the two-hybrid assay originally was developed in yeast, commercial systems (BD Biosciences Clontech, Palo Alto, CA) are now available for studies in bacteria and mammalian cells.

We and other investigators have shown that two-hybrid systems can be used to image protein interactions in living mice with positron emission tomography (PET; Luker et al. 2002, 2003 a–c) or bioluminescence imaging (Ray et al. 2002). For example, to enable noninvasive molecular imaging of protein-protein interactions in vivo by PET and fluorescence imaging, we engineered a fusion reporter gene comprising a mutant herpes simplex virus 1 thymidine kinase

(HSV1-tk) and green fluorescent protein (GFP) for readout of a tetracycline-inducible two-hybrid system in vivo. Using microPET, interactions between p53 tumor suppressor and the large T antigen (TAg) of SV40 virus were visualized in tumor xenografts of HeLa cells stably transfected with the imaging constructs (Luker et al. 2002). However, the two-hybrid method has some limitations. Some types of proteins do not lend themselves to study by the two-hybrid method. For example, because production of signal in the two-hybrid method requires nuclear localization of the hybrid proteins, membrane proteins cannot be studied in their intact state. Also, the time delay associated with both transcriptional activation of the reporter gene and degradation of the reporter protein and mRNA limits its kinetic analysis of protein interactions (Rossi et al. 2000).

2.2 Protein-Fragment Complementation

Protein-fragment complementation (PFC) assays depend on division of a monomeric reporter enzyme into two separate inactive components that can reconstitute function upon association. When these reporter fragments are fused to interacting proteins, the reporter is reactivated upon association of the interacting proteins. PFC strategies based on several enzymes, including β-galactosidase, dihydrofolate reductase (DHFR), β-lactamase, and luciferase have been used to monitor protein-protein interactions in mammalian cells (Rossi et al. 1997; Wehrman et al. 2002; Remy and Michnick 1999; Remy et al. 1999; Galarneau et al. 2002; Ozawa et al. 2001). A fundamental advantage of PFC is that the hybrid proteins directly reconstitute enzymatic activity of the reporter. In principle, therefore, protein interactions may be detected in any subcellular compartment, and assembly of protein complexes may be monitored in real time. A disadvantage of complementation approaches is that reassembly of an enzyme may be susceptible to steric constraints imposed by the interacting proteins. Another potential limitation of PFC for application in living animals is that transient interactions between proteins may produce insufficient amounts of active enzyme to allow noninvasive detection. Nonetheless, because most PFC strategies are based on reconstituting active enzymes, these systems offer the potential bene-

fits of signal amplification to enhance sensitivity for detecting interacting proteins in living animals.

2.3 Optimized Luciferase Fragment Complementation

As discussed, complementation strategies may offer advantages for near real-time applications in living animals, and pilot studies with firefly and *Renilla* luciferases have demonstrated the feasibility of this approach (Ozawa et al. 2001; Paulmurugan and Gambhir 2003). However, the available fragments suffer from considerable constitutive activity of the N-terminus fragments, thereby precluding general use. Thus, no enzyme fragment pair yet has been found that satisfies all criteria for noninvasive analysis of protein-protein interactions and enables interrogation in cell lysates, intact cells, and living animals.

To develop an optimized protein fragment complementation imaging system for broad use in living cells and animals, we screened a combinatorial incremental truncation library for reconstitution of the enzymatic activity of a heterodimeric firefly (*Photinus pyralis*) luciferase (Luker and Piwnica-Worms 2004). This library employed a well-characterized protein interaction system: rapamycin-mediated association of the FRB domain of human mTOR (residues 2024–2113) with FKBP-12 (Remy and Michnick 1999; Galarneau et al. 2002; Chen et al. 1995). Initial fusions of FRB and FKBP with N- and C-terminal fragments of luciferase, respectively, were designed such that the enzymatic activities of the individual overlapping fragments were weak or absent. From these constructs, N- and C-terminal incremental truncation libraries were generated by unidirectional exonuclease digestion and validated essentially as described (Ostermeier et al. 1999). The libraries were coexpressed in *E. coli* and screened in the presence of rapamycin for bioluminescence. From this screen, one could identify an optimal pair of overlapping amino acid sequences for the NLuc fragment and for the CLuc fragment. The optimized combination of fragments produced no signal in the absence of rapamycin and strong bioluminescence in the presence of the dimerizing agent rapamycin.

In live cells and in cell lysates, our optimized complementation system successfully reproduced published apparent K_d values for ra-

pamycin (Remy and Michnick 1999; Galarneau et al. 2002; Luker and Piwnica-Worms 2004; Chen et al. 1995). To test the specificity of the complementation system, we mutated the FRB fragment in the FRB-NLuc construct to a form FRB(S2035I) (Chen et al. 1995), which should be insensitive to rapamycin. We showed that this mutation, even in the presence of rapamycin, produced low bioluminescence signal similar to the optimal pair in the absence of rapamycin. Also, expression of single constructs produced no detectable signal relative to untransfected cells. Thus, our optimized complementation pair eliminated the substantial bioluminescence activity of the N-terminal luciferase fragment that was problematic with previous split-luciferase systems based on simple bisection of luciferase (Paulmurugan et al. 2002).

Furthermore, bioluminescence imaging of animals using charged couple device (CCD) cameras such as the IVIS (Xenogen, Alameda, CA) enabled us to quantify relative expression of the luciferase reporter activity in vivo. In mice bearing implants of cells expressing our FRB-NLuc/CLuc-FKBP fusion pair, repetitive bioluminescence imaging showed dose- and time-dependent luciferase activity induced by rapamycin with a maximal in vivo signal-to-background ratio of greater than 20:1.

2.4 Conclusions

These studies demonstrate that noninvasive molecular imaging of protein-protein interactions may enable investigators to determine how intrinsic binding specificities of proteins are regulated in a wide variety of normal and pathophysiologic conditions. These tools provide a platform for detection of regulated and small molecule-induced protein-protein interactions in intact cells and living animals and should enable a wide range of novel applications in biomedicine, drug discovery, chemical genetics, and proteomics research.

Acknowledgements. We thank colleagues of the Molecular Imaging Center for insightful discussions and excellent technical assistance. Work reviewed herein was supported by a grant from the National Institutes of Health (P50 CA94056).

References

Chen J, Zheng XF, Brown EJ, Schreiber SL (1995) Identification of an 11-kDa FKBP12-rapamycin-binding domain within the 289-kDa FKBP12-rapamycin-associated protein and characterization of a critical serine residue. Proc Natl Acad Sci USA 92:4947–4951

Darnell JE Jr (2002) Transcription factors as targets for cancer therapy. Nat Rev Cancer 2:740–749

Fields S, Song O (1989) A novel genetic system to detect protein-protein interaction. Nature 340:245–246

Galarneau A, Primeau M, Trudeau LE, Michnick S (2002) β-Lactamase protein fragment complementation assays as in vivo and in vitro sensors of protein-protein interactions. Nat Biotechnol 20:619–622

Heldin C (2001) Signal transduction: multiple pathways, multiple options for therapy. Stem Cells 19:295–303

Luker K, Piwnica-Worms D (2004) Optimizing luciferase protein fragment complementation for bioluminescent imaging of protein–protein interactions in live cells and animals. Methods Enzymology 385:349–360

Luker G, Sharma V, Pica C, Dahlheimer J, Li W, Ochesky J, Ryan C, Piwnica-Worms H, Piwnica-Worms D (2002) Noninvasive imaging of protein-protein interactions in living animals. Proc Natl Acad Sci USA 99:6961–6966

Luker G, Sharma V, Pica C, Prior J, Li W, Piwnica-Worms D (2003 a) Molecular imaging of protein-protein Interactions: controlled expression of p53 and large T antigen fusion proteins in vivo. Cancer Res 63:1780–1788

Luker G, Sharma V, Piwnica-Worms D (2003 b) Visualizing protein-protein interactions in living animals. Methods 29:110–122

Luker G, Sharma V, Piwnica-Worms D (2003 c) Noninvasive imaging of protein-protein interactions in living animals. In Conn PM (ed) Handbook of proteomic methods. Humana Press, Inc., Totowa, NJ, pp 283–298

Ogawa H, Ishiguro S, Gaubatz S, Livingston D, Nakatani Y (2002) A complex with chromatin modifiers that occupies E2F- and Myc-responsive genes in G0 cells. Science 296:1132–1136

Ostermeier M, Nixon A, Shim J, Benkovic S (1999) Combinatorial protein engineering by incremental truncation. Proc Natl Acad Sci USA 96: 3562–3567

Ozawa T, Kaihara A, Sato M, Tachihara K, Umezawa Y (2001) Split luciferase as an optical probe for detecting protein-protein interactions in mammalian cells based on protein splicing. Anal Chem 73:2516–2521

Paulmurugan R, Gambhir S (2003) Monitoring protein-protein interactions using split synthetic Renilla luciferase protein-fragment-assisted complementation. Anal Chem 75:1584–1589

Paulmurugan R, Umezawa Y, Gambhir SS (2002) Noninvasive imaging of protein-protein interactions in living subjects by using reporter protein complementation and reconstitution strategies. Proc Natl Acad Sci USA 99:15608–15613

Ray P, Pimenta H, Paulmurugan R, Berger F, Phelps M, Iyer M, Gambhir S (2002) Noninvasive quantitative imaging of protein-protein interactions in living subjects. Proc Natl Acad Sci USA 99:2105–3110

Remy I, Michnick S (1999) Clonal selection and in vivo quantitation of protein interactions with protein-fragment complementation assays. Proc Natl Acad Sci USA 96:5394–5399

Remy I, Wilson I, Michnick S (1999) Erythropoietin receptor activation by a ligand-induced conformation change. Science 283:990–993

Rossi F, Charlton C, Blau H (1997) Monitoring protein-protein interactions in intact eukaryotic cells by β-galactosidase complementation. Proc Natl Acad Sci USA 94:8405–8410

Rossi F, Blakely B, Blau H (2000) Interaction blues: protein interactions monitored in live mammalian cells by β-galactosidase complementation. Trends Cell Biol 10:119–122

Stark G, Kerr I, Williams B, Silverman R, Schreiber R (1998) How cells respond to interferons. Annu Rev Biochem 67:227–264

Toby G, Golemis E (2001) Using the yeast interaction trap and other two-hybrid-based approaches to study protein-protein interactions. Methods 24:201–217

von Mering C, Krause R, Snel B, Cornell M, Oliver S, Fields S, Bork P (2002) Comparative assessment of large-scale sets of protein-protein interactions. Nature 471:399–403

Wehrman T, Kleaveland B, Her JH, Balint RF, Blau HM (2002) Protein-protein interactions monitored in mammalian cells via complementation of β-lactamase enzyme fragments. Proc Natl Acad Sci USA 99:3469–3474

Zhang H, Hu G, Wang H, Sciavolino P, Iler N, Shen M, Abate-Shen C (1997) Heterodimerization of Msx and Dlx homeoproteins results in functional antagonism. Mol Cell Biol 17:2920–2932

3 Radiolabeled Peptides in Nuclear Oncology: Influence of Peptide Structure and Labeling Strategy on Pharmacology

H. R. Maecke

3.1 Introduction

3.1.1 Peptides in Biology and Medicine

Peptides are necessary elements in more fundamental biological processes than any other class of molecules. The most ubiquitous mode for controlling and modulating cellular function, intercellular com-

munication, immune response, and information-transduction pathways is through peptide-protein noncovalent interactions. For example, peptides function as hormones, neurotransmitters, neuromodulators, growth and growth inhibition factors, and cytokines. Although there are numerous exceptions, such as insulin, oxytocin, and calcitonin, most peptide-ligands are not used directly as drugs, and often the most useful ligands for therapy would be analogs that act as agonists or antagonists of the native ligands. The development of peptides or peptide-mimetics that can target the receptors modulating the biological activities is a top priority in biology, chemistry, and medicine.

Peptides also play important roles in growth and other cellular functions not only in normal tissues but also in tumors. Most tumors express receptors for different peptides, frequently in high density, and many of these receptors mediate growth-regulating effects in vitro. Certain types of tumors also respond to the growth-inhibition or growth-promoting signals of peptides in vivo, an effect which has become an important clinical approach to treat tumors in man. An ubiquitous example is the use of somatostatin (SS) analogs (Fig. 1,

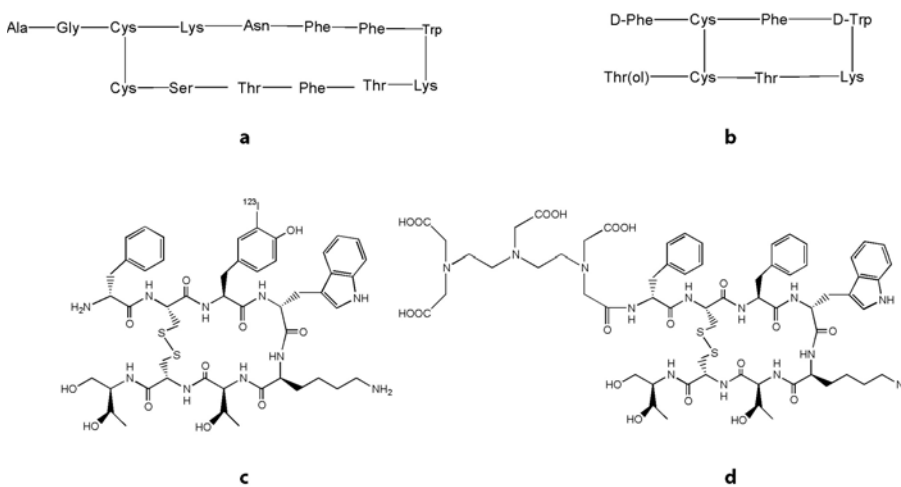

Fig. 1 a–d. Structural formula for: (**a**) SS-14; (**b**) octreotide; (**c**) [^{123}I]-[3-iodo-Tyr^3]-octreotide; (**d**) DTPA-octreotide

see Sect. 3.2.3), whose receptors are overexpressed in many neoplastic tissues. Five human SS receptor subtypes have been identified and cloned (Reisine and Bell 1995). A new development to visualize tumors through peptide receptor targeting began about fifteen years ago when radiolabeled SS analogs were introduced into nuclear medicine for in vivo imaging of human tumors using a gamma camera. Nuclear medicine is mainly a diagnostic discipline; its strength has been the ability to provide images of (patho)physiological functions rather than morphological information. The development in this field advances in the direction of in vivo tissue characterization through imaging of biochemical markers. The use of radiolabeled analogs of regulatory peptides in nuclear oncology is an important step in this direction. The peptides as targeting agents offer several advantages over proteins as, for instance, antibodies. Because of their high molecular weight, antibodies have often shown limited uptake at the target site and slow blood clearance, which results in modest target-to-background ratios (Fischman et al. 1993; Liu and Edwards 1999). In contrast, peptides are readily synthesized via solid phase synthesis, parallel and combinatorial approaches as well as phage-display. They are cheaper and can withstand harsher conditions for modification and labeling. They are less likely to produce immunogenic response, and blood clearance, tissue penetration, and tumor uptake are faster.

However, there are several prerequisites for peptides used as radiopharmaceuticals. Primarily, the corresponding receptors have to be expressed on the target in suitable amounts, overexpression or unique expression being desirable. The peptide ligand should retain the same high affinity to the receptor as the natural compound. For radiotherapeutic applications, internalization appears to be an absolute precondition because of higher residence time. Last, but not least, a main concern of radiolabeled peptides is their metabolic instability, concerning not only the peptide part, but also the stability of the metal-chelator complex or the radiohalogen bond. Other aspects have to be considered when developing radiometal conjugated peptides, i.e., a high rate of complexation, the practicability of radiolabeling, the availability of the radionuclide and some other biochemical properties of the metal and metal-chelator complex that will be discussed later in this chapter.

3.1.2 Radiopeptides and Potential Targets of Radiopeptides in Diagnosis and Therapy

Radiopeptides are composed of a biologically active peptide coupled to a chelator for labeling with radiometals or coupled to prosthetic groups for halogenation. In some cases, direct labeling of peptides is an option if, e.g., the peptide contains Tyr, which can be iodinated, or disulfide bridges, which, upon reductive opening, react with thiophilic ^{99m}Tc(V).

The molecular biology studies preceding successful receptor targeting with radiopeptides include in vitro identification and analysis

Table 1. Expression of receptors on human tumors

Ligand	Receptors	Tumor type
Somatostatin	Somatostatin receptor subtypes sst1–5	Neuroendocrine tumors, SCLC, MTC, tumors of the nervous system, lymphoma (non-Hodgkin's lymphoma, Hodgkin's disease)
VIP/PACAP	$VPAC_1$, $VPAC_2$, PAC_1 receptors	Various adenocarcinomas (stomach, colon, pancreas, lung, etc.)
CCK/gastrin	CCK_1, CCK_2 receptors	MTC, SCLC, stromal ovarian cancer, astrocytoma
LHRH	LHRH receptors	Breast, prostate cancer
α-MSH	MSH receptors	Melanoma
Bombesin/GRP	BB_1, BB_2, BB_3 and BB_4 receptors	SCLC, MTC, glioblastoma, colonic cancer, prostate cancer
Neurotensin	NTR1, NTR2, and NTR3 receptors	Ewing sarcoma, meningioma, MTC, astrocytoma, SCLC, exocrine pancreatic cancer
Opioid	Opioid receptors	SCLC, neuroblastoma, breast cancer
Substance P	NK1 receptors	Glioblastoma, astrocytoma, MTC, breast, peri- and intratumoral blood vessels
GLP-1	Glp-1 receptors	Insulinomas
Oxytocin	Oxytocin receptors	Endometrium, breast cancer
Neuropeptide Y	NPY receptors subtypes Y_1–Y_6	Breast, brain cancer

of receptors with biochemical, biomolecular, and immunological techniques (Reubi 1995). For example, radioligand binding analysis and bioassays with cells or membrane preparations are the means to characterize high-affinity binding sites and the pharmacological profile of a given peptide. Anatomical information about the distribution of receptors in tissues is obtained by quantitative receptor autoradiography, which measures radioligand binding on tissue sections and thus enables localization of receptors at the microscopic level. Only a minority of the large number of potentially useful regulatory peptides and peptide families has been more or less thoroughly investigated so far and future work will probably reveal a multitude of clinically useful peptide-based radioligands. Table 1 gives an overview of some typical receptors for regulatory peptides, which are (over)expressed on various human cancers, and it lists the peptides studied for receptor targeting.

Once the structure of the natural peptide ligand has been obtained, there are several other steps to follow until a new radiopharmaceutical is developed (Heppeler et al. 2000).

3.2 Design of Peptide-Based Radiopharmaceuticals

As indicated above, a radiopeptide is composed of different parts, most importantly being the bioactive peptide, which may be coupled to a spacer and this again to a chelator or a prosthetic group (Fig. 2).

The spacer may be a simple covalent bond but may also be introduced to improve the pharmacologic properties like binding affinity, ability to internalize into tumor cells, suitable biodistribution, etc.

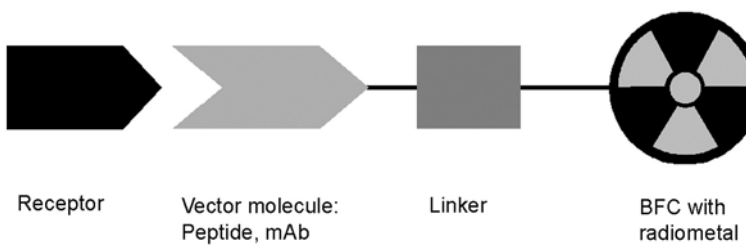

Fig. 2. Design of a receptor-mediated radiopharmaceutical

3.2.1 Important Radionuclides for Imaging and Therapy

The use of metal complexes as diagnostic and therapeutic agents is a relatively new area of medical research. The introduction of radiometals in nuclear medicine started in 1959 when the first ^{99}Mo/^{99m}Tc generator was developed at Brookhaven National Laboratory (Upton, NY). Since then, ^{99m}Tc has been the most widely used radionuclide for diagnostic imaging. Additional important radionuclides useful for imaging are listed in Table 2, including some of the longer-lived positron emitters.

Gamma scintigraphy requires a radiopharmaceutical containing a radionuclide that emits γ-radiation with an energy between 100–250 keV and a gamma camera. Positron emission tomography (PET) requires a radiopharmaceutical labeled with a positron-emitting

Table 2. Nuclear properties of important gamma- and positron-emitting radionuclides for biomolecule labeling

Isotope	Physical half-life (h)	Decay mode	E_γ (keV)	$E_{\beta+}$ (keV) average
^{67}Ga	78.26	EC (100%)	91, 93, 185, 296, 388	
^{99m}Tc	6.0	IT (100%)	141	
^{111}In	67.9	EC (100%)	245, 172	
^{18}F	1.83	β^+ (96.76), EC (3.3%)		649
^{124}I	100.3	β^+ (22.8%), EC (11%)		1,530
^{55}Co	17.5	β^+ (77%), EC (23%)		1,513, 1,037
^{62}Cu	0.16	β^+ (98%), EC (2%)		2,910
^{64}Cu	12.7	β^+ (19%), EC (41%) β^- (40%)		656
^{68}Ga	1.1	β^+ (90%), EC (10%)		1,880, 770
^{86}Y	14.7	β^+ (33%), EC (66%)		2,335, 2,019, 1,603, 1,248, 1,043
^{123}I	13.2	EC (100%)	159	

radionuclide (β^+) and a PET camera. A variety of gamma- and positron-emitters have been used for peptide labeling. Besides the energy of emission, there are some other factors to consider in designing a radionuclide-based peptide radiopharmaceutical, for example, the physical half-life, the type of decay, cost, and availability of the radioisotope.

Unlike radionuclides used for diagnostic imaging, therapeutic radionuclides by definition emit radiations that have a high linear energy transfer (LET) in order to destroy tumor tissue. These radionuclides with potential for therapy fall into three main categories: (a) β-emitting radionuclides; (b) α-emitters; and (c) Auger-electron emitters. Each type of these particles has a different effective range of energy deposition and LET properties.

The physical characteristics and range in tissues of commonly used β- and α-emitters are summarized in Table 3. In cases where

Table 3. Nuclear properties of several therapeutic radionuclides

Isotope	Physical half-life	Decay mode		Range	
		max β^--energy (MeV)	γ (keV) (%)	Mean (mm)	Approx. cell diameters
^{67}Cu	2.58 days	0.577 (20%)	91 (7%) 93 (16%) 185 (48%)	0.27	20
^{90}Y	2.67 days	2.27 (100%)	None	2.8	150
^{131}I	8.04 days	0.606	364 (81%)	0.28	20
^{149}Pm	2.21 days	1.07	286 (3%)	0.71	60
^{166}Dy	3.40 days	0.40	82.5 (13%)	0.18	15
^{177}Lu	6.71 days	0.50 (79%)	208 (11%) 113 (6.4%)	0.24	20
^{186}Re	90.6 h	1.071	137 (8.5%)	0.7	60
^{188}Re	16.98 h	2.116	155 (15%)	2.4	130
^{212}Bi	1 h	1.36 (β, 64%) 6.1 (α, 36%)	727 (7%)	0.09 0.06	2–3 3–4
^{213}Bi	46 min	5.8 (α, 2.2%) 8.4 (α, 97.8%)	440 (27.3%)	0.06 0.08	2–3 3–4
^{225}Ac	10 days	5.83 (α, 100%)	None	0.06	2–3

the γ-ray emission is in the diagnostically useful range, the imaging of the biodistribution of the tracer is also feasible (Kwekkeboom et al. 2001). Radionuclides that decay by β-emission are used most extensively for therapeutic applications in current clinical practice. A unique advantage of β-particle emitters over other therapeutic modalities is that not every cell needs to be targeted to be killed (crossfire effect, high LET). The crossfire effect is efficient for lesions larger in diameter than the average path length. Humm (Humm 1986) has classified β-emitting radionuclides as low-range (mean range <200 µm, i.e., Lu-177), medium-range (mean range 200 mm to <1 mm, i.e., Cu-67, Sm-153), and high range (mean range >1 mm, i.e., Y-90). Radioactive emission of α particles results in high LET over a path length of 3–4 cell diameters. The advantage of this property lies in its capability of producing a high degree of tumoricidal activity while sparing the surrounding normal tissues.

3.2.2 Labeling Methods

3.2.2.1 Direct Labeling

Because of the kinetic lability of hard radiometals like Y^{3+}, Lu^{3+}, and lanthanides in general, but also Cu^{2+}, Co^{2+}, etc. and the competition in human blood and other body fluids by proteins like transferrin, albumin, and anions like PO_4^{3-}, CO_3^{2-}, etc., peptides cannot offer any functional groups which provide enough kinetic stability to ensure intact arrival of the radiometal-peptide conjugate at the target. This is different for the pair Tc and Re, which form kinetically inert metal complexes in several oxidation states. In addition, both metals show a high degree of thiophilicity, which makes sulfur-containing peptidic sequences attractive for the binding of these radiometals. Several groups took advantage of this thiophilicity and labeled disulfide-bridged analogs of SS like octreotide, lanreotide, and vapreotide directly with ^{99m}Tc and ^{188}Re (Fig. 3; see Sect. 3.2.3; Thakur et al. 1997). Unfortunately, none of these peptides is very well characterized; in addition, they are too lipophilic, mainly excreted by the hepatobiliary system, and never made the step from preclinical studies to the clinic. Radiohalogens are being coupled to peptides usually taking advantage of the presence of Tyr. An electro-

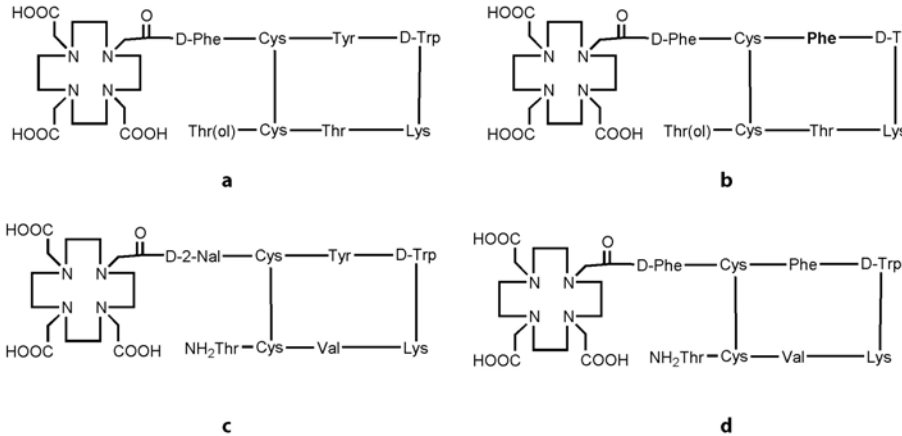

Fig. 3 a–d. Prototypical DOTA-peptides used for radiotherapy: (**a**) DOTA-[Tyr^3]-octreotide (DOTA-TOC); (**b**) DOTA-octreotide (DOTA-OC); (**c**) DOTA-lanreotide (DOTA-LAN); (**d**) DOTA-vapreotide

philic substitution reaction usually gives pure and well-defined radiopeptides.

3.2.2.2 The Bifunctional Chelator Approach

Most often, labeling strategies rely on the utilization of a multidentate ligand capable of chelation of the desired radionuclide. For example, all radiometals except ^{64,67}Cu and ^{55}Co listed in Tables 2 and 3 are hard acids with 3+ as the major oxidation state in solution. As they are kinetically labile, polydentate chelators need to be utilized for an efficient encapsulation and in vivo stabilization.

There are mainly two strategies: the prelabeling and the postlabeling methods. The prelabeling approach involves the formation of the radionuclide-chelator complex prior to conjugation to the peptide. If the radionuclide is introduced into its chelator after the chelator has been attached to the carrier, this is referred to as a postlabeling. The decision on which strategy is to be adopted will be influenced by a variety of considerations. For example, when complex formation can only be achieved under nonaqueous or otherwise harsh conditions

and the biomolecule is sensitive to these conditions, the prelabeling approach is more indicated. Still, this method is complicated and time-consuming because of multiple steps in preparation and purification, and therefore not suitable for routine clinical applications. The postlabeling approach is the most practical method for the development of peptide-based radiopharmaceuticals.

The ideal chelator should satisfy requirements correlating aspects of coordination chemistry with in vivo behavior. Factors to be considered include the kinetic and thermodynamic stability, stereochemistry, charge, lipophilicity and the redox properties of the metal complex. For lanthanides and lanthanide-like radiometals, the bifunctional octadentate chelators satisfy these requirements. Derivatives of diethylenetriaminepentaacetic acid (DTPA) are used for the fast incorporation of radiometals; the first clinically approved peptide-based imaging agent has been the DTPA-derivatized SS analog octreotide labeled with ^{111}In (Fig. 1 d). The coupling to the peptide is achieved either by using DTPA dianhydride or tri-*t*-butyl-DTPA as prochelators (Fig. 4; Achilefu et al. 2000). This potential octadenticity of DTPA may convey additional stability to the radiometal complex as In(DTPA)$^{2-}$ was shown to have coordination number 8 in the solid state and in solution (Maecke et al. 1989). Because of in vivo instability, DTPA is not suitable for any other nuclide than ^{111}In. Attempts to use DTPA-peptide conjugates labeled with ^{90}Y for therapy (Stolz et al. 1996) have not been as successful as the use of macrocyclic bifunctional chelators (BFC) for labeling of peptides (de Jong et al. 1997).

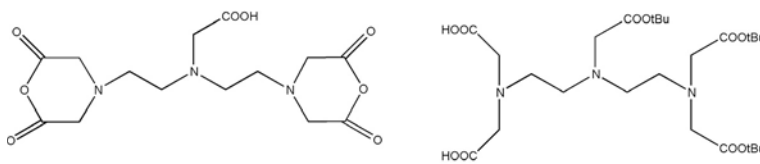

Fig. 4 a, b. Precursors of diethylenetriaminepentaacetic acid (DTPA) for biomolecule coupling: (**a**) DTPA dianhydride (cDTPA); (**b**) tri-*t*-butyl-DTPA (activated via cyclic anhydride formation)

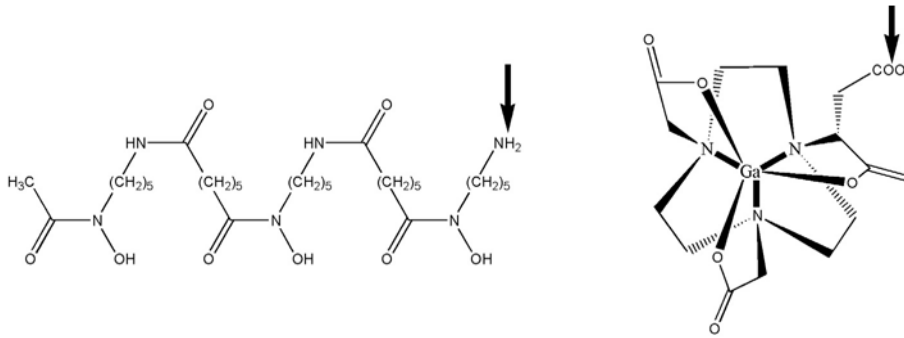

Fig. 5. a Desferrioxamine-B (DFO), a bifunctional chelator for labeling with $^{67/68}$Ga. **b** Ga(NODASA), a (radio)metal complex with three carboxylate groups, protected via the metal, and with potential for biomolecule coupling using the prelabeling approach. The coupling site is indicated by the *arrow*

Radiolabeling with Ga^{III} is of interest because of the access to three radioisotopes for imaging (Table 2). Two approaches were used to label SS analogs with radio-gallium. The use of DFO (desferrioxamine B; Fig. 5 a) allowed fast complexation, whereas the new chelator NODASA (1,4,7-triazacyclononane-1-succinic acid-4,7-diacetic acid; Fig. 5 b; Andre et al. 1998) has three five-membered chelate ring-forming carboxylate groups protected by Ga(III) allowing a free β-carboxylate group for coupling to a SS analog. This prelabeling strategy allows the covalent coupling of a well-defined radiometal complex of high-specific activity to a biomolecule. The same type of chelator has been derivatized in order to make it also available for the postlabeling approach (Eisenwiener et al. 2002).

The DOTA (1,4,7,10-tetraazacyclododecane-1,4,7,10-tetraacetic acid)-based BFCs (Fig. 6 a–c) continue to be the most widely studied ligands for linking trivalent metallic radioisotopes to biomolecules (Cutler et al. 2000; Hu et al. 2002; McDevitt et al. 2001). The most common method involves the attachment of the peptide to one of the four acetate groups via a CO-NH bond. This conjugation can be made either via an activated ester of one carboxylate group (Fig. 6 a), or using a monoreactive DOTA prochelator like

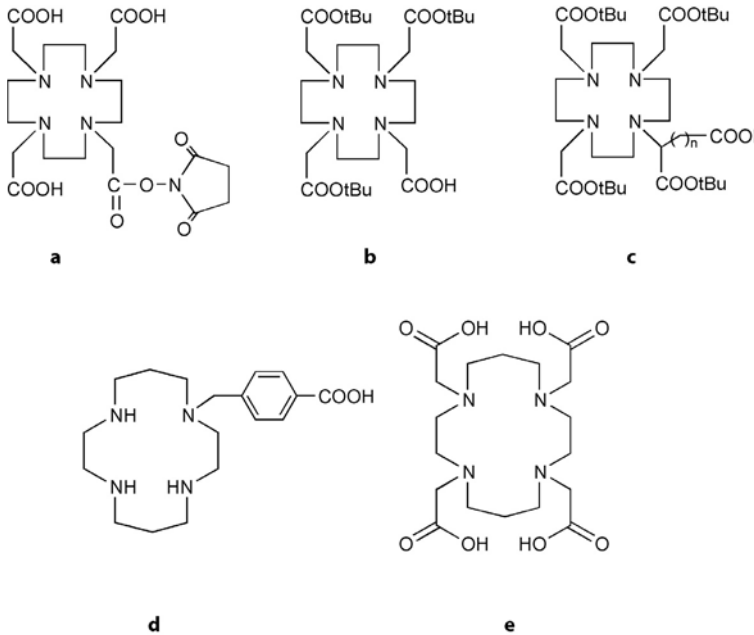

Fig. 6 a–e. Structures of DOTA derivatives: (**a**) *N*-hydroxysuccinimide (NHS) ester of DOTA; (**b**) tri-*t*-butyl-DOTA; (**c**) DOTASA(tBu)$_4$, $n=1$ and DOTAGA(tBu)$_4$, $n=2$; (**d**) CPTA; (**e**) TETA

DOTA(tBu)$_3$ (Fig. 6 b; Heppeler et al. 1999). The prochelator approach is perfectly compatible with peptide synthesis in solid phase or in solution and DOTA(tBu)$_3$ was coupled to SS analogs with 65±5% yields after deprotection and purification. DOTA, used unprotected, was also coupled to the same peptide with about 40% overall yield (Albert et al. 1998).

A disadvantage of this type of conjugation is the loss of one acetate arm for coordination to the radiometal center. To provide eight strong donor atoms for coordination, DOTA has been modified at one of the nitrogen atoms (Fig. 6 c; Eisenwiener et al. 2000). After coupling to the biomolecule and deprotection, a BFC-peptide conjugate is obtained, available for the labeling with different radiometals (^{111}In, ^{90}Y, ^{177}Lu and other lanthanides).

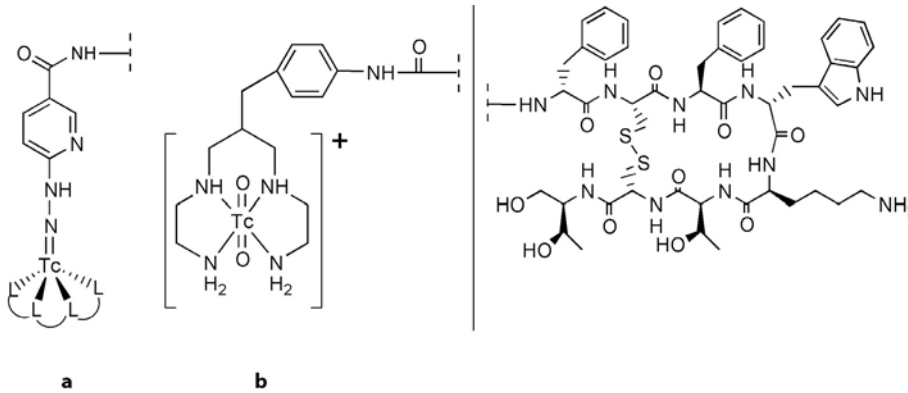

Fig. 7. a Structure of Tc-HYNIC-octreotide; **b** ^{99m}Tc-labeling of octreotide, using the N_4-tetramine chelator

The labeling of peptides with radioisotopes of Cu(II) is of interest mainly because of its two radionuclides ^{64}Cu and ^{67}Cu. The chemistry of copper radiopharmaceuticals has been reviewed extensively and comprehensively (Blower et al. 1996). BFCs for Cu(II) include 4-(1,4,8,11-tetraazacyclotetradec-1-yl)methyl)benzoic acid (CPTA; Fig. 6d), 1,4,8,11-tetraazacyclotetradecane-1,4,8,11-tetraacetic acid (TETA; Fig. 6e) and DOTA. All three chelators were coupled to the SS analogs through a carboxylate group.

Several approaches to label SS analogs with BFCs for ^{99m}Tc labeling have been published. HYNIC (2-hydrazinonicotinic acid; Fig. 7a) is of interest as a ^{99m}Tc-binding unit because of the potential monodenticity of this ligand which leaves coordination sites on the Tc atom free to be completed by different coligands which may be beneficial for the fine tuning of the biodistribution. HYNIC was described before to label successfully different biomolecules with ^{99m}Tc (Abrams et al. 1990; Edwards et al. 1997). [^{99m}Tc-N_4-D-Phe^1]-octreotide (Fig. 7b) was shown to bind with high affinity to the somatostatin releasing inhibiting factor (SRIF) receptor and showed high and specific tumor uptake in a SRIF receptor-positive tumor (Maina et al. 2002).

3.2.3 Prototypical Peptides for Imaging and Targeted Radiotherapy

The first diagnostically studied and also radiotherapeutically employed regulatory peptides were analogs of SS. Throughout this chapter the discussion will solely be based on radiolabeled SS analogs. SS binds with high affinity to SS receptors expressed on target tissues exerting a large number of biological effects. Five such receptor subtypes (hsst1–5) have been cloned in recent years. An important aspect with regard to targeting is the finding that these receptors are overexpressed on a variety of human tumors, mainly of neuroendocrine origin (Schaer et al. 1997). The most relevant receptor subtype is hsst2, but all the other receptor subtypes are to some degree also overexpressed on human tumors. There are two biologically active forms of SS consisting of 14 (SS-14) and 28 (SS-28) amino acids that show only very low metabolic stability in human blood with half lives of 2–3 min and can therefore not be used clinically. Modifications leading to octapeptides afforded SS receptor binding ligands with much lower proteolytic degradation rate. One of the clinically approved peptides is octreotide, a short analog of SS, which retained a high binding affinity to hsst2, reduced affinity to hsst3 and hsst5, and absent affinity to hsst1 and hsst4 (see Table 4). The chemical structures of SS-14 and octreotide are shown in Fig. 1 a, b.

The first radiopeptide used for in vivo localization of tumors was [^{123}I]-[3-iodo-Tyr^{3}]-octreotide (Fig. 1 c). Despite some spectacular early imaging results (Lamberts et al. 1990) and an almost optimal pharmacologic profile showing high hsst2 affinity ($IC_{50} = 2.0 \pm 0.7$ nM) and a high rate of internalization into tumor cells, this radioligand finally turned out not to be useful as a diagnostic tool. The reasons are its lipophilicity causing hepatobiliary excretion and therefore a very low diagnostic sensitivity in the abdomen. In contrast, the chelator-modified molecule, DTPA-octreotide (Fig. 1 d), which was designed to be complexed with the diagnostic radiometal $^{111}In^{3+}$, shows a rather low in vitro pharmacologic profile (low binding affinity to hsst2, $IC_{50} = 22 \pm 3.6$ nM and slow internalization rate), but the hydrophilic metal complex conveys high hydrophilicity to the targeting molecule and changes its pharmacokinetics, including predominant kidney excre-

Table 4. Affinity profiles (IC_{50}) for human sst1-sst5 receptors for a series of somatostatin analogs

Compound	sst1	sst2	sst3	sst4	sst5
SS-28	5.2±0.3	2.7±0.3	7.7±0.9	5.6±0.4	4.0±0.3
Octreotide (OC)	>10,000	2.0±0.7	187±0.355	>1,000	22±6
Y-DOTA-octreotide[a], (DOTA-OC)	>10,000	20±2	27±8	>10,000	57±22
Y-DOTA-[Tyr^3]-octreotide, (DOTA-TOC)	>10,000	11±1.7	389±135	>10,000	114±29
Y^{III}-DOTA-[Tyr^3,Thr^8]-octreotide (DOTA-TATE)	>10,000	1.6±0.4	>1000	523±239	187±50
Y-DOTA-[1-Nal^3]-octreotide	>1,000	3.3±0.2	26±1.9	>1,000	10.4±1.6
In-DOTA-[1-Nal^3]-octreotide, (DOTA-NOC^1)	>10,000	2.9±0.1	8±2	227±18	11.2±3.5
Y-DOTA-[2-Nal^3]-octreotide (DOTA-NOC^2)	>10,000	25±1.0	133±68	>10,000	98±12.5
Y-DOTA-lanreotide[b]	>10,000	23±5	290±105	>10,000	16±3.4
In^{III}-DTPA-octreotide	>10,000	22±3.6	183±13	>1,000	237±52
In^{III}-DTPA-[$Tyr]^3$-octreotate	>10,000	1.3±0.2	>10,000	433±16	>1,000
KE108[c]	2.6±0.4	0.9±0.1	1.5±0.2	1.6±0.1	0.65±0.1

[a] Octreotide: D-Phe-Cys-Phe-D-Trp-Lys-Thr-Cys (disulfide bond).
[b] Lanreotide: [D-2-Nal^1,Tyr^3,Val^6,$ThrNH_2^8$]octreotide.
[c] KE108; see Fig. 12.

tion. Consequently, it became the first imaging vector based on a radiopeptide; the commercial name is Octreoscan (Mid-South Imaging & Therapeutics, Memphis, TN), registered worldwide. In addition, the advantage of the DTPA-peptide conjugate was the highly practical labeling kinetics which can be performed in any nuclear medicine department or even in a private nuclear medicine practice.

In addition to Octreoscan, a ^{99m}Tc-labeled peptide has also been FDA approved recently and registered in several countries. It is based on a carbocyclic hexapeptide, modified with a N_3S-chelator,

and commercialized under the trade name Neotect (Berlex Laboratories, Montville, NJ; ^{99m}Tc-Depreotide).

^{111}In is not a very useful therapeutic radionuclide; therefore, conjugates were designed, synthesized, and evaluated preclinically which fulfilled the need for the labeling with the β-emitters, e.g., ^{90}Y and ^{177}Lu. DOTA was the preferred chelator, forming kinetically and thermodynamically stable metal complexes. The prototypical DOTA-coupled SS-based octapeptides used for radiotherapy are shown in Fig. 3.

3.3 Preclinical Characterization of Somatostatin-Based Radiopeptides

3.3.1 Binding Affinities and Affinity Profiles

The molecular basis of the use of radiopeptides in patient studies is the presence of receptors. Therefore, an important step in the characterization of a radiopeptide is the determination of the receptor affinity and – if receptor subtypes are present – the receptor affinity profile.

Introducing a chelator may strongly affect the biological and pharmacological properties of a peptide. The binding assay can be performed on intact cells or on membrane preparations, either by direct or competitive binding assays, thereby assessing alterations in affinity and specificity of the radiopeptide compared to the natural peptide (Reubi et al. 2000). As shown in Table 1, there are several receptors (over)expressed on different types of tumors, therefore knowing the affinity pattern for receptor subtypes is very important, since each subtype usually has a different expression profile on different tumor types. This is definitely true especially for SS receptors sstr1–5 (Schaer et al. 1997).

3.3.1.1 Peptide-Structure Affinity Relationship

Table 4 displays the affinity profiles of selected SS analogs (some of them shown in Fig. 3a–c) along with their Y(III)/In(III)-chelator-peptide conjugates in comparison with the natural peptide SS-28 and with octreotide. The binding affinities are expressed as IC_{50} values using ^{125}I-[Leu^8, D-Trp^{22}, Tyr^{25}]-SS-28 as radioligand. The assump-

tion made is that nonradioactive metals behave like their radioactive congeners.

The affinity profiles were determined by using cell lines transfected with SS receptor subtypes hsst1–5. Peptide modifications as well as the influence of chelator structure and radiometal (labeling strategy) were studied.

Small structural modifications in the peptide were shown not only to alter the binding affinity but also the subtype binding profile. For instance, modifications in 3-position of DOTA-octreotide [complexed with $^{nat}Y(III)$] leads to a marked improvement of hsstr2 affinity when replacing Phe^3 (Y^{III}-DOTA-OC) for Tyr^3 (Y^{III}-DOTA-TOC) but the hsstr3 affinity decreases by a factor of 15. Furthermore, replacement of Phe with 1-naphthylalanin (1-Nal,DOTA-NOC^1) increases the hsstr2, 3, and 5 affinity, rendering this peptide a very promising candidate for the imaging and targeted radiotherapy of a broader spectrum of human tumors. How subtle structural changes may affect the binding potency is shown by substituting 1-Nal for 2-Nal. This modification results in a peptide with low affinity to hsstr2, 3, and 5. Modifications at the C-terminus have a distinct influence on the sstr2 affinity; Y^{III}-DOTATATE has a sevenfold higher sstr2 affinity if compared to Y^{III}-DOTATOC, whereas the affinities towards sstr3 and 5 decrease.

Focusing on the peptide part in a peptide-based radiopharmaceutical, it is clear that lipophilicity, peptide size, and susceptibility to degradation by peptidases play a vital role (Lister-James et al. 1996).

3.3.1.2 Influence of the Chelate and (Radio)Metal on the Targeting Properties of Radiometallopeptides

In this chapter we will analyze the important role of the radiometal complex geometry as well as charge, size, fluxionality, etc. on DOTA-$[Tyr]^3$-octreotide pharmacology.

Except for the labeling of biomolecules with ^{99m}Tc and $^{186,188}Re$, DOTA has been used for all other radiometals of relevance in nuclear oncology. The use of one single chelator and one single chelator-peptide conjugate for a variety of radiometals allows lyophilized kit formulations and has the advantage that potential clinical applications will be approved easier by ethical committees. Our gold standard molecule for the in vivo localization of SS-receptor-positive tumors and

Table 5. Radiometal dependence on M-DOTATOC affinities to hsstr2

Compound	IC_{50} (nM)
SS-28	2.7±0.3 (19)
Y^{III}-DOTATOC	11±1.7 (6)
Ga^{III}-DOTATOC	2.5±0.5 (6)
Co^{II}-DOTATOC	0.44±0.11 (5)
Bi^{III}-DOTATOC	37±10 (3)
Ga^{III}-DOTATATE	0.2±0.04
Y^{III}-DOTATATE	1.6±0.4
In^{III}-DOTATATE	2.4±1

their targeted radionuclide therapy is [$DOTA^0$-Tyr^3]-octreotide. This molecule has been labeled with $^{66,67,68}Ga^{III}$, $^{111}In^{III}$, $^{90}Y^{III}$, $^{213}Bi^{III}$, and $^{57}Co^{II}$. Table 5 shows the binding characteristics of several metallopeptides to hsstr2 versus a ^{125}I-labeled SS-28 as radioligand.

An important result of this experiment is that obviously the metal ion has a marked influence on the affinity of the metallopeptide, e.g., Co^{II}-DOTATOC shows a better sstr2 binding than Ga^{III}-DOTATOC, Y^{III}-DOTATOC, and Bi^{III}-DOTATOC. As demonstrated, the conjugation of the metal-DOTA complex may even result in an improved ligand compared to the natural peptide. It is not yet clear why the metal ion which is remote from the pharmacologic part of the peptide has such a distinct influence.

Preliminary comparative data using two-dimensional ^{1}H-NMR studies of the Ga^{III}-, In^{III}-, Y^{III}-DOTATOC are not conclusive and the peptides resist crystallization. The model peptides In^{III}-, Y^{III}-, and Ga^{III}-DOTA-D-PheNH_2, however, could be crystallized and their X-ray crystal structure determined. The structures differ in different ways. Ga^{III}-DOTA-D-PheNH_2 (Fig. 8 a) has a pseudo-octahedral structure, the macrocycle showing a *cis*-geometry. The equatorial plane is formed by two transannular nitrogens of the tetraaza ring and two oxygens of the respective carboxylate groups. One carboxylate group is free and the carbonyl oxygen of the peptide bond forming the linkage to D-PheNH_2 is not bound to the Ga^{III}. This is in contrast to Y^{III}(In^{III})-DOTA-D-PheNH_2 (Fig. 8 b), which are octacoordinate complexes including the amide carboxy oxygen (Heppeler et al. 1999).

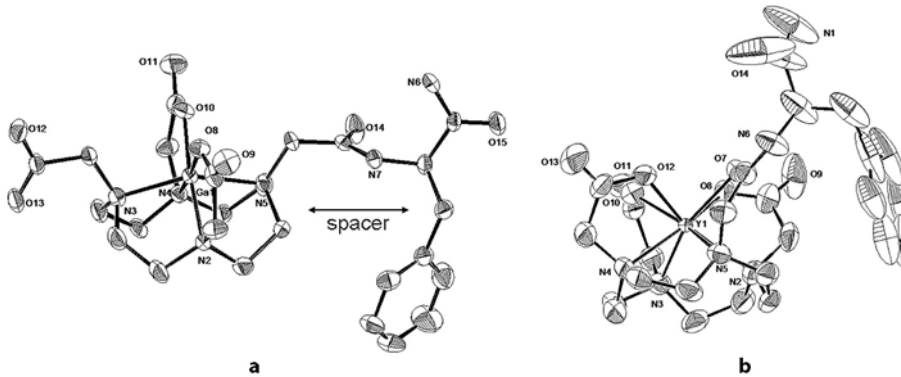

Fig. 8. a ORTEP plot of the crystal structure of [Ga^{III}-DOTA-D-PheNH_2], a pseudo-octahedral structure with a *cis*-geometry of the macrocycle. One carboxylate group is free and the carbonyl oxygen of the peptide bond forming the linkage to D-PheNH_2 is not bound to the Ga^{III}. **b** ORTEP representation of the crystal structure of [Y^{III}-DOTA-D-PheNH_2], an octacoordinate complex including the amide carboxy oxygen (reproduced with permission from Heppeler et al. 1999)

The complex geometry is a somewhat distorted antiprism. ^{1}H-NMR studies showed that also in solution the Ga^{III}-complex is hexacoordinate whereas the Y^{III}-DOTA-D-PheNH_2 and In^{III}-DOTA-D-PheNH_2 complexes are octacoordinate, the latter showing much higher fluxionality (Maecke et al. 2001), which may explain the differences between ^{111}In- and ^{90}Y-DOTA-TOC in the biodistribution study.

The hexacoordination of the Ga^{III}-complex may explain the improved kidney clearance of ^{67}Ga-DOTATOC compared to ^{90}Y-DOTATOC, and the improved pharmacological profile may depend on the free carboxymethyl arm bound to the peptide, allowing for more flexibility due to a spacer function. This hypothesis was tested by developing a conjugate with the optimal chelator for Ga^{III} radioisotopes, NOTA (1,4,7-triaza-1,4,7-triacetic acid). NOTA was modified in order to allow a spacer between the chelator (NODAGA = 1,4,7-triazacyclononane-1-glutaric acid-4,7-diacetic acid) and the peptide, separating the signal producing chelate from the biologically active peptide (Fig. 9). This combination has the additional advantage that the extremely stable Ga^{III}-NOTA complexes make any interference

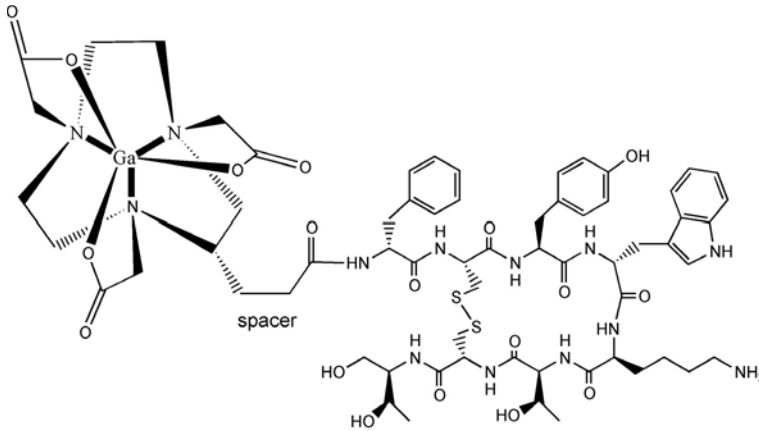

Fig. 9. Structural formula of Ga-NODAGA-TOC

and false interpretation of biological and pharmacological data due to potential transchelation chemistry rather unlikely. Indeed, Ga^{III}-NODAGA-TOC conjugate shows similar pharmacologic and biodistribution parameters like Ga^{III}-DOTATOC (Eisenwiener et al. 2002).

Preliminary data (Heppeler 2000) indicate that Co^{II}-DOTA-D-PheNH_2 has a very similar structure to the Ga^{III} complex and this along with the charge difference may explain the high potency of the corresponding metallopeptide. The low pharmacologic potency and profile of the Bi^{III}-complexed peptide is not understood at all at this time.

3.3.2 Structure Influencing Pharmacokinetics

The in vivo evaluation in animal models of radiopeptides is of major importance, since it is the first "real" indicator of compound pharmacokinetics. As a model, tumor cells for which the peptide is being investigated are transferred from cell culture into nude mice or rats, inducing tumor growth. Upon administration of the labeled peptide in these experimentally grown tumors, the potential of tumor targeting can be evaluated. An important aspect of this is the proof

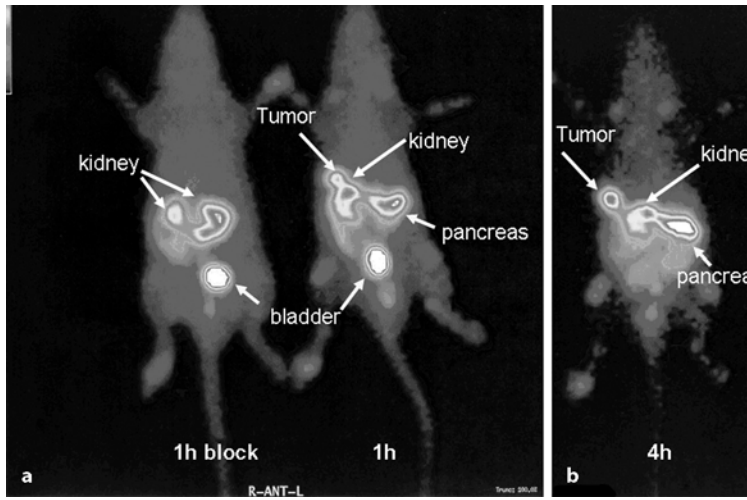

Fig. 10. Four-hour postinjection scintigraphy of two Lewis rats bearing subcutaneous tumors in the left hind leg: (**a**) rat with a coinjection of ^{111}In-DOTATOC and excess of cold peptide; (**b**) rat injected only with ^{111}In-DOTA-TOC

of specificity of tumor targeting due to the possibility of blocking the receptors with excess cold peptide. Such an example is shown in Fig. 10 with two rats bearing subcutaneous tumors in the left hind leg. One animal was only injected with ^{111}In-DOTA-TOC (Fig. 10b) and the tumor is nicely shown, as well as the receptor positive pancreas. In the second rat (Fig. 10a), about 500 times excess of nonradiolabeled peptide is coinjected with ^{111}In-DOTA-TOC, competing for the receptors; no radioactive signal is seen from the tumor and the pancreas.

The aim of biodistribution studies in animal models is the evaluation and optimization of the pharmacokinetics of radiopeptides. The uptake in different organs, especially in the receptor-positive organs and in kidneys have to be optimized. For clinical application, the kidney toxicity is the dose-limiting factor. Peptides are taken up by the tubular cells and radiometal chelates are trapped within the lysosomes, high retention of the radiolabel occurring in the kidneys, eventually causing nephrotoxicity (de Jong et al. 2001).

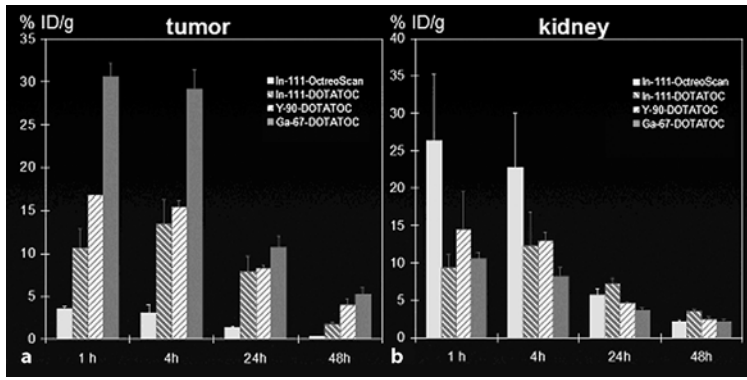

Fig. 11. Tumor (**a**) and kidney (**b**) uptake of ^{111}In-, ^{67}Ga- and ^{90}Y-DOTA-TOC in comparison with Octreoscan

Figure 11 shows a comparison in biodistribution in AR4-2J rat pancreatic-tumor-bearing Lewis rats of four compounds: ^{111}In-Octreoscan (see structure in Fig. 1 d) and DOTA-TOC (see Fig. 3 a) labeled with three different radiometals: ^{111}In, ^{90}Y and ^{67}Ga, respectively (Heppeler et al. 1999). The best tumor-to-kidney ratio corresponds to the gallium-labeled compound, this result being confirmed also in patients. As shown also in Sect. 3.3.1.2, the (radio)metal has a significant influence on the properties (binding affinity, internalization, biodistribution) of the radiopharmaceutical. In addition, this study shows the superiority of the new compounds over the approved ^{111}In-Octreoscan and was the basis to introduce the improved versions into the clinic.

Before therapeutic clinical applications can be performed, radiotherapy studies in animals will be done. For example, Stolz et al. (Stolz et al. 1998) evaluated the therapeutic effect of ^{90}Y-DOTA-TOC on rats bearing CA20948 tumors. Their result showed complete remission of tumors in five out of seven rats. De Jong et al. (de Jong et al. 2001) demonstrated with different SS analogs and different radiometals that the cure rate depends on tumor size, having 100% remission for small tumors.

All these in vivo tests, along with the in vitro assays presented in Sect. 3.3 are helpful for designing and developing new and improved radiopharmaceuticals.

3.3.3 Towards Pan-Somatostatin Ligands

As mentioned above, there are at least five different SS receptor subtypes which may be expressed concomitantly and in various combinations in normal or cancerous tissues (Patel 1999; Reubi et al. 2001). It is therefore of high interest to either develop analogs that bind with high affinity to all five subtypes (pan-SS) for a broader spectrum of tumors or to increase uptake in those tumors which overexpress multiple receptors on their plasma cell membrane. None of the currently used radiopeptides shows such a broad affinity (see Table 4) although some analogs like DOTA-lanreotide (Traub et al. 2001) have been claimed to correspond almost to a pan-SS.

A first example of a universal ligand which can be radioiodinated was recently described by Reubi et al. (Reubi et al. 2002). It is a nonapeptide with reduced size and a metabolically stabilized structure (KE108; Fig. 12; see also Table 4, last entry). It binds with a very high affinity to all five SS receptor subtypes, being equivalent to SS-28 at sstr1 but 2–4 times higher than SS-28 at sstr2–5. In addition, it has agonistic properties at all five subtypes. This peptide was also coupled to DOTA and was shown to still exhibit pan-SS

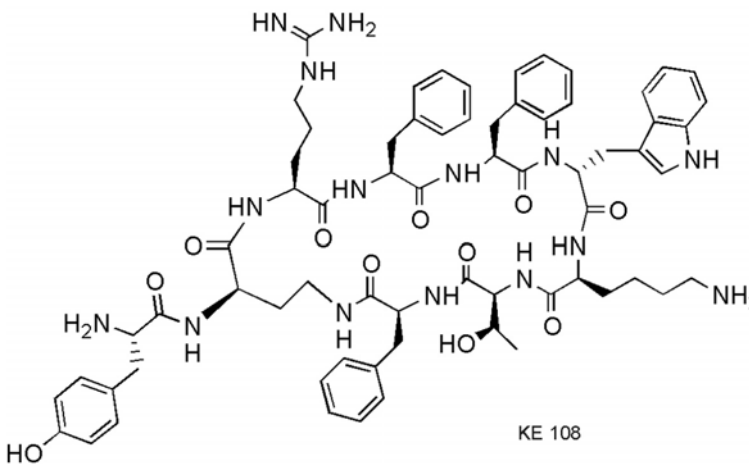

Fig. 12. Structural formula of KE108

character although with slightly reduced affinities to all subtypes (Eisenwiener 2001).

3.4 Patient Studies

As already mentioned, the basis of SS-receptor-targeted radiotherapy is the overexpression of SS receptor subtypes on neuroendocrine tumors.

Herein we present a few patient studies with the gold standard DOTA-[Tyr^3]-octreotide (DOTA-TOC; see Fig. 3a for structure) radiolabeled with different radionuclides for imaging and for therapy, highlighting their superb targeting performance. Fig. 13a and b shows the PET scan of a patient with a neuroendocrine tumor with multiple liver metastases, scanned with ^{68}Ga-DOTA-TOC at 50–80 min after injection. This image reflects the high sensitivity and specificity of the radiogallium-modified peptide, in agreement with the preclinical results found for this radiometallopeptide.

Labeled with the β-emitter, ^{90}Y-DOTA-TOC proved to be very efficient in targeted radiotherapy of some neuroendocrine tumors. Below are two examples which show complete remission even in these radioresistent tumors. The first scan (Fig. 14) shows a patient with a Merkel cell tumor before (left) and after (right) ^{90}Y-DOTATOC therapy. The uptake of ^{111}In-DOTATOC was not visible after four i.v. injections of 50 mCi/m^2 ^{90}Y-DOTATOC; this was judged a complete remission (CR).

Figure 15 shows the image of another patient with an endocrine pancreas tumor and multiple metastases in the liver. After four i.v. injections, the liver metastases disappeared and the outcome was partial remission (PR) overall; the analysis of more than 400 patients treated with this modality in Basel showed 34% objective response (CR and PR) according to WHO criteria. In addition, stabilization of progressive disease was shown in approximately 50%.

The benefit of targeted radiotherapy with radiolabeled SS analogs is documented and has been proven. Still, targeted peptide receptor-mediated radiotherapy is in its infancy and questions remain how one could enhance the efficacy of the therapy. Renal toxicity is the main dose-limiting factor found so far. Infusion of cationic amino

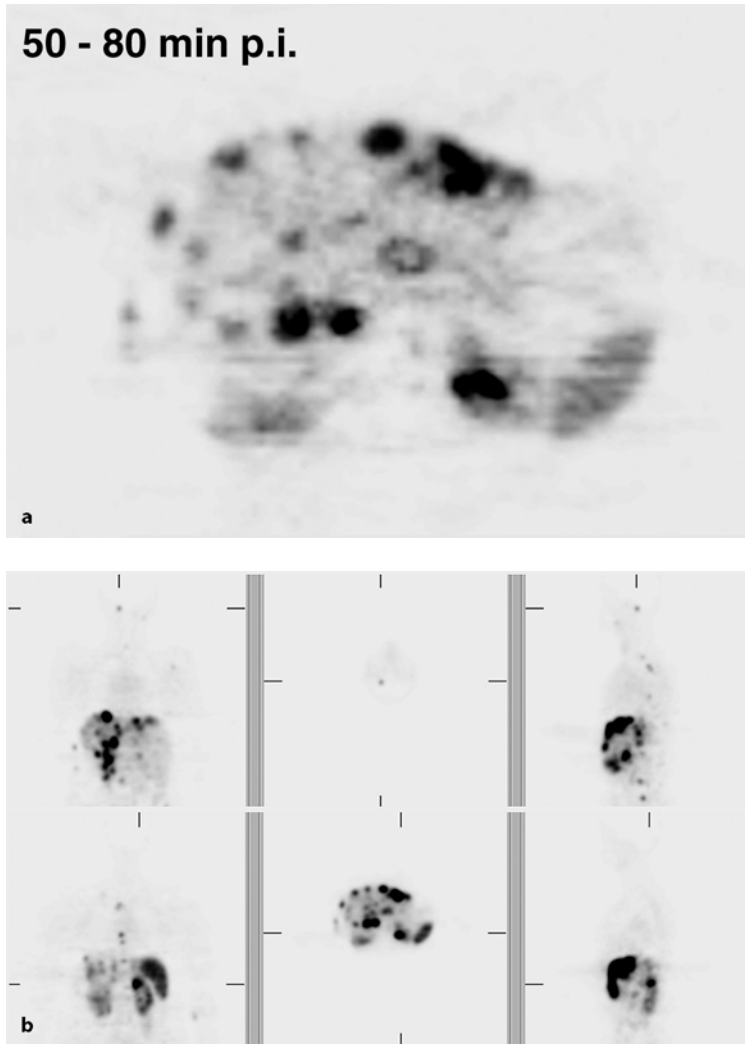

Fig. 13. a UPT: neuroendocrine tumor, ^{68}Ga-DOTATOC PET; multiple liver metastases: minimum ∅ 5 mm, SUV 24.7. **b** UPT: neuroendocrine tumor, ^{68}Ga-DOTATOC PET; previously unknown metastases

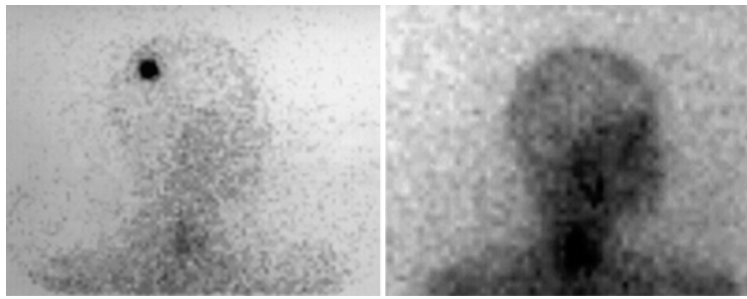

Fig. 14. ^{111}In-DOTATOC scan of a 43-year-old female patient with a Merkel cell tumor before (*left*) and after (*right*) ^{90}Y-DOTATOC treatment

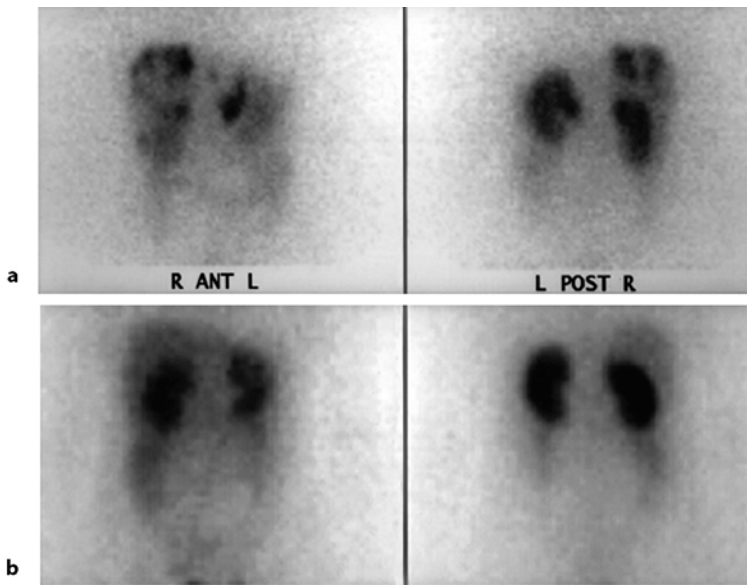

Fig. 15. ^{111}In-DOTATOC scan of the abdomen of a 43-year-old female patient with a recurrence of endocrine pancreatic tumor and multiple liver metastases before (**a**) and after (**b**) ^{90}Y-DOTATOC treatment

acids reduce the uptake of the peptides in the tubular cells of the kidneys. Eventually, structural modifications of the peptides will lead to new radiopeptides with much lower renal uptake. This improvement most likely will come from innovative developments and chelator design from medicinal inorganic chemists.

3.5 Summary and Conclusions

Radiometallo-labeled analogs of SS have shown great benefit in the in vivo localization and targeted radiotherapy of human tumors. The progress and innovation in this clinical application came from the change in strategy, leaving the most widely used radiohalogens for a coordination chemistry approach. The use of chelators appended to the biologically active peptide which convey high thermodynamic and kinetic stability to the radiopeptides did not only improve the pharmacokinetics and pharmacodynamics of the molecules, but surprisingly the biological potency as well.

The most urgent problem to be solved in the field is to improve the kidney clearance of the radiopeptides. The kidney turned out to be the dose-limiting organ in this type of targeted radiotherapy. Coordination chemical strategies have already paved the way to a successful clinical application; it is most likely that chelator modification will further help to improve the renal handling of radiometallopeptides.

Acknowledgements. The authors would like to thank the following for scan pictures: Dr. M. Henze and Prof. U. Haberkorn from the German Cancer Center, Heidelberg; Prof. J. Müller, Dr. C. Waldherr and Dr. M. Walter from University Hospital Basel, Switzerland.

References

Abrams MJ, Juweid M, tenKate CI, Schwartz DA, Hauser MM, Gaul FE, Fuccello AJ, Rubin RH, Strauss HW, Fischman AJ (1990) Technetium-99m-human polyclonal IgG radiolabeled via the hydrazino nicotinamide derivative for imaging focal sites of infection in rats. J Nucl Med 31: 2022–2028

Achilefu S, Wilhelm RR, Jimenez HN, Schmidt MA, Srinivasan A (2000) A new method for the synthesis of tri-tert-butyl diethylenetriaminepentaacetic acid and its derivatives. J Org Chem 65:1562–1565

Albert R, Smith-Jones P, Stolz B, Simeon C, Knecht H, Bruns C, Pless J (1998) Direct synthesis of [DOTA-DPhe^1]-octreotide and [DOTA-DPhe^1,Tyr^3]-octreotide (SMT487): two conjugates for systemic delivery of radiotherapeutical nuclides to somatostatin receptor positive tumors in man. Bioorg Med Chem Lett 8:1207–1210

Andre J, Maecke H, Zehnder M, Macko L, Akyel K (1998) 1,4,7-Triazacyclononane-1-succinic acid-4,7-diacetic acid (NODASA): a new bifunctional chelator for radio gallium-labelling of biomolecules. Chem Commun 12:1301–1302

Blower PJ, Lewis JS, Zweit J (1996) Copper radionuclides and radiopharmaceuticals in nuclear medicine. Nucl Med Biol 23:957–980

Cutler CS, Smith CJ, Ehrhardt GJ, Tyler TT, Jurisson SS, Deutsch E (2000) Current and potential therapeutic uses of lanthanide radioisotopes. Cancer Biother Radiopharm 15:531–545

de Jong M, Bakker WH, Krenning EP, Breeman WA, van der Pluijm ME, Bernard BF, Visser TJ, Jermann E, Béhé M, Powell P, Maecke HR (1997) Yttrium-90 and indium-111 labelling, receptor binding and biodistribution of [DOTA^0,D-Phe^1,Tyr^3]octreotide, a promising somatostatin analog for radionuclide therapy. Eur J Nucl Med 24:368–371

de Jong M, Breeman WA, Bernard BF, Bakker WH, Schaar M, van Gameren A, Bugaj JE, Erion J, Schmidt M, Srinivasan A, Krenning EP (2001) [^{177}Lu-DOTA^0,Tyr^3] octreotate for somatostatin receptor-targeted radionuclide therapy. Int J Cancer 92:628–633

Edwards DS, Liu S, Barrett JA, Harris AR, Looby RJ, Ziegler MC, Hemingway SJ, Carroll TR (1997) New and versatile ternary ligand system for technetium radiopharmaceuticals: water soluble phosphines and tricine as coligands in labeling a hydrazinonicotinamide-modified cyclic glycoprotein IIb/IIIa receptor antagonist with ^{99m}Tc. Bioconjug Chem 8:146–154

Eisenwiener KP (2001) Synthese von makrozyklischen Prochelatoren und ihre Evaluation im Tumortargeting mit regulatorischen Peptiden und im Bereich der Entwicklung neuer auf Gd(III) basierender MRI-Kontrastmittel. PhD thesis: University of Basel

Eisenwiener KP, Powell P, Macke HR (2000) A convenient synthesis of novel bifunctional prochelators for coupling to bioactive peptides for radiometal labelling. Bioorg Med Chem Lett 10:2133–2135

Eisenwiener KP, Prata MI, Buschmann I, Zhang HW, Santos AC, Wenger S, Reubi JC, Macke HR (2002) NODAGATOC, a new chelator-coupled somatostatin analog labeled with [$^{67/68}$Ga] and [^{111}In] for SPECT, PET, and targeted therapeutic applications of somatostatin receptor (hsst2) expressing tumors. Bioconjug Chem 13:530–541

Fischman AJ, Babich JW, Strauss HW (1993) A ticket to ride: peptide radiopharmaceuticals. J Nucl Med 34:2253–2263

Heppeler A (2000) Auswirkungen von Metallkomplexgeometrien verschiedener makrozyklischer Polyaminopolycarboxylat Chelatoren auf die Biologie und Pharmakologie von Metall-Peptid Konjugaten. PhD thesis, University of Basel

Heppeler A, Froidevaux S, Eberle AN, Maecke HR (2000) Receptor targeting for tumor localisation and therapy with radiopeptides. Curr Med Chem 7:971–994

Heppeler A, Froidevaux S, Mäcke HR, Jermann E, Béhé M, Powell P, Hennig M (1999) Radiometal-labelled macrocyclic chelator-derivatized somatostatin analog with superb tumour-targeting properties and potential for receptor-mediated internal radiotherapy. Chem Eur J 5:1016–1023

Hu F, Cutler CS, Hoffman T, Sieckman G, Volkert WA, Jurisson SS (2002) Pm-149 DOTA bombesin analogs for potential radiotherapy. in vivo comparison with Sm-153 and Lu-177 labeled DO_3A-amide-βAla-BBN(7–14) NH_2. Nucl Med Biol 29:423–430

Humm JL (1986) Dosimetric aspects of radiolabeled antibodies for tumor therapy. J Nucl Med 27:1490–1497

Kwekkeboom DJ, Bakker WH, Kooij PP, Konijnenberg MW, Srinivasan A, Erion JL, Schmidt MA, Bugaj JL, de Jong M, Krenning EP (2001) [^{177}Lu-DOTA^{0}Tyr^3]octreotate: comparison with [^{111}In-DTPA^0]octreotide in patients. Eur J Nucl Med 28:1319–1325

Lamberts SW, Bakker WH, Reubi JC, Krenning EP (1990) Somatostatin-receptor imaging in the localization of endocrine tumors. N Engl J Med 323:1246–1249

Lister-James J, Moyer BR, Dean T (1996) Small peptides radiolabeled with ^{99m}Tc. Q J Nucl Med 40:221–233

Liu S, Edwards DS (1999) ^{99m}Tc-labeled small peptides as diagnostic radiopharmaceuticals. Chem Rev 99:2235–2268

Maecke H, Scherer G, Heppeler A, Hennig M (2001) Is In-111 an ideal surrogate for Y-90? If not, why? Eur J Nucl Med 28:967

Maecke HR, Riesen A, Ritter W (1989) The molecular structure of indium-DTPA. J Nucl Med 30:1235–1239

Maina T, Nock B, Nikolopoulou A, Sotiriou P, Loudos G, Maintas D, Cordopatis P, Chiotellis E (2002) [^{99m}Tc]Demotate, a new ^{99m}Tc-based [Tyr^3]octreotate analog for the detection of somatostatin receptor-positive tumours: synthesis and preclinical results. Eur J Nucl Med Mol Imaging 29:742–753

McDevitt MR, Ma D, Lai LT, Simon J, Borchardt P, Frank RK, Wu K, Pellegrini V, Curcio MJ, Miederer M, Bander NH, Scheinberg DA (2001) Tumor therapy with targeted atomic nanogenerators. Science 294:1537–1540

Patel Y (1999) Somatostatin and its receptor family. Front Neuroendocrinol 20:157–198

Reisine T, Bell G (1995) Molecular biology of somatostatin receptors. Endocr Rev 16:427–442

Reubi J, Gugger M, Waser B, Schaer J (2001) Y_1-mediated effect of neuropeptide Y in cancer: breast carcinomas as targets. Cancer Res 61:4636–4641

Reubi J, Schaer J, Waser B, Wenger S, Heppeler A, Schmitt J, Maecke H (2000) Affinity profiles for human somatostatin receptor subtypes SST1-SST5 of somatostatin radiotracers selected for scintigraphic and radiotherapeutic use. Eur J Nucl Med 27:273–282

Reubi JC (1995) Neuropeptide receptors in health and disease: the molecular basis for in vivo imaging. J Nucl Med 36:1825–1835

Reubi JC, Eisenwiener KP, Rink H, Waser B, Maecke H (2002) A new peptide somatostatin agonist with high affinity to all five somatostatin receptors. Eur J Pharmacol 456:45–49

Schaer JC, Waser B, Mengod G, Reubi JC (1997) Somatostatin receptor subtypes sst1, sst2, sst3 and sst5 expression in human pituitary, gastroenteropancreatic and mammary tumors: comparison of mRNA analysis with receptor autoradiography. Int J Cancer 70:530–537

Stolz B, Smith-Jones P, Albert R, Tolcsvai L, Briner U, Ruser G, Macke H, Weckbecker G, Bruns C (1996) Somatostatin analogs for somatostatin-receptor-mediated radiotherapy of cancer. Digestion 57 [Suppl 1]:17–21

Stolz B, Weckbecker G, Smith-Jones PM, Albert R, Raulf F, Bruns C (1998) The somatostatin receptor-targeted radiotherapeutic [^{90}Y-DPTA-DPhe^{1},Tyr^{3}]octreotide (^{90}Y-SMT 487) eradicates experimental rat pancreatic CA 20948 tumours. Eur J Nucl Med 25:668–674

Thakur ML, Kolan H, Li J, Wiaderkiewicz R, Pallela VR, Duggaraju R, Schally AV (1997) Radiolabeled somatostatin analogs in prostate cancer. Nucl Med Biol 24:105–113

Traub T, Petkov V, Ofluoglu S, Pangerl T, Raderer M, Fueger BJ, Schima W, Kurtaran A, Dudczak R, Virgolini I (2001) ^{111}In-DOTA-lanreotide scintigraphy in patients with tumors of the lung. J Nucl Med 42:1309–1315

4 Pretargeted Radioimmunotherapy

G. Paganelli

Strategies for treating most cancers usually employ surgical resection, chemotherapy, and/or radiation therapy. Although surgical resection can be very effective and sometimes curative in localized tumors, the presence of distant sites or inoperable tumors leaves the options of chemotherapy and/or radiotherapy. If chemotherapeutic drugs or radiotherapy could be selectively delivered to tumors, it would be possible to avoid, or at least reduce, unwanted toxicity and improve efficacy (Wawrzynczak 1991).

Monoclonal antibodies (MoAbs) reactive with tumor-associated antigens can be used therapeutically as biologic response modifiers and as delivery systems for chemotherapeutic agent, toxins, and radionuclides. In particular, the utility of MoAbs for targeting radioactive agents to tumor cells, for diagnostic and therapeutic purposes, has been extensively studied (Epenetos et al. 1987; Larson 1985; Buraggi et al. 1985). The concept, which forms the basis of radioimmunoscintigraphy, radioimmuno-guided surgery and radioimmunotherapy (RIT), has been an active area of research in various fields of oncology (Fazio and Paganelli 1993; Kim et al. 1993; Leichner et al. 1993; Chetanneau et al. 1994). Many investigations have focused on several parts of this process, including tumor antigen expression, tumor targeting vehicles, pharmacokinetic aspects and immunogenicity of these recognition units, radioisotopes, and

nuclear imaging technology (Schlom 1986; Hirai 1990; Kuhn et al. 1991; Strand et al. 1993; Hazra et al. 1995). Although several studies have been carried out in this area for almost two decades, many limitations when using radiolabeled MoAbs for treating solid tumors in humans have been encountered. One of the problems in radioimmuno targeting relates to adverse intrinsic tumor characteristics. Tumors often display intrinsic heterogeneity in antigen density. This factor, together with the nonuniformity of tumor vascularization, capillary permeability, degree of tumor necrosis, and difference in interstitial pressure, account for the heterogeneous distribution of antibodies in targeted tumors (Strand et al. 1993). Another problem with such procedures is the relatively low tumor-to-normal tissue radioactivity ratio and the small dose of radioactivity which consequently reaches the target tumor. Accumulation of up to 20%–30% of the injected dose/g of tumor has been observed in mouse tumors model, whereas 0.001%–0.1% injected dose/g is more common in humans (Mann et al. 1984). Other physical and physiological barriers prevent large quantities of MoAb from penetrating into solid masses (Mann et al. 1984; Johnson et al. 1990; Jain 1991) resulting in tumor-to-blood ratios in the range of 1:5. A low tumor-to-background ratio remains the main problem of radio-immunodetection. In an attempt to overcome the low uptake of label by the tumor and improve the tumor-to-blood ratio, various studies have examined the concept of tumor pretargeting based on the separate administration of MoAbs and radiolabeled isotopes (Goodwin et al. 1988; Paganelli et al. 1988, 1991; LeDoussal et al. 1989; Bos et al. 1994; Sung and van Osdol 1995). Such systems require the use of a modified MoAb that permits a second component to bind specifically to it. Conceptually, the modified MoAb is administered first and allowed to distribute throughout the body, to bind to the tissues expressing antigen, and to clear substantially from other tissues. Then the radiolabeled second component is administered and, ideally, it localizes at sites where the modified MoAb has accumulated. If the second component has higher permeation, clearance, and diffusion rates than those of MoAb, more rapid radionuclide localization to the tumor and higher tumor selectivity are possible. MoAbs injection time can be delayed to a time when most of the primary MoAb has been cleared from the blood and normal tissues, thereby decreasing nontumor

binding and achieving, with the use of this strategy, higher tumor-to-nontumor ratios (Magnani et al. 1996).

Among the tumor pretargeting strategies investigated, a three-step method was studied and applied with encouraging results by our group: this model is based on the *avidin-biotin* system (Paganelli et al. 1991 a, b; Magnani et al. 1996). The *avidin-biotin* system is widely used for in vitro applications (Wilchek and Bayer 1984, 1988). *Avidin* [and *Streptavidin*, a nonglycosylated analog (Hamilton et al. 1987)] are functionally defined by their ability to bind *biotin* with high affinity and specificity without recognizing or binding any other physiological compound with any strength. For practical purposes, their binding can be regarded as irreversible (Green 1963). *Avidin* is a small oligomeric protein made up of four identical subunits, bearing a single binding site for biotin. *Biotin* is a 244 Da molecule, and is commercially available with several linkers that facilitate reactions with proteins (Paganelli et al. 1991 b). In the three-step technique, the excess of circulating biotinylated MoAbs is removed as cold complexes, which are taken up and metabolized by the liver (Paganelli et al. 1991 a). This is the major factor in background reduction and is obtained prior to label injection. Schematically, biotinylated MoAbs are first injected (step 1) followed by injection of avidin and streptavidin 1 day later (step 2). The second injection carries a twofold purpose: (1) the removal of excess circulating biotinylated antibodies in the form of cold complexes via avidin (fast clearance); and (2) the targeting of tumor cells with streptavidin (slower clearance). Thereafter, radiolabeled biotin, which will selectively bind to streptavidin and thus to the tumor, is injected (step 3) (Paganelli et al. 1988, 1991). For therapeutic applications, the choice of a suitable isotope is quite limited. Yttrium-90 (^{90}Y), indicated as one of the best therapeutic radionuclides for use in conjunction with tumor-associated antibodies, is certainly very appropriate for that reason and considering that it can easily be obtained with a ^{90}Sr/^{90}Y generator, has a physical half-life of 2.7 days, and is a pure, high energy β-emitter ($E_{max}\,\beta = 2.28$ MeV; $E_{ave}\,\beta = 0.94$ MeV; Wessels and Rogus 1984; Chinol and Hnatowich 1987). The 3-step technique is summarized in Fig. 1.

Lutetium-177 (^{177}Lu), with its longer half-life (6.7 days) and shorter penetration range (maximum 2 mm) could also be a candi-

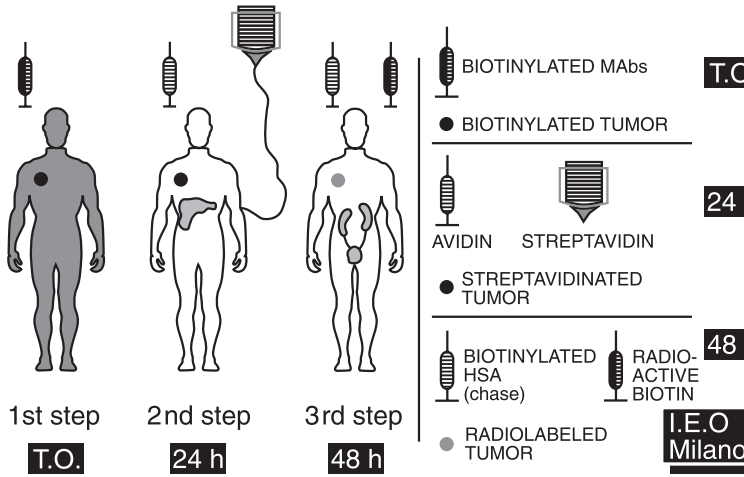

Fig. 1. Three-step strategy. Biotinylated MoAbs are injected (i.v.) and allowed to localize onto the target (*1st step*). One day later avidin and streptavidin are injected (i.v., *2nd step*). After 24 h, when unbound streptavidin and circulating avidin-MoAb complexes have been cleared from circulation, radiolabeled biotin is injected (i.v., *3rd step*)

date for radioimmunotherapy, especially in smaller lesions, as demonstrated by receptor radionuclide therapy trials with ^{177}Lu-octreotide (De Jong et al. 2002).

From a theoretical point of view, a radioimmunotherapy approach can be exploited in all those tumors in which a specific antigen can be targeted by a monoclonal antibody. Brain tumors represent the most favorable model. The hope of therapy for brain tumors and, in particular, for high-grade gliomas (HGG) lies in the potential to extend functional life-span with little additional, and possibly reduced, morbidity, as compared with current aggressive treatment modalities (surgery, radiotherapy, and chemotherapy). Radioimmunotherapy, as a systemic or locoregional application, has the potential to become a well-tolerated therapeutic option in the management of HGG, complementing traditional regimens. HGGs are apt targets for evaluating the therapeutic efficacy of new pretargeting strategies since: (a) the prognosis is poor and patients' life expectancy is less than 1 year;

and (b) a suitable marker, the glycoprotein tenascin, is abundant in the stroma of HGGs, but not in normal cerebral tissues (Zagzag et al. 1996).

In a phase I–II study, we evaluated the toxicity and therapeutic efficacy of the avidin-biotin pretargeting approach in a group of 48 eligible patients with histologically confirmed grade III or IV glioma and documented residual disease or recurrence after conventional treatment (Paganelli et al. 1999). The three-step radioimmunotherapy was performed by intravenous administration of 35 mg/m^2 of biotinylated antitenascin monoclonal antibody (1st step), followed 36 h later by 30 mg of avidin and 50 mg of streptavidin (2nd step), and 18–24 h later by 1–2 mg of Yttrium-90-labeled biotin (3rd step). The injected activity, calculated on the basis of previous studies and dosimetry calculation, ranged from 2.22 to 2.97 GBq/m^2 (60–80 mCi/m^2) per cycle. Three major conclusions emerged from this study. First, three-step radionuclide therapy with high-dose ^{90}Y produced acceptable toxicity at the dose of 60 mCi/m^2 due to the extremely favourable biodistribution of ^{90}Y-DOTA-biotin; with the majority of the nontumor-bound activity eliminated in the first 24 h, the maximum tolerated dose (MTD) has been determined at the level of 80 mCi/m^2. Second, an objective therapeutic effect was documented in an encouraging fraction of our patients, all of whom were no longer responsive to conventional treatments: 52% did not progress any further (the majority suspended cortisone, had reduction in epileptic seizure rate, and improved quality of life), while significant tumor reduction occurred in 25%. Third, immune response to the murine monoclonal antibody, known to interfere with localization in subsequent administrations, was less frequent than in patients treated with the directly labeled MoAbs used in other studies, possibly because of its shorter residence time in the circulation with our procedure. In contrast, Streptavidin was highly immunogenic, preventing the possibility of repeated cycles of therapy.

The encouraging results obtained in this phase I–II study prompted us to apply the same approach in an adjuvant setting, to evaluate: (a) time to relapse, and (b) overall survival (Grana et al. 2002). We studied 37 HGG patients, 17 with grade III glioma and 20 with glioblastoma (GBM), in a controlled open nonrandomized study. All patients underwent surgery and radiotherapy and were dis-

ease-free by neuroradiological examinations. Nineteen patients (treated) received adjuvant treatment with radioimmunotherapy. In the treated GBM patients, the median disease-free interval was 28 months (range, 9–59); median survival was 33.5 months and one patient is still without evidence of disease. All 12 control GBM patients died after a median survival from diagnosis of 8 months. In the treated, grade III glioma patients the median disease-free interval was 56 months (range, 15–60) and survival cannot be calculated as only two in this group died. A number of points arose from the results of this second trial. Firstly, three-step radioimmunotherapy was confirmed as highly active against malignant glioma, yet did not cause major adverse events, as previously described. Secondly, the effect RIT on GBM was interesting: it considerably prolonged disease-free interval and overall survival relative to the untreated group. After this trial, we also became aware of the possibility to further improve the efficacy of the method by modifying its timing. It might be advantageous to administer RIT immediately after debulking surgery, in order to exploit the greater permeability of the blood-brain barrier (BBB) at that time. This would be expected to expose more malignant cells to the radionuclide and hence limit the local spread of the cancer.

However, in clinical practice of HGG, despite all the efforts to prevent the progression, a local relapse coming from the microscopic cellular foci, seeded in the brain-adjacent tumor, is a constant event. This high tendency of glioma to recur locally fully justifies local therapeutic approaches: a second tumor debulking and/or various types of radiotherapy (conformal conventionally fractionated radiotherapy, hypofractionated stereotactic radiotherapy, interstitial brachytherapy and radiosurgery) are usually performed. Clinical experiences, employing more innovative approaches, such as local hyperthermia, intratumoral injection of interleukin-2-activated lymphocytes, α-interferon, recombinant toxins, various chemotherapeutic agents and radiopharmaceuticals, have been reported over the last years (Rand et al. 2000; Barba et al. 1989; Boiardi et al. 1996). The principal advantages of a locally delivered compound (chemotherapeutic agent or radiopharmaceutical) consist mainly of bypassing the BBB, minimizing systemic toxicity, and achieving prolonged local drug concentration. Locoregional radioimmunotherapy using mono-

clonal antibodies labeled with high-energy, β-emitting radionuclides has shown several advantages, including the possibility of destroying large numbers of antigen-negative tumor cells by the so-called crossfire effect. Several studies demonstrated that the locoregional infusion of ^{131}I- or ^{90}Y-labeled antitenascin MoAbs in glioma patients provided a safety profile and the possibility to control the growth of the tumor in the long term (Riva et al. 1999; Hopkins et al. 1995; Cokgor et al. 2000). The three-step pretargeting approach, described above, has also been validated in the locoregional treatment of glioma and peritoneal carcinosis (Paganelli et al. 1992). In a phase I–II study, we investigated the safety profile and antitumor efficacy of a pretargeting three-step method employing ^{90}Y-biotin in the locoregional therapy of recurrent HGG (Paganelli et al. 2001). Twenty-four patients with recurrent glioma underwent second surgical debulking with implantation of an indwelling catheter into the surgical cavity in order to receive the radioimmunotherapeutic agents. Eight patients with anaplastic astrocytoma (AA) and 16 patients with GBM were injected first with biotinylated antitenascin MoAbs (2 mg), then with avidin (10 mg; 24 h later) and finally ^{90}Y-biotin (18 h later). Each patient received two of these treatments 8–10 weeks apart. The injected activity ranged from 0.555 to 1.110 GBq (15–30 mCi). Dosage was escalated by 0.185 GBq (5 mCi) in four consecutive groups. Bremsstrahlung images were acquired to confirm the correct localization of the ^{90}Y-biotin. The treatment was well tolerated without acute side effects up to 0.740 GBq (20 mCi). The maximum tolerated activity was 1.110 GBq (30 mCi) limited by neurologic toxicity. None of the patients developed hematological toxicity. In three patients, infection occurred around the catheter. The average absorbed dose to the normal brain was minimal compared with that received at the surface resection cavity (SRC) interface. At first follow-up, partial (PR) and minor (MR) responses were achieved in three GBM (1 PR, 2 MR) and three AA patients (1 PR, 2 MR) with an overall objective response rate of 25%. Stable disease (SD) was observed in seven GBM and five AA patients (50%). There was disease progression in six GBM patients (25%), but none of the AA patients. This study assessed that with activity ranging from 0.7 to 0.9 GBq per cycle, three-step locoregional radioimmunotherapy was safe and produced an objective response in 25% of patients.

These interesting results have been recently confirmed in a retrospective analysis (manuscript submitted) performed in a group of 73 patients with histologically proven recurrent GBM and immunohistochemical and demonstration of tenascin expression in tumor. All patients had a catheter implanted at second surgery and underwent at least two cycles of locoregional radioimmunotherapy (range 2–7) with a 2-month interval. Thirty-five out of 73 patients were also treated with a novel oral chemotherapy Temozolomide (TMZ). Two cycles of TMZ (200 mg/m^2/day, for 5/28 days) were administered in between each course of LR-RIT. The rationale for combining Temozolomide and radiation-delivering therapies is based on preclinical and clinical data suggesting additional or, at least synergistic activity against GBM. Radiological objective response occurred in 9 patients (3 PR, 6 MR). In a large number of patients (63%), a stabilization of disease was obtained. In the 38 patients treated with LR-RIT alone, median overall survival and progression-free survival were respectively 17.5 months [95% CI=(17–20)] and 5 months [95% CI=(4–8)], while in the 35 treated with the combined treatment (LR-RIT+TMZ) respective values were 25 months [95% CI=(23–30)] and 10 months [95% CI=(9–18)], ($p<0.01$). The addition of TMZ to LR-RIT did not increase neurological toxicity, and no major hematological toxicity was observed. This study confirmed the efficacy and safety of locoregional radioimmunotherapy in GBM, with a significant increase in survival compared to the one obtained with surgery and external radiotherapy alone. In particular, this study shows that this improvement in survival can be further increased by the multimodal approach of combining LR-RIT with Temozolomide. We are aware of possible bias in this retrospective study, such as in the selection of patients. However, these results could represent the basis for further prospective trials, to assess timing and schedule of radioimmunotherapy in the therapeutic algorithm of GBM. We can speculate that the best result may be obtained when LR-RIT will be applied as an adjunct to initial surgery. As the patients tolerate the catheter very well, it could be inserted already during the first surgical intervention. The 2–4-week break, between surgical intervention and external radiotherapy, should be a very convenient period to start LR-RIT.

In conclusion, we emphasize that radioimmunotherapy, both systemic and locoregional, should be used as part of a combined modal-

ity approach. The combined modality approach to treating brain tumors was introduced about 30 years ago; it remains the most effective approach we have. The promise is that the combination of surgery, radiotherapy, chemotherapy, and RIT may provide, at last, a way of increasing life expectancy in HGG patients. The potential advantage in cancer therapy of pretargeting protocols, especially the three-step approach, with respect to the use of directly labeled antibodies, lies in the lower toxicity observed which has allowed for administration of high doses of therapeutic radionuclides, such as ^{90}Y, without bone marrow toxicity.

Acknowledgements. This work was supported by grants of the Italian Association for Cancer (AIFC) and Consiglio Nazionale delle Ricerche (CNR-MIUR)

References

Barba D, Saris SC, Holder C, Rosenberg SA, Oldfield EH (1989) Intratumoral LAK cell and interleukin-2 therapy of human glioma. J Neurosurg 70:175–182

Boiardi A, Salmaggi A, Pozzi A, Broggi G, Silvani A (1996) Interstitial chemotherapy with mitoxantrone in recurrent malignant glioma: preliminary data. J Neurooncol 27:157–162

Bos ES, Kuijpers WHA, Meesters-Winters M, Pham DT, de Haan AS, van Doornmalen AM, Kaspersen FM, van Boeckel CAA, Gougeoun-Bertrand F (1994) In vitro evaluation of DNA-DNA hybridization as a two step approach in radioimmunotherapy of cancer. Cancer Res 54:3479–3486

Buraggi GL, Callegaro L, Mariani G, Turrin A, Cascinelli N, Attili A, Bombardieri E, Terno G, Plassio G, Dovis M (1985) Imaging with ^{131}I-labeled monoclonal antibodies to a high-molecular-weight melanoma-associated antigen in patients with melanoma: Efficacy of whole immunoglobulin and its $F(ab')_2$ fragments. Cancer Res 45:3378–3387

Chetanneau A, Barbet J, Peltier P, Le-Doussal JM, Gruaz-Guyon A, Bernard AM, Resche I, Rouvier E, Bourguet P, Delaage M (1994) Pretargeted imaging of colorectal cancer recurrences using an In-111-labelled bivalent hapten and a biospecific antibody conjugate. Nucl Med Commun 15:972–980

Chinol M, Hnatowich DJ (1987) Generator-produced yttrium-90 for radioimmunotherapy. J Nucl Med 28:1465–1470

Cokgor I, Akabani G, Kuan CT, Friedman HS, Friedman HA, Coleman RE, McLendon RE, Bigner SH, Zhao XG, Garcia-Turner AM, Pegram CN,

Wikstrand CJ, Shafman TD, Herndon JE 2nd, Provenzale JM, Zalutsky MR, Bigner DD (2000) Phase I Trial Results of Iodine-131-labeled antitenascin monoclonal antibody 81c6 treatment of patients with newly diagnosed malignant gliomas. J Clin Oncol 18:3862–3872

De Jong M, Valkema R, Jamar F, Kvols LK, Kwekkeboom DJ, Breeman WA, Bakker WH, Smith C, Pauwels S, Krenning EP (2002) Somatostatin receptor-targeted radionuclide therapy of tumors: preclinical and clinical findings. Semin Nucl Med 32:133–140

Epenetos AA, Munro AJ, Stewart JSW, Rampling R, Lambert HE, McKenzie CG, Soutter WP, Rahemtulla A, Hooker G, Sivolapenko G, Snook D, Courtenay-Luck N, Dhokia B, Krausz T, Taylor-Papadimitriou J, Durbin H, Bodmer WF (1987) Antibody-guided irradiation of advanced ovarian cancer with intraperitoneally administered radiolabelled monoclonal antibodies. J Clin Oncol 5:1890–1899

Fazio F, Paganelli G (1993) Antibody-guided scintigraphy: targeting of the "magic bullet. Eur J Nucl Med 20:1138–1140

Goodwin DA, Meares CF, McCall MJ, McTigue M, Chaovapong W (1988) Pre-targeted immunoscintigraphy of murine tumors with indium-111-labeled bifunctional haptens. J Nucl Med 29:226–234

Grana C, Chinol M, Robertson C, Mazzetta C, Bartolomei M, De Cicco C, Fiorenza M, Gatti M, Caliceti P, Paganelli G (2002) Pretargeted adjuvant radioimmunotherapy with yttrium-90-biotin in malignant glioma patients: a pilot study. Br J Cancer 86:207–212

Green NM (1963) Avidin-1. The use of [^{14}C] biotin for kinetic studies and for assay. Biochem J 89:585–591

Hamilton TC, Ozols RF, Longo DL (1987) Biologic therapy for the treatment of malignant common epithelial tumors of the ovary. Cancer 60 [Suppl 8]:2054–2063

Hazra DK, Britton KE, Lahiri VL, Gupta AK, Khanna P, Saran S (1995) Immunotechnological trend in radioimmuno-targeting: from "magic bullet" to "smart bomb". Nucl Med Commun 16:66–75

Hirai H (1990) Use of tumor receptors for diagnostic imaging. Acta Radiol 374:57–64

Hopkins K, Chandler C, Bullimore J, Sandeman D, Coakham H, Kemshead JT (1995) A pilot study of the treatment of patients with recurrent malignant gliomas with intratumoral yttrium-90 radioimmunoconjugates. Radiother Oncol 34:121–131

Jain RK (1991) Haemodynamic and transport barriers to the treatment of solid tumors. Int J Radiat Biol 60:85–100

Johnson DA, Baker AL, Laguzza BC, Fix DV, Gutowski MC (1990) Antitumor activity of L/1C2-4-desacetylvinblastine-3-carboxyhydrazide immunoconjugate in xenografts. Cancer Res 50:1790–1794

Kim JA, Triozzi PL, Martin EW (1993) Radioimmunoguided surgery for colorectal cancer. Oncology 7:55–60

Kuhn JA, Corbisiero RM, Buras RR, Carroll RG, Wagman LD, Wilson LA, Yamauchi D, Smith MM, Kondo R, Beatty D (1991) Intraoperative gamma detection probe with presurgical antibody imaging in colon cancer. Arch Surg 126:1398–1403

Larson SM (1985) Radiolabelled monoclonal anti-tumor antibodies and therapy. J Nucl Med 26:538–545

LeDoussal JM, Martin M, Gautherot E, Delaage M, Barbet J (1989) In vitro and in vivo targeting of radiolabeled monovalent and divalent haptens with dual specificity monoclonal antibody conjugates: enhanced divalent hapten affinity for cell-bound antibody conjugate. J Nucl Med 30:1358–1366

Leichner PK, Koral KF, Jaszczak RJ, Green AJ, Chen GTY, Roeske JC (1993) An overview of imaging techniques and physical aspects of treatment planning in radioimmunotherapy. Med Physics 20:569–577

Magnani P, Paganelli G, Modorati G, Zito F, Songini C, Sudati F, Koch P, Maecke HR, Brancato R, Siccardi AG, Fazio F (1996) Quantitative comparison of direct antibody labeling and tumor pretargeting in uveal melanoma. J Nucl Med 37:967–971

Mann BD, Cohen MB, Saxton RE, Morton DL, Benedict WF, Korn EL, Spolter L, Graham LS, Chang CC, Burk MW (1984) Imaging of human tumor xenografts in nude mice with radiolabeled monoclonal antibodies. Limitations of specificity due to nonspecific uptake of antibody. Cancer 54:1318–1327

Paganelli G, Riva P, Deleide G, Clivio A, Chiolerio F, Scasselati GA, Malcovati M, Siccardi AG (1988) In vivo labelling of biotinylated monoclonal antibodies by radioactive avidin: a strategy to increase tumor radiolocalization. Int J Cancer 2:121–125

Paganelli G, Magnani P, Zito F, Villa S, Sudati F, Lopalco L, Rossetti C, Malcovati M, Chiolerio F, Seccamani E, Siccardi AG, Fazio F (1991a) Three-step monoclonal antibody tumor targeting in carcinoembryonic antigen-positive patients. Cancer Res 51:5960–5966

Paganelli G, Malcovati M, Fazio F (1991b) Monoclonal antibody pretargetting techniques for tumor localization: the avidin-biotin system. Nucl Med Commun 12:211–234

Paganelli G, Belloni C, Magnani P, Zito F, Pasini A, Sassi I, Meroni M, Mariani M, Vignali M, Siccardi AG, Fazio F (1992) Two-step tumor targeting in ovarian cancer patients using biotinylated monoclonal antibodies and radioactive streptavidin. Eur J Nucl Med 19:322–329

Paganelli G, Grana C, Chinol M, Cremonesi M, De Cicco C, De Braud F, Robertson C, Zurrida S, Casadio C, Zoboli S, Siccardi AG, Veronesi U (1999) Antibody-guided three-step therapy for high grade glioma with yttrium-90 biotin. Eur J Nucl Med 26:348–357

Paganelli G, Bartolomei M, Ferrari M, Cremonesi M, Broggi G, Maira G, Sturiale C, Grana C, Prisco G, Gatti M, Caliceti P, Chinol M (2001) Pretargeted locoregional radioimmunotherapy with ^{90}Y-biotin in glioma

patients: phase I study and preliminary therapeutic results. Cancer Biother Radiopharm 16:227–235

Rand RW, Kreitman RJ, Patronas N, Varricchio F, Pastan I, Puri RK (2000) Intratumoral administration of recombinant circulary permuted interleukin-4-Pseudomonas Exotoxin in patients with high-grade glioma. Clin Cancer Res 6:2157–2165

Riva P, Franceschi G, Frattarelli M, et al. (1999) Loco-regional radioimmunotherapy of high-grade malignant gliomas using specific monoclonal antibodies labeled with ^{90}Y: a Phase I study. Clin Cancer Res 5 [Suppl 10]: 3275s–3280s

Schlom J (1986) Basic principles and application of monoclonal antibodies in the management of carcinomas: the Richard and Hinda Rosenthal Foundation Award Lecture. Cancer Res 46:3225–3238

Strand SE, Zanzonico P, Johnson TK (1993) Pharmacokinetic modeling. Med Physics 20:515–527

Sung C, van Osdol WW (1995) Pharmacokinetic comparison of direct antibody targeting with pretargeting protocols based on streptavidin-biotin binding. J Nucl Med 36:867–876

Wawrzynczak EJ (1991) Systemic immunotoxin therapy of cancer: advances and prospects. Br J Cancer 64:624–630

Wessels BW, Rogus RD (1984) Radionuclide selection and model absorbed dose calculations for radiolabeled tumor associated antibodies. Med Phys 11:638–645

Wilchek M, Bayer EA (1984) The avidin biotin complex in immunology. Immunol Today 5:39–43

Wilchek M, Bayer EA (1988) The avidin biotin complex in bioanalytical applications. Anal Biochem 171:1–32

Zagzag D, Friedlander DR, Dosik J, Chikramane S, Chan W, Greco MA, Allen JC, Dorovini-Zis K, Grumet M (1996) Tenascin-C expression by angiogenic vessels in human astrocytomas and by human brain endothelial cells in vitro. Cancer Res 56:182–189

5 PET/CT: Combining Function and Morphology

T. F. Hany, G. K. von Schulthess

5.1 General Considerations in PET and PET/CT

The basic principle of positron emission tomography (PET) is the use of positron-emitting isotope labeled pharmaceuticals, which bind to a specific receptor or are integrated into a metabolic pathway (Huang et al. 1980). Positron-emitting isotopes are characterized by a β plus-decay, in which a positron is emitted. This positron collides with any of the many shell electrons in the neighboring atoms, with which it annihilates. The annihilation reaction produces two 511 keV gamma rays, which are emitted in almost exactly opposite directions. Carbon-11 (^{11}C), ammonia-13 (^{13}N), oxygen-15 (^{15}O), or fluorine-18 (^{18}F) are the most widely used positron emitters in clinical and research applications. The two photons are detected in coin-

cidence by the PET scanner. In PET scanners, emission data are acquired in either 2-D or 3-D mode. Since the annihilation reaction occurs within the body, photons traveling through the body tissues are attenuated. To obtain quantitative results, attenuation correction is necessary, since photons from decays deep within the body are more attenuated than those coming from decays close to the surface. Attenuation correction is performed using data from a so-called transmission scan, measuring the attenuation of 511 keV photons from an external source of positron-emitting activity (e.g., Germanium pin-source; Jaszczak and Hoffman 1995). This scan must be acquired in addition to the emission scan and takes around 30%–50% of the total imaging time. The shortest duration transmission scans are obtained using X-ray CT, as is possible in the new generation of combined PET/CT scanners (Burger et al. 2002a; Kinahan et al. 1998). On a dedicated PET/CT scanner, CT data are acquired within less than 30 s compared to the 12–15 min for a transmission scan on a PET alone machine. An energy-scaling algorithm is required to convert the transmission images acquired with a CT energy spectrum (from 40–140 keV) to the equivalent images at 511 keV. The great additional advantage of using CT data for this purpose is that the CT images, which are "hardware" coregistered with PET images, can also be used for anatomic referencing for the PET lesions, thereby enhancing the diagnostic accuracy of integrated PET/CT imaging. It has been shown that lesion detection in PET/CT does not improve beyond the relatively low dose of 40 mAs CT scan (Hany et al. 2002).

The most widely clinically evaluated positron-emitting isotope labeled pharmaceutical is fluorine-18 fluoro-2-deoxy-D-glucose (FDG). This glucose analog is transported into the cell by specific transporters and phosphorylated by hexokinase to ^{18}F-FDG-6 phosphate, which is inert to further metabolic processing or transmembrane back-transport outside the cell, and is therefore accumulated within the cells (Phelps 1981). The physical half-life of FDG is around 110 min and makes this PET tracer also attractive for PET imaging at imaging centers without a cyclotron. FDG is used as metabolic marker in oncology, cardiology, neurology, and inflammation imaging. In the following chapters, initial clinical experience using PET/CT are described.

5.2 PET/CT in Oncology

5.2.1 Bronchial Carcinoma

Lung cancer is the most common cancer in men worldwide, accounting for roughly 20% of all cancers. Of all lung cancers, 80% are non-small cell lung cancer (NSCLC) including adenocarcinoma (50%) and squamous cell carcinoma (30%); 15% are small cell lung cancers (SCLC) and 5% are large cell cancer. Surgical resection offers the best chance of cure for NSCLC in the early stages either alone or in combination with chemo- or radiotherapy at the more advanced stages. Unfortunately, many patients present with metastatic disease at the time of diagnosis. SCLC is best treated by chemotherapy and radiation treatment. Staging of lung cancer includes histological work-up of the primary tumor, mediastinoscopy for nodal staging, computed tomography of the thorax including the adrenal glands and detection of bone metastasis by bone scanning.

PET imaging has shown its effectiveness for the differentiation between malignant and nonmalignant disease (Gupta et al. 1996; Patz et al. 1993). It has to be pointed out that the spatial resolution of modern full-ring detector PET scanners is at best 4–5 mm. Therefore, it is not useful to examine solitary lung lesions measuring less than 5–10 mm by PET. Since lesions over 3 cm in diameter can be easily reached by CT-biopsy, PET should be used as an initial diagnostic tool only in selected cases. Lesions with low or even missing FDG uptake can be considered as benign lesions and monitored by CT. All lesions with high FDG uptake should be considered malignant. Unfortunately, active inflammatory disease can also show avid FDG uptake and mimic malignant disease (tuberculosis, histoplasmosis, fungal infection). PET/CT can be helpful in these cases, since morphological information is available at the same time. Only limited data are available, however.

Regarding T-staging, PET alone cannot contribute essential information to the local extent of the primary tumor and is not useful for T-staging. In PET/CT, coregistration of morphological CT information and functional PET information allows for improved detection, particularly of the chest wall and to a lesser extent of mediastinal invasion, and can be used for T-staging. Without contrast-enhanced

CT, invasion of vascular mediastinal structures is not possible. Differentiation of the primary tumor and poststenotic atelectasis is possible when using PET/CT (Lardinois et al. 2003).

For N-staging, sensitivity and specificity in the detection of mediastinal lymph nodes by contrast-enhanced CT is rather low (60%–70%; Webb et al. 1991, 1993). FDG-PET is significantly more accurate (sensitivity 89%, specificity 99%). In addition, integrated PET/CT imaging is more accurate than PET alone in nodal staging (Fig. 1).

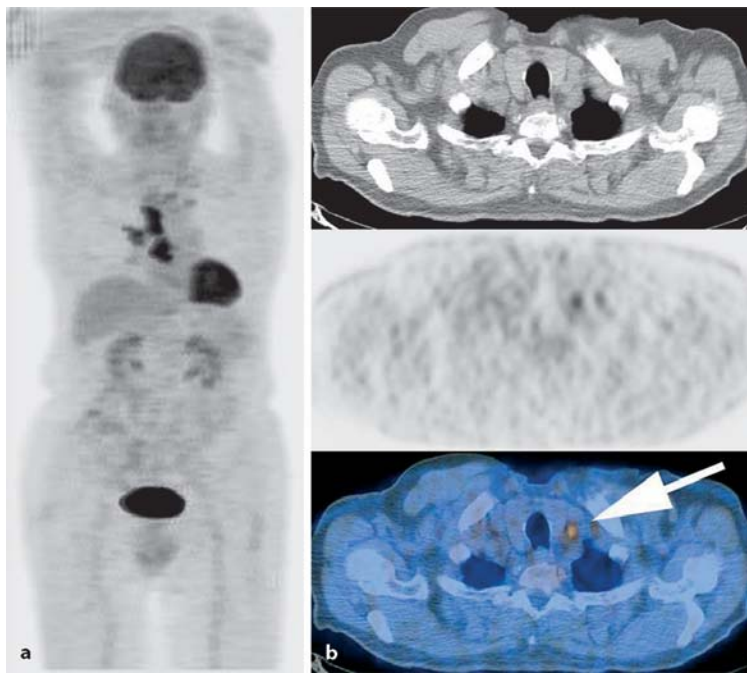

Fig. 1 a, b. A 68-year-old male patient with a para-central squamous cell carcinoma of the lower lobe, referred for staging with FDG-PET/CT. Maximum-intensity projection (MIP). **a** FDG-avid lesions in the infra-carinal and ipsilateral mediastinal region as well as the peribronchial region on the right side. Unfortunately, a metastasis is seen on the contralateral para-vascular site (**b**) and in a scalenus lymph node on the left side (*arrow*), resulting in an inoperable stage IIIB

For M-staging, in 10%–20% of all patients PET detects unexpected extra-thoracic metastasis not found by other conventional imaging modalities. Furthermore, PET is more accurate than CT in differentiation of benign from malignant adrenal lesions. PET/CT can improve exact localization of FDG-avid lesions as well as their classification (Lardinois et al. 2003).

Regarding recurrent disease, PET has a very high accuracy in the detection of recurrent disease and is significantly better than other imaging modalities such as CT or magnetic resonance imaging (MRI; Patz et al. 1994).

Limitations: false negative PET scans are seen in bronchioloalveolar carcinoma and neuroendocrine tumors (Higashi et al. 1998). False positive lesions, as mentioned above, are seen in active inflammatory disease like tuberculosis, histoplasmosis, and fungal infection.

5.2.2 Recurrent Colorectal Disease

Colorectal carcinoma is the most important cause of death due to cancer in the western world after bronchial carcinoma. During 2001, 56,700 people died in the United States alone, and in the same period 183,900 new cases for cancer of the colon, rectum, or anorectum were registered (ACS 2001). Standard patient work-up for detection of recurrence and metastases in colorectal cancer include regular clinical examination, CT scan, colonoscopy, and usually measurement of tumor markers such as CEA (Delbeke et al. 1997). Serological tumor markers are useful, though the CEA level has only 60%–70% sensitivity for recurrence of colorectal cancers. The morphology-based information in CT does not permit distinction between postsurgical changes and tumor recurrence, nor can it detect tumor involvement of normal-sized lymph nodes (Goldberg et al. 1998).

Several studies have shown the superiority of FDG-PET over conventional imaging modalities in the detection and staging of recurrent colorectal carcinoma. The sensitivity and specificity for the detection of recurrent colorectal cancer range from 93% to 98%, respectively (Flamen et al. 1999; Ruers et al. 2002; Falk et al. 1994). These favorable results are due to two advantages of this imaging

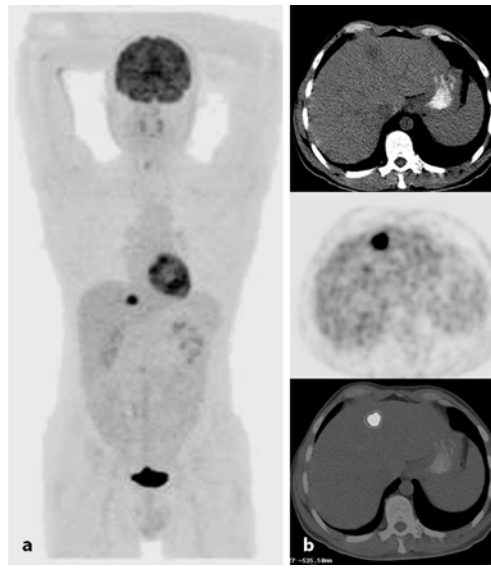

Fig. 2 a, b. A 37-year-old male patient with a history of two meta-chronous colon carcinomas (ascending colon, sigmoid) operated 3 weeks earlier with a suspicious lesion in the liver. FDG-PET-CT reveals focal FDG-uptake in a hypodense lesion in the liver, localized in the left liver (segment 2) with pathological FDG-uptake (**b**; axial image). Otherwise unremarkable PET/CT study

method: FDG-PET detects alterations in tumor metabolism, and it is a whole body imaging technique with relatively high spatial resolution, which can reveal tumor metastases even when morphology is normal. On the other hand, the presence of inflammatory lesions, which also exhibit high FDG-uptake, may lead to false positive results. Another intrinsic disadvantage of FDG-PET is the lack of anatomic landmarks in the image such that even organ borders sometimes cannot be delineated. However, exact anatomical localization of recurrence, e.g., liver involvement versus extra-hepatic localization of tumor burden, represents the most important information when choosing a treatment. PET/CT imaging in restaging colorectal carcinoma improves diagnostic precision compared to PET alone (Fig. 2). The principle advantages of PET/CT imaging are the ability

to correctly localize focal FDG-uptake and to identify pathomorphological structures in anatomical images not seen in PET alone (Burger et al. 2002 b).

5.2.3 Lymphoma

In lymphoma, two groups have to be distinguished: Hodgkin's disease (HD) and non-Hodgkin's lymphoma (NHL). HD, an uncommon lymphoma, accounts for less than 1% of all cases of cancer. More than 70% of all newly diagnosed patients with HD can be cured with combination chemotherapy and/or radiation therapy. Careful staging and treatment planning is required to determine the optimal treatment. NHL lymphomas account for about 5% of all cases of cancer. NHL is less predictable than HD and has a greater predilection to disseminate to extra nodal sites. This disease is divided into two prognostic groups: the low-grade NHL and the aggressive NHL. In general, with modern treatment of patients with NHL, overall survival at 5 years is approximately 50%–60%.

HD and NHL (but not low-grade NHL) show avid FDG-uptake at initial staging (Bangerter et al. 1998; Moog et al. 1997; Stumpe et al. 1998). In most PET studies, both diseases have been studied as one group. In comparison to morphological imaging with contrast-enhanced computed tomography (ceCT), metabolic imaging with FDG-PET showed a higher specificity in staging disease (Moog et al. 1997; Moog et al. 1998 a, b). A major indication for FDG-PET imaging is the evaluation of treatment response after completion of therapy, especially in those patients with residual masses, where it is unclear whether these masses represent tumor persistence (Jerusalem et al. 1999, 2000, 2002). Initial results suggest that PET/CT acquired with a noncontrast-enhanced CT scan is more sensitive and specific than ceCT for the evaluation of lymph node and organ involvement in patients with HD and aggressive NHL, especially regarding exclusion of disease (Schaefer et al. 2003; Fig. 3). However, further prospective studies have to more clearly define the role of PET/CT versus PET and CT in this disease.

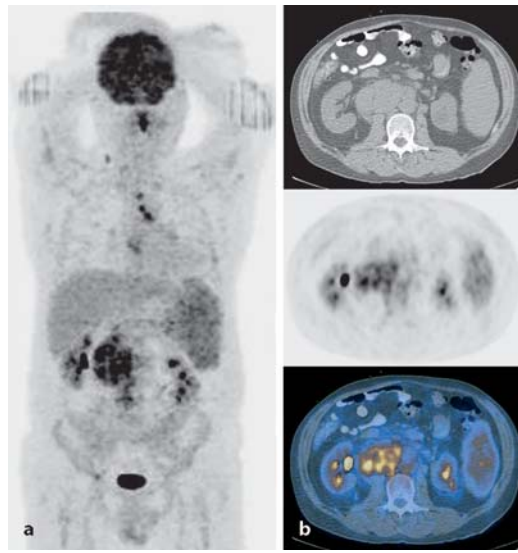

Fig. 3 a, b. A 60-year-old male patient with a Hodgkin's disease stage IIIE. FDG-PET/CT reveals increased FDG-uptake in the spleen (**a**), retroperitoneal lymph nodes (**b**) with clearly enlarged lymph nodes

5.2.4 PET/CT and Head and Neck Cancer

Cancers of the upper aero-digestive tract cause approximately 5% of all cancers with an increasing incidence. Environmental factors, such as alcoholism, smoking, and viruses, such as Herpes or EBV, play a major etiological role in head and neck cancer.

FDG-PET is able to identify primary lesions, lymph node involvement, and distant metastases or secondary tumors in patients with head and neck cancer (Bailet et al. 1992; Adams et al. 1998). PET scanning alone is not suited for T-staging, but is useful for N- and M-staging, crucial for therapy and prognosis. PET is more accurate than CT in the detection of lymph node metastases. Reported sensitivity for node detection at initial staging with PET ranges from 50% to 94% with a specificity ranging from 82% to 100%. In comparison, the sensitivity of CT or MRI ranges from 59% to 86% and the specificity from 25% to 98% (Kau et al. 1999). Distant metasta-

ses or a synchronous secondary cancer are found in approximately 10% of patients at initial staging (Stokkel et al. 1999). Patients with head and neck cancer have a high risk to develop secondary cancers in the aero-digestive tract (head and neck, esophagus and lung). PET/CT scanners can correctly localize lymph node involvement and improve assessment of the primary tumor. Initial results suggest a higher level of confidence using PET/CT compared to PET alone in initial staging of disease. Moreover, PET/CT seems to be equivocal compared to combined analysis of PET alone and ceCT images in initial staging of ENT cancers (Goerres et al. 2003).

5.3 PET/CT and Radiation Treatment Planning

FDG-PET is an established tool for detecting and staging several oncological diseases as mentioned above. The impact of FDG-PET on staging and management in patients referred for radiation treatment has been demonstrated. In a study by Dizendorf et al., in 27% of all patients, FDG-PET findings led to changes in the management in radiation therapy (Dizendorf et al. 2003). Mainly, detection of distant metastases led to cancellation of radiation therapy. In a study by Ciernik et al., volume delineation in plain CT was compared with combined PET/CT in 39 patients. Overall, in 22 patients (56%), gross tumor volume (GTV) was changed significantly. This resulted in changes of the planning target volume (PTV) in 18 of these patients (46%). Further, volume delineation variability was significantly reduced. In this preliminary study, impact on treatment outcome was not assessed (Ciernik et al. 2003).

5.4 PET/CT in Cardiology

To date, coronary angiography is the standard procedure in evaluating coronary artery disease (CAD). Faster scanning and enlarged coverage, allowing acquisition of the entire coronary vasculature using ECG-gated, contrast-enhanced multislice spiral computed tomography (MSCT) have attracted investigators for noninvasive imaging of the coronary vasculature. Concerning both techniques, mor-

phologic angiographic findings are not able to predict the physiologic relevance of a coronary stenosis. Therefore, the concept of coronary flow reserve has been introduced for determination of stenosis severity. This information can be reliably assessed using [^{13}N]ammonia PET imaging of the heart at rest and under stress conditions. Therefore, a combination of MSCT and PET imaging seems to be an optimal approach for noninvasive evaluation of the coronary anato-

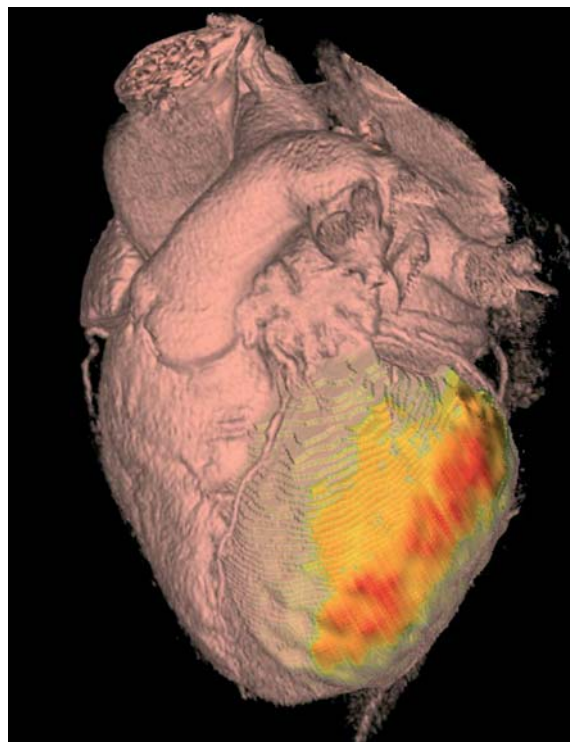

Fig. 4. A 78-year-old male patient with three-vessel coronary artery disease. PET/CT imaging was performed by acquiring contrast-enhanced CT data and [^{13}N]ammonia PET at rest and stress. The figure displays a fused volume-rendered 3-D image of the CT data and the PET flow information. The area in *red* indicates a reduced flow reserve, characteristic of ischemia due to a high-grade stenosis in the left circumflex coronary artery

my and myocardial perfusion. In a study by Namdar et al., PET/CT was compared to CA in the detection of relevant coronary stenosis. Sensitivity and specificity of MSCT alone was lower compared to CA; however, all false-positive findings in MSCT were identified as nonrelevant stenoses by PET imaging, meaning that no ischemia was detected (Fig. 4). A limitation in this study was the suboptimal technique used for MSCT, since only a 4-slice helical CT was available. The encouraging results obtained in this study justify further research to improve the accuracy of PET/CT for the detection of CAD by implementing 8- and 16-slice MSCT scanners into a PET/CT hybrid (Namdar et al. 2003).

5.5 Conclusions

PET/CT is an evolving diagnostic tool, which can be used in three fields in medicine: oncology, radiation treatment planning, and cardiology. In oncology, FDG-PET/CT is practical in the pretherapeutic work-up as well as early and late posttherapy assessment and radiation treatment planning for various cancers. Since state-of-the-art multislice CT scanners are implemented in these systems, any desired contrast-enhanced CT study can be performed and combined with PET information. As a practical application, a combination of contrast-enhanced multislice CT coronary artery imaging and [^{13}N]ammonia PET perfusion data has been successfully achieved.

Future technical developments are aiming to improve hardware performance like higher spatial resolution for PET imaging and faster multislice CT data acquisition. However, a main interest lies within the development of new specific traces like [^{18}N] Choline for prostate cancer imaging (DeGrado et al. 2001).

With PET/CT, combination of molecular imaging and morphology has become clinically routine and may replace single modality imaging in the future.

References

ACS ACS: Cancer Facts & Figures 2001. American Cancer Society, National Home Office, Atlanta, pp 1–44

Adams S, Baum RP, Stuckensen T, et al. (1998) Prospective comparison of ^{18}F-FDG PET with conventional imaging modalities (CT, MRI, US) in lymph node staging of head and neck cancer. Eur J Nucl Med 25:1255–1260

Bailet JW, Abemayor E, Jabour BA, et al. (1992) Positron emission tomography: a new, precise imaging modality for detection of primary head and neck tumors and assessment of cervical adenopathy. Laryngoscope 102:281–288

Bangerter M, Moog F, Buchmann I, et al. (1998) Whole-body 2-[^{18}F]-fluoro-2-deoxy-D-glucose positron emission tomography (FDG-PET) for accurate staging of Hodgkin's disease. Ann Oncol 9:1117–1122

Burger C, Goerres G, Schoenes S, et al. (2002a) PET attenuation coefficients from CT images: experimental evaluation of the transformation of CT into PET 511-keV attenuation coefficients. Eur J Nucl Med Mol Imaging 29:922–927

Burger I, Goerres GW, Von Schulthess GK, et al. (2002b) PET/CT: Diagnostic improvement in recurrent colorectal carcinoma compared to PET alone. Radiology 225:424

Ciernik IF, Dizendorf E, Baumert BG, et al. (2003) Radiation treatment planning with an integrated positron emission and computer tomography (PET/CT): A feasibility study. International Journal of Radiation Oncology Biology Physics 57:853–863

DeGrado TR, Coleman RE, Wang S, et al. (2001) Synthesis and evaluation of ^{18}F-labeled choline as an oncologic tracer for positron emission tomography: initial findings in prostate cancer. Cancer Res 61:110–117

Delbeke D, Vitola JV, Sandler MP, et al. (1997) Staging recurrent metastatic colorectal carcinoma with PET. J Nucl Med 38:1196–1201

Dizendorf EV, Baumert BG, von Schulthess GK, et al. (2003) Impact of whole-body F-18-FDG PET on staging and managing patients for radiation therapy. J Nucl Med 44:24–29

Falk PM, Gupta NC, Thorson AG, et al. (1994) Positron emission tomography for preoperative staging of colorectal carcinoma. Dis Colon Rectum 37:153–156

Flamen P, Stroobants S, Van Cutsem E, et al. (1999) Additional value of whole-body positron emission tomography with fluorine-18–2-fluoro-2-deoxy-D-glucose in recurrent colorectal cancer. J Clin Oncol 17:894–901

Goerres GW, Schmid DT, von Schulthess GK, et al. (2003) FDG PET/CT improves the confidence of anatomic assignment of cancer lesions in the head and neck: a comparison with FDG PET and contrast-enhanced CT. J Nucl Med 44:417–zzz

Goldberg RM, Fleming TR, Tangen CM, et al. (1998) Surgery for recurrent colon cancer: strategies for identifying resectable recurrence and success rates after resection. Eastern Cooperative Oncology Group, the North Central Cancer Treatment Group, and the Southwest Oncology Group. Ann Intern Med 129:27–35

Gupta NC, Maloof J, Gunel E (1996) Probability of malignancy in solitary pulmonary nodules using fluorine-18-FDG and PET. J Nucl Med 37:943–948

Hany TF, Steinert HC, Goerres GW, et al. (2002) PET diagnostic accuracy: improvement with in-line PET-CT system: initial results. Radiology 225:575–581

Higashi K, Ueda Y, Seki H, et al. (1998) Fluorine-18-FDG PET imaging is negative in bronchioloalveolar lung carcinoma. J Nucl Med 39:1016–1020

Huang SC, Phelps ME, Hoffman EJ, et al. (1980) Noninvasive determination of local cerebral metabolic rate of glucose in man. Am J Physiol 238:E69–E82

Jaszczak RJ, Hoffman ED (1995) Positron Emission Tomography (PET): scatter and attenuation, in Wagner HN, Szabo Z, Buchanan JW (eds): Principles of nuclear medicine, 2nd edn. WB Saunders, Philadelphia

Jerusalem G, Beguin Y, Fassotte MF, et al. (2000) Persistent tumor ^{18}F-FDG uptake after a few cycles of polychemotherapy is predictive of treatment failure in non-Hodgkin's lymphoma. Haematologica 85:613–618

Jerusalem G, Beguin Y, Fassotte MF, et al. (1999) Whole-body positron emission tomography using ^{18}F-fluorodeoxyglucose for posttreatment evaluation in Hodgkin's disease and non-Hodgkin's lymphoma has higher diagnostic and prognostic value than classical computed tomography scan imaging. Blood 94:429–433

Jerusalem G, Hustinx R, Beguin Y, et al. (2002) The value of positron emission tomography (PET) imaging in disease staging and therapy assessment. Ann Oncol 13:227–234

Kau RJ, Alexiou C, Laubenbacher C, et al. (1999) Lymph node detection of head and neck squamous cell carcinomas by positron emission tomography with fluorodeoxyglucose F 18 in a routine clinical setting. Arch Otolaryngol Head Neck Surg 125:1322–1328

Kinahan PE, Townsend DW, Beyer T, et al. (1998) Attenuation correction for a combined 3D PET/CT scanner. Med Phys 25:2046–2053

Lardinois D, Weder W, Hany TF, et al. (2003) Staging of non-small-cell lung cancer with integrated positron-emission tomography and computed tomography. N Engl J Med 348:2500–2507

Moog F, Bangerter M, Kotzerke J, et al. (1998a) 18-F-fluorodeoxyglucose-positron emission tomography as a new approach to detect lymphomatous bone marrow. J Clin Oncol 16:603–609

Moog F, Bangerter M, Diederichs CG, et al. (1998b) Extranodal malignant lymphoma: detection with FDG PET versus CT. Radiology 206:475–481

Moog F, Bangerter M, Diederichs CG, et al. (1997) Lymphoma: role of whole-body 2-deoxy-2-[F-18]fluoro-D-glucose (FDG) PET in nodal staging. Radiology 203:795–800

Namdar M, Hany TF, Burger C, et al. (2003) Combined computed tomography-angiogram and positron emission tomography perfusion Imaging for assessment of coronary artery disease in a novel PET/CT: a pilot feasibility study. J Am Coll Cardiol 41:439A

Patz EF, Jr, Lowe VJ, Hoffman JM, et al. (1993) Focal pulmonary abnormalities: evaluation with F-18 fluorodeoxyglucose PET scanning. Radiology 188:487–490

Patz EF, Jr, Lowe VJ, Hoffman JM, et al. (1994) Persistent or recurrent bronchogenic carcinoma: detection with PET and 2-[F-18]-2-deoxy-D-glucose. Radiology 191:379–382

Phelps ME (1981) Positron computed tomography studies of cerebral glucose metabolism in man: theory and application in nuclear medicine. Semin Nucl Med 11:32–49

Ruers TJ, Langenhoff BS, Neeleman N, et al. (2002) Value of positron emission tomography with [F-18]fluorodeoxyglucose in patients with colorectal liver metastases: a prospective study. J Clin Oncol 20:388–395

Schaefer NG, Hany TF, Taverna C, et al. (2003) FDG PET/CT versus contrast enhanced CT in aggressive non-Hodgkin lymphoma and Hodgkin's disease. J Nucl Med 44:272

Stokkel MP, Moons KG, ten Broek FW, et al. (1999) ^{18}F-fluorodeoxyglucose dual-head positron emission tomography as a procedure for detecting simultaneous primary tumors in cases of head and neck cancer. Cancer 86:2370–2377

Stumpe KD, Urbinelli M, Steinert HC, et al. (1998) Whole-body positron emission tomography using fluorodeoxyglucose for staging of lymphoma: effectiveness and comparison with computed tomography. Eur J Nucl Med 25:721–728

Webb WR, Gatsonis C, Zerhouni EA, et al. (1991) CT and MR imaging in staging non-small cell bronchogenic carcinoma: report of the Radiologic Diagnostic Oncology Group. Radiology 178:705–713

Webb WR, Sarin M, Zerhouni EA, et al. (1993) Interobserver variability in CT and MR staging of lung cancer. J Comput Assist Tomogr 17:841–846

6 High Relaxivity Contrast Agents for MRI and Molecular Imaging

S. Aime, A. Barge, E. Gianolio, R. Pagliarin, L. Silengo, L. Tei

6.1 Introduction

The superb spatial resolution and the outstanding capacity of differentiating soft tissues have determined the widespread success of magnetic resonance imaging (MRI) in clinical diagnosis (Young 2000; Rinck 2003). The main determinants of the contrast in an MR image are the proton relaxation times T_1 and T_2. When there is a poor contrast between healthy and pathological regions due to a too-small variation in relaxation times, the use of a contrast agent can be highly beneficial. Contrast agents are chemicals able to alter markedly the relaxation times of water protons in the tissues where they distribute. Their use has led to remarkable improvements in medical diagnosis in terms of higher specificity, better tissue characterization, reduction of image artifacts, and functional information. Depending on whether the dominant effect occurs mainly on T_1 or

T_2, MRI contrast agents can be classified as positive or negative agents, respectively. The most representative class of T_1-positive agents is represented by paramagnetic Gd(III) chelates, whereas iron-oxide particles represent the class of T_2-negative agents (Merbach and Toth 2001).

Currently, about one-third of the MRI scans recorded in clinical settings make use of contrast agents, mainly Gd(III) complexes (Caravan et al. 1999). The effectiveness of a Gd(III) complex to act as MRI contrast agent is first assessed by measuring its relaxivity, i.e., the relaxation enhancement of water protons observed for a millimolar solution of the contrast agent. In the past 15 years, a number of papers addressing the relationship between structure/dynamics and relaxivity of Gd(III) complexes have been published. This has led to a substantial advancement of our understanding of the structural, dynamic, and electronic parameters determining the relaxivity of paramagnetic chelates.

In addition to acting as a catalyst for the relaxation processes of tissutal water protons, a potential MRI-CA has to fulfill several requirements related to tolerance, safety, toxicity, stability, osmolality, viscosity, biodistribution, elimination, and metabolism. The currently used Gd(III) chelates are based on polyaminocarboxylate ligands (Scheme 1), either linear or macrocyclic molecules. All these ligands form very stable complexes (Table 1) so that the risk of dissociation is so low that the danger of acute toxic effects occurring after injection of gadolinium chelates is practically nonexistent with all the products currently in use.

The study of the central nervous system (CNS) is the primary clinical indication for the use of extracellular Gd(III) agents. The majority of these pathologies are brain tumors, and three quarters of them are represented by metastases occurring in patients undergoing treatment for systemic cancer (Fig. 1). Other brain diseases, such as multiple sclerosis and cerebral injuries can be also investigated by contrast-enhanced MRI.

There are several other indications for the use of CAs outside SNC. For instance, in the diagnosis of breast cancer, MRI with contrast agents is becoming an alternative diagnostic procedure to mammography. Particularly interesting is the dynamic use of contrast agents effect. The breast is imaged repeatedly over the first few min-

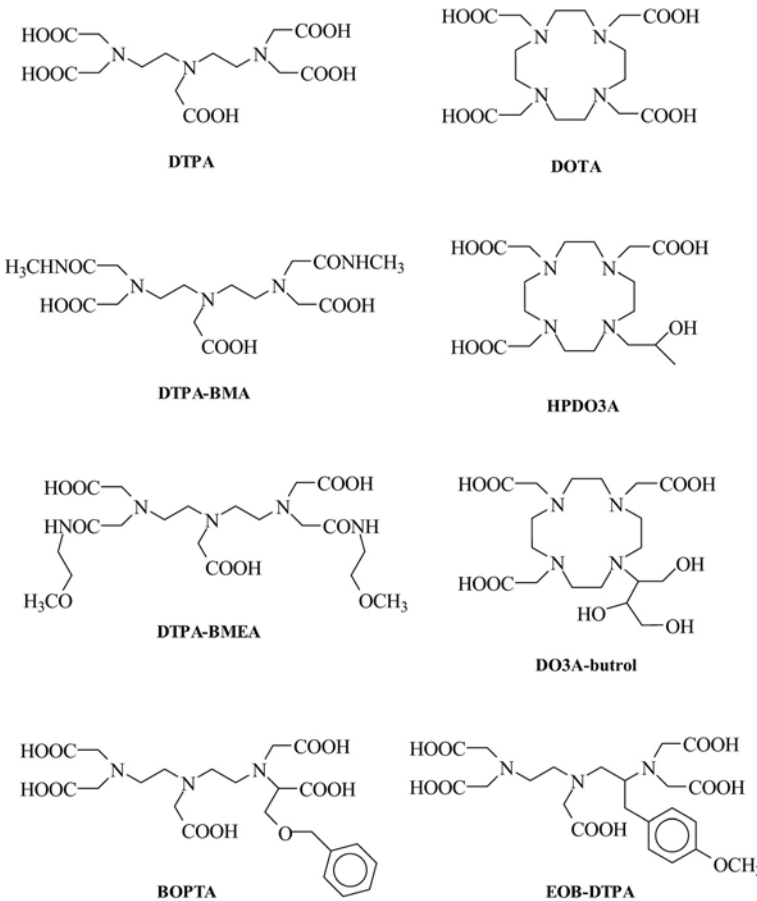

Scheme 1. Polyaminocarboxylate ligands, either linear or macrocyclic, of currently used Gd(III) chelates as commercial MRI contrast agents

utes following contrast agent administration, and a graph reporting the increase of signal for a selected region of interest is plotted as a function of time. The kinetics of the distribution of the contrast agents in the extravascular space is related to the vascular permeability. Neo-formed vessels functional to the tumor growth display a permeability much higher than normal capillaries and the corresponding

Table 1. Clinically accepted Gd(III)-based contrast agents

Complex	Brand name	Company	Log K_{GdL} (8)
Gd-DTPA	Magnevist	Schering	22.5
Gd-DOTA	Dotarem	Guerbet	24.7
Gd-HPDO3A	ProHance	Bracco	23.8
Gd-DO3A-butrol	Gadovist	Schering	20.8
Gd-DTPA-BMA	Omniscan	Nycomed-Amersham	16.8
Gd-DTPA-BMEA	OptiMARK	Mallinckrodt	16.8
Gd-BOPTA	MultiHance	Bracco	22.6
Gd-EOB-DTPA	Eovist	Schering	23.5

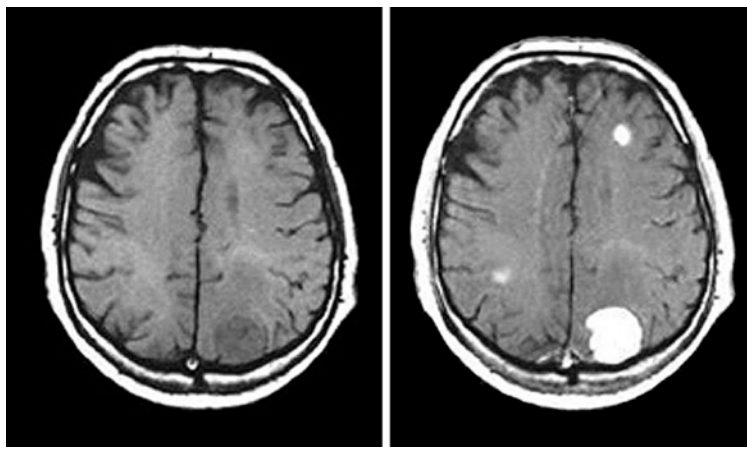

Fig. 1. Metastases in the brain of a patient with brain tumor. The metastases are detected upon intravenously administration of GdDTPA (*right*). Blood vessels (capillaries) are typically quite leaky to small molecules like GdDTPA, allowing them to enter the extracellular space. In the brain, however, the cells forming the walls of capillaries have very tight junctions and prevent small molecules leaving the intravascular space, thereby forming a blood-brain barrier (BBB). Tumors and other pathologies of CNS cause impairment of the BBB, thus allowing the contrast agent to leak from capillaries into extracellular fluid

areas are therefore characterized by high signal intensity (Padhani 2002). Of course, dynamic enhanced MRI is applied to demonstrate the aggressive nature of tumors in several other areas.

The new landscape of molecular imaging applications requires the development of a novel class of CAs characterized by higher contrasting ability and improved targeting capabilities. In this survey, we intend to tackle some basic issues that are of fundamental importance for the use of Gd(III)-based systems in molecular imaging applications, namely: (1) actual understanding of the determinants of T1-relaxivity of Gd(III) complexes, and how to proceed to attain very high relaxivities; (2) how one may envisage efficient routes for the delivery of a high number of Gd(III) complexes at the site of interest; and (3) the most practical ways to pursue the cell-internalization of a high number of Gd(III) complexes.

6.2 Determinants of Relaxivity

First of all, any MRI CA should be endowed with high thermodynamic and kinetic stability, and have at least one water molecule coordinated to the metal ion in fast exchange with the bulk water. This would allow strong influence over the relaxation process of all protons present in the solvent in which the CA is dissolved. The Gd(III) chelate efficiency is commonly estimated in vitro through the measure of its relaxivity (r_1); that for commercial CAs as Magnevist, Dotarem, Prohance, and Omniscan is around 3.4–3.5 mM^{-1} s^{-1} (at 20 MHz and 39 °C). The observed longitudinal relaxation rate (R_1^{obs}) of the water protons in an aqueous solution containing the paramagnetic complex is the sum of three contributions (Banci et al. 1991): (a) the diamagnetic one, whose value corresponds to proton relaxation rate measured in the presence of a diamagnetic (La, Lu, Y) complex of the same ligand; (b) the paramagnetic one, relative to the exchange of water molecules from the inner coordination sphere of the metal ion with bulk water (R_{1p}^{is}); and (c) the paramagnetic one relative to the contribution of water molecules that diffuse in the external coordination sphere of the paramagnetic center (R_{1p}^{os}). Sometimes also a fourth paramagnetic contribution is taken in account, that is due to the presence of mobile protons or water molecules

(normally bound to the chelate through hydrogen bonds) in the second coordination sphere of the metal (Botta 2000). The inner sphere contribution is directly proportional to the molar concentration of the paramagnetic complex, to the number of water molecules coordinated to the paramagnetic center, q, and inversely proportional to the sum of the mean residence lifetime, τ_M, of the coordinated water protons and their relaxation time, T_{1M}. This latter parameter is directly correlated to the sixth power of the distance between the metal center and the coordinated water protons and depends on the molecular reorientational time, τ_R, of the chelate, on the electronic relaxation times, T_{iE} ($i = 1, 2$), of the unpaired electrons of the metal (which depend on the applied magnetic field strength) and on the applied magnetic field strength itself (Fig. 2). The outer sphere contribution depends on T_{iE}, on the distance of maximum approach between the solvent and the paramagnetic solute, on the relative diffusion coefficients and again on the magnetic field strength (Aime et al. 1998). The dependence of R_{1p}^{is} and R_{1p}^{os} on magnetic field is very

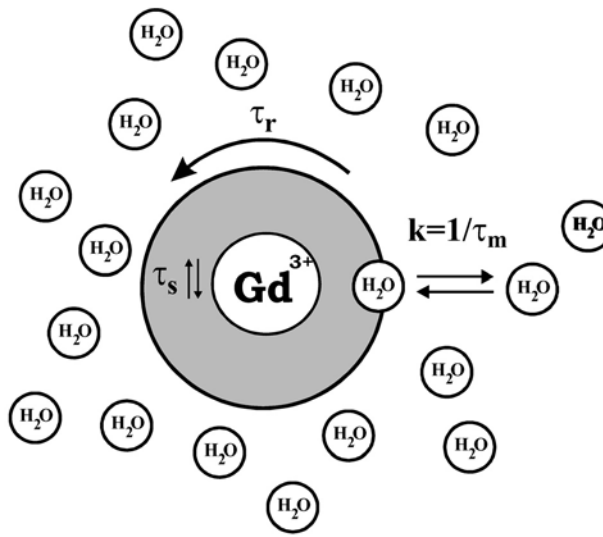

Fig. 2. Schematic representation of relaxation mechanism in an aqueous solution containing a Gd(III)-complex

important because from the analysis of the magnetic field dependence allows the determination of the principal parameters characterizing the relaxivity of a Gd(III) chelate. This information can be obtained through an NMR instrument in which the magnetic field is changed (Field-Cycling Relaxometer) to obtain the measure of r_1 on a wide range of frequencies (typically 0.01–50 MHz). At the frequencies most commonly used in commercial tomographs (20–63 MHz), r_1 is generally determined by the τ_R of the chelate so that high molecular weight systems display a higher relaxivity. A quantitative analysis of r_1 dependence on the different structural and dynamic parameters shows that, for systems with long τ_R (e.g., protein bound complex), the maximum attainable r_1 values can be achieved through the optimization of τ_M and T_{ie} (Banci et al. 1991).

6.3 How to Improve Relaxivity?

6.3.1 Interactions of Gd(III) Complexes with Proteins

Upon interacting with a macromolecule, the relaxation induced by Gd(III) chelates usually displays remarkable changes, primarily related to the increase of the molecular reorientational time τ_R on going from the free to the bound form, which results in a marked increase of the inner sphere R_1^{is} term. From the measurement of the relaxivity enhancement, it is possible to assess the affinity (and the number of binding sites) between the interacting partners (Dwek 1973). Quantitatively, in the presence of a reversible interaction between the paramagnetic species and the macromolecule, the observed enhancement depends on both the molar fraction of the macromolecular adduct χ^b and the relaxivity of the paramagnetic species bound to the macromolecule in the all-bound limit (r_1^b).

Human serum albumin (HSA) has been by far the most investigated protein for binding of Gd(III) chelates. Besides the attainment of high relaxivities, a high binding affinity to HSA enables the Gd(III) chelate with a long intravascular retention time, which is the property required for a good blood-pool agent for MR angiography. In blood, HSA has a concentration of about 0.6 mM and its main physiological role deals with the transport of a huge number of sub-

Table 2. Affinity constant and relaxivity of the adducts of some Gd(III) complexes wiht HSA, calculated at 0.47 T and 298 K. The coordinated water exchange lifetime of free complexes is also reported

Metal complex	$n \times K_A$ (M^{-1})	r_1^b ($mM^{-1}s^{-1}$)	τ_M (ns)	Reference
$[Gd\text{-}DOTA(BOM)(H_2O)]^-$	$<1 \cdot 10^2$			Aime 1996 a
Cis-$[Gd\text{-}DOTA(BOM)_2(H_2O)]^-$	$6.4 \cdot 10^2$	35.2	175	Aime 1996 a
Trans-$[Gd\text{-}DOTA(BOM)_2(H_2O)]^-$	$7.2 \cdot 0^2$	44.2	130	Aime 1996 a
$[Gd\text{-}DOTA(BOM)_3(H_2O)]^-$	$3.4 \cdot 10^3$	53.2	80	Aime 1996 a
MS-325	$3.0 \cdot 10^4$	35.0	250	Aime 1999 c
$[Gd\text{-}BOPTA\ (H_2O)]^{2-}$	$4.0 \cdot 10^2$	33.0	280	Aime 2001; Aime 1999 b
$[Gd\text{-}DTPA(BOM)_2(H_2O)]^{2-}$	$3.6 \cdot 10^3$	28.2	260	Aime 2001; Aime 1999 b
$[Gd\text{-}DTPA(BOM)_3(H_2O)]^{2-}$	$4.0 \cdot 10^4$	44.0	180	Aime 1999 c
$[Gd\text{-}DOTA\text{-}IOP(H_2O)]^-$	$6.2 \cdot 10^2$	24.1	730	Aime 2001
$[Gd\text{-}DOTA\text{-}IOPsp(H_2O)]^-$	$2.9 \cdot 10^3$	20.8	550	Aime 2001
$[Gd\text{-}DOTA\text{-}TIBsp(H_2O)]^-$	$5.3 \cdot 10^2$	23.2	630	Aime 2001
$[Gd\text{-}DTPA\text{-}IOP(H_2O)]^{2-}$	$3.8 \cdot 10^2$	16.1	860	Aime 2001
$[Gd\text{-}DTPA\text{-}IOPsp(H_2O)]^{2-}$	$4.8 \cdot 10^3$	19.9	630	Aime 2001

strates (Carter and Ho 1994). For many of them, the binding region has been identified on the basis of extensive competitive assays. Now, the availability of solid state X-ray crystal structure of HSA allows more insight into the structural details of the binding interaction. The information gained from the studies of the interaction of the various substrates to HSA has been very important in addressing the design of Gd(III)-based blood-pool agents.

In Table 2 a list of Gd(III) complexes and the relevant parameters of their binding interaction to HSA are reported.

Although the theory of the paramagnetic relaxation foresees relaxivities up to 100–120 $mM^{-1}\ s^{-1}$ (at 20 MHz) for complexes bound to macromolecular systems, the data listed in Table 1 show r_1^b values significantly lower than the predicted ones. The primary reason for the quenching of the relaxation enhancement is often associated to the occurrence of a long exchange lifetime, τ_M, of the coordinated water. This may be easily checked by measuring the relaxivity as a function of temperature. The detection of a higher r_1^b value as the

temperature is increased is an unambiguous indication of the occurrence of a too-long τ_M value.

6.3.2 Effect of the Water Exchange Rate on Relaxivity

Slow rates of the coordinated water appear to be primarily characteristic of the complex rather than a consequence of the binding to the protein. Thus, for the attainment of high relaxivities, one has to avoid Gd(III) chelates displaying slow exchange rates. The rational which accounts for the water exchange rates in linear and cyclic polyaminocarboxylate Gd(III) complexes has been elucidated in a number of systems (Aime et al. 2001; Powell et al. 1996). In short, the water-exchange process for the enneacoordinate Gd(III) complexes follows an idealized dissociative pathway. This may be represented by a simple diagram involving the transition state where the metal ion has reduced its coordination number from 9 to 8 (Fig. 3).

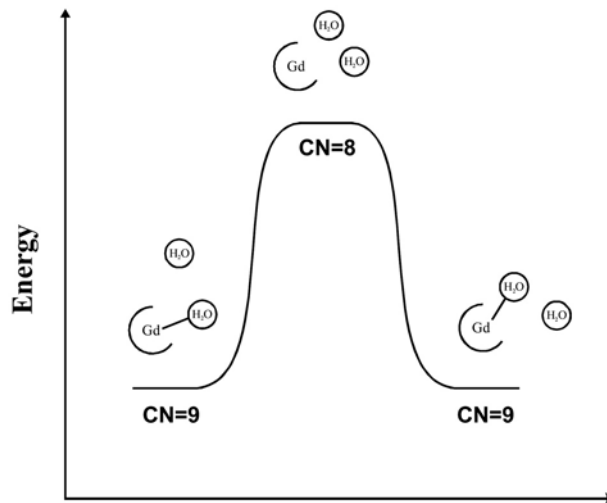

Fig. 3. Energy diagram for the idealized dissociative water exchange mechanism in enneacoordinate Gd(III) complexes

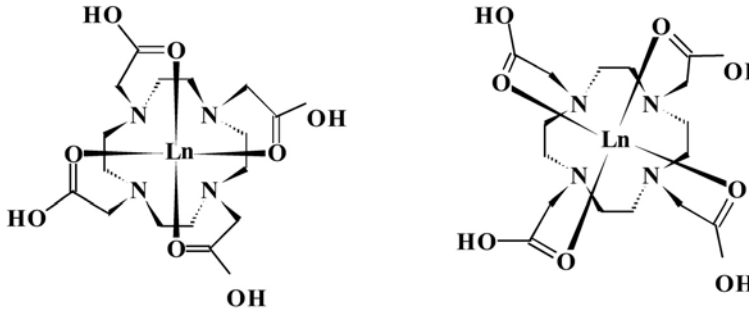

Fig. 4. Structure of the Square Antiprismatic (SA) and Twisted Square Antiprismatic (TSA) isomers in lanthanide DOTA-like complexes

It follows that fast exchange rates can be pursued by decreasing the activation energy and this goal can be addressed either by destabilizing the ground state or stabilizing the intermediate state. Moreover, it has been shown that for DOTA-like systems there is a subtle structural relationship between the exchange rate of the coordinated water and the actual isomeric form. In fact, this class of complexes exists in solution as a mixture of two structural isomers, namely the square antiprismatic (AP) and the twisted square antiprismatic (TAP) isomer (Fig. 4; Aime et al. 1992).

The polyhedron of the AP isomer corresponds closely to the regular square antiprismatic geometry, whereas a twisted square antiprismatic coordination cage with a smaller tilt angle between the two square planes is assigned to the TAP isomer. The latter isomer displays a water exchange rate that is approximately 50 times faster than the corresponding rate in the AP isomer (Aime et al. 1999 a).

Thus, given the above considerations, the functionalization of a ligand for protein targeting requires the choice of a Gd(III) chelate that displays a fast exchange rate of the coordinated water.

In order to get more insight into the problem of why the relaxivity values obtained up to now are significantly lower than those predicted by the theory of paramagnetic relaxation, we have recently

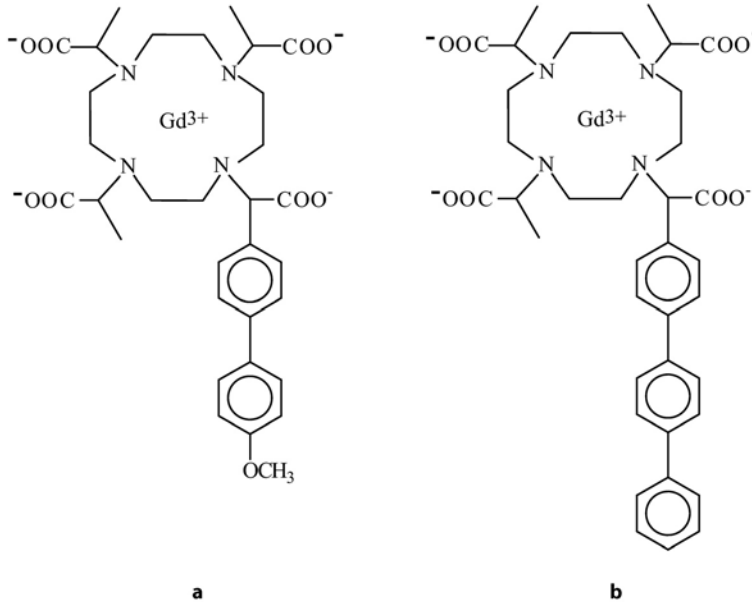

Fig. 5. Structure of two DOTMA derivatives

undertaken a detailed relaxometric study of the interaction of Gd-DOTMA derivatives with HSA (Aime et al., to be published). Gd-DOTMA displays a relatively fast exchange of the coordinated molecule, likely because it possesses a TAP-like structure as shown by ^{1}H-NMR spectra of the Eu(III) and Yb(III) analogs (Aime et al. 1996b; Di Bari et al. 2000). Two new ligands based on DOTMA structure have been synthesized (Fig. 5). ^{1}H-NMR spectra of Eu(III) complexes showed that the TAP geometry found for the parent DOTMA complexes is maintained. Complex A is soluble enough to allow the determination of the water exchange rate by ^{17}O-T_2 measurements at variable temperature. The obtained value ($\tau_M^{298} = 65$ ns) indicates that the replacement of the methyl with the bulkier bis-Phenyl group does not affect the coordination cage, leaving unchanged the water exchange rate. The solubility of complex B was too low to pursue such measurement, but we may safely assume that its τ_M^{298} is similar to that determined for A.

Both A and B binds strongly to HSA, yielding K_a values of 2.7×10^3 M^{-1} and 9.5×10^4 M^{-1} respectively. r_1^b of the A/HSA adduct, at 298 K and 20 MHz, is equal to 35 mM^{-1} s^{-1}. ^{17}O-measurements showed no difference between solutions containing the paramagnetic adduct and HSA alone. Clearly, the expected relaxation enhancement has been "quenched" by a direct interference of the donor groups on the surface of the protein with the inner hydration sphere of the Gd(III) ion. We could not determine whether it results in a replacement of the inner sphere water or simply in a dramatic elongation of its exchange lifetime. Thus, the bis-phenyl moiety does not appear long enough to protrude the chelate moiety outside the interference of the residues on the surface of the protein in proximity of the binding site. However, it is worthwhile to note that the observed relaxation enhancement is due to water molecules/mobile protons on the surface of the protein.

B contains a binding synthon made of three phenyl groups and resulted long enough to avoid such interference. Unfortunately, the low solubility of the adduct prevented the acquisition of ^{17}O-NMR VT spectra, but we got an indirect assessment of the occurrence of the fast exchange of the coordinated water by measuring the water proton relaxation rates as a function of temperature. As shown in Fig. 6, the observed relaxation rate displays an exponential decrease as the temperature increases, i.e., the typical behavior expected for systems not "quenched" by long exchange lifetimes of the coordinated water. However, the observed r_1^b for B/HSA adduct is only 43.5 mM^{-1} s^{-1}, whereas the theory predicts much higher values (Fig. 6) for a system tumbling with the τ_R of HSA (30 ns) and the τ_M value of Gd-DOTMA.

We surmise that the limited relaxation enhancement has to be associated to a molecular reorientational correlation time, for the coordinated water, that is significantly shorter than that one of the macromolecule. This should not depend on an internal motion of the chelate as the binding through the tris-phenyl substituent is tight enough. Rather, the observed behavior should be related to an internal rotation of the coordinated water along its coordination axis, which overlaps with the overall motion of macromolecular adduct. If this suggestion is correct, a challenging question is posed to chemists: how to design a Gd-chelate whose coordinated water is in fast ex-

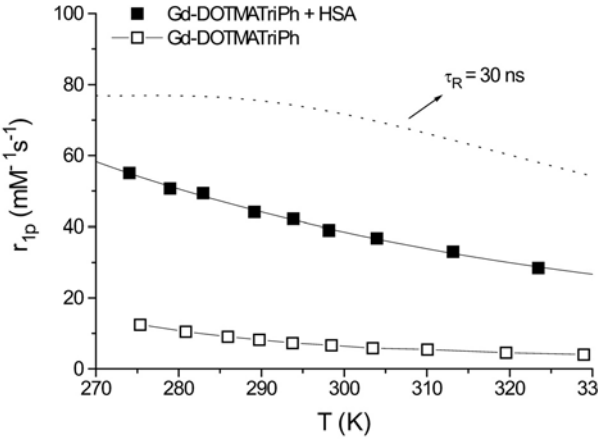

Fig. 6. Longitudinal proton relaxivity as a function of temperature of free complex B (*white boxes*) and of the adduct complex B/HSA (*black boxes*). The *dotted line* represents a simulation of the expected profile with $\tau_R = 30$ ns and $\tau_M = 65$ ns

change with the bulk (short τ_M) and "rigid" inside the coordination cage?

6.4 Targeting Cells with Gd(III) Chelates

Molecular imaging (Weissleder and Mahmood 2001) deals with in vivo characterization and measurement of biological processes at the cellular and molecular level. With molecular imaging, early diagnosis of disease will become possible as the detection of altered biochemical processes largely anticipates the anatomical changes that are at the basis of current diagnostic modalities.

Several modalities have contributed to the early stages of this innovative approach, namely PET, SPECT, MRI, and optical imaging. MRI-Gd(III)-based agents are much less sensitive than radionuclear and optical imaging probes. Therefore, molecular imaging based on MRI invariantly involves the need of accumulating a high number of contrast-enhancing units at the site of interest. The basis for the design of a Gd-containing imaging probes is first dictated from the

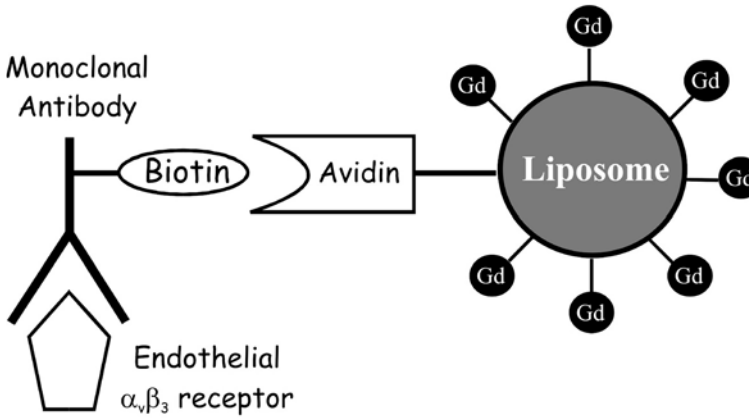

Fig. 7. Targeting of the endothelial integrin $\alpha_v\beta_3$ as a specific angiogenesis marker. The receptor is recognized by a biotinylated antibody that is then bound by an avidin moiety bearing a Gd(III)-loaded liposome

concentration and localization (vascular, extracellular matrix, on the cellular membrane, intracellular) of the target molecule (Aime et al. 2002 a). Of course, the most accessible targets are those present on the surface of endothelial vessels. In principle, they can be visualized by a number of macromolecular conjugates containing many Gd(III) complexes endowed with the proper vector recognizing the given target. A nice example of targeting an endothelial site has been reported by Sipkins et al. (1998) in the targeting of a specific angiogenesis marker, the endothelial integrin $\alpha_v\beta_3$, whose presence has been shown to correlate with tumor grade. The imaging probe used in this work is a Gd-containing polymerized liposome. The target is first bound by a biotinylated antibody against $\alpha_v\beta_3$, which is successfully recognized by an avidin moiety on the surface of the liposome. Each liposome has a mean diameter of 300–350 nm, which appears suitable to avoid the uptake by the reticuloendothelial system (Fig. 7). This approach provided enhanced and detailed detection of rabbit carcinoma through the imaging of the angiogenetic vasculature.

Recently, the same $\alpha_v\beta_3$ target has been addressed with lipidic nanoparticles containing a huge number of Gd-chelated units [94,400 Gd/

particle characterized by $r_1 = 19.1\ s^{-1}mM^{-1}$ (per Gd), $r_1 = 1{,}800{,}000$ per particle]. One of the lipidic components is covalently bound to the $\alpha_v\beta_3$-integrin peptidomimetic antagonist (Winter et al. 2003).

The large molecular size of these constructs limits their delivery to targets on the endothelial walls. To target receptors in solid tissues, other routes have to be followed. Bhujwalla and coworkers (2003) have recently developed and applied a two-component Gd-based avidin-biotin system for the visualization of HER-2/scan receptors. The latter is a member of the epidermal growth factor family and it is amplified in multiple cancers. Their approach consisted of addressing the extracellular domain of the receptors by means of a biotinylated mAb. After clearance of the unbound mAb, Gd-labeled avidin is administered and binds, with high affinity, to the biotinylated mAb. The expression level of the receptor was estimated at 7×10^5 receptors/cell and the average number of Gd-DTPA units per avidin molecule was 12.5. The method has been successfully applied in an experimental mouse model of breast carcinoma.

An interesting route to MR signal amplification has been developed by Weissleder and coworkers (2002). Their approach is based on enzyme-mediated polymerization of paramagnetic substrates into oligomers of higher relaxivity. As substrates they used Gd-chelates functionalized with phenolic substituents which undergo rapid condensation in the presence of H_2O_2 and peroxidase. The increased molecular size of the oligomeric structures causes an increase of the molecular reorientational time which, in turn, results in an increase of the observed relaxivity. This approach has been applied to the imaging of E-selectin-peroxidase conjugate.

As far as the cell internalization of Gd-chelates is concerned, several routes have been explored:

1. Via Pinocytosis. Pinocytosis is the cell-internalized portion of the surrounding fluid by means of the invagination of its membrane and formation of small vesicles ($\leq$150 nm diameter) called endosomes. Therefore, incubation of cells, for a sufficiently long time, in a medium containing the imaging probe at relatively high concentration leads to its internalization at amounts that may be sufficient for MRI visualization. Among a number of systems we have considered, the neutral, highly hydrophilic GdHPDO3A is a good candidate for la-

beling stem cells by the pinocytotic route (Aime et al., in press). The in vivo MR visualization of labeled stem cells will allow their monitoring after transplantation. In a typical experiment of uptake via pinocytosis, a few million stem cells are incubated in a culture medium containing GdHPDO3A in mM concentration range (10–50 mM) for few hours. Upon incubation no saturation effect is observed and the amount of taken up Gd is linearly proportional to the concentration of the paramagnetic agent in the incubation medium. Once cell internalized, the GdHPDO3A molecules end up entrapped in endosomic vesicles as can be seen by observing the cells incubated with EuHPDO3A at the confocal microscope. In fact, Gd and Eu chelates with the same ligands display the same chemical/biological behavior, and the fluorescent response of EuHPDO3A acts as a histological reporter of the localization of GdHPDO3A in the cell. We have proved the potential of this approach by observing a mouse model of angiogenesis, on which blood-derived endothelial progenitor cells (EPCs) have been implanted subcutaneously, within a matrigel plug. After few days, the histologic examination showed large capillary structure transposing the gel plugs. MR images parallel histologic findings as hyperintense spots corresponding to the labeled cells were clearly detected. In Figure 8, we report a MR image taken 14 days after implantation. As control, matrigel-embedding unlabelled cells implanted in the same conditions are always negative for MRI signal.

The cell-labeling procedure described above appears to have general applicability. We have tested it on several tumor cell lines, obtaining invariantly a very efficient uptake with no apparent cytotoxicity. Likely, the entrapment of GdHPDO3A into the endosomic vesicles prevents any impact of the paramagnetic agent on relevant cellular process, meanwhile maintaining the full accessibility to cytoplasmatic water molecules.

2. Via Phagocytosis. Phagocytosis is the process of internalization of particles by cells endowed with phagocytic activity. In such a case, this route appears highly efficient for a single-step internalization of a large amount of imaging probes. However, to be effective on MR images, Gd-chelates must be water soluble. Therefore, the particles must be biodegradable in order to release soluble Gd chelates once

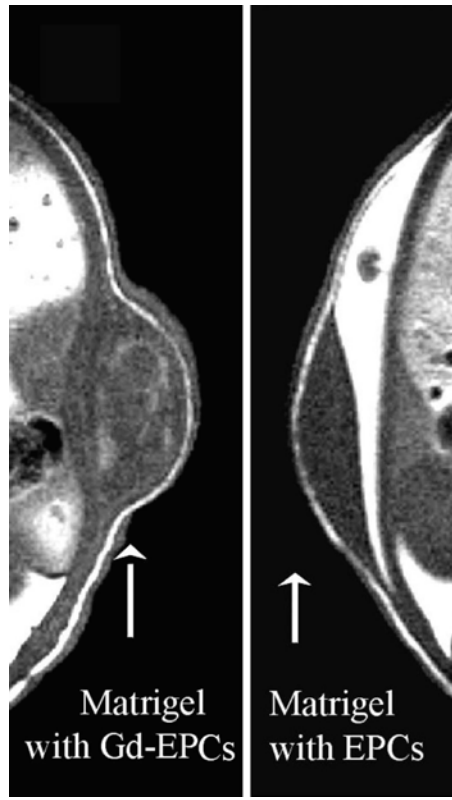

Fig. 8. In vivo T_1-weighted spin echo MR image (7.05 T) of EPCs labeled with GdHPDO3A (*left*). The cells are dispersed into a subcutaneous matrigel plug 7 days after the implantation. On the *right* is the control image of the same in the absence of the paramagnetic label

internalized into phagocytic cells. One may envisage several ways for the release of the Gd chelates. For instance, one may think of gel nano-particles of chitosan loaded with negatively charged Gd-chelates. Such particles (200–400 nm diameter) are easily phagocytosed and slowly degraded once internalized into the cells (S. Aime et al., unpublished results). Another approach to biodegradable Gd-containing particles has been pursued by designing particles whose

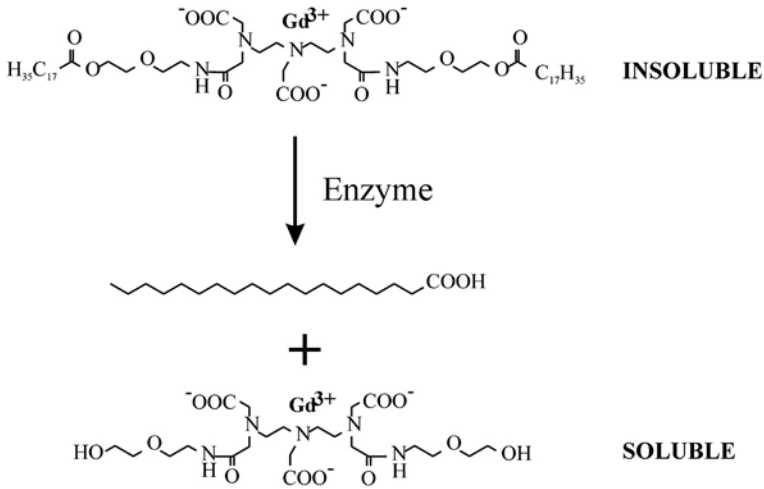

Fig. 9. The insoluble system is represented by a Gd-DTPA-like complex functionalized with a long aliphatic chain which is bound to the chelate moiety through an ester bond. The solubilization is obtained through the enzymatic cleavage of the ester bonds yielding to a soluble Gd(III) complex

insolubility is a property of the Gd-chelates themselves (Aime et al. 2002b). This goal is easily reached by introducing long aliphatic chains on the surface of the ligand. However, one can control the fate of these systems by means of the functionality used to link the insolubilizing moiety to the Gd-chelate. In fact, by using ester or peptidic functionalities, the insolubilizing synthon can be displaced from the Gd chelates by the activity of the proper enzyme (Fig. 9).

3. Via Receptors. Cell-internalization *via* receptors is the route of choice in a number of nuclear medicine assays. For MRI, the design of the imaging probe requires the attachment of one or more Gd(III)-chelates to the ligand molecule. Such structural modification may drastically affect the internalization process with respect to the mechanism occurring for the native ligand.

In order to deal with a system whose structural characteristics were unaltered by the loading with Gd(III) chelates, we choose Apoferritin because it allows the imaging probes to be entrapped inside

its inner cavity (Aime et al. 2002b). The exterior of such Gd(III)-loaded Apoferritin is exactly the same as in the parent Ferritin and then, once administered intravenously, it is quickly cleared-up by the proper receptors on hepatocytes (Osterloch et al. 1996). The process of loading Apoferritin with GdHPDO3A first entails the dissociation of the protein into subunits at pH 2 followed by its reforming at pH 7, thereby trapping the solution components (e.g., GdHPDO3A) within its interior. In such a system, water can freely diffuse through the channels formed at the intersection of the protein subunits (10 channels), but the larger GdHPDO3A molecules cannot. The relaxivity shown by each GdHPDO3A entrapped in the Apoferritin cavity is very high (approximately 80 s^{-1} mM Gd^{-1} at 20 MHz and 25 °C). It has been possible to assess that the Gd-loaded Apoferritin maintains its integrity upon the cell internalization process as the relaxivity observed for the cytoplasmatic extract corresponds to that of the intact system. Finally, the amount of cell-internalized Gd-loaded Apoferritin is similar to that reported for the native Ferritin (6.5×10^6 molecules per cell in 6 h).

4. Via Receptor-Mediated Endocytosis. This is probably the most common route for the internalization of Gd(III) chelates as it is expected to occur any time a given ligand is modified by attaching one or more Gd-chelating units. Thus, the internalization process is no longer the one followed by the native ligand but the binding to the receptor stimulates an endocytotic process which starts with the introflection of a portion of cellular membrane and ends up with the welding of its extremities. Through this process, a number of substances remain entrapped in endosomic vesicles, primarily the molecules bound to the membrane or in close proximity of the portion of membrane involved in the endosome formation.

Weiner et al. (1997) showed that the uptake of a folate-conjugate dendrimer into tumor cells overexpressing high affinity folate receptor (hFR) occurs through this type of endocytotic pathway.

Another example of receptor-mediated endocytosis of a large dendrimer has been recently reported (Kobayashi and Brechbiel 2003). The macromolecular construct comprised of Avidin and a biotinylated dendrimer bearing 254 GdDTPA chelates (AV-G6Gd) has shown to accumulate in vitro into SHIN3 cells (a cell line obtained

originally from human ovarian cancer) 50-fold greater than GdDTPA. The internalization process is driven by avidin molecule, a glycoprotein that binds to β-D-galactose receptors which are present on these tumor cells.

Although not yet proven, it is likely that receptor-mediated endocytosis occurs with a number of systems in which the imaging Gd-probes are linked either to peptides as targeting vectors that bind to specific receptors or to nutrient or pseudo-nutrient moieties that interact with the proper transporter upregulated in tumor cells.

5. Via Transmembrane Carrier Peptides. Another route to enter cells with Gd(III) chelates is based on the use of membrane translocation peptides which have been proven useful for the internalization of a number of substrates like proteins, oligonucleotides, and plasmid DNA. For instance, Bhorade et al. (2000) showed that GdDTPA bound to 13-merHIV-tat peptide is efficiently internalized.

Another example has been recently reported by Allen and Meade (2003), who showed that GdDTPA conjugated to polyarginine (8–16 monomer units) is able to permeate all membranes.

Finally, along this line, an interesting development has been recently reported by Heckl et al. (2003). They synthesized an imaging probe consisting of a Gd-complex, a PNA (Peptide Nucleic Acid) sequence, and a transmembrane carrier peptide. Although the systems enters any type of cell, it accumulates only in tumor cells because of the specific binding of the PNA moiety for the c-*myc* mRNA whose production is upregulated in those cells.

6.5 Concluding Remarks

Gd(III) chelates have played an important role in the development of clinical applications of MRI technique by adding relevant physiological information to the superb anatomical resolution attainable with this imaging modality.

More is still expected with the currently available contrast agents, especially in the field of dynamic contrast enhancement protocols reporting on changes of the vascular permeability associated with the staging and therapeutic follow-up of important pathologies. How-

ever, the major challenges are in the emerging field of molecular imaging where the competition with other imaging modalities can be very tight. Targeting of thrombi and atherosclerotic plaques by peptides functionalized with Gd(III) chelates appears to be the next goal for industrial research. The possibility of identifying and characterizing vulnerable plaques will certainly represent an important task. Clearly, there is a need for new ideas for enhancing the attainable relaxivity at higher fields as the 3-T indication for clinical imagers seems to be quite established. Moreover, it will be necessary to improve the efficiency of the available delivery systems and, possibly, to exploit suitable amplification procedures in order to reach the sensitivity required for the visualization of target molecules present at low concentrations.

The results herein surveyed show that there are several routes for cell entrapment of paramagnetic Gd-agents at concentrations sufficient for MRI visualization. The huge work carried out in a number of laboratories in the last two decades for the development of Gd-based MRI contrast agents provides an excellent platform for designing a new generation of probes for molecular imaging applications. Though one should not underestimate the difficulties that will arise when going from in vitro experiments to in vivo animal studies, we think that the available results suggest that Gd-chelates will have an important role in the armory of imaging probes for cellular and molecular imaging applications.

References

Aime S, Botta M, Ermondi G (1992) Nmr-study of solution structures and dynamics of lanthanide(III) complexes of dota. Inorg Chem 31:4291–4299

Aime S, Botta M, Fasano M, Geninatti Crich S, Terreno E (1996a) Gd(III) complexes as contrast agents for magnetic resonance imaging: a proton relaxation enhancement study of the interaction with human serum albumin. J Biol Inorg Chem 1:312–319

Aime S, Botta M, Fasano M, Terreno E, Kinchesh P, Calabi L, Paleari L (1996b) A new ytterbium chelate as contrast agent in chemical shift imaging and temperature sensitive probe for MR spectroscopy. Magn Res Med 35:648–651

Aime S, Botta M, Fasano M, Terreno E (1998) Lanthanide(III) chelates for NMR biomedical applications. Chem Soc Rev 27:19–29

Aime S, Barge A, Bruce J, Botta M, Howard JAK, Moloney JM, Parker D, de Sousa AS, Woods M (1999a) NMR, relaxometric, and structural studies of the hydration and exchange dynamics of cationic lanthanide complexes of macrocyclic tetraamide ligands. J Am Chem Soc 121:5762–5771

Aime S, Botta M, Fasano M, Terreno E (1999b) Prototropic and water-exchange processes in aqueous solutions of Gd(III) chelates. Acc Chem Res 32:941–949

Aime S, Chiaussa M, Digilio G, Gianolio E, Terreno E (1999c) Contrast agents for magnetic resonance angiographic applications: H-1 and O-17 NMR relaxometric investigations on two gadolinium(III) DTPA-like chelates endowed with high binding affinity to human serum albumin. J Biol Inorg Chem 4:766–774

Aime S, Fasano M, Terreno E, Botta M (2001) In: Merbach AE, Tóth E (eds) The chemistry of contrast agents in medical magnetic resonance imaging. Wiley, Chichester, pp 193–241

Aime S, Cabella C, Colombatto S, Crich SG, Gianolio E, Maggioni F (2002a) Insights into the use of paramagnetic Gd(III) complexes in MR-molecular imaging investigations. J Magn Reson Imaging 16:394–406

Aime S, Frullano L, Geninatti Crich S (2002b) Compartmentalization of a gadolinium complex in the apoferritin cavity: A route to obtain high relaxivity contrast agents for magnetic resonance imaging. Angew Chemie Int Ed 41:1017–1019

Allen MJ, Meade TJ (2003) Synthesis and visualization of a membrane-permeable MRI contrast agent. J Biol Inorg Chem 8:746–750

Banci L, Bertini I, Luchinat C (1991) Nuclear and electronic relaxation. VCH, Weinheim, pp 91–122

Bhorade R, Weissleder R, Nakakoshi T, Moore A, Tung CH (2000) Macrocyclic chelators with paramagnetic cations are internalized into mammalian cells via a HIV-tat derived membrane translocation peptide. Bioconjugate Chem 11:301–305

Bhujwalla ZM, Artemov D, Mori N, Ravi R (2003) Magnetic resonance molecular imaging of the HER-2/neu receptor. Cancer Res 63:2723–2727

Botta M (2000) Second coordination sphere water molecules and relaxivity of gadolinium(III) complexes: implications for MRI contrast agents. Eur J Inorg Chem 3:399–407

Caravan P, Ellison JJ, McMurry TJ, Lauffer RB (1999) Gadolinium(III) chelates as MRI contrast agents: structure, dynamics, and applications. Chem Rev 99:2293–2352

Carter D, Ho JX (1994) Structure of serum-albumin. Adv Prot Chem 45: 153–203

Di Bari L, Pintacuda G, Salvadori P (2000) Solution equilibria in YbDOTMA, a chiral analogue of one of the most successful contrast agents for MRI, GdDOTA. Eur J Inorg Chem 75–82

Dwek RA (1973) Nuclear magnetic resonance in biochemistry, applications to enzyme systems, Clarendon Press, Oxford, pp 174–283

Heckl S, Pipkorn R, Waldeck W, Spring H, Jenne J, von der Lieth CW, Corban-Wilhelm H, Debus J, Braun K (2003) Intracellular visualization of prostate cancer using magnetic resonance imaging. Cancer Res 63:4766–4772

Kobayashi H, Brechbiel MW (2003) Dendrimer-based macromolecular MRI contrast agents: characteristics and application. Mol Imaging 2:1–10

Merbach AE, Tóth E (2001) The chemistry of contrast agents in medical magnetic resonance imaging. Wiley, Chichester

Osterloh K, Aisen P (1989) Pathways in the binding and uptake of ferritin by hepatocytes. Biochem Biophys Acta 1011:40–45

Padhani AR (2002) Dynamic contrast-enhanced MRI in clinical oncology: current status and future directions. J Magn Res 16:407–422

Powell DH, Ni Dhubhghaill OM, Pubanz D, Helm L, Lebedev HS, Schlaepfer W, Merbach AE (1996) Structural and dynamic parameters obtained from O-17 NMR, EPR, and NMRD studies of monomeric and dimeric Gd3+ complexes of interest in magnetic resonance imaging: an integrated and theoretically self consistent approach. J Am Chem Soc 118:9333–9346

Rinck PA (2003) Magnetic resonance in medicine. ABW Wissenschaftsverlag, Berlin

Sipkins DA, Cheresh DA, Kazemi MR, Nevin LM, Bednarski MD, Li KCP (1998) Detection of tumor angiogenesis in vivo by alpha(v)beta(3)-targeted magnetic resonance imaging. Nat Med 4:623–626

Weissleder R, Mahmood U (2001) Molecular imaging. Radiology 219:316–333

Weissleder R, Bogdanov A, Matuszewski L, Bremer C, Petrovski A (2002) Oligomerization of paramagnetic substrates result in signal amplification and can be used for MR imaging of molecular targets. Mol Imag 1:16–23

Wiener EC, Konda S, Shadron A, Brechbiel M, Gansow O (1997) Targeting dendrimer-chelates to tumors and tumor cells expressing the high-affinity folate receptor. Invest Radiol 32:748–754

Winter PM, Caruthers SD, Kassner A, Harris TD, Chinen LK, Allen JS, Lacy EK, Zhang HY, Robertson JD, Wickline SA, Lanza GM (2003) Molecular imaging of angiogenesis in nascent vx-2 rabbit tumors using a novel alpha(v)beta(3)-targeted nanoparticle and 1.5 tesla magnetic resonance imaging. Cancer Res 63:5838–5843

Young IR (2000) Methods in biomedical magnetic resonance imaging and spectroscopy. Wiley, Chichester

7 Luminescent Lanthanide Complexes as Sensors and Imaging Probes

D. Parker, Y. Bretonniere

7.1 Introduction and Background

The use of luminescent probes is now commonplace in biological and clinical applications for the detection and monitoring of a wide range of chemical species, from simple ions to complex bioactive molecules. A wide variety of fluorescent organic molecules is available for this purpose, either incorporating or attached to suitable binding sites for the target species (Haugland 2002). Although this area of research is dominated by purely organic molecules, a considerable research effort in the development of new emissive sensory systems is directed towards luminescent metal complexes, including those of transition metal ions (Demas and de Graff 2001) and of the

lanthanide(III) ions (Parker and Williams 2003). Metal complexes often possess an extensive excited state chemistry, owing to the presence of metal-centered (e.g., *dd* and *ff*) and charge-transfer states involving the metal, in addition to the singlet, triplet, and charge transfer excited states associated with the ligand. Thus, they not only offer additional opportunities for perturbing the emission characteristics, but also may give rise to longer-lived luminescence.

The lowest energy, metal-centered excited states of several of the lanthanide(III) ions have long radiative lifetimes of between 0.1 and 10 ms. As long as deactivation by nonradiative processes is minimized, the observed decay of light emission in solution at ambient temperature may also be of this order. Such long-lived emission is an attractive feature in a luminescent probe, as it allows time-resolved detection methods to be used, offering excellent discrimination between probe and background emission (Lakowicz 1999). A time delay can be introduced between the pulsed excitation of the sample and the measurement of the probe's luminescence, during which the shorter-lived background fluorescence characteristic of biological and clinical samples decays to negligible levels. Such procedures obviate experimental problems associated with light scattering and the large Stokes' shifts of emissive lanthanide complexes also negate the problem of autofluorescence. Although not unique to the lanthanides, long-lived emission *under ambient conditions* is unusual. The triplet-derived phosphorescence of many aromatic molecules, for example, is characterized by long *natural* lifetimes, but is usually quenched too efficiently to be observed in fluid solutions at ambient temperature: deoxygenation and low temperatures are normally required to reduce competitive deactivation processes, rendering such molecules unsuitable for time-gated procedures.

The contracted, "core-like" nature of the 4f orbitals in the tripositive lanthanide ions has three major effects on the optical spectra, leading to markedly different characteristics when compared to the d-d spectra of transition metal ions. First, ligand-field splittings are small, typically around 100 cm^{-1} (1.2 kJ mol^{-1}). Therefore, excited states in compounds or complexes of the lanthanides are effectively the same as for the gas-phase ions. The energy of the *ff* transitions in the spectra is, to a first approximation, independent of the coordination environment. From the point of view of the design of respon-

sive complexes for chemical sensing, this restricts the use of emission wavelength changes as a signaling mechanism, in contrast to many fluorescent sensors. On the other hand, it allows optics to be set up and optimized for fixed emission wavelengths and, in fact, changes in the fine structure of the bands, and especially their relative intensities, can be very informative, especially for Eu(III) complexes. Second, the weakness of the interaction of the *f* orbitals with ligand orbitals leads to minimal mixing of the electronic excited states with ligand vibrations. As for the *dd* transitions of d-block metal ions, it is only through coupling with asymmetric ligand vibrations that the formally forbidden *ff* transitions become partially allowed, so the weakness of the coupling ensures that the transitions remain weak. In absorption, this leads to very low extinction coefficients (ε typically 0.1 $mol^{-1}dm^3cm^{-1}$); in emission, it explains the low transition probabilities and hence the long natural lifetimes. Finally, the emission bands are almost "line-like," i.e., very sharp and narrow, even in solution, because the vibrations of the ligands and concomitant changes in M–L distances have very little effect on the energies of the excited states.

A consequence of the low molar absorption coefficients of the lanthanide(III) ions is that the excited states are not efficiently populated by direct absorption of light by the metal ion, unless laser excitation is used. The most widely-used emissive lanthanides, terbium and europium, can be excited in this way by the 488-nm line of the argon ion laser (matching the Tb $^7F_6 \rightarrow {}^5D_4$ energy gap) and by rhodamine 110 in a dye laser (for the Eu $^7F_0 \rightarrow {}^5D_0$ transition at 580 nm or the $^7F_2 \rightarrow {}^5D_1$ at 557 nm). An alternative solution, which allows lower intensities of light to be used and which opens up additional strategies in the design of responsive luminescent complexes (Sect. 7.2), is that of sensitized emission. A chromophore is built into the structure of a ligand forming a stable complex with the lanthanide ion. It is chosen so that it absorbs light in the range 300–420 nm and transfers its excitation energy to the metal ion (Parker and Williams 1996). If the chromophore has a high extinction coefficient and energy transfer occurs efficiently, then the "effective" molar absorption coefficient of the metal is greatly increased and intense luminescence can result following excitation with conventional lamps or LEDs.

The choice of sensitizer is determined primarily by the energy of the emissive excited state of the metal: the sensitizer must possess an excited state, from which energy transfer can occur, whose energy is at least equal to that of the metal emissive state. The efficiency of the process is dependent on the extent of overlap of the emission spectrum of the donor with the absorption spectrum of the acceptor; in other words, it should be favored by a matching of the energy levels of the donor and acceptor. A further requirement is that the donor excited state must be sufficiently long-lived for energy transfer to compete effectively with other deactivation pathways. An energy transfer rate constant of 10^5–10^7 s^{-1} is typical of Eu^{3+} and Tb^{3+} complexes containing aromatic sensitizers within about 5 Å of the metal ion. This is too slow to allow energy transfer to occur from short-lived singlet states (τ_{obs}^{-1} typically 10^9–10^8 s^{-1}) and most studies in which the energy transfer process has been investigated in detail have revealed the predominance of the longer-lived *triplet* state as the donor (Beeby et al. 2001).

Whilst a triplet energy comparable to, or a little higher than that of the metal emissive state favors the efficiency of sensitization, too small an energy gap (<1,700 cm^{-1}) is detrimental, since thermally activated back energy transfer from the metal to the sensitizer then competes with emission, leading to reduced lifetimes and quantum yields. This limits the choice of sensitizer to those with triplet energies in excess of about 19,000 cm^{-1} for Eu^{3+} and 22,000 cm^{-1} for Tb^{3+} (the emissive states, $^5D_0$ and $^5D_4$, lie at 17,200 and 20,400 cm^{-1} respectively), although a much larger range of sensitizers is possible for lanthanides with lower energy emissive states like Yb^{3+} ($^2F_{5/2}$ at 10,200 cm^{-1}). Further desirable features in the sensitizer are a high quantum yield of triplet formation and a relatively low singlet excited state energy (i.e., a small S_1–T_1 energy gap), to allow excitation to be achieved at long wavelengths (>350 nm), and so avoid the need for quartz optics and competitive absorption by simple biological molecules.

A variety of aromatic chromophores has been considered as sensitizing moieties. Simple naphthyl groups suffer from several problems: they generally possess only very weak absorption beyond 300 nm; their triplet states are only a little higher in energy than the $^5D_4$ of Tb^{3+}, leading to severe back energy transfer; the singlet excited states are quenched by photoinduced electron transfer to Eu^{3+}.

A functionalized 1,10-phenanthroline ligand is used in the commercially available FIAgen bioassay reagent. More recently, phenanthridines (Parker et al. 1998), acridones (Sammes et al. 2000), benzophenones (Beeby et al. 2002), and tetraazatriphenylenes (Werts et al. 2000a, b) have been investigated, which offer efficient sensitization for both europium and terbium, while allowing excitation at wavelengths in the range 340–420 nm.

The next key issue to address is the nature of the ligand to bind the lanthanide. Most applications require the function of the probe complex in aqueous solution and, in the biosciences, in the presence of significant concentrations of competing endogenous ligands (e.g., proteins, phosphorylated anions, lactate, citrate). Complexes are therefore required which have high kinetic and thermodynamic stability with respect to metal ion dissociation, preferably over the pH range 4.5–8. In this respect, the requirements are similar to those demanded by gadolinium-based contrast agents in MRI (Caravan et al. 1999). The high coordination numbers favored by the lanthanide(III) ions necessitate use of multidentate ligands, preferably at least heptadentate, while the high charge density of the tripositive ions is best accommodated by ligands offering anionic or polarizable nitrogen or oxygen donors or a combination thereof. Polyaminocarboxylate ligands based on the acyclic DTPA system or the closely related macrocyclic ligand DOTA are examples of ligands that satisfy each of these requirements, and with analogs incorporating phosphinate or amide groups in place of the carboxylates, constitute a versatile group of ligands, modified to incorporate a variety of sensitizing groups. Other ligand frameworks which have been used as the basis for ligand modification include terpyridines (Toner et al. 1993), bipyridyl-functionalized cryptands (Alpha et al. 1990), and calixarenes (Sabbatini et al. 1995).

7.2 Mechanistic Approach to Modulation of Luminescence

The photochemical pathway that defines the mechanism of sensitized lanthanide luminescence reveals that there are three excited states which may be perturbed, leading to modulation of the emission from the lanthanide ion (Scheme 1; Parker and Williams 2003).

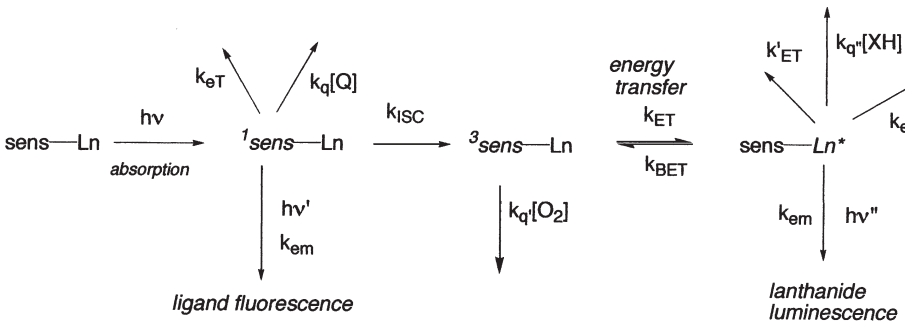

Scheme 1. Lanthanide luminescence

First, the singlet excited state of the sensitizing chromophore may be quenched by an electron or charge-transfer process which can be inter- or intramolecular in nature. This quenching process competes with intersystem crossing, depletes the population of the singlet excited state, may be accompanied by fluorescence quenching, and is echoed by a reduction in the intensity of emission from the lanthanide ion. Another way of perturbing the singlet excited state involves a reversible binding process of the chromophore itself, e.g., following protonation or metal coordination, leading to a change in the energy of the singlet excited state. This will modulate the relative intensity of lanthanide emission but more significantly leads to a change in the corresponding excitation spectra, allowing ratiometric measurements to be performed (Blair et al. 2001). Second, the intermediate triplet of the chromophore may be perturbed. Its energy may also be changed by reversible metal binding or protonation at an integral basic site leading to differences in the rate of forward or reverse energy transfer (Parker et al. 1998; Parker and Williams 2003). This process also modulates the lifetime of the lanthanide excited state. Aromatic triplet states are particularly sensitive to collisional quenching by molecular oxygen. In cases where $k_q[O_2]$ is of the same order as k_{ET}, the lanthanide emission lifetime and intensity is sensitive to variations in dissolved oxygen concentration (Blair et al. 2002). In addition, enhanced oxygen sensitivity may occur when there is a finite rate of reverse energy transfer from the Ln^{3+} excited state, leading to a repopulation of the chromophore triplet state. This

thermally activated process is only significant when the energy gap between the two states is less than 1,500 cm^{-1}. Most examples have involved the $^5D_4$ excited state of Tb^{3+}. It lies at 20,400 cm^{-1} and is close in energy to a large number of aryl triplet states. Pronounced modulation of the lifetime of the lanthanide excited state results from collisional deactivation of the aryl triplet by oxygen. The measured dependence of lanthanide emission/lifetime variation on oxygen concentration may be kinetically complex, being determined by two coupled first-order differential equations.

Finally, the lanthanide excited state itself may be quenched. Here, there are three different cases: vibrational energy transfer involving energy-matched XH oscillators [especially hydroxy (OH) and amino (NH) groups]; energy transfer to an acceptor of appropriate energy; and electron transfer involving the metal-centered excited state. In the first case, the displacement of bound water molecules by inter or intramolecular anion binding leads to an increase in Ln emission intensity and lifetime and modifies the form of the emission spectrum. This allows ratiometric analyses to be undertaken (Bruce et al. 2000; Lowe et al. 2001). Analysis of emission spectra changes is easiest for europium complexes, because of the absence of degeneracy of the ^5D_o emissive state. Examples involving energy transfer are less common; suitable acceptors for Eu^{3+} include the dye bromothymol blue or the protein allophycocyanine which fluoresces at 665 nm with the lifetime of the donor europium complex (Mathis 1995). Cases of charge transfer quenching of the Ln^{3+} excited state are even less common but include deactivation of a cationic terbium-tetraazatriphenylene complex, following its binding to GC base pairs in poly (dGdC) or calf thymus DNA (Bobba et al. 2002).

7.2.1 Singlet Excited State Perturbation

The best-defined examples of singlet excited state quenching in lanthanide conjugates involve halide anions. The chloride ion fulfils a series of key functions inside a variety of different cell types, including ion transport, pH homeostasis and the regulation of cell volume and intermediary metabolism. The accumulation of chloride above its equilibrium state has been recognized in smooth muscle

contraction (Chipperfield and Harper 2000) and is hypothesized to be linked with modulation of (Na^++K^++Cl^-) cotransport and the perturbation of HCO_3^-/Cl^- exchange. Considerable interest exists in devising better ways of monitoring intracellular chloride concentrations (30–70 mM range) using optical methods. So far this has been achieved by examining the quenching of fluorescence of zwitterionic N-alkylated quinolinium or acridinium species. This phenomenon involves collisional quenching of the singlet excited state, but gives intensity modulation only, with short wavelength excitation and interference from proteins via PET quenching from protein amino groups.

In the stable Eu complex [Eu**1**]$^+$, addition of halide ions led to a reduction in phenanthridinium fluorescence (405 nm), echoed by a diminution in europium emission intensity (e.g., at 616 nm). With chloride, Stern-Volmer quenching constants (K_{SV}^{-1}) were in the range 40 to 50 mM, and were independent of added lactate, phosphate, citrate and hydrogen carbonate (Parker et al. 1998). Quenching followed the order I>Br>Cl. In the analogous terbium complexes while phenanthridinium fluorescence was modulated to the same extent, the Tb emission intensity was much less sensitive to added Cl^-, because of competitive quenching of the T_1 state by O_2 (Sect. 7.2.2), suggesting a possible use of Tb/Eu complexes in tandem to assay chloride by ratiometric methods.

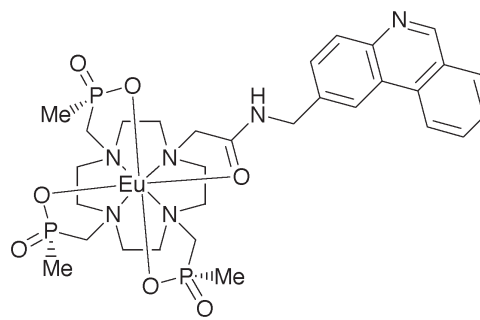

[Eu.**1**]

7.2.2 Triplet Perturbation

Measurement of the level of dissolved oxygen in water is important in many biological and environmental systems: in river waters, for example, hypoxia may lead to the death of fish when the oxygen concentration falls from 0.27 mM (normal) to below 0.04 mM. Knowledge of oxygen gradients in complex biological samples is required for many processes that involve aerobic energy metabolism. Optical methods are used widely (Demas et al. 1999) as they are amenable to miniaturization (e.g., fibre-optic optodes), exhibit fast response times, and rarely are subject to interference. The majority are based on quenching metal to ligand charge transfer (MLCT) states in Ru or Os di-imine complexes of ligand-centered triplet states in Pd and Pt porphyrins. In emissive lanthanide complexes, the long-lived lanthanide excited state is not sensitive to O_2. It is the triplet state of the sensitizing moiety which may be subject to collisional quenching either because of a slow rate of competing energy transfer or because it is long-lived as a result of repopulation by a back energy transfer process.

A series of near-IR luminescent complexes has been described (Nd, Er, Yb) in which an integral fluorescein, eosin, or metalloporphyrin group acts as a sensitizing chromophore (Werts et al. 2000a, b). Intramolecular energy transfer competes with triplet quenching by O_2, giving rise to O_2 sensitivity in emission lifetime and intensity. Examples of oxygen sensing using Eu complexes operating at the gas/solid interface have been reported. Europium β-diketonate complexes bearing a phenanthroline chromophore (λ_{exc} 340 nm) have been immobilized in polystyrene films and exhibit modest oxygen sensitivity (Imao et al. 2000). Perhaps the greatest opportunity for devising practicable pO_2-dependent Ln^{3+} luminescence involves sensitized terbium emission. The long-lived Tb $^5D_4$ excited state ($\tau \sim 1$–3 ms) lies at 20,400 cm^{-1}, within range of many common aryl triplet states. When the energy gap is less than about 1,000 cm^{-1}, thermally activated back energy transfer significantly depletes the emissive $^5D_4$ level, and oxygen sensitivity results. Examples of aryl triplets with such energy include substituted coumarins, N-alkyl or protonated phenanthridiniums and quinoliniums, triphenylenes, and naphthalenes. The dependence of the Tb emission

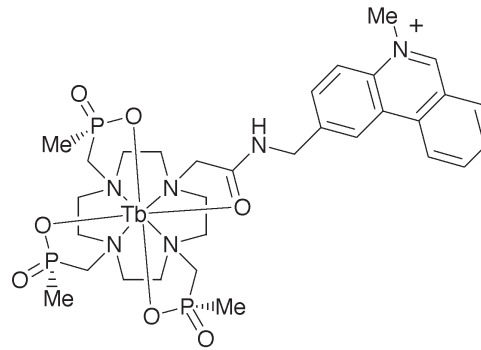

[Tb.**2**]$^{+}$

lifetime on pO_2 may follow Stern-Volmer behavior in homogeneous solution, but can be kinetically complex in immobilized systems. Simple calibrations have been established (Blair et al. 2002), e.g., for Tb-N methylphenanthridinium conjugates such as [Tb.**2**]$^{+}$, immobilized in sol-gel matrices, which possess an overall quantum yield efficiency of 20%, with respect to O_2 quenching in aqueous media.

7.2.3 Lanthanide Excited State Perturbation

Each of the excited Ln^{3+} ions is subject to quenching by vibrational energy transfer involving harmonics of energy-matched XH oscillators. Directly coordinated water molecules afford the most common example of this quenching, so if a species can bind directly to the Ln^{3+} center, reversibly displacing these waters, both the emission intensity and lifetime increase and the form of the emission spectrum will also change, allowing ratiometric analyses. With chiral complexes, the local helicity at the metal center may be perturbed as well, allowing modulation of the circular polarization of the emitted light (Lopinski et al. 2002). Examples of intermolecular binding include the reversible binding of anions (HCO_3^-, lactate, citrate, phosphate, DNA) at diaqua-lanthanide centers (see Sect. 7.3.1). Intramolecular examples have been reported in which an integral sulfona-

mide nitrogen binds reversibly, in a pH- (or metal ion-) dependent manner (Lowe et al. 2001).

The Ln^{3+} excited state may also be quenched by a nonradiative charge-transfer interaction. Such a process leads to a reduction in emission lifetime and intensity and has been reported in cases where the Ln^{3+} ion is directly coordinated to an electron-poor heteroaromatic, e.g., the chiral Eu and Tb complexes of the emissive ($\phi_{H_2O}^{Eu} = 21\%$); ($\phi_{H_2O}^{Tb} = 40\%; \lambda_{exc}$ 355 nm) nine-coordinate tetraazatriphenylene conjugate, [Ln.**3**] (Bobba et al. 2002). The complex binds strongly to DNA and engages in a charge transfer interaction which is more well defined with GC base pairs, building up charge on the heteroaromatic moiety. This is signaled by a marked hypochromism and a shift to the red of the aromatic absorption band. At the same time, a change in the polarizability of the Ln-bound N donors occurs, leading to a build-up of positive charge at the metal center. Such a process is more efficient for Tb^{3+} than Eu^{3+} (i.e., an MLCT type of process) and is accompanied by a change in the form of the hypersensitive $\Delta J = 4$ manifold in Eu^{3+} emission spectra, allowing ratiometric analysis of the binding interaction. This behavior is consistent with modulation of the polarizability of the "axially" bound tetraazatriphenylene N in the monocapped-square antiprismatic complex (Bruce et al. 2003).

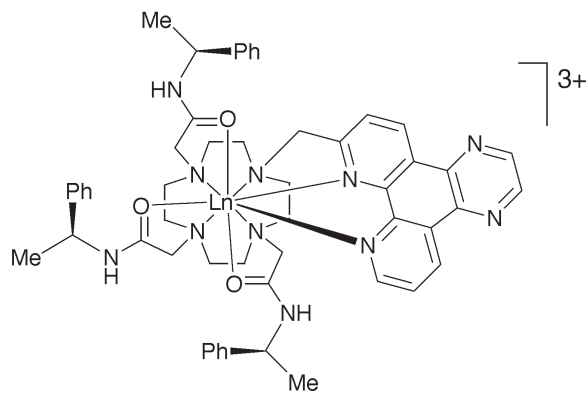

(SSS)-Δ-[Ln.**3**]$^{3+}$

7.3 Tailoring the Lanthanide Complex for Use "In Cellulo"

The above discussion summarizes the guiding chemical principles that have been used to establish the probe and sensor properties of responsive lanthanide complexes over the past 10 years. To date, most applications of luminescent lanthanide complexes in biochemistry and biology have related to the development of time-resolved immunoassays (Mathis 1995) or the introduction of lanthanide complexes as long-lived donors in fluorescence resonance energy transfer (FRET) analyses (Jones et al. 2001). For use in live cell imaging, the requirements of the luminescent probe are more exacting: luminescence at wavelengths shifted from the excitation wavelength; an excitation wavelength well removed from absorption by endogenous cellular chromophores; good absorption characteristics (high ε), and a large overall emission quantum yield; cellular permeability or better still, preferential uptake or retention by different cell types or cell compartments; no cell toxicity; high chemical stability with respect to complex degradation and resistance to photo-bleaching and photo-fading. In addition, the responsive complex must not only bind the target analyte with appropriate avidity (match K_d) and selectivity, but also signal that selective binding event by sufficient changes in emission form (ratiometric methods), polarization, or lifetime to allow calibration.

7.3.1 Anion Analysis: Selectivity for Hydrogen Carbonate

Most work to date has addressed the reversible displacement of one or both waters in diaqua complexes by anion ligation to the lanthanide center (Bruce et al. 2000; Dickins et al. 2002; Parker et al. 2002). This event is signaled by changes in the intensity and form of Ln emission, allowing ratiometric analyses to be undertaken. Such methods are most appropriate in analyses of Eu emission spectra. The relative intensity of the magnetic-dipole-allowed $\Delta J = 1$ transitions (around 590 nm) is insensitive to the associated change in coordination environment while the intensity of the electric-dipole-allowed $\Delta J = 2$ (616 nm) and $\Delta J = 4$ (around 702 nm) manifold changes considerably, particularly if the "hard" axial water molecule

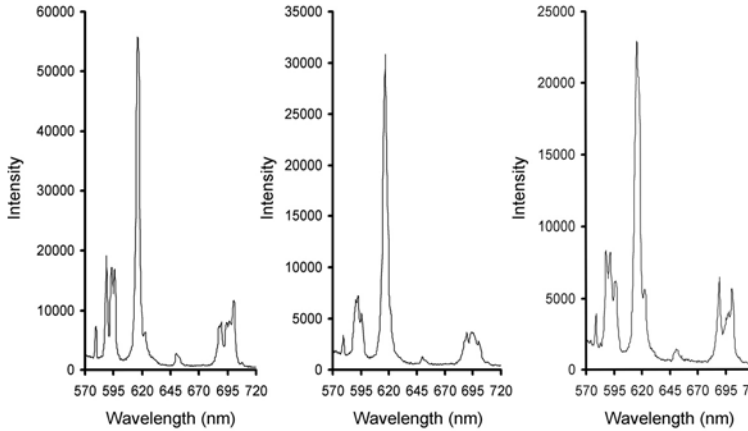

Fig. 1. Europium emission spectra for $[Eu.\mathbf{4}]^{3-}$ (0.1 mM, 1 mM anion, pH 7.4, λ_{exc} 410 nm) in the presence of (*S*)-lactate (*left*), bicarbonate (*center*) and hydrogen phosphate, showing the changes in the form of the emission spectrum signaling reversible anion coordination

is displaced by a more polarizable charged donor. An example of such emission spectra (Fig. 1) highlights the increase in the relative intensity of the $\Delta J=2$ band (618 nm) for the carbonate-bound species – compared to lactate and citrate – and exemplifies how each bound anion gives a "fingerprint" emission spectral profile, allowing simple identification and ratiometric analysis. This information is required in the application of such methods in intracellular media – where a large number of anions may compete in binding to the lanthanide center. The structure of several of these ternary complexes has been defined by X-ray crystallography (e.g., in chelated adducts with lactate, citrate, several amino-acids, acetate; Dickins et al. 2002) and by NMR studies on Eu and Yb analogs. Relative binding affinities have been assessed in simple competitive analyses or in fixed interference studies. They reveal that in the millimolar range, it is the more polarizable (higher energy HOMO) oxygen in HCO_3^- (bound as CO_3^{2-}) and various phosphorylated di-anions (e.g., glucose-6-*O*-phosphate; AMP but *not* cAMP) which bind most avidly, and at ambient pH, it is the bicarbonate anion (range 3–25 mM) which wins the competition between endogenous anions.

The bicarbonate ion is an essential component of biological systems and is vital to many cellular processes in mammals, such as intracellular pH homeostasis, kidney function, and sperm maturation. However, almost nothing is known about how bicarbonate concentrations fluctuate within a cell in response to cell stimuli and such analyses are currently limited to radiochemical measurement of overall $H^{14}CO_3^-$ uptake and inferences based upon changes in intracellular pH. Information about how HCO_3^- is localized and varies within cell compartments is needed in order to understand the diverse physiological processes it may control, e.g., cyclic-AMP regulation, through pH-independent, reversible binding to a soluble adenylyl cyclase enzyme (Cann et al. 2000). Moreover, the pathological consequences of perturbing some of these physiological processes may be very significant: mis-expression of carbonic anhydrase (CA) is linked to the presence of a variety of tumor types and CA-II deficiency syndrome in humans is characterized by renal tubular acidosis, osteoporosis, and mental retardation. There is a pressing need for a direct method to allow changes in HCO_3^- concentration to be measured within a cell, and to monitor the changes in different compartments (e.g., mitochondria) in real time.

A series of europium-acridone conjugates has been reported (Bretonniere et al. 2002) that reveal a fourfold change in the intensity ratio of the Eu 618/588 nm emission bands in the physiologically relevant bicarbonate concentration range, 5–25 mM. The system has been calibrated in the presence of competing anions and protein, e.g., in a cell lysate. The affinity for bicarbonate has been controlled by changing the peripheral electrostatic gradient in the Eu complexes. Thus, anionic, zwitterionic and cationic complexes have been examined, ([Eu.**4**]: the cationic version is the ethyl ester analog of those shown). The zwitterionic and anionic complexes possess the desired affinity and selectivity for bicarbonate (Fig. 2). The complexes are nontoxic to cells (5 mM), and the imaging of cells by confocal microscopy reveals uptake and clear intracellular staining. Preliminary colocalization studies with established compartmentalized organic dyes, such as Mitotracker Green and Lysotracker Green are consistent with localization in lysosomes and possibly mitochondria (Fig. 3). Key experiments remain to be undertaken to address the following: can a ratiometric method be used in real time to im-

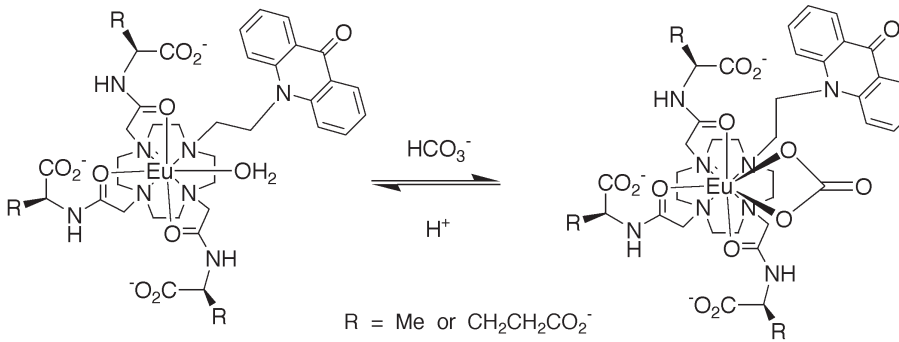

[Eu.**4**]

age bicarbonate fluctuations? Can the Eu complex be targeted to other cell compartments? What is the mechanism of cellular uptake? The early work is encouraging and augurs well for the application of these probes to image intracellular HCO_3^- fluctuations, and hence enhance our understanding of the biological significance of the most important C_1 oxyanion.

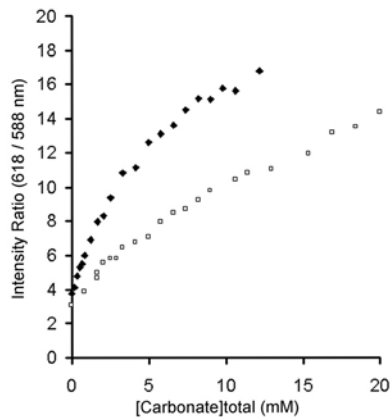

Fig. 2. Calibration curves showing the response of the europium complexes ([Eu.**4**]: 0.1 mM; *open squares*, glutarate derivative; *filled diamonds*, alanine (zwitterionic); 1 mM anion, pH 7.4, λ_{exc} 410 nm) to total added bicarbonate/carbonate in a cell lysate (NIH 3T3 cells)

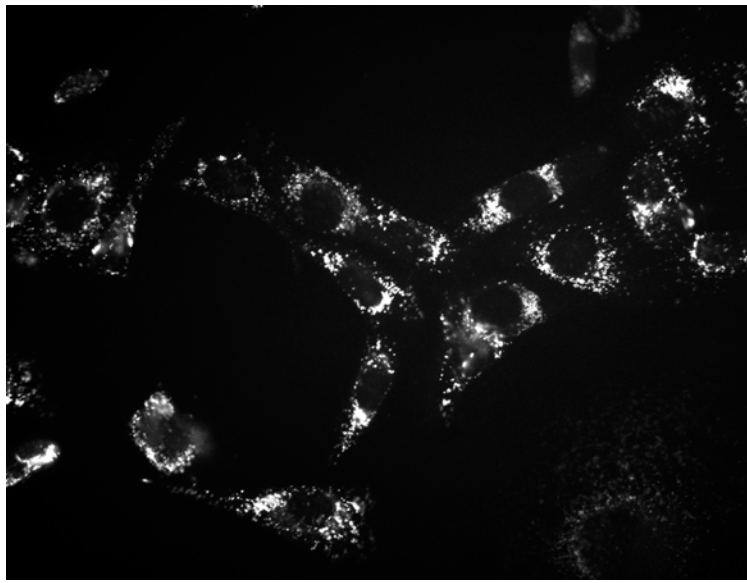

Fig. 3. Microscopy image showing the localization of the anionic complex, [Eu.**4**] (as the glutarate derivative), 3 h postinoculation in NIH 3T3 cells

7.3.2 Targeting the Cell Nucleus: DNA Binding Complexes

Although chiral, octahedral complexes of the late d-block metals have been studied for over 20 years in vitro as structural and reactive probes for nucleic acids, relatively little has been reported on their behavior in living cells. Typical examples include the Δ and Λ isomers of $Ru(phen)_3^{2+}$ and a large series of mixed ligand dipyridophenazine (dppz) complexes of ruthenium, rhodium, and osmium, e.g., $[Os(bpy)(dppz)]^{2+}$. These complexes are reputed to bind to DNA by preferential intercalation of the phenazine moiety from the minor groove and the perturbation of the metal-ligand charge transfer transitions that accompanies DNA binding provides a sensitive spectroscopic handle to study the nature of the bound complex.

Until very recently, there were no well-defined examples of chiral lanthanide complexes suitable for binding to the polyanionic nucleic acids. In general, the literature reports that discuss lanthanide-nu-

cleic acid interactions have been dominated by the interactions of the aqua ions themselves. Such work has often focused on the selective sensitization of selected ions, e.g., Tb^{3+}, and advantage has been taken of this effect in several assays directed at the detection of selected nucleic acids. Another theme of current activity relates to the ability of certain lanthanide ions to cause nucleic acid cleavage and attempts have been made to target certain sequences using an antisense strategy.

Recently, a series of cationic lanthanide complexes has been defined incorporating a phenanthridinium moiety, in which the configuration of a remote carbon stereogenic center determines the helicity of the overall complex. In the prototypical example, $[Ln.\mathbf{5}]^{4+}$, a primary component of the free energy of binding to oligonucleotides and DNA, has been linked to an intercalative interaction, supported by absorption, CD, and fluorescence quenching behavior. The lanthanide coordination environment and local helicity remained unchanged but the oligonucleotide underwent distinctive changes in local helicity and pitch that were sensitive to the handedness of the Ln complex and in certain cases to the nature of the Ln ion (Yb versus Eu). A limitation of this system is that the singlet excited state of the phenanthridinium complex is quenched on DNA binding via a nonradiative charge transfer interaction with GC base-pairs. The

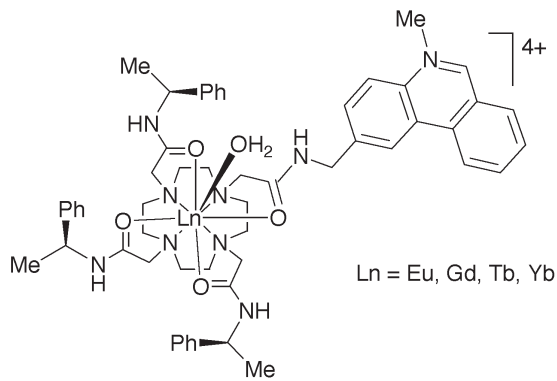

(SSS)-Δ- $[Ln.\mathbf{5}]^{4+}$

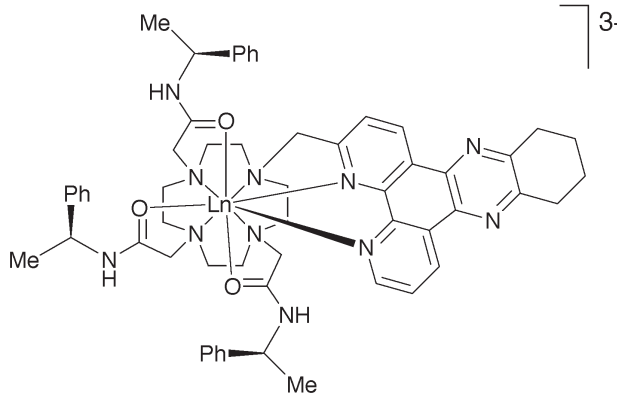

(SSS)-Δ-[Ln.**6**]$^{3+}$

lanthanide emission is therefore also switched off on binding, limiting the scope for assessing the intracellular activity of such probes (Dickins et al. 2002).

More promising behavior is shown by the highly emissive, enantiopure Δ and Λ tetrazatriphenylene complexes, [Ln.**3**]$^{3+}$ and [Ln.**6**]$^{3+}$, which bind to DNA stereoselectively via an electrostatic and intercalative mechanism (Bobba et al. 2002). The lanthanide emission reduces in intensity (approximately 50%) but is not "switched off" on DNA binding. Moreover, it is modulated in form. Of particular interest is the ability of these complexes to enter live cells, target the cell nucleus, and on prolonged irradiation lead to cell death (Frias et al. 2003). Control experiments reveal $<10\%$ cell death in the absence of complex or irradiation. Cells were examined by fluorescence microscopy from 1–48 h after incubation with the complex. Images taken over a period of 48 h showed that cells internalize each complex but that uptake of the Eu complex appears faster than the Tb analog. The microscopy images (Figs. 4, 5) reveal the migration of the probes through the cytoplasm, across the nuclear membrane into the nucleus, revealing substructures within the nucleus. Surprisingly, the Tb complex appeared to remain in the cytoplasm for longer periods and was apparently slower to migrate to

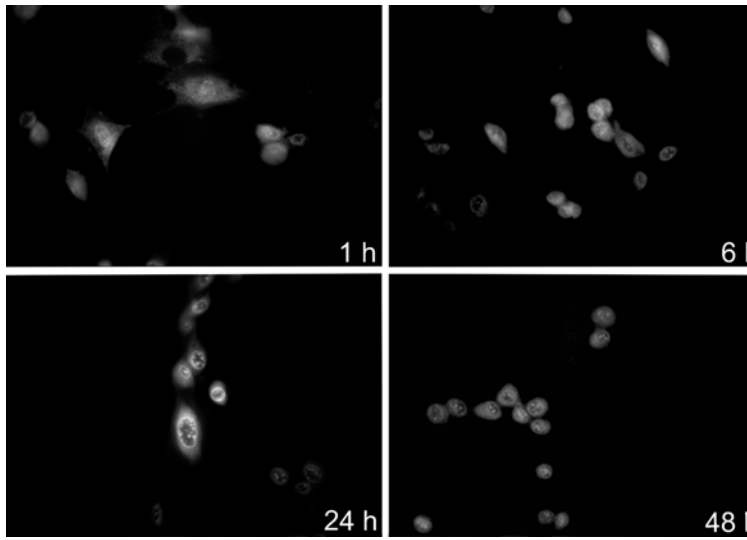

Fig. 4. Microscopy images, at different time points postinoculation, showing the uptake of the DNA-binding complex $[Eu.\mathbf{6}]^{3+}$ into the cell nucleus of NIH 3T3 cells

the nucleus. Parallel in vitro studies had indicated that emission from the Tb complexes was quenched to a greater extent when bound to DNA than for the Eu analogs. When uptake of the Δ and Λ enantiomeric complexes was compared, no significant differences were noted.

In a separate experiment, the cells were inoculated for a period of 3 h, to ensure that the complex had been internalized and was located in the nucleus (Fig. 6). Unbound complex was removed by washing with phosphate-buffered saline solution. The images revealed a transfer of the luminescence from the nucleus to the cytoplasm after a few hours and indicated that the complex remains in the cytoplasm for sustained periods. The egress of the complex from the nucleus back into the cytoplasm was not observed in localization studies carried out with an excess of complex, suggesting that entry into the cell nucleus requires a favorable concentration gradient of the complex.

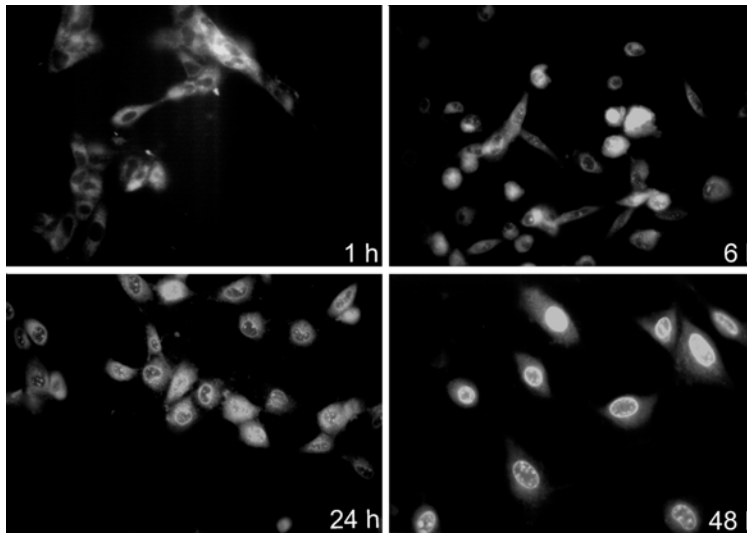

Fig. 5. Microscopy images, at different time points, postinoculation, showing the uptake of the DNA-binding complex $[Tb.\mathbf{6}]^{3+}$ into the cell nucleus of NIH 3T3 cells

The mechanism by which the cells take up the complex remains to be defined. These probes (tripositive charge and MW >1,000) are unlikely to enter by any passive diffusion process across the plasma membrane and therefore active uptake is more likely. No obvious vesicular structures were apparent in the cytoplasm by fluorescence microscopy, so an endocytotic uptake mechanism also seems unlikely.

7.4 Conclusions and Future Perspectives

There remains a great deal of work to do before luminescent lanthanide complexes are used in practice in cell biology. Nevertheless, they show considerable promise as luminescent probes, and once time-gated microscopy equipment is more generally available, and charge coupled device (CCD) cameras can be added to facilitate ratiometric analyses, one might expect further applications to develop.

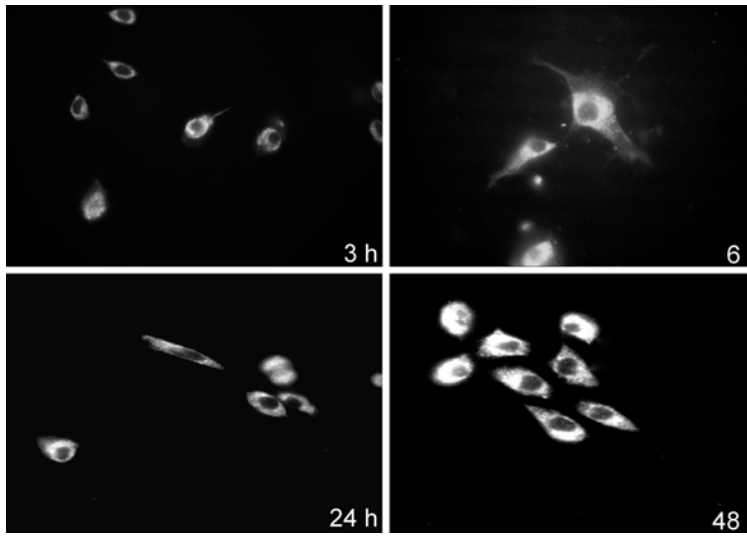

Fig. 6. Microscopy images showing the transit of the complex, $[Eu.\mathbf{6}]^{3+}$ out of the cell nucleus over a period of time, in the absence of added complex

The more important challenge for the molecular scientists is to devise practicable methods for monitoring the spatio-temporal variations in the concentration of essential bioactive ions. Great progress was made in cell biology following the development of Ca-sensitive fluorophores by Tsien, but we still need *new chemistry* and biochemical assays to be discovered, to allow us to understand the biological role of many simple ionic species such as bicarbonate, phosphopeptides and small proteins and molecules such as carbon monoxide and nitric oxide.

References

Alpha B, Ballardini R, Balzani V, Lehn J-M, Perathones S, Sabbatini N (1990) Antenna effect in luminescent lanthanide cryptates: a photophysical study. Photochem Photobiol 52:299–306

Beeby A, Faulkner S, Parker D, Williams JAG (2001) Sensitised luminescence from phenanthridine appended lanthanide complexes: analysis of

triplet mediated energy transfer processes in terbium, europium and neodymium complexes. J Chem Soc Perkin Trans 2:1268–1273
Beeby A, Bushby LM, Maffeo D, Williams JAG (2002) Intramolecular sensitisation of lanthanide(III) luminescence by acetophenone-containing ligands: the effect of para substituents and solvent. Dalton Trans 48–54
Blair S, Lowe MP, Mathieu CE, Parker D, Senanayake KP (2001) Optical pH sensors based on luminescent europium and terbium complexes immobilised in a sol-gel glass. Inorg Chem 40:5860–5867
Blair S, Kataky R, Parker D (2002) Sol gel immobilised terbium complexes for luminescence sensing of dissolved oxygen in aqueous solution by analysis of lanthanide emission decay. New J Chem 26:530–535
Bobba G, Frias J-C, Parker D (2002) Highly emissive, nine-coordinate enantiopure lanthanide complexes incorporating tetraazatriphenylenes as probes for DNA. Chem Commun Camb 8:890–891
Bretonniere Y, Cann MJ, Parker D, Slater R (2002) Ratiometric probes for hydrogen carbonate analysis in intracellular or extracellular environments using europium luminescence. Chem Commun Camb 17:1930–1931
Bruce JI, Dickins RS, Govenlock LJ, Gunnlaugsson T, Lopinski S, Lowe MP, Parker D, Peacock RD, Perry JJB, Aime S, Botta M (2000) The selectivity of reversible oxy-anion binding in aqueous solution at a europium and terbium centre; signalling of carbonate chelation by changes in the form and circular polarisation of luminescence emission. J Am Chem Soc 122:9674–9684
Bruce JI, Dickins RS, Parker D, Tozer DJ (2003) Correlation of optical and ^{1}H NMR spectral information with coordination variation for axially symmetric europium and ytterbium(III) complexes: importance of axial donor polarisability in determining affinity and ligand field. Dalton Trans, pp 1264–1271
Cann MJ, Chen Y, Litvin TN, Iourgenko V, Sinclair ML, Levin LR, Buck J (2000) Soluble adenylyl cyclase as an evolutionarily conserved bicarbonate sensor. Science 289:625–628
Caravan P, Ellison J, McMurry TJ, Lauffer RB (1999) Gadolinium (III) chelates as MRI contrast agents: structure, dynamics and applications. Chem Rev 99:2293–2345
Chipperfield AR, Harper AA (2000) Chloride in smooth muscle. Progr Biophys Mol Biol 74:175–221
Demas JN, DeGraff BA (2001) Applications of luminescent platinum group metal complexes to sensor technology and molecular probes. Coord Chem Rev 211:317–351
Demas JN, DeGraff BA, Coleman PB (1999) Oxygen sensors based on luminescence quenching. Anal Chem 71:793A–800A
Dickins RS, Aime S, Batsanov AS, Beeby A, Botta M, Bruce JI, Howard JAK, Love CS, Parker D, Peacock RD, Puschmann H (2002) Structural, luminescence and NMR studies of the reversible binding of acetate, lac-

tate, citrate and selected amino-acids to chiral di-aqua ytterbium and europium complexes. J Am Chem Soc 124:12697–12705
Frias JC, Bobba G, Cann MJ, Parker D, Hutchison CJ (2003) Luminescent nonacoordinate cationic lanthanide complexes as potential cellular imaging and reactive probes. Org Biomol Chem 1:905–907
Haugland RP (2002) Handbook of fluorescent probes and research chemicals, 9th edn. Molecular Probes, Eugene, Oregon
Imao Y, Okura I, Miyashita T (2000) Optical oxygen sensing based on quenching of europium(III) complex immobilised in fluoropolymer film. Bull Chem Soc Jpn 73:2663–2668
Jones SG, Lee DY, Wright JF, Jones CN, Tee ME, Gregory SY, Burns DD (2001) Improvements in the sensitivity of time-resolved fluorescence energy transfer. J Fluoresc 11:13–18
Lakowicz JR (1999) Principles of fluorescence spectroscopy, 2nd edn. Kluwer Academic/Plenum, New York
Lopinski S, Bruce JI, Parker D, Peacock RD (2002) Survey of factors determining the circularly polarised luminescence of macrocyclic lanthanide complexes in solution. Chirality 14:562–567
Lowe MP, Parker D, Reany O, Aime S, Botta M, Castellano G, Gianolio E, Pagliarin R (2001) pH Dependent modulation of relaxivity in macrocyclic gadolinium complexes based on reversible intramolecular sulfonamide ligation. J Am Chem Soc 123:7601–7609
Mathis G (1995) Probing molecular interactions with homogeneous techniques based on rare earth cryptates and fluorescence energy transfer. Clin Chem 41:1391–1397
Parker D, Williams JAG (1996) Getting excited about lanthanide complexation chemistry. J Chem Soc Dalton Trans, pp 3613–3628
Parker D, Williams JAG (2003) Responsive luminescent lanthanide complexes. In: Sigel H, Sigel A (eds) Metal ions in biological systems: the lanthanides and their interrelations with biosystems. Marcel Decker, New York, pp 233–280
Parker D, Senanayake PK, Williams JAG (1998) Luminescent sensors for pH, pO_2, halide and hydroxide ions using phenanthridine as a photosensitiser in macrocyclic europium and terbium complexes. J Chem Soc Perkin Trans 2:2129–2141
Parker D, Dickins RS, Puschmann H, Crossland C, Howard JAK (2002) Being excited by lanthanide coordination chemistry: aqua species, chirality, excited state chemistry and exchange dynamics. Chem Rev 102: 1977–2010
Sabbatini N, Guardigli M, Manet I, Ungaro R, Casnati R, Fischer C, Ziessel R, Ulrich G (1995) Synthesis and luminescence of Eu and Tb complexes with novel calyx[4]arene ligands carrying 2,2′-bipyridine subunits. New J Chem 19:137–140

Sammes PG, Dadabhoy A, Faulkner S (2000) Small singlet-triplet energy gap of acridone enables longer wavelength sensitisation of europium(III) luminescence. J Chem Soc Perkin Trans 2:2359–2360

Toner JL, Saha AK, Kross K, Kloszewski ED, Upson DA, Snow RA, Black CDV, Desai VC (1993) Time resolved fluorescence of a new europium chelate complex – demonstration of highly sensitive detection of protein and DNA samples. J Am Chem Soc 115:11032–11033

Werts MHV, Verhoeven JW, Hofstraat JW (2000a) Efficient visible light sensitisation of water soluble near infra-red luminescent lanthanide complexes. J Chem Soc Perkin Trans 2:433–439

Werts MHV, Wondenberg RH, Emmerink PG, van Gassel R, Hofstraat JW, Verhoeven JW (2000b) A near infra-red luminescent label based on Yb(III) ions and its application to a fluoroimmunoassay. Angew Chem Int Ed Engl 39:4542–4544

8 Magnetic Resonance Signal Amplification Probes

A. A. Bogdanov Jr., J. W. Chen, H. W. Kang, R. Weissleder

The ability to image specific molecular biomarkers in vivo would have important implications for the earliest detection of cancer, in assessing specific targeted therapies, and for monitoring dynamic changes in expression patterns during disease progression. However, many molecular biomarkers are expressed in low numbers, necessitating novel imaging signal amplification strategies.

Among various signal amplification strategies described so far (reviewed in Aime et al. 2002; Bogdanov and Weissleder 1998) we chose to focus on: (1) internalization of superparamagnetic particles via receptor-mediated endocytosis (Kang et al. 2002) and (2) magnetic resonance (MR) signal amplification mediated by enzymes (Bogdanov et al. 2002).

8.1 Receptor-Mediated Internalization

8.1.1 Transferrin Receptor Imaging

Initially, the receptor-mediated amplification approach has been investigated by using transferrin receptor (TfR) as a molecular shuttling system (Fig. 1). The expression of this receptor has been a subject of extensive research in molecular oncology because of its role in mediating macromolecular transport across the microvascular endothelium of the blood-brain barrier (Huwyler et al. 1996) and is overexpressed in many tumors. The latter observation suggested potential targetability of TfR for cancer therapy or tumor detection (Kresse et al. 1998; Weissleder et al. 2000). The potential of the receptor for gene expression imaging by MRI was also identified (Koretsky et al. 1996). MRI research suggested that receptor overex-

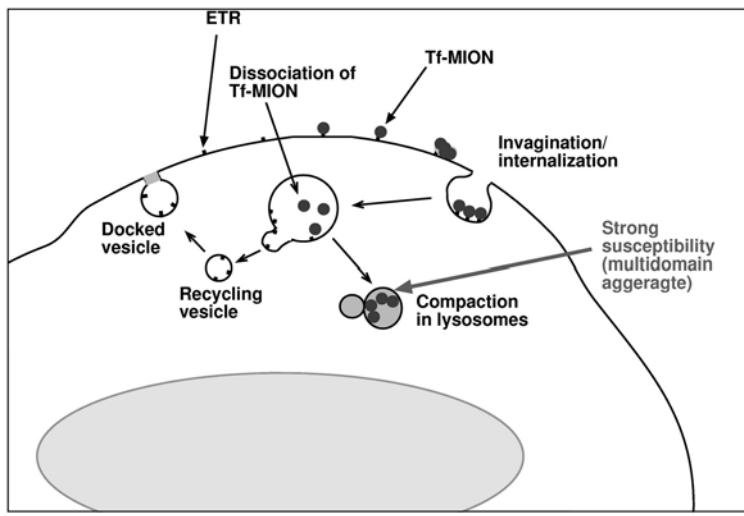

Fig. 1. Amplification through cellular internalization of iron oxide nanoparticles. Amplification is achieved as a result of iron oxide (magnetite) superparamagnetic susceptibility effect plus through nonregulated uptake and storage of iron oxide in intracellular compartment (formation of interacting multiple-domain systems)

pression could lead to iron accumulation in cells detectable by imaging (Kresse et al. 1998). The molecular basis of the observed effects is in the ability of TfR to internalize into the cells and to recycle back to the cell surface very rapidly. However, intracellular iron transport is tightly controlled and is a subject of feedback downregulation with resultant low efficiency of transferrin receptor as a vehicle for paramagnetic iron delivery into cells. We hypothesized that it would be possible to (1) circumvent the iron-mediated downregulation of transferrin receptor by "masking" iron in dextran-coated iron oxide nanoparticles (MION) conjugated with transferrin (Tf-MION), and (2) that Tf-MION would amplify the MR signal as a result of internalization and compartmentalization inside the cell. The amplification effect was expected because of the susceptibility effects generated by iron oxide microscopic magnetic field gradients from iron oxide particles that become stronger as the superparamagnetic crystalline domains (and magnetic moments) of several particles interact as they are confined in an intercellular vesicle (Moore et al. 1998). Diffusion of water protons in the vicinity of such gradients results in efficient transverse relaxation and susceptibility (the increase of R2 and R2*). Therefore, efficient internalization of iron oxide would result in increased transverse relaxivity of cells and, as a consequence, better detectability of receptor-positive cells. The results obtained in mouse xenografts suggested that transgene expression in tumors could be visualized noninvasively by MR imaging (Weissleder et al. 2000). The studies demonstrated that specific recognition of cell-surface receptor by targeted MR imaging probe with subsequent internalization could lead to dramatic relaxation time changes and susceptibility effects.

8.1.2 Inducible Endothelial Receptor Imaging

One of the most promising molecular imaging applications that can be accomplished using MRI is "precision" imaging of cell-surface molecules associated with the expression of mitotic or otherwise activated phenotypes. This important task can be potentially accomplished by using cell-surface targeted agents. We hypothesized that the prominent marker of endothelial activation and proinflammatory

molecule, E-selectin (ELAM-1) expression in tumor endothelium can be of prime importance for imaging tumor angiogenesis. The expression of E-selectin is transcriptionally upregulated as a result of endothelial cell exposure to several cytokines (e.g., IL-1β and TNFα) and lipopolysaccharide (Luscinskas et al. 1989; Montgomery et al. 1991). As demonstrated previously, several monoclonal antibodies to human E-selectin detect inducible E-selectin expression in human endothelial cells with high specificity (Bevilacqua et al. 1987; Peters 1998). E-selectin-targeted immunoliposomes and anti-E-selectin-hirudin conjugates prepared using H18/7 antibody were previously shown to bind to activated human endothelial cells in vitro at levels exceeding 200-fold those of control cells. These findings suggest that H18/7 antibody or its fragments can potentially serve as excellent targeting ligands for designing imaging probes.

One of the properties of E-selectin that made iron oxide-mediated targeting approach especially attractive is the ability of E-selectin to internalize soon after expression on the cell surface (Chuang et al. 1997; von Asmuth et al. 1992). Internalization of E-selectin is a tubulin-dependent process governed by the signal expressed in the cytoplasmic domain of E-selectin. It has already been established that E-selectin-bound mAb can be recovered in intracellular compartments with a tubular morphology (apparently, tubular lysosomes). Therefore, we set forth to design a highly superparamagnetic conjugate of CLIO (cross-linked iron oxide) and $F(ab')_2$ fragment isolated from H18/7 antibody.

In experiments involving the binding of CLIO-$F(ab')_2$ to human endothelial umbilical cord cells (HUVEC) that are either IL-1β activated or control cells, we observed a very highly specific binding to activated endothelial cells in vitro (Table 1). By using a ^{125}I-labeled CLIO-$F(ab')_2$ preparation we determined that on the average $0.14 \pm 0.05\%$ of initial iron oxide added was bound to IL-1β-treated HUVEC if CLIO-$F(ab')_2$ was added to cells at the concentration of 1.2–2.4 μg iron/ml. In the absence of IL-1β pretreatment, only 0.02%–0.06% of iron was taken up by the endothelial cells at the same concentration of iron added. Thus, our results indicate that CLIO-bound antibody preserved its specificity (approximately 50-fold higher binding to activated than to control cells) and that the HUVECs bind CLIO-$F(ab')_2$ with high efficiency (approximately

Table 1. Different binding of CLIO-F(ab′)$_2$ to HUVEC cells in the presence or absence of IL-1β pretreatment

Preparation	CLIO-F(ab′)$_2$ [a]	
HUVEC, IL-1β treatment	+	–
Iron binding, ng/mln cells [b]	104 ± 12	2.1
F(ab′)$_2$ binding, ng/mln cells [b]	5.5 ± 0.8	0.1
T2, ms	29 ± 2	> 1,500

[a] CLIO-F(ab′)$_2$: Fe 0.6 mg/ml, F(ab′)$_2$ 40.8 mg/ml, Fe/F(ab′)$_2$ = 15.
[b] Data presented as mean ± SD (n = 2).

0.1 pg iron/cell). The shortening of T2 relaxation times of water was proportional to the amount of iron associated with the cells (Table 1). Cells treated with CLIO-F(ab′)$_2$ conjugate were pelleted and studied using MR imaging to determine whether differential binding of CLIO-F(ab′)$_2$ to nontreated versus IL-1β-treated cells would be reflected in differential effects on MR signal intensity. T2-weighted MR spin-echo images reveal remarkable differences in signal intensities of IL-1β-treated and control cells. Endothelial cells stimulated with IL-1β showed a substantially stronger contrast enhancement. There was no detectable signal in pellets of cells incubated with CLIO-F(ab′)$_2$ without pretreatment with IL-1β. This result is thus in agreement with the quantitative analysis of CLIO-F(ab′)$_2$ binding to HUVECs (Table 1). Since an increase of CLIO-F(ab′)$_2$ uptake after IL-1β treatment could be a result of additional cytokine-mediated activation of adsorptive endocytosis or pinocytosis, we tested this using several control preparations. We compared binding of H18/7 F(ab′)$_2$ conjugated to cross-linked iron oxides (CLIO). Results of MR imaging clearly demonstrate that the profound signal intensity changes detected in IL-1β-activated HUVECs incubated with CLIO-F(ab′)$_2$ do not stem from the augmentation of nonspecific uptake mechanisms since cells incubated in the presence of control nanoparticles did not show any measurable uptake before or after IL-1β treatment. Interestingly, the excess of free H18/7 F(ab′)$_2$ inhibited binding and uptake by IL-1β-treated cells only by 20% on the average, suggesting a multipoint interaction of CLIO-F(ab′)$_2$ with the cell surface, i.e., a higher avidity of the resultant conjugate.

The obtained data demonstrate that: (1) H18/7 or control $F(ab')_2$ fragments can be covalently modified with *N*-Succinimidyl-acetyl-thioacetate (SATA) and attached to superparamagnetic nanoparticles using thiol-disulfide exchange reaction, (2) anti-E selectin nanoparticles bound with high specificity to IL-1β-stimulated HUVECs, and (3) specific interaction between CLIO-$F(ab')_2$ and HUVEC can be directly imaged using MRI. Our experiments provided evidence of the feasibility of E-selectin imaging and justified further development of MR-targeted agents for monitoring proinflammatory markers associated with tumor vascular endothelial proliferation, angiogenesis, and atherosclerosis.

8.2 Enzyme-Mediated MR Signal Amplification

Several MR amplification strategies can be used to increase the atomic relaxivity of paramagnetic lanthanides, which is critical for detecting low numbers of target molecules. This is commonly achieved by modulating the rotational correlation time (τ_r). So far, three different ways of decreasing rotational mobility of metal complexes had been considered: (1) dispersing paramagnetic chelated metal ions into a high viscosity compartments, (2) covalent attachment of paramagnetic complexes to macromolecules, and (3) noncovalent binding of chelated complexes to macromolecules. We hypothesized that there exists a fourth strategy leading to a similar τ_r increase. This strategy would include condensation (or polymerization) of low relaxivity complexes into higher relaxivity products. Therefore, we originally developed and subsequently explored a generic method of signal amplification that relies on enzyme-mediated substrate conversion into magnetically active oligomers, exemplified by DOTA(Gd) tyramide polymerization (MRamp). The major advantage of MRamp is in that a single substrate can potentially be used as a reporter for thousands of targets, using an antibody-enzyme conjugate as the primary reporter, similar to that of a traditional enzyme-linked immunoassay (Fig. 2). Specifically, we assumed that the oxidoreductases (e.g., peroxidases, designated as $E^{\bullet}$ below, of which horseradish peroxidase and myeloperoxidase have been already tested) would catalyze the reduction of peroxide using a low-

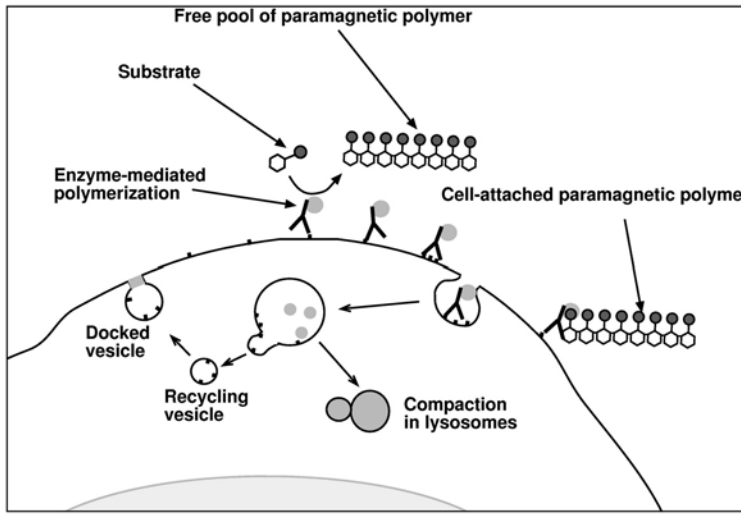

Fig. 2. Magnetic resonance amplification as a result of enzyme-mediated polymerization of paramagnetic substrates: hypothetical mechanisms of amplification after binding of enzyme-tagged, target-specific molecules (e.g., antibodies) to the cell surface

relaxivity, paramagnetic substrate (AH) as a donor of electrons (reaction 1).

$$2\,\mathrm{AH} + [\mathrm{E}^{\bullet}\mathrm{H_2O_2}] \rightarrow 2\,[*\mathrm{A}] + 2\,\mathrm{H_2O} + \mathrm{E} \quad (1)$$

$$\mathrm{n}[*\mathrm{A}] \rightarrow [\mathrm{A}]\mathrm{n} \quad (2)$$

Oxidized substrate molecules (*A) would then self-polymerize (oligomerize) into the larger, high relaxivity paramagnetic oligomers ([A]n, reaction 2). Catalytic generation of hydrogen peroxide (serving as oxidizer in this reaction) can be used by including glucose oxidase as the second enzymatic component in this reaction in vitro and in vivo. Relaxometric measurements and theoretical calculations have shown a 2.5-fold increase in relaxivity at imaging field strengths that is primarily modulated by an increase in the rotational correlation time as a result of the oligomerization.

Another class of enzymes that catalyze polymerization of monophenols, tyrosinases (monophenol, oxygen oxidoreductases), could be potentially utilized as an alternative to the glucose oxidase/peroxidase system. Unlike peroxidase, tyrosinase catalyzes two consecutive reactions using monophenols for hydroxylation and subsequent oxidation to quinones. Self-polymerizing quinones bearing a paramagnetic label can form large-molecular weight products and thus contribute to an increase of atomic relaxivity of paramagnetic lantanides.

Therefore, the potential advantages of MRamp are: (1) it utilizes low molecular weight lanthanide complexes which are converted into large molecules "on site," (2) the development of these low molecular weight precursors is clinically viable, (3) the observed relaxivity changes are higher or similar to that of other amplification strategies, (4) the oligomerized products can be designed to reside locally, and (5) the method can be used in a variety of generic ways, potentially allowing the read-out of many different targets. So far, we have shown that the method holds promise in the (1) MR detection of a model ligand using an enzyme-linked immunoadsorbent assay format, (2) imaging of a proinflammatory marker, E-selectin, on the surface of endothelial cells, and (3) detection of endogenous enzymes – tyrosinase and myeloperoxidase. Two primary targets are currently under investigation: a mutant, constitutively active ΔEGFR and angiogenesis-modulated E-selectin. ΔEGFR expression strongly upregulates VEGF expression which, in turn, upregulates E-selectin and tube formation by endothelial cells. These targets were chosen because of their importance in tumor proliferation, modulation by chemotherapy (e.g., EGFR tyrosine kinase inhibitors) and the current lack of imaging probes directed against them. To further increase the sensitivity of MRamp, we are investigating novel paramagnetic substrates to exploit changes in T1 (gadolinium) and T2/T2* effect (dysprosium).

8.2.1 Myeloperoxidase-Specific Substrates

Myeloperoxidase (MPO) is an endogenous enzyme of clinical interest because it is secreted by activated macrophages and neutrophils

in response to injury. MR imaging of MPO activity in vivo has the potential to reveal detailed knowledge of inflammatory diseases such as rheumatoid arthritis and atherosclerosis. To investigate the application of the MRamp strategy to imaging MPO, we developed and tested various substrates against MPO. We found that DOTA(Gd) 5-hydroxytryptamine, in the presence of MPO and peroxide, such as that produced by glucose oxidase, rapidly oligomerizes. The oligomer demonstrates an increase in T1 relaxivity similar to that of DOTA(Gd) tyramide with horseradish peroxidase. Furthermore, the degree of enhancement appears to be proportional to the amount of MPO present. In vitro imaging experiments performed at 1.5 T in phantoms containing matrigel demonstrates the ability of the 5-hydroxytryptamine substrate to polymerize at the surface of the Matrigel^{TM} in the presence of MPO and glucose oxidase, resulting in the selective enhancement on T1 weighted images of the interface/border of the matrigel.

8.2.2 Dysprosium-Based Substrates

Dysprosium has a large magnetic susceptibility, making it a potential T2/T2* imaging agent. We have investigated the potential of the MRamp strategy to cause T2/T2* shortening (reverse amplification) utilizing the substrate DOTA(Dy) tyramide. In the presence of a peroxidase such as horseradish peroxidase, there is a 30% shortening of T2/T2* at both 1.5 T and 7 T, and this shortening is further amplified when the substrates are compartmentalized in liposomes. Because T2/T2* relaxivity increases with field strength, a dramatic signal difference is obtained at 7 T on T2 weighted images. Combining with the ability to target enzyme activity, dysprosium-based MRamp substrates are potential high field enzyme reporter agents.

Acknowledgements. The authors received support from NIH grants, Schering AG and RSNA Seed Grant.

References

Aime S, Cabella C, Colombatto S, Geninatti Crich S, Gianolio E, Maggioni F (2002) Insights into the use of paramagnetic Gd(III) complexes in MR-molecular imaging investigations. J Magn Reson Imaging 16:394–406

Bevilacqua MP, Pober JS, Mendrick DL, Cotran RS, Gimbrone MA, Jr (1987) Identification of an inducible endothelial-leukocyte adhesion molecule. Proc Natl Acad Sci 84:9238–9242

Bogdanov A, Jr, Weissleder R (1998) The development of in vivo imaging systems to study gene expression. Trends Biotechnol 16:5–10

Bogdanov A, Jr, Matuszewski L, Bremer C, Petrovsky A, Weissleder R (2002) Oligomerization of paramagnetic substrates results in signal amplification and can be used for MR imaging of molecular targets. Mol Imaging 1:16–23

Chuang PI, Young BA, Thiagarajan RR, Cornejo C, Winn RK, Harlan JM (1997) Cytoplasmic domain of E-selectin contains a non-tyrosine endocytosis signal. J Biol Chem 272:24813–24818

Huwyler J, Wu D, Pardridge W (1996) Brain drug delivery of small molecules using immunoliposomes. Proc Natl Acad Sci 93:14164–14169

Kang HW, Josephson L, Petrovsky A, Weissleder R, Bogdanov A, Jr (2002) Magnetic resonance imaging of inducible E-selectin expression in human endothelial cell culture. Bioconj Chem 13:122–127

Koretsky A, Lin Y, Schorle H, Jaenisch R (1996) Genetic control of MRI contrast by expression of the transferrin receptor. In: Proceedings of the Fourth Meeting of the International Society for Magnetic Resonance in Medicine, Berkeley, CA, 1996. International Society for Magnetic Resonance in Medicine, New York, pp 69

Kresse M, Wagner S, Pfefferer D, Lawaczeck R, Elste V, Semmler W (1998) Targeting of ultrasmall superparamagnetic iron oxide (USPIO) particles to tumor cells in vivo by using transferrin receptor pathways. Magn Reson Med 40:236–242

Luscinskas FW, Brock AF, Arnaout MA, Gimbrone MA (1989) Endothelial-leukocyte adhesion molecule-1-dependent and leukocyte (CD11/CD18)-dependent mechanisms contribute to polymorphonuclear leukocyte adhesion to cytokine-activated human vascular endothelium. J Immunol 142:2257–2263

Montgomery KF, Osborn L, Hession C, Tizard R, Goff D, Vassallo C, Tarr PI, Bomsztyk K, Lobb R, Harlan JM (1991) Activation of endothelial-leukocyte adhesion molecule 1 (ELAM-1) gene transcription. Proc Natl Acad Sci 88:6523–6527

Moore A, Basilion J, Chiocca A, Weissleder R (1998) Measuring transferrin receptor gene expression by NMR imaging. Biochim Biophys Acta 1402: 239–249

Peters AM (1998) The use of nuclear medicine in infections. Brit J Radiol 71:252–261

von Asmuth EJ, Smeets EF, Ginsel LA, Onderwater JJ, Leeuwenberg JF, Buurman WA (1992) Evidence for endocytosis of E-selectin in human endothelial cells. Eur J Immunol 22:2519–2526

Weissleder R, Moore A, Mahmood U, Bhorade R, Benveniste H, Chiocca EA, Basilion JP (2000) In vivo magnetic resonance imaging of transgene expression. Nature Med 6:351–355

9 Imaging of Proteases for Tumor Detection and Differentiation

C. Bremer

9.1 Introduction

Major challenges for the molecular imaging community are (a) defining diagnostically relevant targets and (b) developing suitable imaging methods to noninvasively depict those targets. Various molecular substrates such as DNA, RNA, or proteins could serve as potential imaging targets. However, targeting intracellular structures in vivo is a major pharmacological challenge since several delivery barriers have to be overcome. Moreover, there is a natural "signal amplification" in the transcription and translation process resulting in several copies of RNA from one DNA template and again multiple protein copies of the mRNA. Therefore "downstream imaging" (i.e., molecular imaging on the protein level) should be the most promising approach to detecting molecular structures in an intact organism.

Compared to conventional imaging approaches even targeting whole cells, which measure 5–20 μm in diameter in size, is an ambitious goal. However, looking at protein structures is an even more challenging task and therefore requires efficient contrasting strategies with excellent signal-to-noise ratios (SNR). Nuclear imaging modalities have been the mainstay for in vivo probing of molecular substrates since radioactive tracers are employed without any natural background signal and therefore high SNR can be achieved. In contrast, detecting molecular structures by magnetic resonance imaging (MRI) is a very challenging task as protons are omnipresent within the body because approximately 65% of the body consists of water, contributing to a high background signal. More recently, very promising approaches have been undertaken to exploit "smart" MR-contrast agents as well as carbon or fluorine compounds serving as specific molecular contrast agents in vivo.

9.2 Light for Molecular Imaging

Using light for in vivo imaging is an emerging imaging modality which offers some unique advantages for molecular in vivo imaging:

1. Different optical techniques have already been used for many years in the molecular biology community to probe tissue samples or cells (such as the use of fluorescent proteins, fluorescently labeled antibodies, etc.) and can be adapted for in vivo applications.
2. In the near infrared range (NIR) very little tissue auto-fluorescence can be observed offering excellent signal-to-noise ratios (SNR) comparable to conventional nuclear imaging techniques. Besides offering high SNR, light in the NIR can traverse tissue very efficiently as the absorption by water and hemoglobin is relatively low in this spectrum ("diagnostic window"; Ntziachristos and Weissleder 2001).
3. Functional paradigms can be applied for optical contrast agents (such as fluorescence resonance energy transfer or bioluminescence) in order to detect specific target interactions in vivo (such as enzyme activity).

9.3 Optical Contrast Agents

Various strategies can be pursued to obtain optical information from the tissue ranging from nonspecific perfusion contrast agents to targeted or "smart" optical probes (Fig. 1).

While nonspecific perfusion agents such as indocyanine green (ICG) can only depict tumor physiology such as perfusion, vessel permeability, or tissue blood volume, molecular information can not be obtained using this approach.

Targeted contrast agents, however, are linked to affinity ligands imparting molecular specificity to the optical probe. Ideally, these

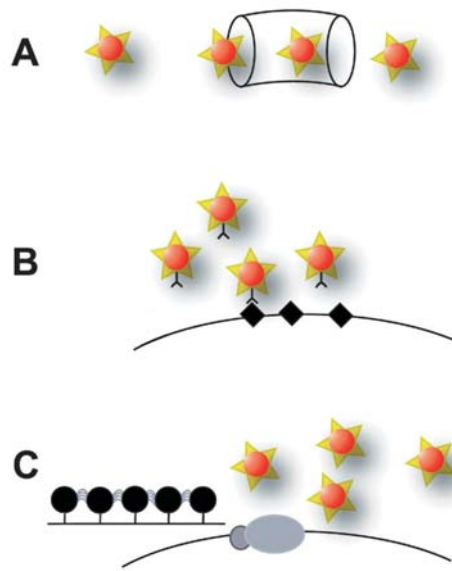

Fig. 1A–C. Design of different optical contrast agents. Nonspecific fluorochromes such as indocyanine green (**A**) show perfusion and/or permeability properties of the tissue. Targeted probes (**B**) bind via specific ligands to protein structures on the cell surface such as tumor-associated receptors; unbound probe contributes to background signal, lowering the SNR. "Smart" probes (**C**) are activated by enzymatic conversion yielding a strong fluorescence increase once the fluorochromes are released from the backbone (*right*). Tumor-associated proteases can be detected using this approach (reprinted with permission from Bremer et al. 2003)

contrast agents are accumulated at the target over time offering a strong signal in the region of interest (Fig. 1). However, there is – especially in the early phase after injection – a fair amount of unbound circulating material contributing to background signal and therefore lowering the SNR. Different targeted contrast agents have been described and experimentally validated using large molecules such as antibodies (AB) or AB fragments to small peptide derivatives serving as tissue-specific affinity ligands (e.g., bombesin, somatostatin, or the folated receptor; (Becker et al. 2001; Licha et al. 2002)).

"Smart" optical probes change their signal characteristics upon interaction with the target. They ideally undergo a status of zero signal in their native state to a strong signal after target interaction. A class of smart optical contrast agents was recently described, which undergo conformational changes after cleavage by various enzymes (Weissleder et al. 1999; Fig. 1C). In 1999, the first autoquenched fluorescent probe was developed, which is converted from a non-fluorescence to fluorescence state by proteolytic activation (Weissleder et al. 1999).

The first generation of this smart contrast agent consists of a long circulating carrier molecule (poly-lysine backbone, ~ 450 kDa) shielded by multiple methoxy-polyethylene-glycol sidechains (PLL-MPEG). Twelve to 14 cyanine dyes (Cy 5.5) are loaded onto this carrier molecule resulting in a signal quench due to fluorescence resonance energy transfer (FRET; Weissleder et al. 1999). Thus, in its native state the molecule exhibits very little to no fluorescence, whereas after enzymatic cleavage a strong fluorescence signal increase (up to several 100-fold) can be detected (dequenching; Fig. 1C). Inhibition experiments revealed that this first generation of protease-sensing optical probes are activated mainly by lysosomal cysteine or serine proteases such as cathepsin-B (Weissleder et al. 1999).

The selectivity of this smart optical probe can be tailored to other enzymes by insertion of enzyme-specific peptide stalks between the carrier and the fluorochromes. In order to impart MMP-2 selectivity, for instance, a peptide stalk with the following sequence: -Gly-Pro-Leu-Gly-Val-Arg-Gly-Lys- was inserted between the backbone and the fluorochrome. This peptide sequence is recognized by MMP-2 with a high affinity resulting in an efficient dequenching of the completely

assembled MMP-2 probe by the purified enzyme. A control-probe that was synthesized using a scrambled peptide sequence (-Gly-Val-Arg-Leu-Gly-Pro-Gly-Lys-) remained quenched after incubation with the enzyme. Besides MMPs, other enzyme systems such as cathepsin-D or thrombin could be targeted using this approach (Weissleder et al. 1999; Bremer et al. 2001 a, b).

9.3.1 Oncological Imaging

Different proteases are known to be key players in a whole variety of pathologies ranging from carcinogenesis to immune diseases (Edwards and Murphy 1998). It is known that various proteases such as cathepsins and matrix-metalloproteinases are involved in a cascade of enzymes, which finally yields to the digestion of the extracellular matrix and thus local as well as metastatic tumor cell infiltration (Edwards and Murphy 1998; Fang et al. 2000; Folkman 1999; Aparicio et al. 1999; Herszenyi et al. 1999; Koblinski et al. 2000). Indeed, clinical data suggest that tumoral protease burden correlates with clinical outcome (McCarthy et al. 1999; Kanayama et al. 1998; Davidson et al. 1999).

The first experimental studies using a LX-1 tumor xenograft model showed that even small tumor nodules could be sensitively contrasted with the cathepsin-B sensing optical probe, suggesting that protease imaging might be a feasible approach for early cancer detection (Weissleder et al. 1999; Mahmood et al. 1999). Indeed, there is evidence that protease overexpression is an early step involved in malignant cell transformation. In colon cancer, for example, cathepsin-B and matrix-metalloproteinases have been found to be upregulated within the invasive tumor margins (Campo et al. 1994; Emmert-Buck et al. 1994; Khan et al. 1998 a, b). In line with this observation is the fact that even premalignant gastrointestinal lesions could be detected by enyzme-sensing molecular beacons (Marten et al. 2002). Dysplastic colon polyps in aged $APC^{Min/+}$ mice serving as a model for spontaneous adenomatosis coli could be sensitively detected using the cathepsin-B sensing optical probe (Marten et al. 2002). Even lesions in the submillimeter range (50 μm in diameter), which were invisible with white-light inspection, could be visualized

using this approach. Lesion conspicuity could be significantly enhanced compared to visual inspection, yielding a sensitivity of about 96% and a specificity of about 93% (Marten et al. 2002).

Highly invasive cancers have been linked to a higher load of proteases in both clinical and experimental investigations (McCarthy et

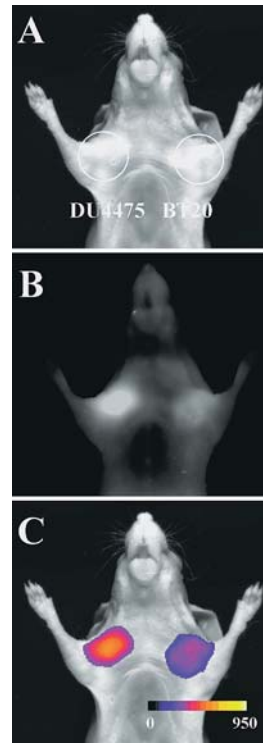

Fig. 2A–C. Tumor differentiation with NIRF imaging using protease-sensing probes. Fluorescence reflectance imaging using a cathepsin-B sensing optical probe. The animal was implanted with a highly invasive (DU4475; *right chest*) and a well-differentiated breast adenocarcinoma (BT20; *left chest*); light image (**A**), raw NIRF image (**B**), and color-encoded NIRF signal (AU of NIRF-intensity) superimposed on light image (**C**). Due to a higher protease load, the invasive breast lesion activated the probe more efficiently, resulting in a higher NIRF signal of the tumor (**B**, **C** reprinted with permission from Bremer et al. 2002)

al. 1999; Kanayama et al. 1998; Davidson et al. 1999; Kuniyasu et al. 1999; Murray et al. 1996; Sakakibara et al. 1999). Therefore, noninvasive tumor grading might be another application of protease imaging. In a breast cancer xenograft model, a highly invasive human adenocarcinoma (DU4475) was tested against a well-differentiated breast adenocarcinoma (BT20; Bremer et al. 2002; Fig. 2). In accordance with the literature, the protease load (cathepsin-B) of the DU4475 tumor cells was about 1.7-fold higher compared to the well-differentiated adenocarcinoma. Fluorescence reflectance imaging (FRI) of the tumors revealed significantly stronger probe activation by the highly invasive compared to the well-differentiated tumor (Bremer et al. 2002). A grading of tumor types according to protease load can therefore be envisioned using protease sensing optical probes.

Treatment effects of novel protease inhibitors can also be visualized using protease-sensing optical probes (Bremer et al. 2001 a, b). Nude mice implanted with MMP overexpressing fibrosarcomas (HT1080) were treated with an MMP-protease inhibitor (AG3340, Aguron/Pfizer, San Diego, CA) and imaged by FRI using the MMP-sensing optical probe (see Sect. 9.3). Treatment resulted in a significant reduction of protease-induced NIRF signal which could be detected as early as 48 h after initiation of the treatment, long before phenotypical changes (such as regression of tumor size, rarefication of vasculature, etc.) can be seen (Bremer et al. 2001 b). Thus protease imaging is a very sensitive means to assess novel antitumor therapies (Bremer et al. 2001 b).

9.4 Nononcological Imaging

Protease imaging can potentially be applied to imaging the activity of autoimmune diseases such as rheumatoid arthritis (Ji et al. 2002). In a model of inducible rheumatoid arthritis, FRI with a cathepsin-B sensing probe detected inflammatory activity in the joints as early as 20 h after disease induction while clinical manifestations of the disease were still discrete (Ji et al. 2002).

Inflammatory activity in atherosclerotic soft plaques were recently visualized by FRI using the cathepsin B probe (Chen et al.

2002). Twenty four hours after probe injection, aortic atherosclerotic plaques showed strong probe activation in ApoE-deficient mouse strains that were kept on a Western-style, lipid-rich diet (Chen et al. 2002). There was a clear colocalization of tissue fluorescence and soft plaques in the mouse aorta. Cathepsin B expression was confirmed by immunohistochemistry of plaques sections. Moreover, thrombin activity was recently visualized using a dedicated thrombin-sensitive optical probe (Tung et al. 2002). Since thrombin is a key enzyme in hemostasis and thrombotic events, a screening for clotting disorders or thrombosis might be possible with this molecular sensor (Tung et al. 2002).

9.5 Potential Clinical Applications

With the advent of three-dimensional, quantitative imaging methods for detection of fluorochrome distribution such as fluorescence-mediated tomography (FMT; Ntziachristos and Weissleder 2001; Ntziachristos et al. 2001, 2002a, b), a wide range of clinical applications of optical imaging can be envisioned (Fig. 3). Numerical simulations based on current laboratory data suggest that FMT can be upscaled for human use (Ntziachristos et al. 2002c). Moreover, in a clinical study combing gadolinium-enhanced MRI with indocyanine-green-enhanced diffuse optical tomography (DOT), breast lesions could be optically resolved, which serves as a proof of principle for the applicability of this concept for human use.

Combining detailed anatomical resolution by MRI or CT with molecular information generated by optical signatures or contrast media, respectively, would greatly enhance the sensitivity and, most of all, the specificity of biomedical imaging. Contrast-enhanced optical breast imaging will be the first application to come and the first clinical studies are currently underway. However, other aspects of cancer imaging can potentially be addressed using FMT and smart or targeted optical probes including musculoskeletal, head and neck, and pediatric imaging applications.

Besides tomographic sensors, a combination of endoscopic or laparoscopic devices with optical fibers for fluorochrome detection should be feasible to build. Moreover, handheld scanning devices

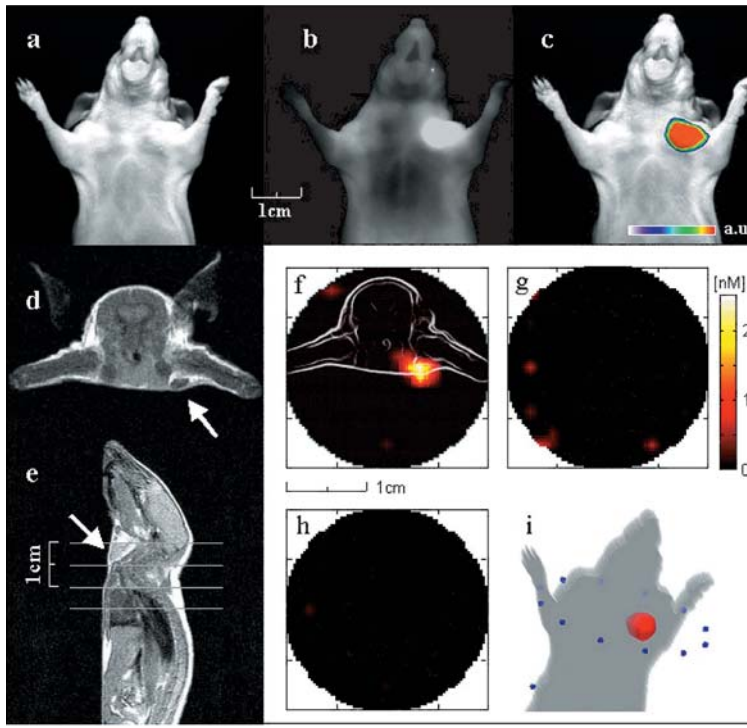

Fig. 3 a–i. Fluorescence mediated tomography (FMT). FMT allows for three-dimensional, quantitative imaging of fluorochrome distribution in vivo. **a** Intrinsic light image obtained with reflectance imaging. **b** Fluorescence image obtained with reflectance imaging. **c** Superposition of **b** onto **a** after threshold application. **d** MRI axial slice at the level of the uppermost FMT slice acquired, with an *arrow* denoting the tumor location. **e** MRI sagittal slice with lines denoting the three-slice volume segmentation assumed by FMT. A fibrosarcoma was implanted in the mammary fat pad of a nude mouse. An *arrow* denotes the tumor location. **f–h** Reconstructed FMT slices. The outline of the axial MRI slice is shown superimposed in **f** for registration purposes. **i** Volume rendering of the FMT dataset (*red*). *Blue spheres* denote the locations of the most superior ring of detectors. Note that three-dimensional, quantitative assessment of fluorochrome distribution is feasible using FMT (reprinted with permission from Ntziachristos et al. 2002a)

comparable to ultrasound probes may be useful to screen for superficial fluorochrome detection.

In summary, optical imaging techniques provide excellent tools for probing molecular information in vivo both for experimental and clinical applications.

References

Aparicio T, Kermorgant S, Dessirier V, Lewin MJ, Lehy T (1999) Matrix metalloproteinase inhibition prevents colon cancer peritoneal carcinomatosis development and prolongs survival in rats. Carcinogenesis 20:1445–1451

Becker A, Hessenius C, Licha K, Ebert B, Sukowski U, Semmler W, Wiedenmann B, Grotzinger C (2001) Receptor-targeted optical imaging of tumors with near-infrared fluorescent ligands. Nat Biotechnol 19:327–331

Bremer C, Tung CH, Weissleder R (2001) In vivo molecular target assessment of matrix metalloproteinase inhibition. Nat Med 7:743–748

Bremer C, Bredow S, Mahmood U, Weissleder R, Tung CH (2001 a) Optical imaging of matrix metalloproteinase-2 activity in tumors: feasibility study in a mouse model. Radiology 221:523–529

Bremer C, Tung CH, Bogdanov A, Jr, Weissleder R (2002) Imaging of differential protease expression in breast cancers for detection of aggressive tumor phenotypes. Radiology 222:814–818

Bremer C, Ntziachristos V, Weissleder R (2003 b) Optical-based molecular imaging: contrast agents and potential medical applications. Eur Radiol 13:231–243

Campo E, Munoz J, Miquel R, Palacin A, Cardesa A, Sloane BF, Emmert-Buck MR (1994) Cathepsin B expression in colorectal carcinomas correlates with tumor progression and shortened patient survival. Am J Pathol 145:301–309

Chen J, Tung CH, Mahmood U, Ntziachristos V, Gyurko R, Fishman MC, Huang PL, Weissleder R (2002) In vivo imaging of proteolytic activity in atherosclerosis. Circulation 105:2766–2771

Davidson B, Goldberg I, Kopolovic J, Lerner-Geva L, Gotlieb WH, Ben-Baruch G, Reich R (1999) MMP-2 and TIMP-2 expression correlates with poor prognosis in cervical carcinoma – a clinicopathologic study using immunohistochemistry and mRNA in situ hybridization. Gynecol Oncol 73:372–382

Edwards DR, Murphy G (1998) Cancer. Proteases – invasion and more. Nature 394:527–528

Emmert-Buck MR, Roth MJ, Zhuang Z, Campo E, Rozhin J, Sloane BF, Liotta LA, Stetler-Stevenson WG (1994) Increased gelatinase A (MMP-

2) and cathepsin B activity in invasive tumor regions of human colon cancer samples. Am J Pathol 145:1285–1290

Fang J, Shing Y, Wiederschain D, Yan L, Butterfield C, Jackson G, Harper J, Tamvakopoulos G, Moses MA (2000) Matrix metalloproteinase-2 is required for the switch to the angiogenic phenotype in a tumor model. Proc Natl Acad Sci USA 97:3884–3889

Folkman J (1999) Angiogenic zip code. Nat Biotechnol 17:749

Herszenyi L, Plebani M, Carraro P, De Paoli M, Roveroni G, Cardin R, Tulassay Z, Naccarato R, Farinati F (1999) The role of cysteine and serine proteases in colorectal carcinoma. Cancer 86:1135–1142

Ji H, Ohmura K, Mahmood U, Lee DM, Hofhuis FM, Boackle SA, Takahashi K, Holers VM, Walport M, Gerard C, Ezekowitz A, Carroll MC, Brenner M, Weissleder R, Verbeek JS, Duchatelle V, Degott C, Benoist C, Mathis D (2002) Arthritis critically dependent on innate immune system players. Immunity 16:157–168

Kanayama H, Yokota K, Kurokawa Y, Murakami Y, Nishitani M, Kagawa S (1998) Prognostic values of matrix metalloproteinase-2 and tissue inhibitor of metalloproteinase-2 expression in bladder cancer. Cancer 82:1359–1366

Khan A, Krishna M, Baker SP, Banner BF (1998 a) Cathepsin B and tumor-associated laminin expression in the progression of colorectal adenoma to carcinoma. Mod Pathol 11:704–708

Khan A, Krishna M, Baker SP, Malhothra R, Banner BF (1998 b) Cathepsin B expression and its correlation with tumor-associated laminin and tumor progression in gastric cancer. Arch Pathol Lab Med 122:172–177

Koblinski JE, Ahram M, Sloane BF (2000) Unraveling the role of proteases in cancer. Clin Chim Acta 291:113–135

Kuniyasu H, Ellis LM, Evans DB, Abbruzzese JL, Fenoglio CJ, Bucana CD, Cleary KR, Tahara E, Fidler IJ (1999) Relative expression of E-cadherin and type IV collagenase genes predicts disease outcome in patients with resectable pancreatic carcinoma. Clin Cancer Res 5:25–33

Licha K, Riefke B, Ebert B, Grotzinger C (2002) Cyanine dyes as contrast agents in biomedical optical imaging. Acad Radiol 9 [Suppl 2]:S320–322

Mahmood U, Tung CH, Bogdanov A, Jr, Weissleder R (1999) Near-infrared optical imaging of protease activity for tumor detection. Radiology 213: 866–870

Marten K, Bremer C, Khazaie K, Sameni M, Sloane B, Tung CH, Weissleder R (2002) Detection of dysplastic intestinal adenomas using enzyme-sensing molecular beacons in mice. Gastroenterol 122:406–414

McCarthy K, Maguire T, McGreal G, McDermott E, O'Higgins N, Duffy MJ (1999) High levels of tissue inhibitor of metalloproteinase-1 predict poor outcome in patients with breast cancer. Int J Cancer 84:44–48

Murray GI, Duncan ME, O'Neil P, Melvin WT, Fothergill JE (1996) Matrix metalloproteinase-1 is associated with poor prognosis in colorectal cancer. Nat Med 2:461–462

Ntziachristos V, Weissleder R (2001) Experimental three-dimensional fluorescence reconstruction of diffuse media by use of a normalized Born approximation. Optics Lett 26:893–895

Ntziachristos V, Tung C, Bremer C, Weissleder R (2001) Fluorescence-mediated tomography resolves protease activity in vivo. Nat Med 8:757–760

Ntziachristos V, Bremer C, Weissleder R (2002a) Fluorescence imaging with near-infrared light: new technological advances that enable in vivo molecular imaging. Eur Radiol 13:195–208

Ntziachristos V, Bremer C, Graves EE, Ripoll J, Weissleder R (2002b) In vivo tomographic imaging of near-infrared fluorescent probes. Mol Imaging 1:82–88

Ntziachristos V, Ripoll J, Weissleder R (2002c) Would near-infrared fluorescence signals propagate through large human organs for clinical studies. Optics Lett 27:527–529

Sakakibara M, Koizumi S, Saikawa Y, Wada H, Ichihara T, Sato H, Horita S, Mugishima H, Kaneko Y, Koike K (1999) Membrane-type matrix metalloproteinase-1 expression and activation of gelatinase A as prognostic markers in advanced pediatric neuroblastoma. Cancer 85:231–239

Tung CH, Gerszten RE, Jaffer FA, Weissleder R (2002) A novel near-infrared fluorescence sensor for detection of thrombin activation in blood. Chembiochem 3:207–211

Weissleder R (2001) A clearer vision for in vivo imaging. Nat Biotechnol 19:316–317

Weissleder R, Tung CH, Mahmood U, Bogdanov A, Jr (1999) In vivo imaging of tumors with protease-activated near-infrared fluorescent probes. Nat Biotechnol 17:375–378

10 Molecular Imaging with Targeted Ultrasound Contrast Microbubbles

A. L. Klibanov

10.1 Introduction

Molecular imaging is rapidly gaining momentum as the next-generation approach to the general goal of personalized medicine (Pither 2003). The front-runners of molecular imaging are nuclear medicine and PET modalities, which allow noninvasive monitoring of metabolic pathways and help detect certain molecules (e.g., receptors) such as tumor-specific antigens, angiogenesis, or apoptosis markers in the disease tissues. However, the most widespread imaging equipment worldwide is not a gamma camera/SPECT/PET, but ultrasound. Ultrasound imaging systems are abundant (tens of thousands units), easy to use, and inexpensive; they are small (portable, even laptop devices are available commercially), so they are quite suitable for the doctor's private practice use, for ambulance, field, or emer-

gency room applications. Therefore, if worldwide molecular imaging application is desired, capabilities of ultrasound should not be overlooked. The use of parenteral contrast will be needed to enable ultrasound in the molecular imaging.

Ultrasound contrast materials were proposed several decades ago (Gramiak and Shah 1968; reviewed in Goldberg et al. 2001). Contrast particles are usually micron-sized gas-filled microbubbles, that are injected intravenously and circulate with the flow of blood, gradually losing gas as it diffuses out of the bubble, dissolves in the surrounding biological fluids, and is eventually exhaled. Some such agents are already approved for clinical use in the United States, Canada, European countries, and Japan. Typically, up to several billions of contrast particles (with the combined particle mass of less than a milligram, overall gas volume of several microliters, dispersed in several ml of aqueous medium) are administered to the patient. Ultrasound contrast is well tolerated and could be applied for aiding organ delineation (e.g., myocardial border delineation and left ventricle opacification) or in radiology (e.g., to aid in imaging of liver malignancies; Dill-Macky et al. 2002). Successful studies of myocardial perfusion imaging have been reported (Lindner et al. 1999). The mechanism of action of ultrasound contrast is as follows. The contrast particle, being filled with gas, is much more compressible than surrounding aqueous biological fluid. Therefore, medical imaging ultrasound pressure waves (in MHz range) result in the compression and expansion of microbubbles, and effective ultrasound backscatter (Leighton 1997). These scattered ultrasound waves are detected by the imaging system transducer.

The general idea for using ultrasound contrast in molecular imaging is very straightforward. A targeting ligand (a protein, antibody, peptide, etc.) is attached to the surface of the contrast particles. Particles are administered in the circulation, where they selectively bind to the molecular receptors on the diseased tissues and accumulate there. Excess circulating particles are cleared from the bloodstream, and the target/normal tissue ratio of the ultrasound signal becomes high enough for selective imaging of the upregulated receptors distribution.

In order to design a successful ultrasound contrast material capable of targeted molecular imaging, the following criteria should be

applied. The contrast agent is harmless to the patient and generates no undesirable or toxic side effects. The agent is easily detected by ultrasound imaging equipment in small quantities. The ligand is attached to the contrast particles in a manner that does not impede its binding to the target receptors. The contrast material circulates in the bloodstream for the time sufficient to reach the target and bind to it (i.e., contrast has a chance and ability to reach the target). Targeted particles are attached firmly onto the surface of target tissue; particles are stable for the duration of the imaging exam (i.e., contrast on the target is stable enough so that diagnostic imaging could be performed). Contrast material should be inexpensive and easy to make, stable on storage, robust, and easy to handle.

In the following sections of the review we demonstrate how to design such ultrasound contrast materials, and attach targeting ligands to them. We describe targeting experiments performed with these contrast agents in vitro and in animal models in vivo. In a limited review setting it is not possible to discuss in detail all the research that takes place in the exciting area of targeted ultrasound imaging, and only some of the representative experimental studies and approaches will be discussed. The general aim is to show that targeted ultrasound contrast imaging may provide a viable alternative to nuclear medicine approaches, and bring molecular imaging into widespread clinical use.

10.2 Microbubble-Based Ultrasound Contrast Agents: General Design and Preparation

There are several types of ultrasound contrast agents, such as liquid emulsions (Andre et al. 1993; Lanza et al. 1996), liposomes (Alkan-Onyuksel et al. 1996), and gas-filled microbubbles (Fritz et al. 1997; Skyba et al. 1996; Schutt et al. 2003). We will focus this review on the microbubble-based contrast agents, due to their excellent ultrasound response, combined with good stability and targetability.

One would not expect that unprotected gas-filled bubbles would possess any reasonable degree of stability. The lifespan of a bubble in an aqueous medium is usually defined by the time it takes for the particle to float to the top of the solution and fuse with the atmo-

sphere or vial headspace (it may take up to an hour for a small micron-size bubble to reach the surface even in a high-viscosity medium, but long-term storage stability is a problem). Furthermore, if a gas microbubble is placed (or newly generated) in an aqueous medium, Laplace pressure is produced by surface tension, resulting in high internal pressure inside the bubble, which squeezes gas out of the bubble with its rapid dissolution in the surrounding medium (Epstein and Plesset 1950). Therefore, microbubble particles require a protective shell that will prevent gas loss and particle fusion; the shell will also aid in the improvement of the circulation time and stability in vivo. This protective shell may consist of lipid (Fritz et al. 1997), protein (Skyba et al. 1996), polymer (Villanueva et al. 2001), or combinations of these materials.

Obviously, one of the most convenient shell designs is based on lipid monolayers (Fig. 1). Lipid monolayer structures are usually prepared by self-assembly techniques. Surfactants from the aqueous medium are transferred to the newly generated gas-liquid interface as gas is dispersed in the liquid and position themselves at the interface, with the hydrophobic lipid tails facing towards the gas phase,

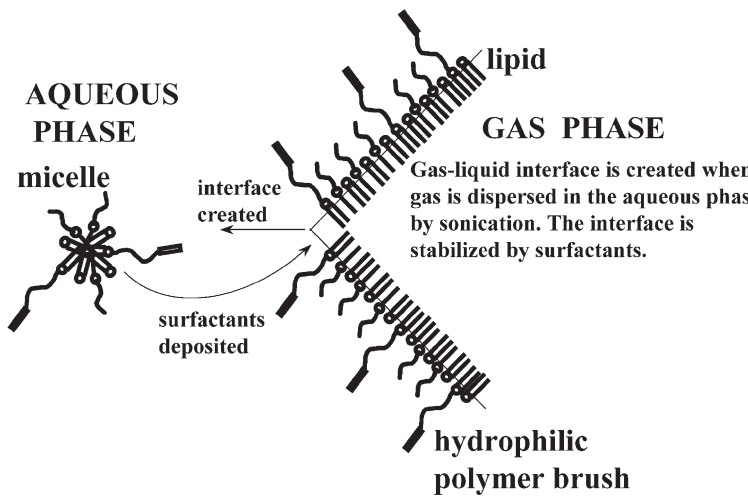

Fig. 1. Preparation of a microbubble coated with a lipid monolayer

and hydrophilic polar residues in the aqueous medium. If the monolayer is made of the molecules that do not possess a high level of cohesion, surfactant lateral diffusion would be high. This type of coating would not be able to serve as a good protective barrier. Storage stability of microbubbles prepared with such a coating will be quite poor. It is required to have a solid shell with little or no lateral diffusion or surface defects, so that resulting microbubbles will not be able to fuse with their neighbors upon storage. To eliminate gas loss due to Laplace pressure effect (Epstein and Plesset 1950), surface tension on such a bubble shell should be close to zero. One would expect that only thicker shells, such as those made of denatured proteins (albumin; Skyba et al. 1996) or organic polymers, like polylactide/glycolide (Yao et al. 2002), would be able to achieve this goal. However, solid phospholipid monolayer-coated microbubbles offer very reasonable stability at temperatures below the main transition temperature of the main lipid component (Lee et al. 2001; Borden and Longo 2002). Introduction of a grafted brush of hydrophilic poly(ethylene glycol) (PEG) polymer into the microbubble shell provides an additional degree of steric protection; in our experience, bubbles manufactured from distearoyl phosphatidylcholine (Tc $\sim 55\,^{\circ}$C) and PEG stearate were stable for months in refrigerated storage (Klibanov et al. 1999 a).

Actual preparation of such microbubbles is performed by simply dispersing gas (air, or preferably a poorly soluble gas, decafluorobutane) that is bubbled through the aqueous micellar solution (typically, several mg/ml) of a phospholipid, e.g., phosphatidylcholine, and PEG-containing surfactant, e.g., PEG stearate. Dispersion is performed with the aid of the probe-type sonicator (Klibanov et al. 1999 a), or other types of high-shear mixing (e.g., Fritz et al. 1997). As the new bubbles of gas are generated by high shear in the aqueous medium, they are immediately stabilized by deposition of the surfactant/phospholipid mixture on the bubble surface, with a monolayer self-assembly (Fig. 1). Gas is locked inside the bubble shell, and bubbles become protected from fusion with their neighbors and the atmosphere by the combination of "solid" phospholipid shell and a grafted PEG brush. The major advantage of this approach is in its flexibility: if one wants to introduce another lipid or surfactant in the bubble shell, it can be added to the aqueous solution at the mi-

celle preparation stage, usually at several mol %, prior to the bubble preparation stage (Klibanov et al. 1999a). This way, targeting ligands (outfitted with lipid anchors) or hydrophobic fluorescent probes can be introduced in the microbubble coating.

10.3 Targeting Ligand Attachment to Microbubbles

In order to achieve targetability of ultrasound contrast, selective ligands have to be attached to the microbubble shell. General ligand conjugation chemistry has been developed quite extensively during the past two decades, mostly for targeted nuclear scintigraphy agents and MRI contrast. Similar coupling schemes can be applied for the attachment of ligands to microbubbles. The major points to pay attention to in the established procedures are (a) the necessity to retain ligand ability to bind to the target upon coupling, (b) avoidance of reagents undesirable for parenteral applications, and (c) the ability to achieve high coupling yield and high surface density of the ligand on the bubble shell.

The most convenient technique, especially suitable for the early research stage, is the avidin-biotin coupling method (Fig. 2; Lindner et al. 2001). Biotinylated phospholipid derivative (preferably with a long PEG spacer arm) is synthesized and incorporated in the microbubble shell during bubble preparation as described above. After the bubbles are prepared, they need to be washed from the excess of the aqueous micellar lipid; this is usually accomplished by multiple centrifugal flotation. Streptavidin is then added to the microbubble preparation in excess to avoid homo- and heterocrosslinking of biotins on the bubble surface. Excess of free streptavidin is also removed by centrifugal flotation, and biotinylated ligand is added to the dispersion; it binds to the unoccupied biotin-binding moieties on streptavidin molecules. The main advantage of this approach lies in its ability to quickly add to the bubbles various new ligands for early research-stage testing; a large variety of targeting ligands, such as monoclonal antibodies, are available commercially, often in biotinylated form. Another advantage of this technique is that only a small amount of precious biotinylated ligand is needed for the preparation, and a ligand-to-bubble initial ratio can be chosen so that most of the

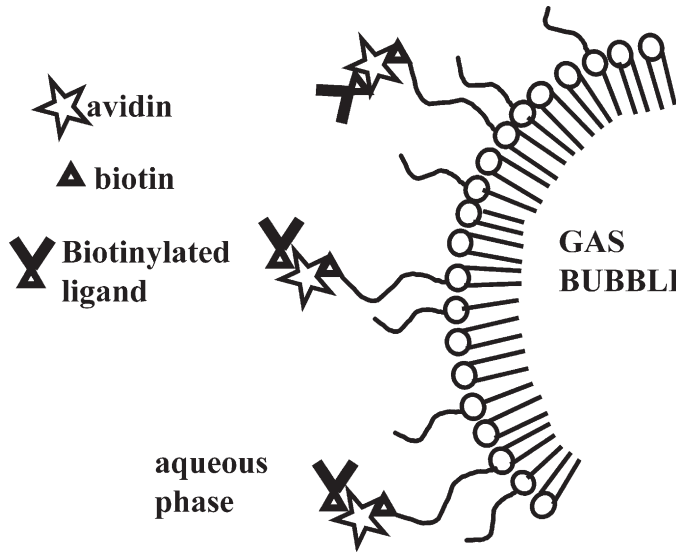

Fig. 2. Attachment of targeting ligands to microbubble surface via biotin-streptavidin bridge

added ligand is bound to bubbles. Two major disadvantages make it difficult to consider this technique for clinical diagnostic imaging use: first is the fact that streptavidin is a foreign protein and a possible immunogen, and second is the need for multiple centrifugal washes required for this multistep procedure. A preferred clinically applicable technique would be the covalent attachment of the ligand to the microbubble shell.

The obvious first choice of the covalent coupling method is the formation of an amide bond between the activated carboxyl of the lipid (or PEG-lipid) derivative and a primary amino group on the ligand molecule. In research settings, a monoclonal IgG antibody is usually applied as a first-choice ligand, because antibodies are available commercially against a wide variety of antigens. The IgG molecule has several dozen lysines in its sequence, and random attachment of one of these residues to the surface of a microbubble would not result in the loss of the antigen-binding capability. Coupling is typically performed by the active ester technique, where the carboxy-

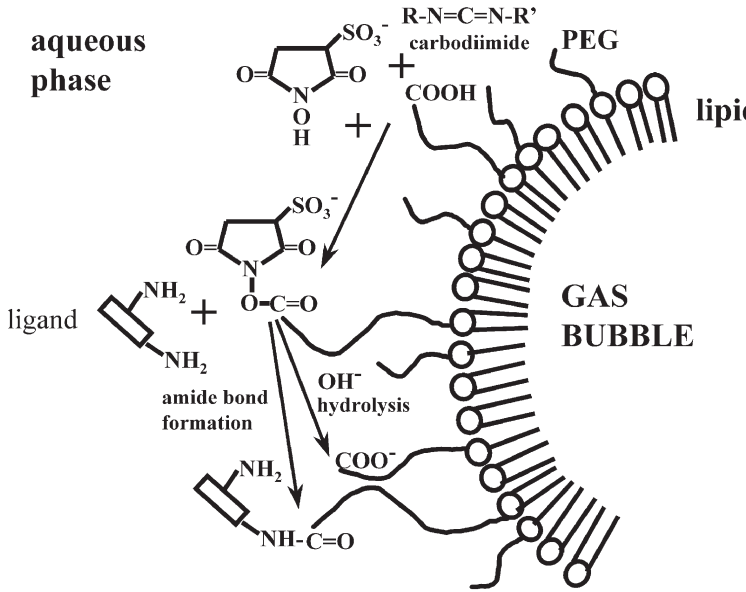

Fig. 3. Attachment of targeting ligands to microbubble via active ester coupling

late of the microbubble-associated PEG-lipid is first activated by water-soluble carbodiimide and converted to sulfo-*N*-hydroxysuccinimide (NHS) ester by the addition of sulfo-*N*-hydroxysuccinimide (at pH $\sim$ 4–5; Fig. 3; Villanueva et al. 1998). Activated microbubble preparation is then added to the antibody (or other aminoligand) solution (at pH $\sim$ 7–8), and coupling of ligand to the bubble occurs with the formation of the amide bond. In the mild alkaline conditions that are required for the successful progression of the amide bond formation, most of the active ester is hydrolyzed (an undesirable side reaction), and does not have a chance to bind to the antibody. Therefore, in order to couple a reasonably high amount (tens of thousands of molecules) of antibodies per microbubble to achieve successful targeting, one would require large excess of antibody, most of which would not be bound to the bubbles and wasted/removed in the subsequent bubble purification washes.

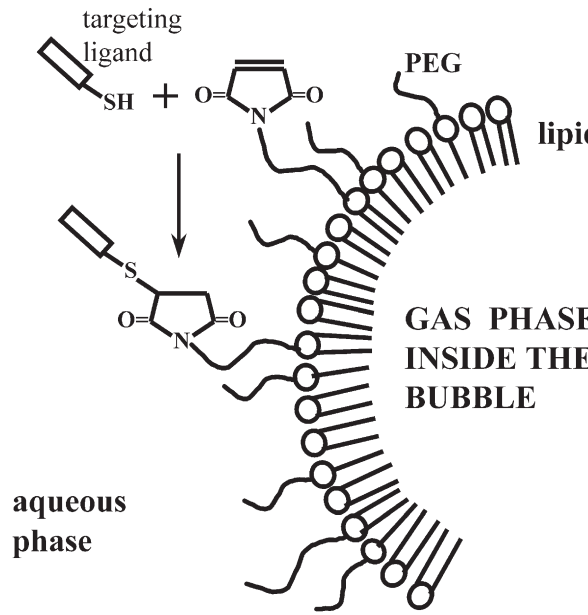

Fig. 4. Attachment of targeting ligands to microbubble via thiol-maleimide coupling

The most suitable technique for coupling ligands onto the microbubble surface seems to be thiol-maleimide chemistry, as developed for targeted liposome applications (Kirpotin et al. 1997). In this case, active maleimide lipid derivative (available commercially) would be incorporated into the microbubble shell, and after the flotation wash to remove free lipids not associated with the bubbles, microbubbles would be added to the solution of thiol ligand derivative (Fig. 4). Maleimide residue on the bubble surface is stable for days; however, its reaction with thiol is completed within less than an hour. Consequently, reaction yield is improved. Large excesses of the ligand would not be required for the preparation, so loss of this expensive material can be avoided. Another advantage of this approach is the ability to generate a single thiol in a ligand molecule, either by synthesis or by controlled cleavage (such as Fab′-fragments generation from IgG antibodies); the ligand will then be

attached to the microbubbles in a controlled, oriented fashion, so that all of the ligands will be available for target binding without inactivation.

10.4 In Vitro Targeting: Binding Studies in Model Systems

Testing of targeted microbubble functionality was initially performed in vitro in model systems, such as plastic or glass surfaces coated with the model receptor, with ligand attached to the surface of microbubbles as described. Microbubbles were first placed into the dish that contained the model target, with the dish inverted so that the bubbles would float to the target surface and touch it; after several minutes of incubation, free nonattached bubbles would be washed off the dish, and detection of targeted bubbles would be performed by microscopy and/or ultrasound imaging. The first model targeting receptor tested was avidin, with the targeting ligand being biotin, attached to the microbubble surface via a phosphatidylethanolamine anchor (preferably with a PEG spacer arm; Klibanov et al. 1997, 1999b). When biotinylated microbubbles had an opportunity to touch avidin-coated target and bind, their hold to the target surface was quite firm (aqueous medium flow rates up to 0.6 m/s were required to dislodge the bubbles, depending on the amount of biotin on the bubble surface; Klibanov et al. 1999b). When an antigen-antibody ligand-receptor system was tested instead of avidin-biotin, the strength of the bubble-target bond was not as high, and detachment occurred at slower flows (Klibanov et al. 1999b).

A more realistic experimental approach would be not to allow microbubbles to bind to the target in the static conditions first, but to let them flow through the target area like it would occur in the actual targeted imaging application setting (Fig. 5). A parallel plate flow chamber has been used to characterize particle and cell-targeted binding in the flow conditions (Lawrence et al. 1987); it is easily applied to targeted microbubble testing (it only needs to be turned upside down so that bubbles would have a chance to roll by the target surface). Targeted bubbles carrying fluorescein ligand attached to the antifluorescein scFv receptor-coated flow chamber deck from the flowing aqueous medium at $\sim 140\ s^{-1}$ shear rate;

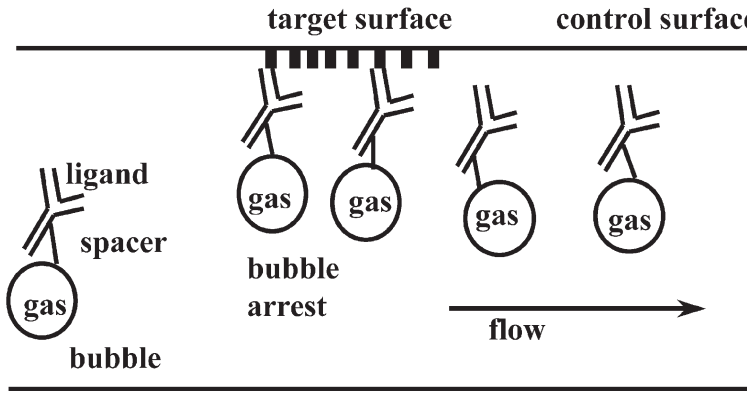

Fig. 5. Targeting of microbubbles in the flow of liquid

control nontargeted bubbles floated by without attachment (Klibanov et al. 1999 b).

Direct measurement of the bubble-target bond strength was performed with the use of a micromanipulation system (Kim et al. 2000). An avidin-coated glass microbead, held by micropipette under suction pressure, was brought in contact with the biotinylated bubble held by another micropipette, and binding allowed to occur. The critical pull manometric pressure required for the detachment of the target bead from the bubble was then determined. The detachment force was calculated based on the cross-section surface area. A force of up to tens of nanoNewtons (saturated at biotin concentration over ~ 3 mol% of total lipid present) was required for bubble-target detachment. Interestingly, comparison of biotin-PEG-lipid anchor (Fig. 6 a) and shorter biotinamidocaproyl-lipid derivative (Fig. 6 b) revealed nearly complete lack of ability of the short-arm anchor to produce targeted binding, probably due to the steric hindrance for the access of avidin target surface to biotin through the dense PEG brush that covered the surface of both types of bubbles.

Once selective targeting of microbubbles to model receptors was demonstrated, the issue of the sensitivity of ultrasound imaging and its ability to detect contrast particles was evaluated. Surprisingly, even with the older, fundamental imaging ultrasound systems, a very

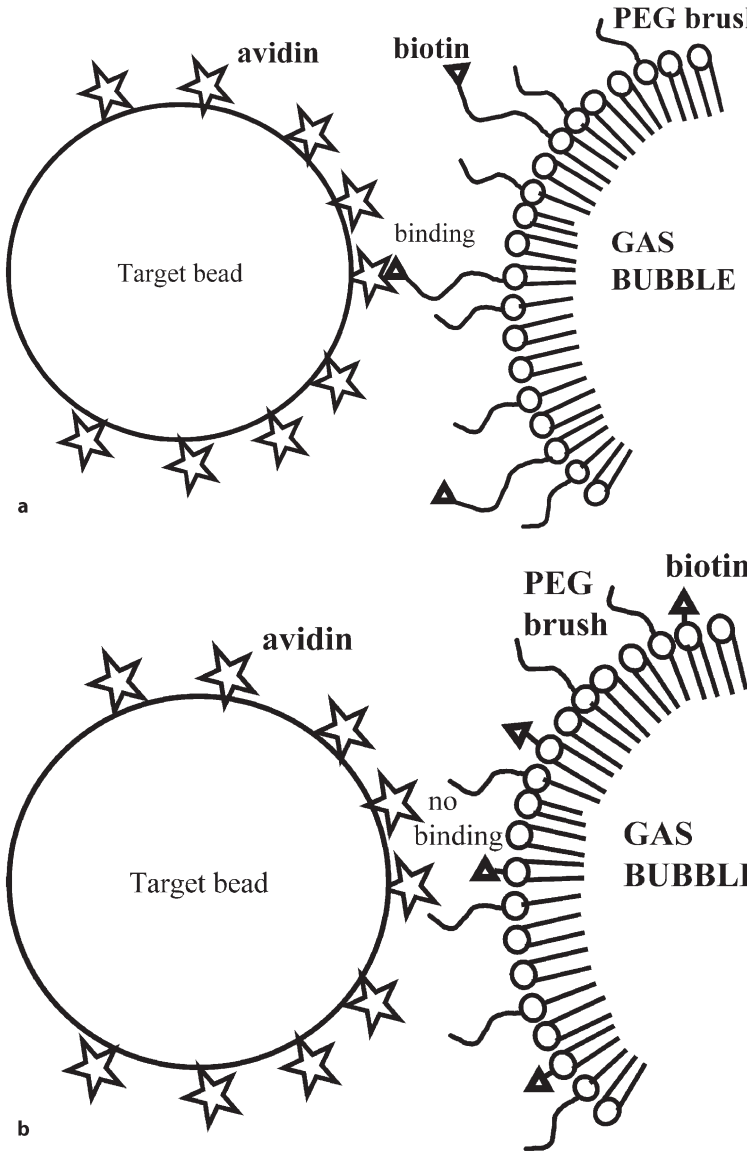

Fig. 6. a Advantage of long PEG spacer arm for microbubble targeting. **b** Disadvantage of short spacer arm for microbubble targeting

small number of microbubble contrast particles targeted to the surface of the Petri dish were visualized (Klibanov et al. 1997). Bubble patches as small as 1×2 mm on the flat, receptor-coated plastic surface were visualized as bright spots by ultrasound imaging, i.e., several thousands of bubble particles with the overall mass in the nanogram range were detectable (Klibanov et al. 1997, 1999b). Technically, the modern contrast ultrasound imaging modalities, such as pulse inversion, ultraharmonic, or power modulation imaging techniques, are very sensitive to the presence of microbubbles, and allow detection of individual microbubbles in the aqueous dispersion (each microbubble has a mass in the picogram range; Klibanov et al. 2002). Furthermore, it was recently shown (Klibanov et al. 2004) that an individually targeted microbubble in vitro, attached to the Petri dish surface, could also be detected by ultrasound imaging in the pulse inversion mode. All these results imply that detectable doses of microbubbles can be easily achieved during in vivo accumulation in the target tissues.

10.5 In Vivo Microbubble Targeting: Biodistribution, Nonspecific and Targeted Accumulation and Ultrasound Imaging

Two basic techniques are in use to evaluate in vivo behavior of targeted microbubbles. One is intravital microscopy, which is normally performed in the cremaster muscle model setting, aided by the fact that fluorescence lipid probes can be easily incorporated in the microbubble shell and visualized by fluorescence epi-illumination imaging in real time. The other imaging technique is actual ultrasound, usually performed with the clinically oriented systems, where the presence of microbubbles in the particular tissue or organ is evaluated by echo response.

Prior to describing results of targeted accumulation of ligand-carrying microbubbles in the tissues of experimental animals, we should first evaluate the nonspecific uptake of the microbubble contrast agents into various organs, tissues, and cells. This information will help to assess the ability of targeted microbubble contrast to

achieve high target-to-normal tissue accumulation ratios, which is the main prerequisite for success of targeted imaging.

Microbubbles after intravenous administration are freely circulating in the bloodstream, not exiting the vasculature. It has been shown (Keller et al. 1989) that the rheological behavior of microbubbles in the flow of blood is quite comparable to the behavior of red blood cells. Depending on the shell composition, such as inclusion of apoptosis marker phosphatidylserine (Christiansen et al. 2002), microbubbles may demonstrate accelerated uptake by leukocytes deposited in the postcapillary venules or, possibly, by Kupffer cells in the liver. Surface charge and composition may also have an influence on the interaction of the microbubbles with leukocytes on the endothelium lining of the vasculature, either directly (Lindner et al. 2000) or via complement activation and complement C3 shell deposition mechanisms (Lindner et al. 2000; Fisher et al. 2002). In the presence of a strong negative surface charge, nonspecific adhesion and accumulation of microbubbles on the vascular endothelium has been noted both in the cremaster muscle model setting by microscopy and in the echocardiography setting in the large animal model (Fisher et al. 2002). Even the presence on the bubble surface of PEG brush, which is often used as a steric protective layer on pharmaceutical nanoparticles, only partially reduced this charge-related microbubble retention. Therefore, in order to reduce undesirable nonspecific deposition of targeted microbubbles on endothelium and uptake by leukocytes, microbubble surface charge should be kept close to neutral.

Selective targeting with microbubbles is generally directed to the specific receptors of pathological conditions on the surface of the endothelium. Because of the size of microbubbles (typically, several microns), it is presumed that only the intravascular structures can be within reach for contact with the ligands on the microbubble surface, so the imaging targets are limited to thrombi (Schumann et al. 2002) or the molecules located on the luminal surface of the endothelium, especially the molecules that are overexpressed in certain pathological conditions, such as inflammation, ischemia/reperfusion injury, or angiogenesis (Lindner et al. 2001; Villanueva et al. 1998). Via these markers, vascular endothelium provides information to the immune system about the status of the underlying tissues. P-selectin,

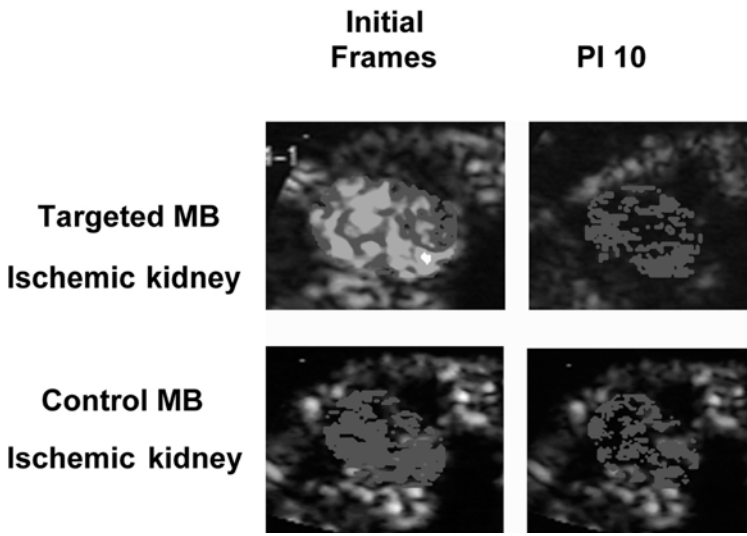

Fig. 7. Background-subtracted color-coded ultrasound images of kidneys 1 h after ischemia-reperfusion injury in wild-type mice. Initial images acquired 8 min after intravenous injection of microbubbles and images subsequently obtained at PI of 10 s are shown (reprinted with permission from Lippincott, copyright 2001, from Lindner et al. Color images not available here)

an endothelial cell adhesion molecule, is an obvious object of interest for targeted imaging. In the areas of inflammation it is substantially upregulated on the surface of the vascular endothelium. When a monoclonal antibody (RB40.34 against mouse P-selectin) was attached to microbubbles via a biotin-streptavidin scheme, such microbubbles showed a statistically significant increase of accumulation in the cremaster muscle tissue that was treated by proinflammatory stimuli (TNF-α), as compared with control, nontargeted bubbles (Lindner et al. 2001). In addition to inflammation caused by TNF, upregulation of P-selectin expression is caused by ischemia-reperfusion injury. Hence, when RB40.34 antibody-carrying bubbles were administered to mice in which one of the kidneys was subjected to transient (30 min) ischemia followed by 1 h reperfusion, selective accumulation of targeted microbubbles in the target kidney was demonstrated (Fig. 7; Lindner et al. 2001).

Background subtraction image processing is a powerful technique crucial for the analysis of these contrasted targeted images. First, a control precontrast image was obtained, then contrast was administered and microbubbles were allowed to circulate for 8–15 min, so that target accumulation could occur. Then, contrast ultrasound imaging was performed and the contrast image was subtracted from the background and color-coded (Fig. 7, left panel). Finally, high-intensity ultrasound pulses were used to destroy all the bubbles in the tissue, and after a 10-s interval contrast imaging was performed again, to evaluate the residual amount of circulating microbubbles (Fig. 7, right panel). In a separate study, the same biotinylated microbubbles carrying biotinylated monoclonal antibody against ICAM-1 integrin were prepared by streptavidin bridging and tested in the rejected heart transplant rat model (Weller et al. 2003). ICAM-1 is upregulated on the endothelium of rejected hearts. Respectively, a statistically significant increase of contrast ultrasound video intensity was demonstrated in the rejecting heart with the injection of targeted bubbles over control, nonrejecting hearts (with little accumulation of nontargeted control bubbles in either; Weller et al. 2003).

The application of targeted ultrasound contrast is not limited to visualization of inflammation or transplant rejection: an important potential application of this technology is the imaging of angiogenesis. Angiogenic endothelium is known to overexpress $\alpha_v\beta_3$ integrin (Brooks et al. 1994); this molecule may be a sensible target for the evaluation of the status of the endothelium (i.e., development of neovasculature or blood supply) in tumors (Winter et al. 2003; Sipkins et al. 1998), or perhaps a marker for the monitoring of proangiogenic therapy in ischemic tissues. Antibodies against $\alpha_v\beta_3$ are available, as well as smaller targeting ligands, e.g., disintegrin peptide echistatin (Yahalom et al. 2002); both molecules could be biotinylated and attached to the bubbles by the above-mentioned streptavidin scheme.

The angiogenesis animal model first used to test this targeted contrast agent was an FGF-2 matrigel plug in a mouse setting; both confocal microscopy and ultrasound imaging revealed selective accumulation of targeted microbubbles in the angiogenic area (Fig. 8), which was confirmed by intravital microscopy of the FGF-2-treated

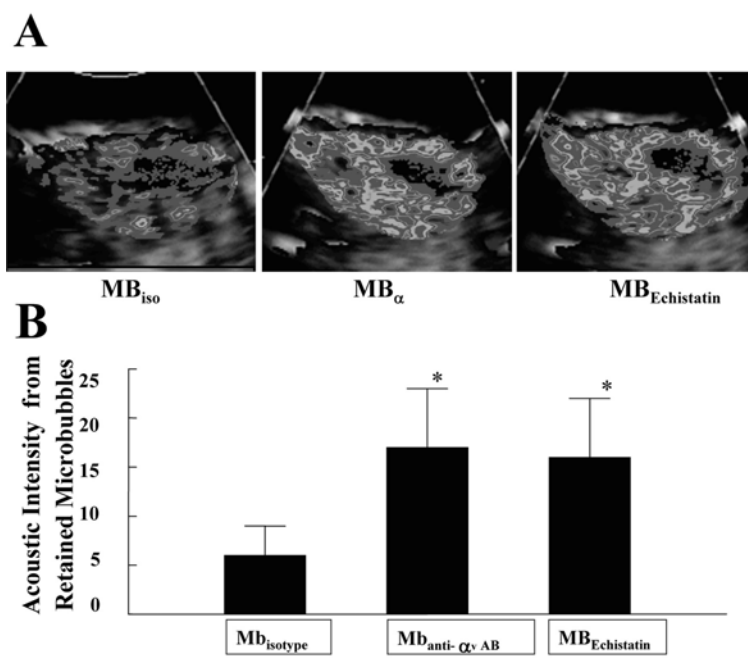

Fig. 8A,B. CEU assessment of microbubble retention in matrigel. **A** Examples of background-subtracted color-coded CEU images reflecting signal from microbubbles retained in matrigel plugs 15 min after intravenous injection of microbubbles. **B** Mean (+SD) background-subtracted acoustic intensity for retained microbubbles. $*P<0.01$ compared with MBc (reprinted with permission from Lippincott, copyright 2003, from Leong-Poi et al. Color images not available here)

cremaster (Leong-Poi et al. 2003). Further studies were performed in a rat glioma setting, where angiogenesis during the time course of tumor development was evaluated both by nontargeted, circulating ultrasound contrast microbubbles and echistatin-coated targeted microbubbles (Ellegala et al. 2003). A statistically significant increase of targeted microbubble accumulation in the areas of tumor angiogenesis was reported, as compared with the control tumor-free hemisphere, or with the administration of control ligand-free microbubbles. Selective targeting of echistatin-carrying bubbles to the angio-

genic endothelium was confirmed by confocal microscopy. Tumor intravascular blood volume showed good correlation with the targeted microbubbles' acoustic intensity in the tissue. Overall, this technique offers a noninvasive method to evaluate the level of upregulation of an angiogenesis marker in the tumor-related vasculature, which is one of the major goals of molecular imaging.

10.6 Conclusions

Microbubbles were prepared from insoluble perfluorocarbon gas, stabilized with a monolayer of phospholipid with a grafted PEG brush and decorated with targeting ligands, such as monoclonal antibodies or peptides on a flexible PEG spacer arm. Such targeted bubbles selectively and firmly bind to the surfaces coated with the specific receptors in vitro. Bubble deposition areas can be detected by ultrasound imaging. Single bubble detection sensitivity is possible.

Targeting of microbubbles to areas of inflammation, ischemia-reperfusion injury, and angiogenesis (including tumors) was achieved in vivo in experimental animal studies, by the use of microbubbles directed towards P-selectin or $\alpha_v\beta_3$, respectively. Selective accumulation of ligand-carrying bubbles in the tissues of interest was confirmed by fluorescence microscopy (intravital and confocal) and ultrasound imaging.

Acknowledgements. The author thanks the Cardiovascular Imaging Center, Cardiovascular Research Center, University of Virginia Cardiovascular Division, Sanjiv Kaul, Jonathan Lindner and Klaus Ley for help and support. Donation of laboratory equipment by Mallinckrodt Inc. (St. Louis, MO) to A. Klibanov's laboratory at UVA Cardiovascular Imaging Center is gratefully acknowledged.

References

Alkan-Onyuksel H, Demos SM, Lanza GM, Vonesh MJ, Klegerman ME, Kane BJ, Kuszak J, McPherson DD (1996) Development of inherently echogenic liposomes as an ultrasonic contrast agent. J Pharm Sci 85:486–490

Andre MP, Steinbach G, Mattrey RF (1993) Enhancement of the echogenicity of flowing blood by the contrast agent perflubron. Invest Radiol 28:502–506

Borden MA, Longo ML (2002) Dissolution behavior of lipid-monolayer-coated, air-filled microbubbles: effect of lipid hydrophobic chain length. Langmuir 18:9225–9233

Brooks PC, Clark RA, Cheresh DA (1994) Requirement of vascular integrin alpha(v)beta3 for angiogenesis. Science 264:569–571

Christiansen JP, Leong-Poi H, Klibanov AL, Kaul S, Lindner JR (2002) Noninvasive imaging of myocardial reperfusion injury using leukocyte-targeted contrast echocardiography. Circulation 105:1764–1767

Dill-Macky MJ, Burns PN, Khalili K, Wilson SR (2002) Focal hepatic masses: enhancement patterns with SH U 508A and pulse-inversion US. Radiology 222:95–102

Ellegala DB, Leong-Poi H, Carpenter JE, Klibanov AL, Kaul S, Shaffrey ME, Sklenar J, Lindner JR (2003) Imaging tumor angiogenesis with contrast ultrasound and microbubbles targeted to alpha(v)beta3. Circulation 108:336–341

Epstein PS, Plesset MS (1950) On the stability of gas bubbles in liquid-gas solutions. J Chem Phys 18:1505–1509

Fisher NG, Christiansen JP, Klibanov AL, Taylor RP, Kaul S, Lindner JR (2002) Influence of microbubble surface charge on capillary transit and myocardial contrast enhancement. J Am Coll Cardiol 40:811–819

Fritz TA, Unger EC, Sutherland G, Sahn D (1997) Phase I clinical trials of MRX-115, a new ultrasound contrast agent. Invest Radiol 32:735–740

Goldberg BB, Raichlen JS, Forsberg S (eds) (2001) Ultrasound contrast agents: basic principles and clinical applications. Martin Dunitz, London

Gramiak R, Shah PM (1968) Echocardiography of the aortic root. Invest Radiol 3:356–366

Keller MW, Segal SS, Kaul S, Duling B (1989) The behavior of sonicated albumin microbubbles within the microcirculation: a basis for their use during myocardial contrast echocardiography. Circ Res 65:458–467

Kim DH, Klibanov AL, Needham D (2000) The influence of tiered layers of surface-grafted poly(ethylene glycol) on receptor-ligand-mediated adhesion between phospholipid monolayer-stabilized microbubbles and coated glass beads. Langmuir 16:2808–2817

Kirpotin D, Park JW, Hong K, Zalipsky S, Li WL, Carter P, Benz CC, Papahadjopoulos D (1997) Sterically stabilized anti-HER2 immunoliposomes:

design and targeting to human breast cancer cells in vitro. Biochemistry 36:66–75

Klibanov AL, Hughes MS, Marsh JN, Hall CS, Miller JG, Wible JH, Brandenburger GH (1997) Targeting of ultrasound contrast material. An in vitro feasibility study. Acta Radiol Suppl 412:113–120

Klibanov AL, Gu H, Wojdyla JK, Wible JH, Kim DH, Needham D, Villanueva FS, Brandenburger GH (1999 a) Attachment of ligands to gas-filled microbubbles via PEG spacer and lipid residues anchored at the interface. In: Proceedings of the 26th international symposium on controlled release of bioactive materials. Controlled release society, Boston, pp 124 –125

Klibanov AL, Hughes MS, Villanueva FS, Jankowski RJ, Wagner WR, Wojdyla JK, Wible JH, Brandenburger GH (1999 b) Targeting and ultrasound imaging of microbubble-based contrast agents. MAGMA 8:177–184

Klibanov AL, Rasche PT, Hughes MS, Wojdyla JK, Galen KP, Wible JH Jr, Brandenburger GH (2002) Detection of individual microbubbles of an ultrasound contrast agent: fundamental and pulse inversion imaging. Acad Radiol 2:S279–S281

Klibanov AL, Rasche PT, Hughes MS, Wojdyla JK, Galen KP, Wible JH Jr, Brandenburger GH (2004) Detection of individual microbubbles of ultrasound contrast agents: imaging of free-floating and targeted bubbles. Invest Radiol 39:187–195

Lanza GM, Wallace KD, Scott MJ, Cacheris WP, Abendschein DR, Christy DH, Sharkey AM, Miller JG, Gaffney PJ, Wickline SA (1996) A novel site-targeted ultrasonic contrast agent with broad biomedical application. Circulation 94:3334–3340

Lawrence MB, McIntire LV, Eskin SG (1987) Effect of flow on polymorphonuclear leukocyte/endothelial cell adhesion. Blood 70:1284–1290

Lee S, Kim DH, Needham D (2001) Equilibrium and dynamic interfacial tension measurements at microscopic interfaces using a micropipet technique. 2. Dynamics of phospholipid monolayer formation and equilibrium tensions at the water-air interface. Langmuir 17:5544–5550

Leighton TG (1997) The acoustic bubble. Academic Press, NY

Leong-Poi H, Christiansen J, Klibanov AL, Kaul S, Lindner JR (2003) Noninvasive assessment of angiogenesis by ultrasound and microbubbles targeted to alpha(v)-integrins. Circulation 107:455–460

Lindner JR, Wei K, Kaul S (1999) Imaging of myocardial perfusion with SonoVue in patients with a prior myocardial infarction. Echocardiography 16:753–760

Lindner JR, Coggins MP, Kaul S, Klibanov AL, Brandenburger GH, Ley K (2000) Microbubble persistence in the microcirculation during ischemia/reperfusion and inflammation is caused by integrin- and complement-mediated adherence to activated leukocytes. Circulation 101:668–675

Lindner JR, Song J, Christiansen J, Klibanov AL, Xu F, Ley K (2001) Ultrasound assessment of inflammation and renal tissue injury with microbubbles targeted to P-selectin. Circulation 104:2107–2112

Pither R (2003) PET and the role of in vivo molecular imaging in personalized medicine. Expert Rev Mol Diagn 3:703–713

Schumann PA, Christiansen JP, Quigley RM, McCreery TP, Sweitzer RH, Unger EC, Lindner JR, Matsunaga TO (2002) Targeted-microbubble binding selectively to GPIIbIIIa receptors of platelet thrombi. Invest Radiol 37:587–593

Schutt EG, Klein DH, Mattrey RM, Riess JG (2003) Injectable microbubbles as contrast agents for diagnostic ultrasound imaging: the key role of perfluorochemicals. Angew Chem Int Ed Engl 42:3218–3235

Sipkins DA, Cheresh DA, Kazemi MR, Nevin LM, Bednarski MD, Li KC (1998) Detection of tumor angiogenesis in vivo by alphaVbeta3-targeted magnetic resonance imaging. Nat Med 4:623–626

Skyba DM, Camarano G, Goodman NC, Price RJ, Skalak TC, Kaul S (1996) Hemodynamic characteristics, myocardial kinetics and microvascular rheology of FS-069, a second-generation echocardiographic contrast agent capable of producing myocardial opacification from a venous injection. J Am Coll Cardiol 28:1292–1300

Villanueva FS, Jankowski RJ, Klibanov S, Pina ML, Alber SM, Watkins SC, Brandenburger GH, Wagner WR (1998) Microbubbles targeted to intercellular adhesion molecule-1 bind to activated coronary artery endothelial cells. Circulation 98:1–5

Villanueva FS, Gertz EW, Csikari M, Pulido G, Fisher D, Sklenar J (2001) Detection of coronary artery stenosis with power Doppler imaging. Circulation 103:2624–2630

Weller GE, Lu E, Csikari MM, Klibanov AL, Fischer D, Wagner WR, Villanueva FS (2003) Ultrasound imaging of acute cardiac transplant rejection with microbubbles targeted to intercellular adhesion molecule-1. Circulation 108:218–224

Winter PM, Caruthers SD, Kassner A, Harris TD, Chinen LK, Allen JS, Lacy EK, Zhang H, Robertson JD, Wickline SA, Lanza GM (2003) Molecular imaging of angiogenesis in nascent Vx-2 rabbit tumors using a novel alpha(V)beta3-targeted nanoparticle and 1.5 tesla magnetic resonance imaging. Cancer Res 63:5838–5843

Yahalom D, Wittelsberger A, Mierke DF, Rosenblatt M, Alexander JM, Chorev M (2002) Identification of the principal binding site for RGD-containing ligands in the alphaVbeta3 integrin: a photoaffinity cross-linking study. Biochemistry 41:8321–8331

Yao J, Takeuchi M, Teupe C, Sheahan M, Connolly R, Walovitch RC, Fetterman RC, Church CC, Udelson JE, Pandian NG (2002) Evaluation of a new ultrasound contrast agent (AI-700) using two-dimensional and three-dimensional imaging during acute ischemia. J Am Soc Echocardiogr 15:686–694

11 Noninvasive Real-Time In Vivo Bioluminescent Imaging of Gene Expression and of Tumor Progression and Metastasis

C. W. G. M. Lowik, M. G. Cecchini, A. Maggi, G. van der Pluijm

11.1 General Introduction

In 2003, the human genome project ended with the completion of the entire human genetic sequence. Now that most genes have been identified, the big challenge for the future is to try to discover where the genes are expressed, how they are regulated, and what is their exact function in the homeostasis of specific cell types. This so-called functional genomics research will lead to a better understanding of the molecular, cellular, and biological processes involved in normal physiology and pathology in a variety of diseases. It will also allow us to find new drug targets and, consequently, better management of diseases.

In order to study the location and regulation of gene expression in vitro as well as in vivo, reporter genes (e.g., β-galactosidase, CAT, green fluorescent protein, luciferase) have been widely used and are essential tools. They are also used for developing gene delivery systems for gene therapy and for tracking the fate of cells injected systemically in small experimental animals. Until recently, the proteins translated from the reporter gene-constructs were either visualized in histological tissue sections or detected biochemically in tissue extracts after sacrifice of the animal. However, bioluminescent imaging (BLI) coupled to luciferase as reporter gene currently allows very sensitive image recording of the topographical expression of this enzyme noninvasively and repetitively in the living animal.

11.2 Principles of Bioluminescent Imaging

Bioluminescence refers to the enzymatic generation of visible light by living organisms. The most commonly used bioluminescent reporter gene for research purposes has been luciferase from the North American firefly *Photinus pyralis*. The enzyme catalyzes the transformation of its substrate D-Luciferin into oxyluciferin in an oxygen and ATP-dependent process, leading to the emission of photons. The first report of real-time in vivo imaging of gene expression using firefly luciferase as a reporter was from Millar and coworkers in plants, in which they used a low-light video imaging system to establish that luciferase bioluminescence in vivo accurately reports the

temporal and spatial regulation of cab2 transcription in single seedlings (Millar et al. 1992).

Biological sources of light (bioluminescence) have sufficient intensity to cross animal tissues, provided that the endogenous light has a wavelength >550 nm. Above this wavelength the tissues do not absorb photons. The firefly luciferase/luciferin reaction emits photons at wavelengths from 500 to 620 nm and is therefore suitable for external detection. Apart from fulfilling this criterion, another important feature is that the substrate luciferin diffuses within a few minutes from intravenous or peritoneal injection throughout the entire body of small animals and is rapidly taken up by cells (Contag et al. 1997, 1998). Besides firefly luciferase, Renilla luciferase can also be used as a reporter in combination with its specific substrate coelenterazine. Although this reaction will emit mainly blue light, the emission spectrum is very broad and a small part also exceeds the wavelength of 580 nm, making it suitable for BLI (Bhaumik and Gambhir 2002).

Recent technical advances for imaging weak visible light sources using cooled charged coupled device (CCCD) cameras, peltier-cooled detectors and microplate channel intensifiers allow detection of bioluminescent emission from inside the tissues of the animal (see Table 1 for available BLI systems).

This technical development made it possible to monitor gene expression in live animals via a *luc*-reporter gene linked to specific pro-

Table 1. Several currently available BLI systems

Company	System name	BLI technology
Xenogen	IVIS-100	Liquid nitrogen-cooled CCD camera
Berthold	Nightowl	Peltier-cooled CCD camera
Hamamatsu + Improvision	VIM Camera model C2400-47	Intensified CCD camera
Roper Scientic	ChemiPro	Cryogenic-cooled CCD camera
Biospace	photoImager	Intensified CCD camera

moters (Carlsen et al. 2002; Zhang et al. 2001, 2003, 2004; Ciana et al. 2003) or to follow in real time the fate of luciferase (*luc*) transfected tumor cells (Edinger et al. 1999, 2003; Sweeney et al. 1999; Contag et al. 2000; Wetterwald et al. 2002; El Hilali et al. 2002) or immune cells (Hardy et al. 2001; Mandl et al. 2002) injected in living animals. One of the many advantages of this methodology is that it is non-invasive and therefore allows investigations in the same animal at different time points. Accordingly, the number of the animal groups in the experimental setting is greatly reduced.

There are further important advantages of using luciferase as a reporter.

1. The luciferase protein, in contrast to other reporter proteins, has a relatively short half-live of about 1–1.5 h. This feature makes it ideally suited for kinetic and dynamic analysis of gene expression within short time frames and, therefore, to identify circadian or even infradian rhythms of gene expression.
2. There is no background activity, making it very specific and sensitive. This in contrast to β-galactosidase activity, which is also found endogenously in some tissues or GFP signals which are disturbed by auto-fluorescence of some tissues.
3. Luciferase activity can easily and sensitively be quantitatively assayed in tissue extracts.
4. Luciferase protein can also be detected in tissue section using immunohistochemistry.

We will discuss examples in the two major areas of application of the bioluminescent technology: gene expression in transgenic *luc*-reporter mice and cancer research where it allows early detection and reliable quantification of primary tumor growth, and of micro- and macrometastatic tumor spread.

11.3 Transgenic *Luc*-Reporter Mice to Study Specific Gene Expression

Transgenic mice offer one of the most efficient and elegant ways to determine gene function in vivo. However, gene function is usually assessed by time-consuming and sometimes difficult phenotypic and

biochemical assays performed ex vivo. In contrast, detection of the bioluminescent activity in vivo of the luciferase enzyme as a transcriptional reporter facilitates rapid and repetitive screening for both the presence and function of transgenes in intact living mice. Using transgenic ERE-*luc* reporter mice, we were able to image transcriptionally active estrogen receptors (Ciana et al. 2003) in vivo. Using transgenic mice expressing luciferase under the control of the human osteocalcin (OC) promoter we could show skeletal sites of active bone formation/remodeling since osteocalcin is a bone-specific gene expressed by the bone-synthesizing cells, the osteoblasts.

11.3.1 Monitoring Estrogen Receptor Transcriptional Activity In Vivo

It is now well established that estrogens control not only reproductive functions, but also modulate other important physiological processes such as cognitive brain function, adipogenesis, lipid metabolism, blood pressure, and bone turnover. Estrogen deficiency related to menopause is clearly associated with increased incidence of neurodegenerative disorders, like Alzheimer's disease, and of obesity, cardiovascular disease, and postmenopausal osteoporosis. Identification of compounds with tissue-selective activity (SERMs, selective estrogen receptor modulators) will lead to new drugs mimicking the beneficial effects of estrogen on the prevention of osteoporosis, and cardiovascular or neurodegenerative diseases, while avoiding its detrimental proliferative effects which can lead to cancer. For this purpose the group of Adriana Maggi in Milan (Ciana et al. 2001, 2003) engineered a transgenic mouse that ubiquitously expresses a luciferase reporter gene in all known estrogen target tissues. The construct used for transgenesis consisted of the reporter gene driven by a dimerized estrogen-responsive element (ERE) and a minimal promoter. The key to the successful realization of this model was most probably the use of insulators. It is well known that the expression of transgenes driven by weak promoters is heavily influenced by enhancers/silencers surrounding the regions of insertion. In addition, methylation may gradually extinguish their transcriptional activity. Insulators have been successfully used to counteract these effects in

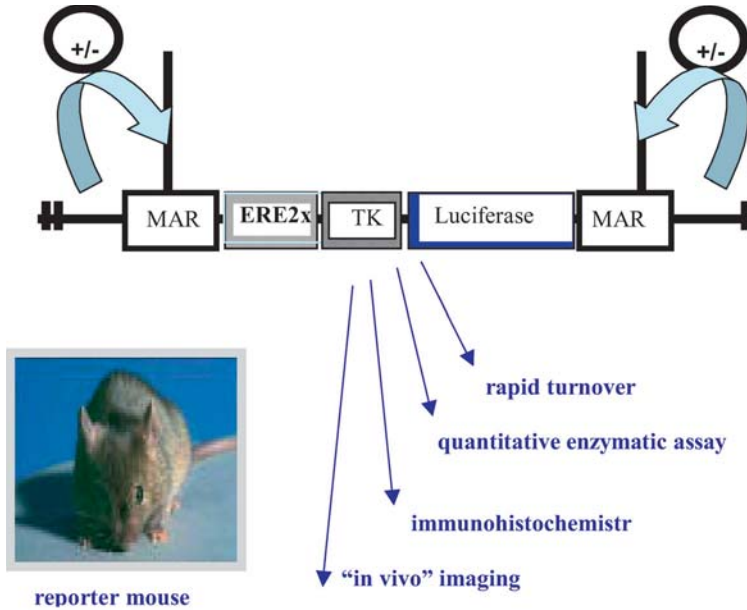

Fig. 1. The constructs for transgenesis consist of the reporter gene driven by a dimerized estrogen-responsive element (*ERE*) and a minimal TK promoter. The construct is flanked by matrix attachment region (*MAR*) insulator sequences to achieve a generalized, hormone-responsive luciferase expression. The advantage of using this kind of luciferase construct to make transgenics is indicated: rapid turnover of the luciferase protein, luciferase activity can be quantitatively assayed, luciferase can be detected using immunohistochemistry, luciferase activity can be used for BLI

specific tissues. In the transgenic animals used for BLI, the matrix attachment region (MAR) sequence was used as an insulator to flank the construct and, thus, to achieve a uniform and consistent, hormone-responsive luciferase expression in all target tissues (see Fig. 1).

Apart from the advantage of using insulators to obtain a uniform, hormone-responsive luciferase expression, the use of luciferase offered the additional and important advantages of this reporter listed above. Accordingly, the ERE-*luc* mouse allowed us to monitor, in a

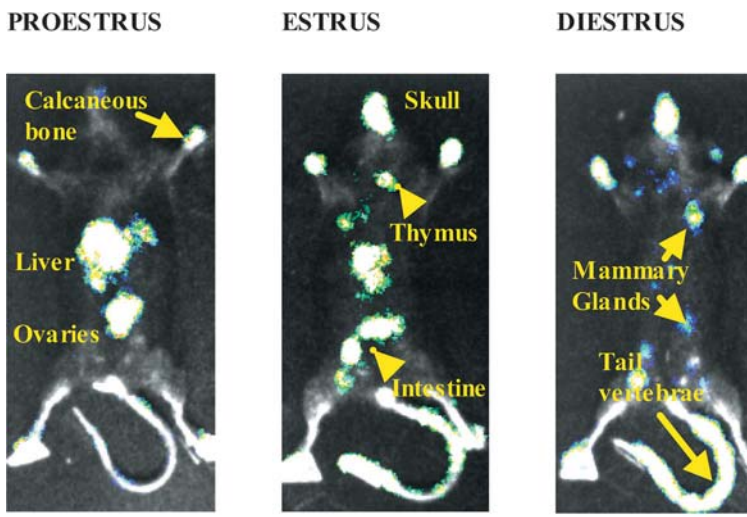

Fig. 2. In the three *upper panels* BLI of ER transcriptional activity is shown at 3 consecutive days. In the *lower panel* plasma estradiol levels in cycling mice is shown

spatiotemporal manner, the transcriptional activity of ER genes in intact or hormonally manipulated mice.

Figure 2 shows the ER transcriptional activity measured by BLI during the 5 day estrous cycle of female ERE-*luc* mice. The phase of the estrous cycle was determined by vaginal smears. For 3 consecutive days the mice were anaesthetized at a fixed time point in the morning (9:00 a.m.) and injected with 100 µl D-luciferin (25 mg/ml) 10 min before imaging. In these experiments the imaging system consisted of an intensified charge-coupled device camera (VIM camera, model C2400-47; Hamamatsu Photonics, Hamamatsu, Japan) fitted to a light-tight chamber (Hamamatsu Photonics) and equipped with an 80 mm/f 0.9 f Schneider lens. The images are generated on an Argus-20 image processor (Hamamatsu Photonics) and transferred via SCSI using a software module (Openlab; Improvision, Coventry, UK) to a computer (Macintosh G4; Apple Computer, Cupertino, CA) and processed by image analysis software (Openlab; Improvision, Coventry, UK).

As shown in Fig. 2, the level of estradiol is highest at pro-estrus and at this time point the highest photon emission was observed in the liver and ovaries with very little activity in limbs and tail (vertebrae) and none in the area corresponding to the brain. The next morning, in estrus, when the same mouse was imaged again, a very different pattern of luciferase/luciferin-related photon emission, showing much lower emission in areas corresponding to liver and ovaries than the previous day, was observed. Now photon emission was clearly seen in areas corresponding to the head (=brain+bone), bone (ankles, wrists, and tail) and intestine and thymus. The following day when the mouse was in diestrus-1, there was much less signal coming from liver and ovaries, but the strongest signals were now coming from the head, which includes brain and skull bones, the mechanically loaded ankle and wrist bones and tail vertebrae (note the increase over time in the tail vertebrae). At the same time point there was also detectable expression in some of the mammary glands. This pattern of ER transcriptional activity as detected by BLI during the estrous cycle was very reproducible and indicated that there are tissues with either estrogen (ligand)-dependent or -independent activation of ER transcriptional activity. This was confirmed by biochemical measurement of luciferase enzyme activity in the same tissues at different phases of the cycle. What was extremely interesting is the fact that in tissues with reproductive functions, like the ovaries, uterus, mammary glands, hypothalamus, and liver, the activity was highest during pro-estrus, when estrogen levels were also the highest. In the nonreproductive tissues like bone, brain, intestine, kidney, lungs, and thymus, maximum luciferase activity was found at di-estrus, when estradiol levels are low. In line with this was the finding that progesterone receptor content, a direct downstream ER target, was maximal in liver at pro-estrus and maximal in bone at di-estrus. These results suggest that ER transcriptional activity in reproductive tissues is essentially dependent on the presence of the ligand, while in nonreproductive tissues it is not.

Further evidence for estrogen-independent activation of ER transcriptional activity came from the observations that in situations where gonadal estrogen synthesis is absent, as in 10-day-old immature female mice and 3 weeks after ovariectomy (OVX), luciferase activity could still be detected. In the immature mice, luciferase ac-

tivity was even higher in the nonreproductive tissues like bone and brain compared to adult mice, whereas in the estrogen-dependent liver, ER transcriptional activity, as expected, was lower in the immature mice compared to adult mice. Similarly, 3 weeks after OVX both the imaging and biochemical detection of luciferase expression showed appreciable activity under basal conditions in bone, brain, and the intestine, being the activity in bone and brain 50%–60% of the maximal activity measured during the cycle. As expected, the ligand-dependent tissues, liver and uterus, had 13% and 7% of the highest activity as measured during pro-estrus of normal cycling female mice.

Although these data strongly indicate a different regulation of estrogen receptor transcriptional activity in the liver and reproductive organs compared to the nonreproductive organs, when estrogen is administered exogenously to 3-weeks ovariectomized mice, all tissues tested responded by an increase in ER transcriptional activity. However, the response to 5 μg/kg 17β-estradiol, which is comparable to levels at pro-estrus, was much higher in liver and uterus (eight- and sixfold) compared to brain and bone (about twofold). This difference can be explained by a difference in basal activity of ERE-*luc* after OVX, which, as mentioned earlier, is higher for bone and brain compared to liver and uterus. These findings show that the observed differences in ER transcriptional activation are not due to their ability to respond to circulating estrogen per se. Furthermore, administration of the specific ER-antagonist ICI182,780 to either immature mice or to adult female mice resulted in a strong reduction in luciferase activity in all organs, although the relative decrease was stronger in liver compared to brain and bone. This suggests that even in the absence of estrogen the luciferase activity strongly depends on activated ERs.

All together, the findings described above and described in more detail elsewhere (Ciana et al. 2003) strongly suggest that both in immature and adult cycling mice ER can be activated by estrogen-independent mechanisms in nonreproductive tissues. Since it has been shown both in vitro and in vivo that ER activity can also be modulated independently of estrogen by signaling pathways downstream from growth factors and neurotransmitters, these are likely candidates involved in the estrogen-independent activation (Kato 2001).

In fact, it has been shown that IGF-1 administration to OVX ERE-*luc* mice resulted in an increase in luciferase activity in the uterus and in nonreproductive organs (Klotz et al. 2002). Preliminary data in the ERE-luc mice using an inhibitor of IGF-1 signaling indicate that it mainly blocked the activation in the nonreproductive organs, suggesting that indeed IGF-1 is a major player in this process (A. Maggi, personal communication). This is also in agreement with the knowledge that during the estrous cycle in mammals circulating IGF-1 levels increase at estrus and decline during the luteal phase (Hashizume et al. 2002). Since most of the circulating IGF-1 is derived from the liver, it is very possible that during pro-estrus, when estrogen levels are high, estrogen activates ER, leading to enhanced IGF-1 production as has been shown in other organs and cell types (Kassem et al. 1998; Shingo et al. 2003). This in turn would lead to activation of the ER in the nonreproductive organs.

These new exciting findings may have great implications for hormone replacement therapy (HRT) and were initially discovered due to transgenic mice in which recording of gene expression was greatly facilitated by BLI. The search for new tissue selective modulators of ER activity (SERMs), either synthetic or natural, will be made much easier using these kind of transgenic reporter animals in combination with BLI.

11.3.2 Osteocalcin-*luc* Reporter Mice to Monitor Bone Formation and Remodeling

Osteocalcin, a noncollagenous bone protein synthesized by the osteoblast, has been suggested as a good biochemical marker for bone turnover or bone formation (Young 2003). Osteocalcin is one of the most abundant noncollagenous proteins in bone and expressed by mature osteoblasts, osteocytes, and to some extent in odontoblasts, and hypertrophic chondrocytes. Osteocalcin is a bone-specific protein that binds calcium and has strong affinity for hydroxyapatite, and its production by osteoblasts adjacent to mineralizing surfaces coincides with mineralization of developing bone. In vitro experiments in developing osteoblast cultures has shown that osteocalcin starts to be expressed at the onset of mineralization. Moreover, the

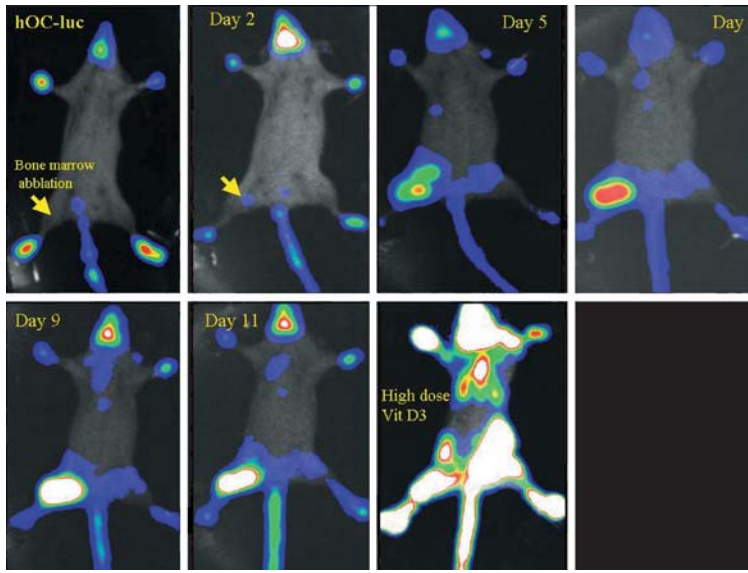

Fig. 3. Bone formation model. BLI of a hOC-*luc* mouse under basal conditions and after bone marrow ablation, which is known to result in very strong and local bone formation during the first 10–12 days after the ablation. In the *last frame* a mouse is shown after stimulation with 1.25(OH)2D3, a known stimulator of human osteocalcin expression. The mice were monitored every morning at the same time and BLI was performed with the animal lying in the same position on its back

human and rat osteocalcin gene contains a vitamin D response element (VDRE) and, therefore, its expression is regulated by 1.25(OH)2D3 (Desai 1995).

Clemens and coworkers (Clemens et al. 1997) has generated transgenic mice in which the luciferase (*luc*) reporter gene was under the regulation of the human osteocalcin (hOC) promoter. Using these hOC-*luc* mice in combination with BLI, one can study the human osteocalcin gene expression in vivo noninvasively and in principle detect changes in bone formation and/or remodeling.

As shown in Fig. 3, under basal conditions the hOC-*luc* mouse strongly expresses the gene at all sites of the body with high mechanical loading, like the ankle and wrist bones, the jaw, and the tail

vertebrae. It is known from studies in humans that especially the calcaneus (ankle) bones are undergoing high mechanical forces during mechanical loading due to walking, running, and jumping (Lehtonen-Veromaa et al. 2001). Since mice are walking on 4 feet, all the calcaneus bones show high luciferase activity. The luciferase expression shown in the bones of the jaw is the result of the high remodeling of alveolar bone as a result of the constant growth of the incisor teeth, which is characteristic of the rodents. In the hOC-*luc* mice the expression in the jaw varied during the day most probably consequent to the known circadian rhythm of the incisor growth and mastication due to feeding schedule (Ohtsuka and Shinoda 1995). Finally, the tail vertebrae of mice are mechanically loaded by continuous tail movements.

Depending on the physical activity of the mice and food intake, the gene expression of the human osteocalcin gene varied, most probably due to differences in mechanical loading. This was in line with our observations that mice that have been inactivated for a while show much less activity in calcaneus bones and tail vertebrae.

Femoral bone marrow ablation in rodents has been shown to lead to a strong but temporary increase in new bone formation with a peak around 10–12 days after the ablation (Bab 1995). During this period, the total marrow space is completely filled with new bone trabeculae. Hereafter, the osteoclast will come in and completely resorb the new trabecular bone back to its original size within 8–10 days. Thus, in this model bone formation and resorption are nicely separated in time. When a bone marrow ablation was performed on the femur of the right hind leg of the hOC-*luc* mouse an increase of OC-*luc* expression could be visualized by BLI 2 days after the ablation and peak activity was obtained at day 9 (see Fig. 3). These data are in line with the recent findings of Iris and coworkers (Iris et al. 2003). When after 3 weeks the expression was back to normal, the mouse received one single high dose of 1.25(OH)2D3 which, as expected, resulted in an enormous increase in luciferase activity all over the entire skeleton due to increased OC-*luc* expression in almost all skeletal elements since the human OC-promotor is known to be activated by vitamin D3 (Clemens et al. 1997).

These findings show that the hOC-*luc* mouse model in combination with BLI is nicely suited to study effects of mechanical loading and drugs like vitamin D and related analogs.

These studies with transgenic *luc*-reporter mice show that BLI allows rapid and convenient assessment of changes in gene expression in time and place noninvasively. It also allowed us to make new, unexpected discoveries that are not easily made with conventional technologies.

11.4 Tumor Progression and Bone/Bone Marrow Metastasis of Breast and Prostate Cancer

11.4.1 Skeletal Metastasis and Minimal Residual Disease

Metastatic disease is the major cause of death in cancer patients. Bone marrow is a preferential site of metastasis in a variety of cancers. However, only a restricted number of solid cancers, especially breast and prostate cancer, are responsible for the majority of skeletal metastases. According to the "Seed and Soil" theory, this propensity to metastasize to bone is related to chemoattraction, survival, and growth factor support, specific for these cancers, that is provided by the bone marrow/bone microenvironment. Experimental evidence suggests that this support mechanism is active during bone resorption. Micrometastatic spread is often present in bone marrow of cancer patients devoid of clinically evident metastases (minimal residual disease) and represent the pathophysiological basis for cancer relapse as overt bone metastases (see Fig. 4). Established micrometastases can stay dormant in G_0-status for a long time, but can be activated through a local mesenchymal stroma reaction, usually cytokines or growth factors. Dormancy also explains the failure of chemotherapy or radiotherapy, which aims at inhibition of proliferation. Once the micrometastases starts growing into a macrometastases it can grow until a size of 2–3 mm^3 without the need of new blood vessels by co-option with the existing blood vessels. When this size is reached, hypoxia will occur, leading to induction of VEGFs and angiogenesis. Until now, there has been no good animal model to study minimal residual disease because the detection limit of tumor

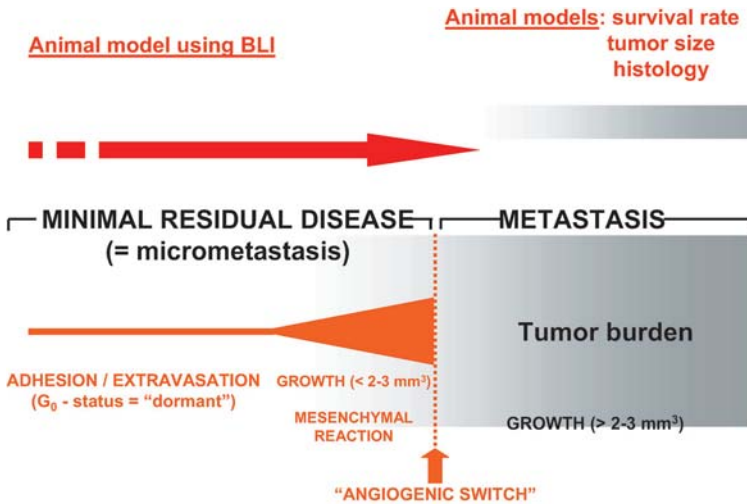

Fig. 4. An animal model for studying minimal residual disease using BLI

cells is not sensitive enough. In most current models tumor volume of subcutaneously transplanted tumors, survival rate, and histology are still used to monitor therapeutic effects. However, BLI now offers the possibility to measure tumor development, progression, and metastasis in a very rapid and time-sensitive manner.

An emerging concept identifies the growth support provided by a specific organ microenvironment as the principal target for adjuvant therapies aiming to prevent progression of micrometastases to overt metastases. The tumor-host interface in bone metastasis represents a unique opportunity to test this hypothesis, since, differently from other organs, therapeutic means that lower bone resorption and, consequently, tumor growth support are available.

Recently, we developed a BLI-based, highly sensitive method to monitor, continuously and reliably, development and progression of experimental bone metastases in living animals (Wetterwald et al. 2002). After intracardiac injection of the tumor cells, very small amounts of tumor cells can be detected in bone marrow/bone, mimicking micrometastatic spread. Therefore, this model is also a nice model for minimal residual disease and effectively allows sensitive

localization and growth monitoring of minimal metastatic deposits in the bone marrow at a stage largely preceding tumor-induced osteolysis. Below, the BLI models will be discussed and we will show, as an example, how they can be used to investigate the effects of a potent nitrogen-containing bisphosphonate (Olpadronate) on the development and progression of osteolytic metastases.

Our investigations may help to better identify situations at risk for bone metastasis and novel therapeutic strategies that could be extended to the clinical reality.

11.4.2 Bone Metastasis of Breast and Prostate Cancer

Because of the progress made in early detection and surgical treatment of the primary tumor, mortality in cancer patients is increasingly linked to metastatic disease. Bone is the second most frequent site of metastasis. However, only a restricted number of solid cancers, especially breast cancer (BCa) and prostate cancer (PCa), are responsible for the majority of skeletal metastases. These are a major cause of morbidity, characterized by severe pain and high incidence of skeletal and hemopoietic complications (fractures, spinal cord compression, and bone marrow aplasia) requiring hospitalization. They represent a relevant problem for health care because the patients may show a long clinical course. Furthermore, the quality of life of these patients and their families is greatly affected.

Despite the frequency of skeletal metastases in BCa and PCa, the molecular mechanisms for their propensity to colonize bone are poorly understood. This is also reflected by the fact that treatment options for bone metastasis, namely chemotherapy, radiotherapy, hormonal ablation, and surgery, are unsatisfactory.

Metastasis is a multistep process characterized sequentially by loss of intercellular cohesion, and induction of cell migration, angiogenesis, access to the systemic blood circulation, and subsequent extravasation at distant organs. In animal models, it has been estimated that $3–4\times10^6$ cancer cells/g of tumor can reach the bloodstream per day (Butler and Gullino 1975). However, according to the “Seed and Soil” theory (Paget 1889), for the final development of a metastasis it is essential that the metastatic cells can adapt, and therefore sur-

vive and grow, to the specific organ environment that they colonize. Genetic instability within the cancer cell population(s) of the primary tumor is responsible for the acquisition of these new properties. However, acquisition of "all" these properties is a relatively rare event and, consequently, the metastatic process is highly inefficient and only a restricted minority of cancer cells reaching the blood will survive and grow at the distant sites (Fidler 1970). It derives that therapeutic interference with the ultimate survival/growth step, targeting a small minority of cancer cells, should be far more efficient than inhibition of later steps of the metastatic process, which seems to be accomplished by a much greater number of cancer cells.

11.4.3 Bone Turnover

Bone is a highly dynamic tissue that is continuously remodeled by microscopic patches of bone resorption and subsequent bone formation. The result is replacement of old bone with new bone, thus maintaining structural integrity of the skeleton throughout adult life. These morphological entities, together with their cellular components, are called "basic multicellular units" (BMU; Eriksen et al. 1994). The number and the activity of these BMU determine the rate of bone turnover and they are under the control of mechanical stress, cytokines, and hormones. During the bone remodeling process, osteoblasts and osteoclasts, the cellular components of the BMU, secrete paracrine growth factors. Furthermore, there is experimental evidence that growth factors are exposed from the bone matrix and activated during bone resorption (Mundy and Yoneda 1996; see Fig. 5). Direct evidence that tumor cells do not have intrinsic ability to resorb bone and that osteoclasts are required for tumor-induced osteolysis and tumor growth was provided in osteoclast-deficient mice (Clohisy and Ramnaraine 1998). As described in the next section (see also legend to Fig. 5), increased bone resorption, especially near the site of tumor seeds, favors the growth of breast cancer cells. Furthermore, there is some clinical evidence that increased bone resorption is associated with a higher incidence of breast cancer bone metastasis.

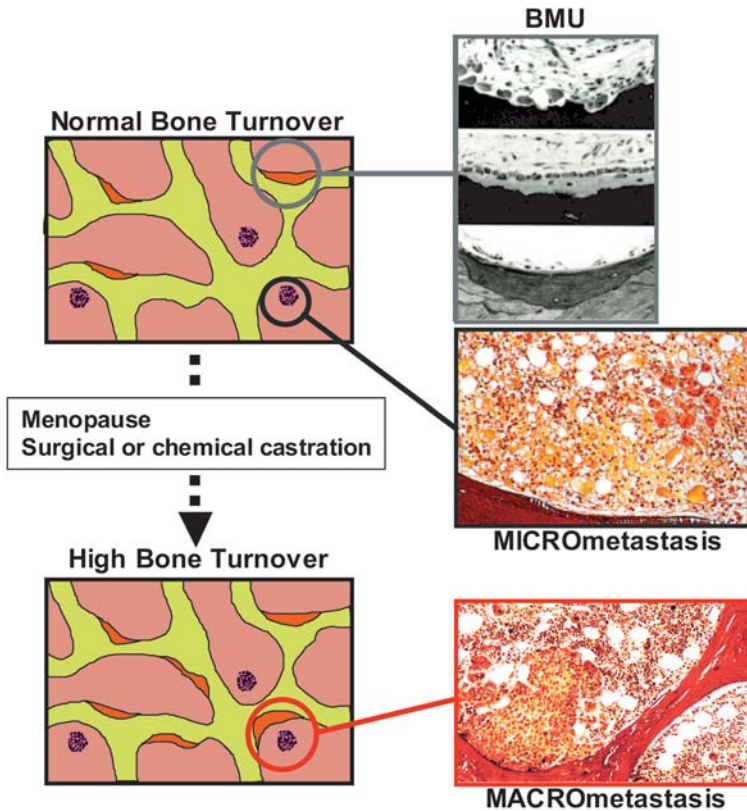

Fig. 5. Role of bone turnover in bone metastasis. During normal bone turnover, several BMUs are opened in which bone remodeling (bone resorption followed by bone formation) takes place. In this area, the bone marrow stroma is locally activated by cytokines to induce osteoclast and osteoblast formation from bone-marrow derived progenitors. If only a few BMUs are present, the statistical chance of activating a new BMU near a dormant micrometastases is relatively small. This changes dramatically when the number of new BMUs are opened, leading to a much higher risk of activating the dormant tumor cells and the formation of macrometastases

11.4.4 "Vicious Cycle" Hypothesis of Bone Metastasis

The bone/bone marrow microenvironment may contribute to development of metastasis at this site through chemoattraction, adhesion, survival- and growth-promoting molecules locally released during bone resorption/formation. The primary epithelial tumor cells lose their cell-cell adherence (E-Cadherin) and acquire an invasive phenotype (increase in proteolytic enzymes, i.e. cathepsins and MMPs). They increase the production of angiogenic factors (i.e., VEGF, FGF) and intravasate into the blood vessels. Recent findings show that chemokine receptor CXCR4 and its ligand SDF-1 (stromal derived factor 1), which is also produced by bone marrow stroma cells, play a critical role in metastasis to bone marrow (Muller et al. 2001). We have shown that β-integrins play an important role in adhesion to bone marrow stroma. Secretion of parathyroid hormone-related protein (PTHrP) by tumor cells present in the bone microenvironment activates osteoblasts to produce receptor activator of nuclear factor-κB ligand (RANK-L) and to downregulate osteoprotegerin (OPG). As a result, osteoclast recruitment and activity are stimulated, and bone resorption is increased. The consequent release of growth factors, such as transforming growth factor-β (TGF-β), insulin-like growth factor-1 (IGF-1), and other cytokines stimulates tumor growth and further secretion of PTHrP and VEGFs, thus establishing a "vicious cycle" (Guise et al. 1996; Guise 1999; Mundy 2002; see Fig. 6). Accordingly, pharmacological suppression of bone turnover (i.e., bisphosphonates, BP) should interfere with its growth support and, thus, prevent development and progression of bone metastases.

11.4.5 Micrometastases and Minimal Residual Disease

Due to improved and earlier diagnosis, an increased proportion of cancer patients, including those affected by BCa and PCa, shows no macroscopic metastasis at the moment of first diagnosis. Nevertheless, 30% of these patients will develop macroscopic metastasis in the following 5 years. It is now clear that already at the moment of the original diagnosis these patients have microscopic deposits of

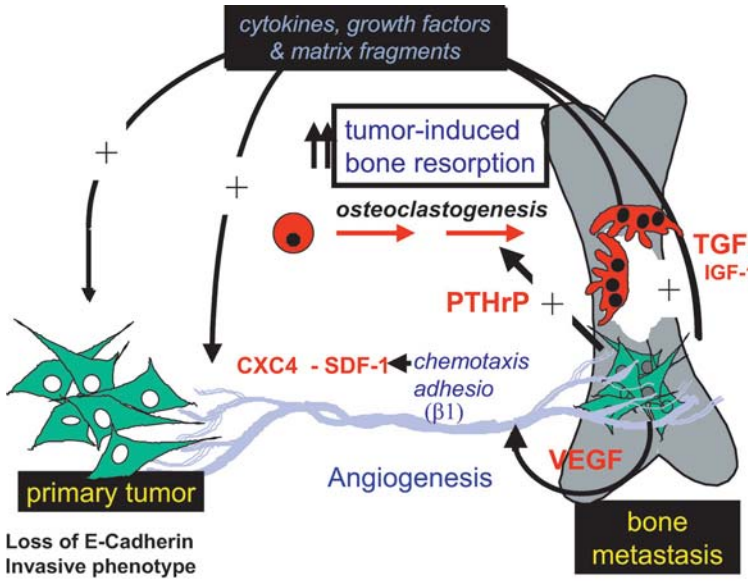

Fig. 6. The "vicious cycle" hypothesis of bone metastasis

cancer cells in various tissues that cannot be identified by current diagnostic methods. In clinical studies, micrometastases have been detected in a vast proportion of the bone marrow aspirates of subjects affected by mammary and prostate carcinoma with no radiological or scintigraphic evidence of bone metastases (Braun et al. 2000; Mansi et al. 1987; Melchior et al. 1997; Gao et al. 1999). This has led to the hypothesis that most cancer patients harbor neoplastic cells in their bone marrow at the time of diagnosis (Lange and Vasella 1999). However, analysis of their cell cycling status shows that most of these cancer cells are dormant (G_0-status; Pantel et al. 1993). After resection of the primary tumor, the proportion of bone marrow aspirates that are positive for cancer cells dramatically declines and, eventually, revert to a negative status within 6–9 months (Lange and Vasella 1999). This indicates that the presence of micrometastases is a relatively early event in the disease process and it is due to the continuous supply of blood circulating cancer cells as a

result of cell shedding from the primary tumor. The G_0-status of these micrometastatic cells may explain failure of chemotherapy and suggests that alternative adjuvant therapies, aiming to repress microenvironmental growth support during the period following surgery, are a better therapeutic rationale.

11.5 Use of Bioluminescent Imaging in Animal Models of Skeletal Metastasis

11.5.1 Breast Cancer Bone Metastasis Model

In 1988, Arguello and coworkers showed that injection of cancer cell lines into the left cardiac ventricle of immunodeficient (*nu/nu*) mice will lead to colonization of specific sites of the skeleton. This model is now a widely used animal model of bone/bone marrow metastasis. We and others have applied this model to study human breast cancer metastasis (Arguello et al 1988, 1992; Sasaki et al. 1995; Yin et al. 1999; van der Pluijm et al. 2000, 2001, 2002a, b; Wetterwald et al. 2002). For this we use the highly malignant human breast carcinoma cell line MDA-MB-231, that metastasizes to bone marrow and will rapidly cause multiple osteolytic lesions that can be detected using X-ray radiography. However, radiological-evident osteolytic/osteosclerotic metastases are a late and macroscopic event in the development of metastatic bone disease. Thus, the model lacks the sensitivity that would be necessary to dissect the initial processes essential for tumor progression. Furthermore, the radiological detection of osteolytic (or osteosclerotic, as seen in prostate cancer) metastases is an indirect measure of the tumor burden. Therefore, we developed a more sensitive method to detect and monitor directly metastatic growth in bone marrow/bone using whole animal BLI (Wetterwald et al. 2002).

To use BLI to monitor osteolytic bone metastasis of breast cancer, we use a stably *luc*-transfected, bone-seeking sub-clone (MDA-231-B) derived from four sequential cycles of intracardiac inoculation in vivo and expansion in vitro of the cell population recovered from the resulting bone metastases. Using BLI in this model has the following advantages:

1. Early detection of minimal bone metastatic sites (=0.3 mm^3 volume/approximately 5,000 cells; when the metastases are not yet osteolytic), as compared to conventional radiography detecting almost exclusively the osteolytic sites (2–3 weeks vs. 5 weeks)
2. Much higher precision and reliability, as compared to radiography
3. The possibility to quantify the tumor burden for each metastatic site
4. The possibility to follow the kinetics of tumor growth in the same animal
5. Targeted dissection of all the metastatic sites for end-point histological and/or molecular analysis
6. Detect possible nonosteolytic and soft tissue metastases.

11.5.1.1 Intracardiac Injection Model

Figure 7 shows the principle of the intracardiac injection model.

11.5.1.2 Intraosseous Implantation Model

Figure 8 depicts the principle of the intraosseous implantation model.

11.5.2 Bisphosphonates

Bisphosphonates (BP) are nonhydrolysable pyrophosphate analogs that exert a strong inhibitory effect on osteoclastic bone resorption (Fleish 1998; Rodan 1998). Typically, BP show a very high affinity to bone mineral and, consequently, in vivo they exclusively accumulate in bone (Fleish 1998). Nitrogen-containing BP inhibit the prenylation (mevalonate pathway) of guanidine triphosphate-binding proteins required for osteoclast development, function, and survival (Luckman et al. 1998; van Beek et al. 1999a, b; Russell et al. 1999). Nonnitrogen containing BP, such as Clodronate, acts prevalently by generation of cytotoxic ATP analogs (Frith et al. 1997).

Bisphosphonates have been reported to exert direct antiproliferative and proapoptotic effects on cancer cells in vitro (Shipman et al. 1997; Seneratne et al. 2000; Lee et al. 2001), to interfere with cancer cell adhesion to bone matrix proteins (van der Pluijm et al. 1996; Boissier et al. 1997), and to inhibit matrix metalloproteinases (Heikkila et al. 2002; Teronen et al. 1999) and cancer cell migration

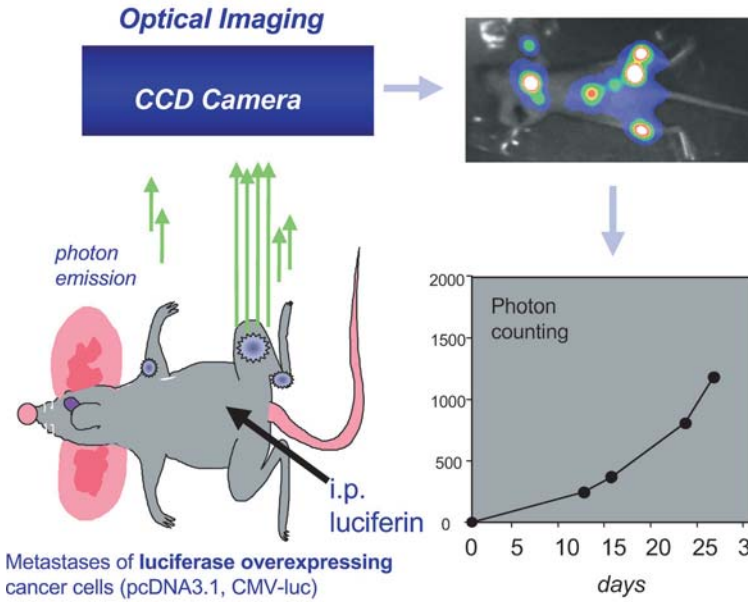

Fig. 7. Intracardiac injection model. Injection of 100,000 MD-231 B-*luc* cells into the left heart ventricle of 8-week-old female nude mice causes multiple skeletal metastases. At any given time point the animals can be monitored using BLI. For this the animals were anesthetized and 25 µl of a 250-mmol/l aqueous solution of luciferin was injected intraperitoneally 10 min before beginning photon recording. Mice were placed in the light-tight chamber and a gray-scale image of the animal was first recorded with dimmed light. Photon emission was then measured and recorded as pseudo-color images. For colocalization of the bioluminescent photon emission on the animal body, gray-scale and pseudo-color images were merged by using imaging software. The progression of each individual metastases can be monitored in time as indicated

and invasion (Boissier et al. 2000). An antiangiogenic effect has also been described (Wood et al. 2002; Fournier et al. 2002). All these effects are possibly relevant for cancer disease (Clezardin et al. 2003; Green 2002). However, in most of the cases they have been obtained at concentrations that are too high to be reached in vivo in the extracellular fluid.

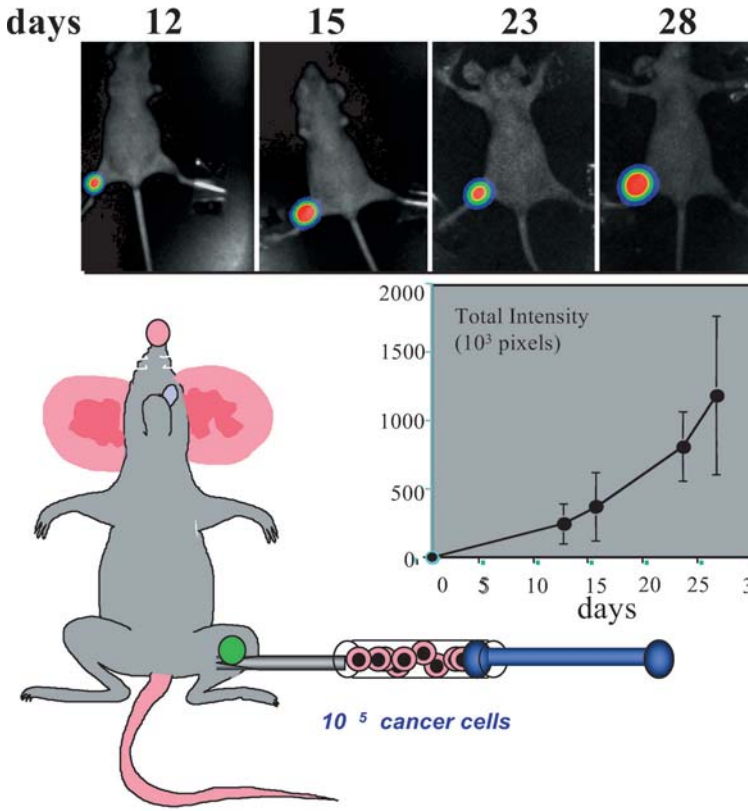

Fig. 8. Intraosseous implantation model. For direct intraosseous implantation of MDA-231B-*Luc* cells, two holes, 4–5 mm distant from each other and each with a diameter of 0.35 mm, were drilled through the bone cortex of the upper third of the right tibia with the aid of a dental drill. Space in the marrow cavity was created by flushing out the bone marrow of the proximal segment of the bone shaft. The upper hole was sealed with surgical bone wax and a single cell suspension of MDA-231B-*Luc* cells (1×10^5/25 µl of PBS) slowly inoculated via a 30-gauge needle inserted through the lower hole. Finally, the lower hole was sealed with surgical bone wax and the cutaneous wound was sutured. Local tumor development was monitored with BLI

In animal models of bone metastasis, BP have been reported to reduce the tumor burden in established bone metastases, but not in soft tissue and visceral metastases. This effect was suggested to be mediated by induction of apoptosis in the cancer cells (Hiraga et al. 2001). Prophylactic treatment with BP, given prior to the development of evident metastasis, resulted in a marked reduction of the number of bone metastases (Hall and Stoica 1994; Sasaki et al. 1995). However, in one preventive study it was reported that BP pretreatment leads to an increased tumor burden in the developing bone metastases, but not in extraosseous metastases (Kostenuik et al. 1993). Nevertheless, these results further supported the concept that BP inhibition of osteoclastic bone resorption could be a useful adjunctive therapy for the treatment of cancers that have colonized bone.

In clinical practice, BP have been widely used to control the skeletal complications (bone metastasis and humoral hypercalcemia of malignancy) in various neoplastic diseases. In established bone metastases, BP reduce the number of skeletal-related events (Elomaa et al. 1983; Berenson et al. 1996, 1998; van Holten-Verzantvoort et al. 1993; Hortobagyi et al. 1996). Other clinical studies have also shown that BP may prevent development of new bone metastatic foci in patients either with bone metastasis already present or with no bone metastasis at the beginning of the treatment (Kanis et al. 1996; Conte et al. 1996). However, a similar study failed to demonstrate a reduction in the number of metastases (van Holten-Verzantvoort et al. 1996). Three clinical trials have primarily focused their investigation on the possibility that BP may prevent the development of metastases in women affected by mammary carcinoma, but free of bone metastases at the moment of diagnosis. In two of these studies (Powles et al. 2002; Diel et al. 1998), the preventive administration of BP reduced significantly the number of patients developing bone metastases and, in those who developed bone metastases, the number of the bone metastases. In one study (Diel et al. 1998) there was also a significant reduction of the number of visceral metastases. However, in the third study (Saarto et al. 2001) BP treatment did not prevent the development of bone metastases and seemed even to increase the development of nonskeletal metastases. In prostate cancer similar prevention trials are ongoing, but the definitive results are not yet known.

The contradictory results reported above still leave some open questions concerning the efficacy of BP as adjuvant therapy for preventing bone metastasis in cancer disease. First of all, it is unresolved whether BP act directly on cancer cells or indirectly, via inhibition of bone resorption and, thus, release of growth factor support for cancer cells. Second, the stage of metastatic disease and the bone turnover status for which BP should find their best indication are not yet defined.

11.5.2.1 Treatment with the Potent Antiresorptive Bisphosphonate Olpadronate Inhibits Osteolysis But Does Not Inhibit Tumor Progression of Established MDA-B-*luc* Tumors in Bone

In order to determine if bisphosphonate treatment also effects tumor progression of breast cancer tumors in bone, either directly or indirectly via inhibition of bone resorption, the following experiments were performed. One hundred thousand MDA-B-*luc* tumor cells were inoculated directly into the bone marrow space and 14 days later, when small photon-emitting tumors had formed, daily Olpadronate treatment (1.6 μM/kg/day subcutaneous) started and lasted 28 days. Tumor-induced osteolysis was determined using X-ray radiography and depicted as lytic area (mm^2). Changes in tumor volume were determined using BLI and depicted as total intensity (number of pixels).

In the left upper panel of Fig. 9, it is shown that Olpadronate treatment strongly inhibits tumor-induced osteolysis. However, as shown in the right upper panel, Olpadronate treatment does not have an inhibitory effect on tumor progression as measured by BLI. This was confirmed by histological examination of the bones. It is clear that in the vehicle-treated animal, the bone (in green) is completely lost and fractured and that the tumor is now also growing outside of bone. In the Olpadronate-treated animal, the bone collar is still intact and the bone is not fractured. However, the tumor is also growing outside of bone. The reason for this is that due to inhibition of bone resorption the tumor cell can not grow any further within the bone marrow compartment and will migrate outside of the bone marrow space via the vascular channels. These data show that Olpadronate has no direct antitumor effect and that inhibition of bone re-

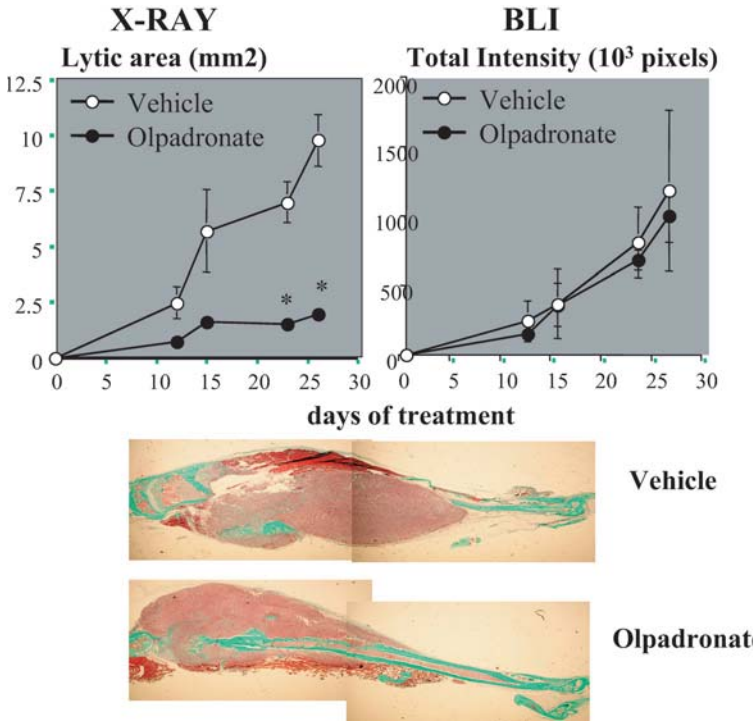

Fig. 9. Effect of the potent antiresorptive bisphosphonate Olpadronate on established MDA-B-*luc* tumors growing in bone. For this purpose, 100,000 MDA-B-*luc* cells were intraosseously inoculated and daily treatment with Olpadronate started 14 days after inoculation, when small tumors were established. Osteolysis was measured using X-ray radiography and tumor progression was measured using BLI

sorption does not lead to a slower progression of already-established tumors within bone.

11.5.2.2 Olpadronate Inhibits the Formation of New Bone Metastases

To test whether prophylactic Olpadronate treatment could reduce the number of metastases formed, the following experiments were performed. Two days before intracardiac injection of the MDA-B-*Luc*

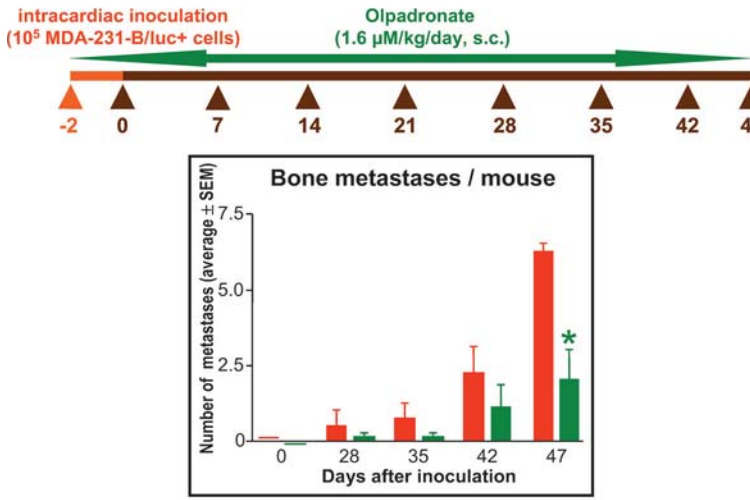

Fig. 10. Effect of prophylactic Olpadronate treatment on the development of bone metastases after intracardiac inoculation of MDA-B-*luc* breast cancer cell

cells, the daily treatment with Olpadronate (1.6 µM/kg/day subcutaneous) started and lasted 47 days. The number of metastatic sites in the whole animal was determined using BLI (see also Fig. 7). As depicted in Fig. 10, when Olpadronate was given daily starting 2 days before the inoculation of the tumor cells, there was a significant reduction in the number of metastases formed.

These findings lead us to conclude that bisphosphonates, via their antiresorptive activity, can reduce breast cancer metastasis to bone, most probably by reducing bone remodeling, leading to a decrease of local factors that are normally released during the resorption process and that are involved in activation of micrometastases. However, our data also suggest that once a micrometastases has turned into a macrometastases or small tumor, it becomes independent of local bone turnover for its growth and, therefore, bisphosphonate treatment will not slow down tumor progression. We also did not find any evidence for a direct effect of Olpadronate on tumor growth. It might still be possible that, dependent on the structure of

the bisphosphonate used, compounds with lower bone affinity that are also slowly released from the bone surface can have direct effects on the nearby tumor itself. In our preliminary experiments we did not find an increase in soft tissue metastases. However, it is important to note that our studies were performed with a selected clone of MDA-MB-231 cells which almost exclusively give rise to bone metastases. Other studies are needed to investigate this in more detail.

11.6 Conclusions and Future Perspectives

It is clear from the work presented in this chapter and from work by others that BLI is perfectly suited to monitor gene expression in transgenic reporter mice and to detect and follow small numbers of cells noninvasively. As we have shown, it also enables the quantification of tumor cells within internal organs in animal models of cancer. BLI is a powerful tool in functional genomics of cancer development, progression, and metastasis and will allow us to identify in vivo molecular targets of cancer and their metastasis. The application of BLI in combination with new animal models for cancer will allow us to study very rapidly and conveniently the efficacy of new therapeutic approaches such as gene therapy stem cell therapy and antiangiogenic therapy, and when successful can be a first step towards clinical application. Furthermore, the development of new smart luciferase-based reporter constructs as well as new possibilities to create transgenic animals containing these reporter constructs will make noninvasive in vivo BLI also a powerful new tool in other small animal models of human biology and disease.

References

Arguello F, Baggs RB, Frantz CN (1988) A murine model of experimental metastasis to bone and bone marrow. Cancer Res 48:6876–6881

Arguello F, Baggs RB, Graves BT, Harwell SE, Cohen HJ, Frantz CN (1992) Effect of IL-1 on experimental bone/bone-marrow metastases. Int J Cancer 52:802–807

Bab IA (1995) Postablation bone marrow regeneration: an in vivo model to study differential regulation of bone formation and resorption. Bone [4 Suppl]:437S–441S

Berenson JR, Lichtenstein A, Porter L, Dimopoulos MA, Bordoni R, George S, Lipton A, Keller A, Ballester O, Kovacs MJ, Blacklock HA, Bell R, Simeone J, Reitsma DJ, Heffernan M, Seaman J, Knight RD (1996) Efficacy of pamidronate in reducing skeletal events in patients with advanced multiple myeloma. Myeloma Aredia Study Group. N Engl J Med 334: 488–493

Berenson JR, Lichtenstein A, Porter L, Dimopoulos MA, Bordoni R, George S, Lipton A, Keller A, Ballester O, Kovacs M, Blacklock H, Bell R, Simeone JF, Reitsma DJ, Heffernan M, Seaman J, Knight RD (1998) Long-term pamidronate treatment of advanced multiple myeloma patients reduces skeletal events. Myeloma Aredia Study Group. J Clin Oncol 16: 593–602

Bhaumik S, Gambhir SS (2002) Optical imaging of Renilla luciferase reporter gene expression in living mice. Proc Natl Acad Sci USA 99:377–382

Boissier S, Magnetto S, Frappart L, Cuzin B, Ebetino FH, Delmas PD, Clezardin P (1997) Bisphosphonates inhibit prostate and breast carcinoma cell adhesion to unmineralized and mineralized bone extracellular matrices. Cancer Res 57:3890–3894

Boissier S, Ferreras M, Peyruchaud O, Magnetto S, Ebetino FH, Colombel M, Delmas P, Delaisse JM, Clezardin P (2000) Bisphosphonates inhibit breast and prostate carcinoma cell invasion, an early event in the formation of bone metastases. Cancer Res 60:2949–2954

Braun S, Pantel K, Muller P, Janni W, Hepp F, Kentenich CR, Gastroph S, Wischnik A, Dimpfl T, Kindermann G, Riethmuller G, Schlimok G (2000) Cytokeratin-positive cells in the bone marrow and survival of patients with stage I, II, or III breast cancer. N Engl J Med 342:525–533

Butler TP, Gullino PM (1975) Quantitation of cell shedding into efferent blood of mammary adenocarcinoma. Cancer Res 35:512–516

Carlsen H, Moskaug JO, Fromm SH, Blomhoff R (2002) In vivo imaging of NF-kappa B activity. J Immunol 168:1441–1446

Ciana P, Di Luccio G, Belcredito S, Pollio G, Vegeto E, Tatangelo L, Tiveron C, Maggi A (2001) Engineering of a mouse for the in vivo profiling of estrogen receptor activity. Mol Endocrinol 15:1104–1113

Ciana P, Raviscioni M, Mussi P, Vegeto E, Que I, Parker MG, Lowik C, Maggi A (2003) In vivo imaging of transcriptionally active estrogen receptors. Nat Med 9:82–86

Clemens TL, Tang H, Maeda S, Kesterson RA, Demayo F, Pike JW, Gundberg CM (1997) Analysis of osteocalcin expression in transgenic mice reveals a species difference in vitamin D regulation of mouse and human osteocalcin genes. J Bone Miner Res 12:1570–1576

Clezardin P, Fournier P, Boissier S, Peyruchaud O (2003) In vitro and in vivo antitumor effects of bisphosphonates. Curr Med Chem 10:173–180

Clohisy DR, Ramnaraine ML (1998) Osteoclasts are required for bone tumors to grow and destroy bone. J Orthop Res 16:660–666

Contag CH, Spilman SD, Contag PR, Oshiro M, Eames B, Dennery P, Stevenson DK, Benaron DA (1997) Visualizing gene expression in living mammals using a bioluminescent reporter. Photochem Photobiol 66:523–531

Contag PR, Olomu IN, Stevenson DK, Contag CH (1998) Bioluminescent indicators in living mammals. Nat Med 4:245–247

Contag CH, Jenkins D, Contag PR, Negrin RS (2000) Use of reporter genes for optical measurements of neoplastic disease in vivo. Neoplasia 2:41–52

Conte PF, Latreille J, Mauriac L, Calabresi F, Santos R, Campos D, Bonneterre J, Francini G, Ford JM (1996) Delay in progression of bone metastases in breast cancer patients treated with intravenous pamidronate: results from a multinational randomized controlled trial. The Aredia Multinational Cooperative Group. J Clin Oncol 14:2552–2559

Desai RK, van Wijnen AJ, Stein JL, Stein GS, Lian JB (1995) Control of 1,25-dihydroxyvitamin D3 receptor-mediated enhancement of osteocalcin gene transcription: effects of perturbing phosphorylation pathways by okadaic acid and staurosporine. Endocrinology 136:5685–5693

Diel IJ, Solomayer EF, Costa SD, Gollan C, Goerner R, Wallwiener D, Kaufmann M, Bastert G (1998) Reduction in new metastases in breast cancer with adjuvant clodronate treatment. N Engl J Med 339:357–363

Edinger M, Cao YA, Verneris MR, Bachmann MH, Contag CH, Negrin RS (2003) Revealing lymphoma growth and the efficacy of immune cell therapies using in vivo bioluminescence imaging. Blood 101:640–648

Edinger M, Sweeney TJ, Tucker AA, Olomu AB, Negrin RS, Contag CH (1999) Noninvasive assessment of tumor cell proliferation in animal models. Neoplasia 1:303–310

El Hilali N, Rubio N, Martinez-Villacampa M, Blanco J (2002) Combined noninvasive imaging and luminometric quantification of luciferase-labeled human prostate tumors and metastases. Lab Invest 82:1563–1571

Elomaa I, Blomqvist C, Grohn P, Porkka L, Kairento AL, Selander K, Lamberg-Allardt C, Holmstrom T (1983) Long-term controlled trial with diphosphonate in patients with osteolytic bone metastases. Lancet 1:146–149

Eriksen EF, Axelrod DW, Melsen F (1994) Bone histomorphometry. Raven Press, New York, pp 3–12

Fidler IJ (1970) Metastasis: quantitative analysis of distribution and fate of tumor emboli labeled with ^{125}I-5-iodo-2′-deoxyuridine. J Natl Cancer Inst 45:773–782

Fournier P, Boissier S, Filleur S, Guglielmi J, Cabon F, Colombel M, Clezardin P (2002) Bisphosphonates inhibit angiogenesis in vitro and testosterone-stimulated vascular regrowth in the ventral prostate in castrated rats. Cancer Res 62:6538–6544

Frith JC, Monkkonen J, Blackburn GM, Russell RG, Rogers MJ (1997) Clodronate and liposome-encapsulated clodronate are metabolized to a toxic ATP analog, adenosine 5′-(β,γ-dichloromethylene) triphosphate, by mammalian cells in vitro. J Bone Miner Res 12:1358–1367

Gao CL, Dean RC, Pinto A, Mooneyhan R, Connelly RR, McLeod DG, Srivastava S, Moul JW (1999) Detection of circulating prostate specific antigen expressing prostatic cells in the bone marrow of radical prostatectomy patients by sensitive reverse transcriptase polymerase chain reaction. J Urol 161:1070–1076

Green JR (2002) Bisphosphonates in cancer therapy. Curr Opin Oncol 14: 609–615

Guise TA (1999) TGF-β signaling blockade inhibits PTHrP secretion by breast cancer cells and bone metastases development. J Clin Invest 103:197–206

Guise TA, Yin JJ, Taylor SD, Kumagai Y, Dallas M, Boyce BF, Yoneda T, Mundy GR (1996) Evidence for a causal role of parathyroid hormone-related protein in the pathogenesis of human breast cancer-mediated osteolysis. J Clin Invest 98:1544–1549

Hall DG, Stoica G (1994) Effect of the bisphosphonate risedronate on bone metastases in a rat mammary adenocarcinoma model system. J Bone Miner Res 9:221–230

Hardy J, Edinger M, Bachmann MH, Negrin RS, Fathman CG, Contag CH (2001) Bioluminescence imaging of lymphocyte trafficking in vivo. Exp Hematol 29:1353–1360

Hashizume T, Kumahara A, Fujino M, Okada K (2002) Insulin-like growth factor I enhances gonadotropin-releasing hormone-stimulated luteinizing hormone release from bovine anterior pituitary cells. Anim Reprod Sci 70:13–21

Heikkila P, Teronen O, Moilanen M, Konttinen YT, Hanemaaijer R, Laitinen M, Maisi P, van der Pluijm G, Bartlett JD, Salo T, Sorsa T (2002) Bisphosphonates inhibit stromelysin-1 (MMP-3), matrix metalloelastase (MMP-12), collagenase-3 (MMP-13) and enamelysin (MMP-20), but not urokinase-type plasminogen activator, and diminish invasion and migration of human malignant and endothelial cell lines. Anticancer Drugs 13:245–254

Hiraga T, Williams PJ, Mundy GR, Yoneda T (2001) The bisphosphonate ibandronate promotes apoptosis in MDA-MB-231 human breast cancer cells in bone metastases. Cancer Res 61:4418–4424

Hortobagyi GN, Theriault RL, Porter L, Blayney D, Lipton A, Sinoff C, Wheeler H, Simeone JF, Seaman J, Knight RD (1996) Efficacy of pamidronate in reducing skeletal complications in patients with breast cancer and lytic bone metastases. Protocol 19 Aredia Breast Cancer Study Group. N Engl J Med 335:1785–1791

Iris B, Zilberman Y, Zeira E, Galun E, Honigman A, Turgeman G, Clemens T, Gazit Z, Gazit D (2003) Molecular imaging of the skeleton: quantitative real-time bioluminescence. J Bone Miner Res 18:570–578

Kanis JA, Powles T, Paterson AH, McCloskey EV, Ashley S (1996) Clodronate decreases the frequency of skeletal metastases in women with breast cancer. Bone 19:663–667

Kassem M, Okazaki R, Harris SA, Spelsberg TC, Conover CA, Riggs BL (1998) Estrogen effects on insulin-like growth factor gene expression in a human osteoblastic cell line with high levels of estrogen receptor. Calcif Tissue Int 62:60–66

Kato S (2001) Estrogen receptor-mediated cross-talk with growth factor signaling pathways. Breast Cancer 8:3–9

Klotz DM, Hewitt SC, Ciana P, Raviscioni M, Lindzey JK, Foley J, Maggi A, DiAugustine RP, Korach KS (2002) Requirement of estrogen receptor-alpha in insulin-like growth factor-1 (IGF-1)-induced uterine responses and in vivo evidence for IGF-1/estrogen receptor cross-talk. J Biol Chem 277:8531–8537

Kostenuik PJ, Singh G, Suyama KL, Orr FW (1993) Stimulation of bone resorption results in a selective increase in the growth rate of spontaneously metastatic Walker 256 cancer cells in bone. Clin Exp Metastasis 10:411–418

Lange PH, Vessella RL (1999) Mechanisms, hypotheses and questions regarding prostate cancer micrometastases to bone. Cancer Metastasis Rev 17:331–336

Lee MV, Fong EM, Singer FR, Guenette RS (2001) Bisphosphonate treatment inhibits the growth of prostate cancer cells. Cancer Res 61:2602–2608

Lehtonen-Veromaa M, Mottonen T, Kautiainen H, Heinonen OJ, Viikari J (2001) Influence of physical activity and cessation of training on calcaneal quantitative ultrasound measurements in peripubertal girls: a 1-year prospective study. Calcif Tissue Int 68:146–150

Luckman SP, Hughes DE, Coxon FP, Graham R, Russell G, Rogers MJ (1998) Nitrogen-containing bisphosphonates inhibit the mevalonate pathway and prevent post-translational prenylation of GTP-binding proteins, including Ras. J Bone Miner Res 13:581–589

Mandl S, Schimmelpfennig C, Edinger M, Negrin RS, Contag CH (2002) Understanding immune cell trafficking patterns via in vivo bioluminescence imaging. J Cell Biochem [Suppl] 39:239–248

Mansi JL, Berger U, Easton D, McDonnell T, Redding WH, Gazet JC, McKinna A, Powles TJ, Coombes RC (1987) Micrometastases in bone marrow in patients with primary breast cancer: evaluation as an early predictor of bone metastases. Br Med J (Clin Res Ed) 295:1093–1096

Melchior SW, Corey E, Ellis WJ, Ross AA, Layton TJ, Oswin MM, Lange PH, Vessella RL (1997) Early tumor cell dissemination in patients with

clinically localized carcinoma of the prostate. Clin Cancer Res 3:249–256

Millar AJ, Short SR, Chua NH, Kay SA (1992) A novel circadian phenotype based on firefly luciferase expression in transgenic plants. Plant Cell 4:1075–1087

Muller A, Homey B, Soto H, Ge N, Catron D, Buchanan ME, McClanahan T, Murphy E, Yuan W, Wagner SN, Barrera JL, Mohar A, Verastegui E, Zlotnik A (2001) Involvement of chemokine receptors in breast cancer metastasis. Nature 410:50–56

Mundy GR (2002) Metastasis to bone: causes, consequences and therapeutic opportunities. Nat Rev Cancer 2:584–593

Mundy GR, Yoneda T (1996) Mechanisms of bone metastasis. In: Orr FW, Singh G (eds) Bone metastasis – mechanisms and pathophysiology. Springer, Berlin Heidelberg New York, pp 1–16

Ohtsuka M, Shinoda H (1995) Ontogeny of circadian dentinogenesis in the rat incisor. Arch Oral Biol 40:481–485

Paget S (1889) The distribution of secondary growths in cancer of the breast. Lancet 1:571–573

Pantel K, Schlimok G, Braun S, Kutter D, Lindemann F, Schaller G, Funke I, Izbicki JR, Riethmuller G (1993) Differential expression of proliferation-associated molecules in individual micrometastatic carcinoma cells. J Natl Cancer Inst 85:1419–1424

Powles T, Paterson S, Kanis JA, McCloskey E, Ashley S, Tidy A, Rosenqvist K, Smith I, Ottestad L, Legault S, Pajunen M, Nevantaus A, Mannisto E, Suovuori A, Atula S, Nevalainen J, Pylkkanen L (2002) Randomized, placebo-controlled trial of clodronate in patients with primary operable breast cancer. J Clin Oncol 20:3219–3224

Rodan GA (1998) Mechanisms of action of bisphosphonates. Annu Rev Pharmacol Toxicol 38:375–388

Russell RG, Rogers MJ, Frith JC, Luckman SP, Coxon FP, Benford HL, Croucher PI, Shipman C, Fleisch HA (1999) The pharmacology of bisphosphonates and new insights into their mechanisms of action. J Bone Miner Res 14 [Suppl 2]:53–65

Saarto T, Blomqvist C, Virkkunen P, Elomaa I (2001) Adjuvant clodronate treatment does not reduce the frequency of skeletal metastases in node-positive breast cancer patients: 5-year results of a randomized controlled trial. J Clin Oncol 19:10–17

Sasaki A, Boyce BF, Story B, Wright KR, Chapman M, Boyce R, Mundy GR, Yoneda T (1995) Bisphosphonate risedronate reduces metastatic human breast cancer burden in bone in nude mice. Cancer Res 55:3551–3557

Senaratne SG, Pirianov G, Mansi JL, Arnett TR, Colston KW (2000) Bisphosphonates induce apoptosis in human breast cancer cell lines. Br J Cancer 82:1459–1468

Shingo AS, Kito S (2003) Estrogen induces insulin-like growth factor-1 mRNA expression in the immortalized hippocampal cell: determination by quantitative real-time polymerase chain reaction. Neurochem Res 28: 1379–1383

Shipman CM, Rogers MJ, Apperley JF, Russell RG, Croucher PI (1997) Bisphosphonates induce apoptosis in human myeloma cell lines: a novel antitumor activity. Br J Haematol 98:665–672

Sweeney TJ, Mailander V, Tucker AA, Olomu AB, Zhang W, Cao Y, Negrin RS, Contag CH (1999) Visualizing the kinetics of tumor-cell clearance in living animals. Proc Natl Acad Sci USA 96:12044–12049

Teronen O, Heikkila P, Konttinen YT, Laitinen M, Salo T, Hanemaaijer R, Teronen A, Maisi P, Sorsa T (1999) MMP inhibition and downregulation by bisphosphonates. Ann N Y Acad Sci 878:453–465

van Beek E, Lowik C, van der Pluijm G, Papapoulos S (1999 a) The role of geranylgeranylation in bone resorption and its suppression by bisphosphonates in fetal bone explants in vitro: a clue to the mechanism of action of nitrogen-containing bisphosphonates. J Bone Miner Res 14:722–729

van Beek E, Pieterman E, Cohen L, Lowik C, Papapoulos S (1999 b) Farnesyl pyrophosphate synthase is the molecular target of nitrogen-containing bisphosphonates. Biochem Biophys Res Commun 264:108–111

van der Pluijm G, Vloedgraven H, van Beek E, van der Wee-Pals L, Lowik C, Papapoulos S (1996) Bisphosphonates inhibit the adhesion of breast cancer cells to bone matrices in vitro. J Clin Invest 98:698–705

van der Pluijm G, Lowik C, Papapoulos S (2000) Tumor progression and angiogenesis in bone metastasis from breast cancer: new approaches to an old problem. Cancer Treat Rev 26:11–27

van der Pluijm G, Sijmons B, Vloedgraven H, Deckers M, Papapoulos S, Lowik C (2001) Monitoring metastatic behavior of human tumor cells in mice with species-specific polymerase chain reaction: elevated expression of angiogenesis and bone resorption stimulators by breast cancer in bone metastases. J Bone Miner Res 16:1077–1091

van der Pluijm G, Karperien M, Löwik CWGM, Wetterwald A, Thalmann GN, Cecchini MG (2002 a) Whole body optical imaging of bone turnover and skeletal metastases: pathogenic relationship and therapeutic rationale (abstract). Clin Exp Metastasis 19:T-11

van der Pluijm G, Sijmons B, Que I, Buijs J, Cecchini M, Löwik C, Papapoulos S (2002 b) Monitoring progression of breast cancer cells in bone/bone marrow by optical imaging: bisphosphonates do not suppress tumor growth rate and tumor burden (abstract). J Bone Miner Res 17:1091

van Holten-Verzantvoort AT, Kroon HM, Bijvoet OL, Cleton FJ, Beex LV, Blijham G, Hermans J, Neijt JP, Papapoulos SE, Sleeboom HP, et al. (1993) Palliative pamidronate treatment in patients with bone metastases from breast cancer. J Clin Oncol 11:491–498

van Holten-Verzantvoort AT, Hermans J, Beex LV, Blijham G, Cleton FJ, van Eck-Smit BC, Sleeboom HP, Papapoulos SE (1996) Does supportive pamidronate treatment prevent or delay the first manifestation of bone metastases in breast cancer patients? Eur J Cancer 32A:450–454

Wetterwald A, van der Pluijm G, Que I, Sijmons B, Buijs J, Karperien M, Lowik CW, Gautschi E, Thalmann GN, Cecchini MG (2002) Optical imaging of cancer metastasis to bone marrow: a mouse model of minimal residual disease. Am J Pathol 160:1143–1153

Wood J, Bonjean K, Ruetz S, Bellahcene A, Devy L, Foidart JM, Castronovo V, Green JR (2002) Novel antiangiogenic effects of the bisphosphonate compound zoledronic acid. J Pharmacol Exp Ther 302:1055–1061

Yin JJ, Selander K, Chirgwin JM, Dallas M, Grubbs BG, Wieser R, Massague J, Mundy GR, Guise TA (1999) TGF-β signaling blockade inhibits PTHrP secretion by breast cancer cells and bone metastases development. J Clin Invest 103:197–206

Young M (2003) Bone matrix proteins: their function, regulation, and relationship to osteoporosis. Osteoporos Int 14 [Suppl 3]:S35–42

Zhang N, Fang Z, Contag PR, Purchio AF, West DB (2004) Tracking angiogenesis induced by skin wounding and contact hypersensitivity using a Vegfr2-luciferase transgenic mouse. Blood 103:617–626

Zhang W, Feng JQ, Harris SE, Contag PR, Stevenson DK, Contag CH (2001) Rapid in vivo functional analysis of transgenes in mice using whole body imaging of luciferase expression. Transgenic Res 10:423–434

Zhang W, Purchio AF, Chen K, Wu J, Lu L, Coffee R, Contag PR, West DB (2003) A transgenic mouse model with a luciferase reporter for studying in vivo transcriptional regulation of the human CYP3A4 gene. Drug Metab Dispos 8:1054–1064

12 Targeted Optical Imaging and Photodynamic Therapy

N. Solban, B. Ortel, B. Pogue, T. Hasan

12.1 Introduction

Optically activable agents (OAA), molecules that absorb light and emit fluorescence, can be useful probes for diagnostic applications and for the study of basic cellular processes (Hasan et al. 2003). If

these same molecules can, from their activated states, also initiate photochemistry so as to destroy cells/tissues locally, they can serve the dual purpose of being diagnostic and therapeutic agents. Photodynamic therapy (PDT), an emerging therapeutic modality, incorporates such molecular probes called photosensitizers (PS). Since most PS are fluorescent, drug localization can be determined by macroscopic and microscopic fluorescence imaging. Hence, throughout this chapter we will use the term PS interchangeably with OAA. These agents achieve selectivity by two complementary paths: biological-chemical targeting enhances localization/accumulation of the PS at desired sites, and optical targeting confines light delivery to target tissues. Once the PS is located at the site of interest, it is activated by the appropriate wavelength of light to its first excited state (S_1). The PS can then follow various paths for energy dissipation: it can return to its ground state (S_0) with the emission of fluorescence, which, with appropriate imaging and/or spectroscopic technology, can be used for diagnostic purposes. Alternatively, the activated PS in its S_1 state can undergo intersystem crossing to another electronically excited state at a slightly lowered energy level, called the first triplet state T_1. In this state the OAA is more efficient at initiating photochemically induced species due to the increased lifetime of the triplet state relative to other excited states. Figure 1 depicts the different pathways of molecular excited states. The best-known biomedical application of triplet state-induced photochemistry is PDT, where the production of singlet oxygen is largely thought to be the dominant mechanism of tissue damage. If the triplet state is not quenched by interaction with other molecules, it will generally relax back to its S_0 state with the emission of phosphorescence in the process, which, although more difficult to detect, may also be useful for diagnostic purposes.

This chapter outlines recent developments in biological-chemical targeting of PS with a focus on cancer applications. However, molecular optical imaging and therapy is rapidly expanding to the diagnosis and treatment of other diseases and a few examples are presented here. In the first section we will describe the nonspecific accumulation of PS in tumors. The following section will focus on imaging with two PS commonly used in our laboratory: benzoporphyrin derivative monoacid A (BPD-MA) and δ-aminolevulinic acid

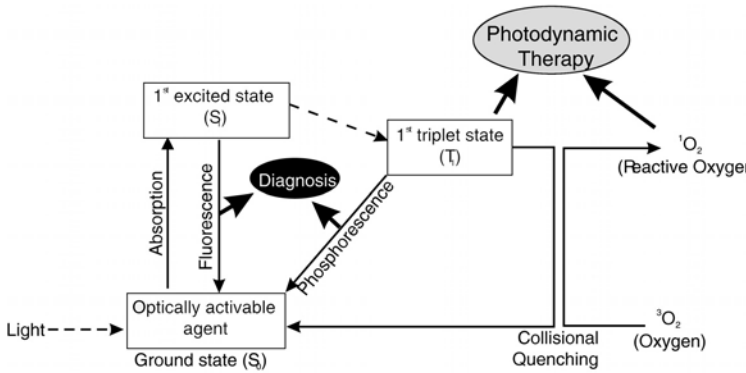

Fig. 1. A simplified energy level diagram for the photoexcitation of an optically active molecule. Absorption of a photon results in the excitation of the absorbing molecule from the ground singlet state (S_0), to the first excited singlet state (S_1). Fluorescence, which can be used for diagnostic purposes, comes during de-excitation from S_1, back to the ground state S_0. Alternatively, the first triple state (T_1) is generated after intersystem crossing from S_1. Phosphorescence is emitted when the molecule relax back to S_0 from T_1. T_1 can initiate photochemical reactions directly, giving rise to reactive free radicals, or transfer its energy to the ground state oxygen molecules ($^3O_2$) to give rise to excited singlet state oxygen molecules ($^1O_2$) (adapted from Pogue and Hasan 2003)

(ALA)-derived protoporphyrin IX (PpIX). In the third section we will describe some methods used to specifically target the PS to tumor tissue, the fourth section focuses on optical targeting, and finally in the fifth section we will give a general overview of the mechanisms of photodynamic therapy.

12.2 Photosensitizer Localization in Tumors

Based on two therapeutically relevant compartments of malignant tumors, PS are often classified as cellular or vascular, a reference to the primary site of action under the conditions studied. However, the transport, in vivo, is a dynamic process for every PS. The timing of the light exposure is very important. The appropriate choice of different delay times after PS administration may allow targeting differ-

ent compartments within the tissue (e.g., vascular and extravascular) using the very same PS. The concentration of agents varies between the blood, interstitial space, and tumor parenchymal cells and with time. Hydrophilic molecules usually remain in circulation until excreted, while hydrophobic compounds leak rapidly out of the vessels and are retained in tumor tissue (Freitas 1990). This dynamic process results in a preferential accumulation of PS in tumors, and early clearance from the blood after injection.

The reason for the preferential accumulation of PS in tumors compared to normal tissue is not clearly understood but several properties of tumor tissue may contribute to this selective accumulation. It may be a result of the greater proliferative rates of neoplastic cells, poorer lymphatic drainage, leaky vasculature, or more specific interaction between the PS and marker molecules on neoplastic cells [for example, elevated numbers of low-density lipoprotein receptors (Polo et al. 2002)]. Furthermore, tumor stroma contains a high amount of collagen, shown to bind porphyrins (Nelson et al. 1988), and a high amount of lipid, that has a high affinity for lipophilic PS (Freitas 1990). Cationic PS are suggested to be cellularly localized after a short intravascular phase and thus act at the tumor cell level. These compounds accumulate in tumor cells because of the much steeper electrical potential across the mitochondrial membrane of tumor cells compared to normal cells (Cernay and Zimmermann 1996; Dummin et al. 1997). The best developed of the series are the benzophenothiazine dyes, and animal studies using these dyes show high cure rates following light activation (Cincotta et al. 1994, 1996).

Most of the PS in use are hydrophobic molecules, since it was noted that accumulation in tumors increases upon increasing the degree of hydrophobicity (Oenbrink et al. 1988). However, since these molecules are not very water soluble, intravenous treatment is hampered. This prompted the use of delivery vehicles such as: liposomes, oil-dispersions, polymers, and polymeric particles to facilitate drug delivery (Konan et al. 2002). Therefore, novel PS are often formulated in lipid-based delivery systems. It has been suggested that LDL receptors on tumor cells and on tumor vascular endothelial cells (Barel et al. 1986; Kessel 1992) play a role in the uptake of PS since it has been shown that PS can bind LDL (Allison et al. 1994).

In general, hydrophobic dyes are associated with lipoproteins, while their hydrophilic counterparts bind preferentially to other serum proteins. For example, it was shown that liposomal benzoporphyrin derivative (BPD) enters tissues more rapidly and has a higher accumulation in tumor than nonliposomal BPD (Richter et al. 1993). Furthermore, recent studies showed that liposomal BPD is rapidly transferred to lipoprotein: close to 91% of liposomal BPD is associated with lipoprotein after 1 h, as compared to 50% with the nonliposomal BPD (Richter et al. 1993). This may explain the rapid delivery to tissues (Chowdhary et al. 2003).

12.3 Photosensitizing Agents

Several thousand patients have been treated with PDT for a variety of neoplasms. Randomized clinical trials were initiated in 1987, using a purified form of Hematoporphyrin derivative (HPD), Photofrin (PF, Porfimer sodium). These first randomized trials compared the efficacy of PDT with that of other forms of therapy for bladder, esophageal, and lung cancers. Within the past 7 years regulatory approval has been obtained for a variety of indications. Currently, between Europe and the United States there are five photosensitizing agents approved for the treatment of a variety of diseases. Applications for the treatment of several other indications, including for early cancers, have been filed in the United States, Canada, Japan, and Europe, and approvals are currently pending.

12.3.1 Imaging with Photosensitizing Agents

Although there are a large number of PS under investigation, both preclinically and clinically (Hasan et al. 2003), we focus only on two of them: benzoporphyrin derivative monoacid A (BPD-MA) and δ-aminolevulinic acid (ALA)-derived protoporphyrin IX (PpIX) as examples since these are currently the most frequently used clinically.

12.3.1.1 Benzoporphyrin Derivative Monoacid A

The majority of clinical experience in PDT has been with PF, which was first approved by the FDA in 1995 for palliative treatment of esophageal cancer. However, its use may be associated with prolonged cutaneous phototoxicity of up to 6 weeks. Furthermore, the therapeutically relevant absorption peak of PF at 630 nm is not ideal for deep tissue treatment (Hasan et al. 2003). Typically, the effective penetration depth at 630 nm is only about 2–3 mm and the penetration depth increases to 5–6 mm at longer wavelengths (700–800 nm) (Taroni et al. 2003). Newer PS show improved selectivity for the tumors, therefore reducing cutaneous phototoxicity and usually have red shifted absorption spectra allowing deeper tissue treatment. Of the newer compounds, the most developed is benzoporphyrin derivative monoacid A (BPD-MA). For clinical applications, BPD-MA is liposomally formulated (verteporfin). The FDA-approved application of PDT for the treatment of age-related macular degeneration (AMD) is based on the dynamic nature of the PS transport through tissue. In the treatment of AMD, the goal is to destroy newly developed, pathological blood vessels, in the subretinal region, hence the illumination is performed within 15 min of intravenous injection of the PS (vascular localization), yielding almost exclusive vascular damage. Conversely, light exposure at a longer time after BPD-MA injection will preferentially target the cellular spaces, shutting down cellular respiration and killing the cells. This latter regimen is much more suitable for tumor targeting (Schmidt-Erfurth et al. 1994).

In Fig. 2, BPD-MA fluorescence is shown in a rat prostate tumor shortly after injection (a) and at 3 h after injection (b). Early on the compound is clearly seen in the vasculature, while 3 h later it is located in the tumor parenchyma with vessels appearing nonfluorescent. Thus, the leakage of the drug into the tissue provides a dynamic localization change over time through nonspecific targeting (Pogue and Hasan 2003).

12.3.1.2 *δ*-Aminolevulinic Acid-Based Imaging and Photodynamic Therapy

A relatively novel way of PS targeting is the use of a prodrug approach, where the molecule is not a presynthesized PS, but is converted into a PS in situ. This is the case with aminolevulinic acid

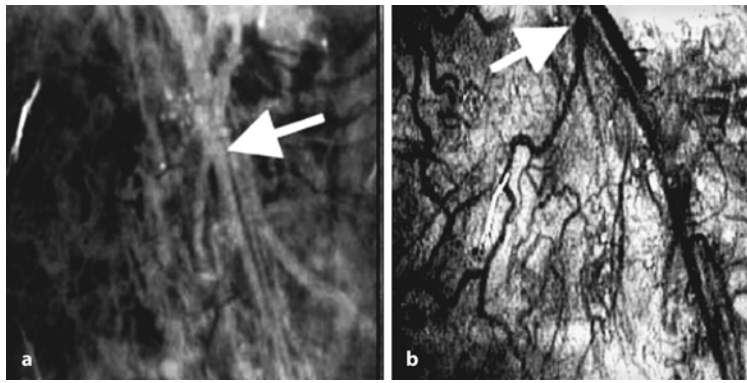

Fig. 2a,b. Localization of BPD fluorescence after injection. At an early time after injection the drug is mostly in the vasculature (**a**). Three hours after injection a major fraction has leaked out and is localized in the parenchyma (**b**). *Arrows* indicate blood vessels (reproduced with permission from Pogue and Hasan 2003)

(ALA) or its esters. Every cell requires heme proteins for a number of functions, including ATP formation. Therefore, each cell has the capacity to synthesize heme (Fig. 3). Under physiological conditions, heme production in nonerythroid cells is regulated by the expression levels of the enzyme ALA-synthase (ALA-S), which is under a negative feedback control by free heme. ALA-S provides ALA, the first committed precursor of heme formation. When exogenous ALA is added, this rate-limiting step is bypassed and downstream metabolites are synthesized in excess. The last step in this pathway involves the conversion of PpIX, a PS, to heme (a nonphotosensitizing species). When exogenous ALA is added, ferrochelatase, the enzyme responsible for the insertion of iron into PpIX, becomes rate limiting. It is unable to utilize the excess PpIX that is formed. PpIX therefore accumulates in the cells and renders them photosensitive (Kennedy et al. 1996). When esters of ALA are used, they first have to be hydrolyzed before ALA can enter the heme synthetic pathway.

Along with photosensitivity comes fluorescence, and thus the use of ALA-induced PpIX has gained much interest in diagnostic applications. Exogenous ALA-dependent PpIX fluorescence is being de-

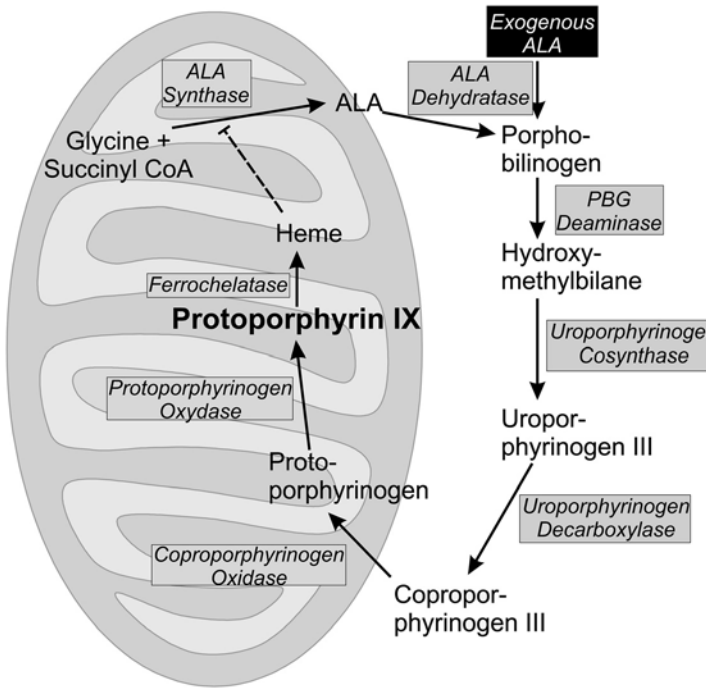

Fig. 3. Heme production. The enzymes and metabolites are located in the mitochondria and the cytosol. Heme can negatively regulate ALA synthase at several points. Exogenous ALA induces excess formation of heme precursors, including PpIX that can be used for photosensitization

veloped for the detection of early malignancies, carcinomas in situ, and certain cancer precursor lesions. The detection of localized pathologies is based on increased PpIX formation in diseased as compared to normal surrounding tissue. The reason for this selectivity is not entirely clear and several components may contribute to a different extent depending on the organ and tissue that is probed. In some epithelial tissues such as the epidermis, the disturbance of the physiological barrier function in lesional skin accounts for increased ALA penetration (Fig. 4).

In brain tumors, the disruption of the blood-brain barrier seems to be instrumental in increasing lesional ALA delivery and thus PpIX

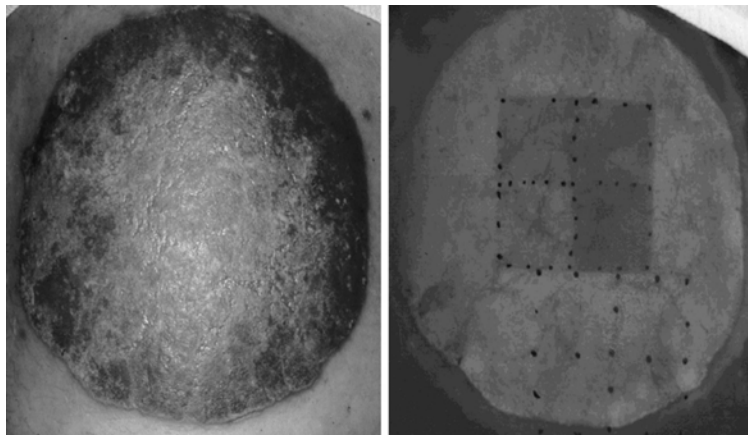

Fig. 4. ALA-induced porphyrin fluorescence in psoriatic skin. In psoriasis, inflammation and hyperproliferation lead to thickened, bright red skin areas (plaques), covered with large scales (*left panel*). The same plaque shows red fluorescence after treatment with topical ALA (*right panel*, *pale colored area*). The psoriatic skin allows more efficient uptake of ALA due to a disturbed epidermal barrier function. The *squares* in the center of the plaque were irradiated clockwise with increasing doses of blue light, resulting in increased photobleaching and thus reduction of the fluorescence intensity (*darker area at center of panel*)

formation. The most accessible organs were the first to be tested, including the skin (Fritsch et al. 1998; Marcus et al. 1996), the bladder (Riedl et al. 1999), oral cavity (Leunig et al. 2000), lungs (Baumgartner et al. 1996), and the upper and lower gastrointestinal tract (Messmann 2000). The hollow organs can be reasonably conveniently viewed with optical devices and PpIX fluorescence is used to identify pathologies that are less or not at all visible with conventional white-light-based inspection. Visible PpIX fluorescence indicates suspicious areas for guided biopsy and therapy.

In urology, ALA-induced PpIX fluorescence is used for the early diagnosis of urothelial dysplasia and carcinoma using a modified cystoscope (Riedl et al. 2001). Patients have their bladder filled with an ALA solution. After 4–6 h, the physician first performs cystoscopy under white-light illumination. Then, filtered blue light is

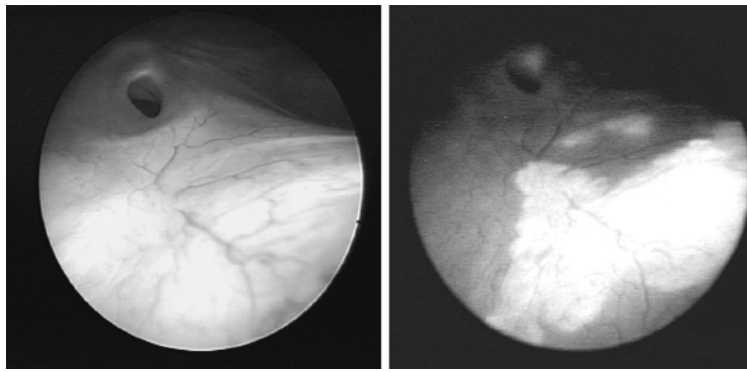

Fig 5. Clinical fluorescence diagnosis of urothelial dysplasia in the bladder. Cystoscopic images of the bladder wall of patients after instillation of 50 ml of a 3% ALA solution for 2 h for the induction of PpIX formation. The conventional white light image (*left panel*) did not show the extent of the neoplastic lesions, which is revealed by PpIX fluorescence under blue illumination of the same view (*right panel*, *white area*) (images courtesy of Reinhold Boumgartner, PhD)

used to excite the red porphyrin fluorescence, which is observed through the cystoscope (Fig. 5).

The specificity of ALA-PpIX-based cystoscopic diagnosis is not very high because of a relatively high number of false positives. However, using fluorescence diagnosis, the sensitivity has been clearly increased over conventional cystoscopy much to the benefit of patients. Fluorescence imaging following surgical resection has also been shown to be a useful tool to identify remaining dysplastic tissue, thereby reducing the recurrence of cancer following surgery (Riedl et al. 2001). Besides ALA, its hexylester has shown great potential for bladder cancer diagnosis (Marti et al. 2003). The rationale behind using ALA esters is the alteration of physicochemical properties of the compound (Casas and Batlle 2002). For example, the lipophilicity increases with esterification with aliphatic alcohols such as hexanol. Consequently, the pharmacokinetic properties in vitro and in vivo of the ALA esters differ considerably from ALA.

ALA-PpIX has been shown to be useful not only for detecting premalignant or malignant tissue, but also for the detection of tumor

margins. During surgery for primary brain tumors, the surgical challenge is to remove the malignant tissue as radically as possible, while preserving as much of the healthy brain tissue as possible. The finger-like extensions of these so-called gliomas infiltrate the healthy tissue and thus it is often difficult to distinguish the tumor margins. If the patient ingests ALA prior to surgery, the tumor-associated disruption of the blood-brain barrier results in increased ALA delivery to tumor areas and consequently higher localized PpIX concentrations. Under a modified operating microscope blue-light-induced PpIX fluorescence is then used to guide the targeted resection of the fluorescent malignant tissue with careful sparing of nonfluorescent normal brain. This strategy has been employed successfully in clinical studies and has resulted in prolonged patient survival, which is a sensitive measure of efficient surgery in brain tumors (Friesen et al. 2002).

12.4 Targeted Optical Imaging and Photodynamic Therapy

An important determinant of successful PDT is the localization of the PS in neoplastic tissue, specifically with respect to its selectivity, which is the ratio of lesional and normal tissue concentrations of the PS. More precise OAA targeting is therefore desirable in order to ensure success but also to reduce toxicity to uninvolved tissues and organs in complex sites, such as in the abdominal cavity. The use of molecular delivery systems that recognize specific molecular markers are highly desirable and under active investigation. It is important to note that contrary to conventional targeted chemotherapy where the drug has to be released from the carrier moiety to elicit a response, this is not a prerequisite when carrier molecules are used for delivery of PS in PDT. Furthermore, the requirements for specificity of the delivery molecule are less stringent in PDT. This is due to the dual selectivity of the treatment. As long as the delivery agent has preferential (not necessarily exclusive) affinity for the target tissue, selective phototoxicity is expected. Thus, carrier-mediated PDT offers the possibility of using targeting molecules that are not only found on tumors, providing a greater repertoire of usable compounds. However, the problems associated with the use of large mol-

ecules, such as complicated synthesis, transport barriers, and potential systemic toxicity, are similar for PS conjugates and for other conjugates. In this section we will describe some macromolecular carriers used to specifically target PS to tumor tissues. In the case of imaging, similar arguments apply if imaging is in localized areas as for guided surgery or detection of malignancies in specific organs or sites. For generalized whole-body imaging the stringency of selectivity requirements would be higher but certainly without the long-term hazards of radioisotope imaging.

12.4.1 Photoimmunotargeting

Tumor targeting with antibodies is based on the concept that molecular markers are present on tumor cells, and the ability to obtain specific monoclonal antibodies (MAb) that recognize these markers. It is thought that neoplastic transformation generates new and specific antigens not present on normal cells. However, this is not the case with all tumors, and MAb with a high level of specificity for tumor markers are extremely rare. Photoimmunotargeting (PIT) has therefore many advantages over standard immunotherapies because it combines two therapeutic principles. The molecule recognized by the MAb doesn't have to be expressed exclusively on neoplastic tissues and the MAb doesn't need to have an intrinsic effector function. This means the MAb does not need to initiate on its own a reaction that would lead to tumor destruction. However, PIT requires conjugates with high PS to MAb ratios, which makes the synthesis complicated. PS can be linked chemically to the MAbs directly or via polymers (Hasan et al. 1989; Yarmush et al. 1993). The chemical reactions that are necessary for the synthesis and the resulting structural alterations of the molecules' environments may lead to a loss of activity of the MAb (reduced affinity), the PS (reduced singlet oxygen yield upon irradiation), or both. In an ideal scenario the PS and antibody activities will be preserved, while at the same time allowing maximal PS incorporation (Jiang et al. 1990).

12.4.2 Receptor-Targeted Photoimmunotargeting

Most PS are able to cross the cell membrane because they are hydrophobic molecules. By the same token these molecules tend to aggregate readily in aqueous solutions. When targeting tumors with antibodies, these are sometimes internalized; therefore, hydrophilic PS conjugated to internalizing antibodies could be used. A recent study (Vrouenraets et al. 2000) tested this hypothesis. Using the hydrophilic PS TrisMPyP-Phico(2)H conjugated to the internalizing antibodies cMAb U36 or MAb 425, it was shown that these conjugate were phototoxic to A431 cells, while noninternalizing Ab conjugates and free PS were harmless at the same concentration. The same group also showed that this method was effective in targeting aluminum (III) phthalocyanine tetrasulfonate, another hydrophilic PS, to tumors using delivery by the same internalizing antibodies (Vrouenraets et al. 2001).

In other applications of PIT, specific biomolecules on pathological cells and tissues can be targeted. For example, a much sought-after target is the epidermal growth factor receptor (EGFR). Clearly, similar approaches can be used for many other intra- and extracellular molecular targets.

The real utility of PIT may lie in its use as a detection modality and therapeutic response monitoring methodology. With this as a focus, we have tested an anti-EGFR MAb coupled to either the near infrared fluorescent dye Cy5.5 for detection or to the photochemically active dye, chlorin (e6) (ce_6) for therapy of premalignancy in the hamster cheek pouch carcinogenesis model (Soukos et al. 2001). Head and neck cancers including oral cancer and precancer overexpress EGFR. Furthermore, EGFR overexpression was also detected in the chemically induced malignant transformation leading to carcinoma in the hamster cheek pouch model (Shin et al. 1990). These findings suggested that the overexpression of EGFR might be used as a marker for early diagnosis and treatment of oral precancer. Targeting the EGFR with antibody-delivered photoactive molecules may destroy the EGFR overexpressing cells, while the normal, low expression levels of EGFR in the healthy tissue do not lead to high enough PS concentration in the normal mucosa. Targeted PDT thus

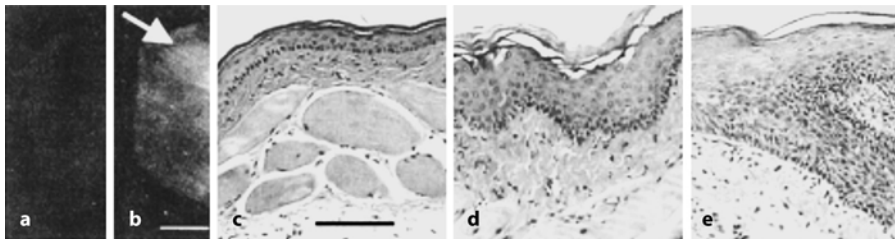

Fig. 6. Fluorescence images of normal (**a**) and carcinogen-treated (**b**) hamster cheek pouches, 6 days after the injection of the EGFR-Cy5.5 conjugated Mab (*bar*, 5 mm). An area of increased fluorescence can be seen within the carcinogen treated cheek pouch (*arrow*). H&E histology shows (**c**) normal mucosal epithelium for the carcinogen-untreated cheek pouch (*bar*, 100 μm), (**d**) mild dysplasia for the carcinogen-treated cheek pouch, and (**e**) moderate dysplasia for the hot spot (reproduced with permission from Soukos et al. 2001)

will cause the premalignant lesion to regress. The MAb-bound OAA may also allow monitoring of the progress of the treatment.

Figure 6 shows a representative image from an animal with an oral papillary tumor measuring 5 mm in diameter. The normal cheek pouch has no visible fluorescence (Fig. 6a), whereas the tumor-bearing pouch has a clearly delineated tumor in the fluorescence image (Fig. 6b) after systemic injection of anti-EGFR-Cy5.5 MAb conjugate (Soukos et al. 2001). Cy5.5 has several advantages over fluorescein, a dye commonly used for diagnosis in animals and humans: it has good solubility, high fluorescence quantum yield, and a longer emission wavelength (emits at 702 nm after 675 nm excitation). This leads to increased sensitivity of detection of premalignant lesions because fluorescence from OAA localized deeper in the tissue can be detected, and background autofluorescence is minimized because the endogenous fluorophores present in tissue do not absorb at 675 nm.

We have also conjugated EGFR-MAb to the PS ce_6. Following PDT with this conjugate we found that the overexpression of EGFR in carcinogen-treated hamsters was significantly reduced to background levels compared to nonilluminated areas. No difference between illuminated and dark areas was seen in the normal cheek

pouch. These results demonstrate the potential for development of immunotargeted photodiagnosis as a diagnostic tool and as a method of monitoring response to therapy.

12.4.3 Peptide-Mediated Targeting

To enhance the delivery of PS to hepatocytes, Akhlynina et al. (1995) conjugated ce_6 to insulin. This study demonstrated specific receptor-mediated internalization and phototoxicity hundred times higher than that obtained with free ce_6. Furthermore, specific inhibition of endocytosis of the conjugate abrogated phototoxicity. Despite these interesting results, the use of insulin conjugates in cancer therapy is limited since not all hepatoma cell lines possess a great number of insulin receptors.

On the other hand, EGFR is overexpressed in many carcinomas. We described in a previous section (Sect. 12.4.2) the use of an anti-EGFR MAb to specifically target PS to tumors. A recent study (Gijsens et al. 2000) used epidermal growth factor (EGF) conjugated to ce_6 to target EGFR-positive tumors. The conjugate was highly phototoxic, while incubation with a competing concentration of unconjugated EGF reduced phototoxicity.

The transferrin receptor is often overexpressed in hyperproliferative cells, while it is usually present at low levels in normal tissue. The PS ce_6 was conjugated to transferrin. This conjugate was efficient in killing mammary adenocarcinoma cells in culture (Cavanaugh 2002).

To improve the selectivity of PpIX toward cancerous cells, Rahimipour et al. (2003) conjugated PpIX to a gonadotropin-releasing hormone (GnRH) agonist and to a GnRH antagonist. These conjugates would specifically target cancerous cells that express gonadotropin-releasing hormone receptors. This study showed that the hormone conjugate had lower binding affinity to the receptor, but proved to be long acting in vivo. Furthermore, both conjugates were more phototoxic toward pituitary gonadotrope αT3-1 cell line than unconjugated PpIX. In a primary pituitary cell culture the efficacy of the antagonist conjugate was approximately ten times higher than unconjugated PpIX.

The neurotensin receptor (NTR) is expressed in several human tumors; therefore, it can be targeted for the delivery of cytotoxic drugs and imaging agents. This receptor binds neurotensin, a tridecapeptide with a very short plasma half-life. A recent study (Achilefu et al. 2003) showed that modification of neurotensin increased its stability for more than 4 h without affecting its binding affinity. The additional conjugation of the modified neurotensin to fluorescein for optical imaging did not reduce binding affinity to NTR. This study also showed that the compound was primarily retained in tumor tissue. The same group also conjugated a fluorescent agent to somatostatin (Bugaj et al. 2001) and observed specific tumor targeting. The efficacy of targeting somatostatin receptor-expressing tumors with somatostatin was demonstrated in a previous study (Stolz et al. 1998). The conjugation of a PS to neurotensin or to somatostatin could potentially be developed for targeted PS delivery to tumors overexpressing NTR or the somatostatin receptor.

12.4.4 Other Approaches to Photosensitizer Targeting

The purpose of the brief discussion below is primarily to inform the reader of other approaches to selective photoactivation. The examples are primarily therapeutic, but there is no reason for not exploiting these same strategies for imaging and diagnostic purposes. Alternative ways of targeting PS to a specific cell population need to take advantage of certain properties of these cells, which either distinguish them from other cell or tissue types, or differentiate malignant from normal cells. The following approach, which was recently used by Zhang (Zhang et al. 2003), is based on altered sugar metabolism in cancer cells. They demonstrated that the PS pyropheophorbide 2-deoxyglucosamide (pyro-2DG) selectively accumulated in tumors. Rapidly growing tumors are able to maintain high glucose catabolic rate by upregulation of hexokinase. This enzyme phosphorylates glucose to glucose-6-phosphate, which is then retained in the cell (Mathupala et al. 1997). Pyro-2DG is taken up by cells and becomes a substrate for hexokinase and the chemically altered PS is retained in the cells. Since cancer cells upregulate this enzyme, more of the PS is retained in tumor cells than in normal cells. This strategy of

PS administration and subsequent photoactivation caused efficient mitochondrial damage.

Another approach exploits the biological changes associated with T-cell activation. Activated T-cells play an important role in many inflammatory diseases and malignancies of lymphocytes (lymphomas). The P-glycoprotein, product of the *MDR1* gene, plays an important role in multidrug resistance of cancer cells by extruding cytotoxic chemicals (Sakaeda et al. 2003). However, upon activation of T cells with mitogens, inactivation of the P-glycoprotein has been reported (Gupta 1995). A recent study (Guimond et al. 2002) used this characteristic to specifically target activated T cells with the PS TH9402. This study showed that only activated T cells retained the PS and photoactivation resulted in their selective depletion. This targeting strategy could potentially be used to monitor and treat graft-versus-host disease or other diseases mediated by activated T cells.

Macrophage targeting is currently being developed for the detection and treatment of vulnerable plaque, a noncancer, life-threatening pathology. Using ce6 conjugated to maleylated albumin, Hamblin et al. (2003) were able to specifically target macrophages in the vulnerable plaques in a rabbit model of atherosclerosis. Figure 7 shows aortic rings segment taken from an uninjected atherosclerotic rabbit (Fig. 7, column 1), a conjugate-injected normal rabbit (Fig. 7, column 2), and a conjugate-injected atherosclerotic rabbit (Fig. 7, column 3). The uninjected atherosclerotic sections show typical autofluorescence. The conjugate-injected aortic section from a normal rabbit shows a small amount of specific fluorescence, while the conjugate-injected atherosclerotic rabbit shows a large amount of fluorescence in the thick plaque. These data suggest that macrophage targeting could be used for the detection/treatment of vulnerable plaques.

12.5 Optical Targeting

An additional level of targeting is available to optical methods due to the ability to direct light to specific areas or volumes. The following sections deal with aspects of “light-targeting” that may be important both in imaging and therapeutic applications of optical technologies.

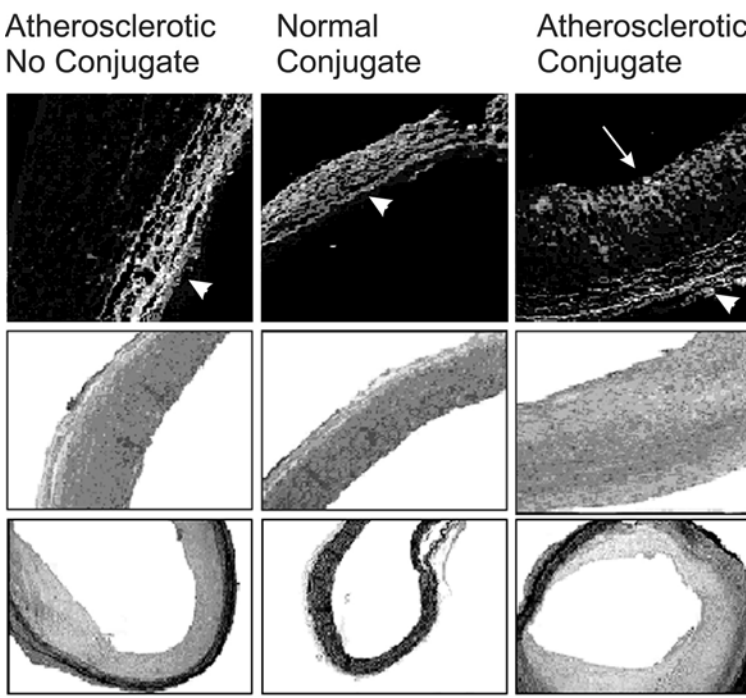

Fig. 7. Rings taken from the aortic segments from an uninjected atherosclerotic rabbit (*column 1*), a conjugate-injected rabbit (*column 2*), and a conjugate-injected atherosclerotic rabbit (*column 3*) were snap frozen and 10 μm cryosections cut. Adjacent sections were examined with confocal laser scanning fluorescence microscopy (*row 1*) and stained with hematoxylin and eosin (*row 2*), and with Verhoeff's elastic lamina stain (*row 3*). *Arrowhead* shows typical autofluorescence. *Arrow* indicate area of targeted macrophage (images courtesy of Michael R. Hamblin, PhD, Hamblin et al. 2003)

12.5.1 In Vivo Microscopy Approaches

In recent years, optical microscopy tools for in vivo diagnostic use have gradually been developed from standard bench top systems towards useful in vivo devices. In vivo microscopes have become standard as preclinical (Hadjantonakis and Nagy 2001; Liang et al. 2002) and clinical tools (Fulljames et al. 1999). Both fluorescence

and phosphorescence imaging of exogenous agents such as OAA provide fundamental insight into the physiology or pathophysiologic changes in tissue. Most simply, targeting can be explicitly achieved by focusing light to different depths in tissue, or through the use of confocal detection. Confocal sectioning in both reflectance and fluorescence mode has been developed into useful in vivo tools (Murray 1992). In particular, two-photon imaging provides a great opportunity to see into tissue, due to excitation wavelengths in the near-infrared region, where penetration of light in tissue is maximal (Cahalan et al. 2002). Sectioning light via coherence, lifetime, and polarization are alternative methods to sample differing volumes and layers of tissues, and as preclinical studies progress, they will find specific niches for medical use.

12.5.2 In Vivo Fluorescence Probes for Photodynamic Therapy Dosimetry

PDT tissue damage is a function of PS dose present in tissue, and methods used to quantify the PS dose present in tissue typically rely upon fluorescence of the drug (Frisoli et al. 1993). In vivo there is clear evidence emerging that the variation of drug concentration between subjects can be very high, and that even the variation within tumor can be very high. Estimates for the RIF-1 tumor indicated that for mice with all the same tumor size, this variation was near 75% standard deviation (Lee et al. 2003) even when all mice were handled in the same manner. Thus, the rationale for developing online monitors of PS fluorescence to estimate its concentration in clinical applications has been steadily growing. Validation of these tools is always done by correlating their measurements with ex vivo quantifications. However, the latter does not reflect the complexity of the microenvironment and its implications such as photochemical quenching changes that occur (Lee et al. 2001). It is likely that direct in vivo measurements of fluorescence, when taken with carefully designed instrumentation, will yield more accurate data on PS concentration than biopsy sampling will. This is especially important for those PS that are hydrophobic on whole or in part, and are known to aggregate. Fiberoptic devices that are designed to work in

vivo, and specifically with minimized interaction with the tissue have been proposed (Wagnieres et al. 1998; Pogue and Burke 1998; Bigio et al. 1999; Utzinger and Richards-Kortum 2003). As PDT gets translated into viable clinical treatments, these tools will become increasingly important.

12.5.3 In Vivo Light Transport in Photodynamic Therapy Dosimetry and Diagnosis

Dosimetry for radiation therapy has become a standard of care in oncology, and similar developments must occur as PDT becomes accepted. Understanding light transport in tissue is challenging, due to the complexity of interactions and the difficulty in modeling precise light dosimetry in realistic tissue volumes. When light is used to image or treat large regions of tissue from the surface, the resulting intensity is largely confined to the upper layers of the tissue, due to the high degree of elastic scattering in tissue. The probability that a photon will be scattered in tissue is effectively 10–100 times higher than its probability to be absorbed. Modeling light transport with Monte Carlo methods over short distances and diffusion theory models over longer distances has gained widespread acceptance, and allows good estimates of light fluence patterns in tissues (Patterson et al. 1990a, b). Optical dose measurements have been shown to be crucially important in PDT (Vulcan et al. 2000), and it is possible that several failed clinical trials can be attributed to lack of accurate optical dosimetry, resulting in incomplete treatments. Use of interstitial, surface, or feedback dosimetry tools is thought to be essential for optimal PDT treatment (Marijnissen et al. 1993; Braichotte et al. 1996; Wilson et al. 1997).

In diagnostic applications, delivery of light several centimeters deep into tissue is commonplace in medicine, for applications such as pulse oxymetry of the finger. When diagnosis is the primary aim, it is possible to observe light signals through up to 12 cm of tissue. In particular, red and near-infrared radiation has the lowest scattering and absorption probability in tissue of all wavelength ranges, with an effective penetration depth of approximately 5 mm for a decrease to 1/e times the incident fluence. Using numerical modeling

of light transport in tissue, it is possible to predict the light fluence pattern, and to work out from where the relative contributions to the signal are derived. This type of analysis continues to be studied for use in cancer imaging (Pogue et al. 2001). The potential applications of fluorophore reporter imaging also hold significant promise. Experimental studies with rodent and dog tumor models have confirmed that fluorescent imaging can be accurate and quantitative through several centimeters of tissue (Hawrysz and Sevick-Muraca 2000). Development in the area of diagnostic imaging with molecular markers is now more influenced by the specific agents being developed and the potential pathologic markers that are being targeted (Ntziachristos et al. 2002, 2003).

12.6 Photodynamic Therapy

Photodynamic therapy (PDT) has already been mentioned in the introduction. It is based on the concept that PS can be localized in neoplastic tissue, and can be activated with the appropriate wavelength of light to generate active molecular species, such as free radicals and singlet oxygen ($^1O_2$) that are toxic to cells and tissues. An inherent advantage (and limitation) of PDT is its dual selectivity: the PS can be specifically targeted to a particular tissue and irradiation can be limited to a specified volume. Provided that the PS is not toxic, only the irradiated area will be affected, even if the PS accumulates in normal tissues. For photoactivation, the wavelength of light is matched to the electronic absorption spectrum of the PS. Endogenous molecules, in particular hemoglobin, strongly absorb light below 600 nm (capture its photons); therefore, the range of activating light is typically between 600 nm and 900 nm; this range is called the therapeutic window for PDT in vivo. Above 900 nm the penetration depth is also good, but the PS excited state energetics are not sufficient to produce $^1O_2$, a major effector of phototherapy with most PS.

12.6.1 Mechanisms

12.6.1.1 Cellular Mechanisms

In complex environments, such as cells and tissues, the subcellular localization of the PS is important for effective photochemistry to occur. For example, chlorin p6 localizes in lysosomes (Kessel et al. 1995 a), a monocationic porphyrin localizes in membranes (Kessel et al. 1995 b), while the porphycene monomer localizes in mitochondria (Kessel and Luo 1998). Since most PDT sensitizers do not accumulate in the cell nuclei, PDT has generally a low potential of causing DNA damage, mutations, and carcinogenesis. Electron transfer reactions (type I reaction) occur when the excited sensitizer interacts with a donor or acceptor molecule; when these molecules are cellular targets, photobiologic effects occur. Energy transfer reaction (type II reaction) involving reactive oxygen ($^1O_2$) require close proximity of sensitizer and target since $^1O_2$ can diffuse only about 20 nm in cells due to efficient quenching in biological environments (Moan and Berg 1991). Hence, cellular structures close to both a high sensitizer and high oxygen concentration will be damaged following illumination. Sensitizers that localize to the mitochondria are rapid inducers of apoptosis (Kessel and Luo 1999), initiated by the release of cytochrome c from the mitochondria into the cytosol (Granville et al. 2001). In contrast, lysosomal PS usually induce necrosis, possibly by releasing toxic lysosomal enzymes (Wood et al. 1997) into the cytosol following illumination.

12.6.1.2 In Vivo Mechanisms

Three primary mechanisms of PDT-mediated tumor destruction in vivo have been proposed: cellular, vascular (Fingar et al. 2000), and immunologic (Hunt and Chan 2000). The contribution of these mechanisms depends not only on the nature of the PS and its localization within the tumor tissue at the time of irradiation, but also on the tumor type (vascularity and macrophage content). When the PS is intravascular at the time of irradiation, vascular shutdown begins almost immediately after initiation of light exposure. When the PS content is high within the tumor cells at the time of irradiation, direct cell destruction may dominate. It is worth mentioning that under the typical protocols vascular damage is considered the domi-

nant mechanism of tumor death in vivo for most PS being investigated clinically.

12.6.2 Photodynamic Therapy and Oxygen

In principle, a photodynamic response happens wherever a PS and light occur simultaneously. The extent of the response is modulated by PS concentration and by light. There appears to be a threshold for PDT effects to be lethal, below which tissue damage is repaired (Patterson et al. 1990c). However, with most PS under investigation, PDT efficacy is also oxygen dependent. This oxygen dependence is due to the generation of singlet oxygen during treatment. Under anoxic conditions, the PDT effect of certain PS can be abolished. In clinical settings, higher subthermal fluence rates (the rate of photon delivery) have been thought to be favorable because total irradiation time could be reduced. Surprisingly, reduced efficacy of tumor destruction has been reported when fluence rates in the range typically applied to clinical studies were used in PDT (Sitnik et al. 1998; Sitnik and Henderson 1998). This lowered efficacy has been attributed to oxygen depletion during irradiation due to oxygen consumption in the photochemical reaction at a rate greater than the rate of reperfusion. The effect of fluence rate and light fractionation on PDT is currently under investigation in order to optimize treatment protocols (Iinuma et al. 1999).

12.7 Conclusion

This review of photodiagnosis and phototherapy is a summary of specific aspects of optical targeting. It is not meant to be a comprehensive review, rather it is expected to serve both as an introduction of the approach for an audience outside the field of optical technologies. As such it is somewhat subjective and it is important for the reader to be aware that this is a very brief summary of literature and concepts in a rapidly emerging field. With the advent of new molecular probes and light delivery and light capturing techniques, it is likely that the field of optical treatment and diagnosis will have de-

veloped to such an extent in the next 5 years so as to make this writing irrelevant!

Many of the PS described throughout this chapter are potentially useful for both diagnosis and therapy. The fluorescence produced by these compounds may be exploited for several purposes: the identification and delineation of malignant tissues, the quantification of PS at the tumor site, and potentially the monitoring of oxygen and PS consumption during therapeutic light exposure. In an optimal scenario, targeted delivery identifies diseased tissue and in the same procedure treatment is delivered. A targeting molecule (MAb or peptide based) would deliver an optically activable agent specifically to tumors. This OAA would be used for diagnosis and treatment. The progressive improvement of remote imaging devices and molecular targeting strategies make this an attractive aim of preclinical and clinical development.

Acknowledgements. Support for the authors was provided by the National Institutes of Health Grants RO1 AR40352 (T.H.), PO1 CA84203 (T.H., B.O., B.W.P.).

References

Achilefu S, Srinivasan A, Schmidt MA, Jimenez HN, Bugaj JE, Erion JL (2003) Novel bioactive and stable neurotensin peptide analogues capable of delivering radiopharmaceuticals and molecular beacons to tumors. J Med Chem 46:3403–3411

Akhlynina TV, Rosenkranz AA, Jans DA, Sobolev AS (1995) Insulin-mediated intracellular targeting enhances the photodynamic activity of chlorin e6. Cancer Res 55:1014–1019

Allison BA, Pritchard PH, Levy JG (1994) Evidence for low-density lipoprotein receptor-mediated uptake of benzoporphyrin derivative. Br J Cancer 69:833–839

Barel A, Jori G, Perin A, Romandini P, Pagnan A, Biffanti S (1986) Role of high-, low- and very low-density lipoproteins in the transport and tumor-delivery of hematoporphyrin in vivo. Cancer Lett 32:145–150

Baumgartner R, Huber RM, Schulz H, Stepp H, Rick K, Gamarra F, Leberig A, Roth C (1996) Inhalation of 5-aminolevulinic acid: a new technique for fluorescence detection of early stage lung cancer. J Photochem Photobiol B 36:169–174

Bigio IJ, Mourant JR, Los G (1999) Noninvasive, in-situ measurement of drug concentrations in tissue using optical spectroscopy. J Gravit Physiol 6:P173–175

Braichotte DR, Savary JF, Monnier P, van den Bergh HE (1996) Optimizing light dosimetry in photodynamic therapy of early stage carcinomas of the esophagus using fluorescence spectroscopy. Lasers Surg Med 19:340–346

Bugaj JE, Achilefu S, Dorshow RB, Rajagopalan R (2001) Novel fluorescent contrast agents for optical imaging of in vivo tumors based on a receptor-targeted dye-peptide conjugate platform. J Biomed Opt 6:122–133

Cahalan MD, Parker I, Wei SH, Miller MJ (2002) Two-photon tissue imaging: seeing the immune system in a fresh light. Nat Rev Immunol 2:872–880

Casas A, Batlle A (2002) Rational design of 5-aminolevulinic acid derivatives aimed at improving photodynamic therapy. Curr Med Chem Anti-Canc Agents 2:465–475

Cavanaugh PG (2002) Synthesis of chlorin e6-transferrin and demonstration of its light-dependent in vitro breast cancer cell killing ability. Breast Cancer Res Treat 72:117–130

Cernay T, Zimmermann HW (1996) Selective photosensitization of mitochondria by the lipophilic cationic porphyrin POR10. J Photochem Photobiol B 34:191–196

Chowdhary RK, Shariff I, Dolphin D (2003) Drug release characteristics of lipid based benzoporphyrin derivative. J Pharm Sci 6:13–19

Cincotta L, Foley JW, MacEachern T, Lampros E, Cincotta AH (1994) Novel photodynamic effects of a benzophenothiazine on two different murine sarcomas. Cancer Res 54:1249–1258

Cincotta L, Szeto D, Lampros E, Hasan T, Cincotta AH (1996) Benzophenothiazine and benzoporphyrin derivative combination phototherapy effectively eradicates large murine sarcomas. Photochem Photobiol 63:229–237

Dummin H, Cernay T, Zimmermann HW (1997) Selective photosensitization of mitochondria in HeLa cells by cationic Zn (II) phthalocyanines with lipophilic side-chains. J Photochem Photobiol B 37:219–229

Fingar VH, Taber SW, Haydon PS, Harrison LT, Kempf SJ, Wieman TJ (2000) Vascular damage after photodynamic therapy of solid tumors: a view and comparison of effect in pre-clinical and clinical models at the University of Louisville. In Vivo 14:93–100

Freitas I (1990) Lipid accumulation: the common feature to photosensitizer-retaining normal and malignant tissues. J Photochem Photobiol B 7:359–361

Friesen SA, Hjortland GO, Madsen SJ, Hirschberg H, Engebraten O, Nesland JM, Peng Q (2002) 5-Aminolevulinic acid-based photodynamic detection and therapy of brain tumors (review). Int J Oncol 21:577–582

Frisoli JK, Tudor EG, Flotte TJ, Hasan T, Deutsch TF, Schomacker KT (1993) Pharmacokinetics of a fluorescent drug using laser-induced fluorescence. Cancer Res 53:5954–5961

Fritsch C, Lang K, Neuse W, Ruzicka T, Lehmann P (1998) Photodynamic diagnosis and therapy in dermatology. Skin Pharmacol Appl Skin Physiol 11:358–373

Fulljames C, Stone N, Bennett D, Barr H (1999) Beyond white light endoscopy – the prospect for endoscopic optical biopsy. Ital J Gastroenterol Hepatol 31:695–704

Gijsens A, Missiaen L, Merlevede W, de Witte P (2000) Epidermal growth factor-mediated targeting of chlorin e6 selectively potentiates its photodynamic activity. Cancer Res 60:2197–2202

Granville DJ, Cassidy BA, Ruehlmann DO, Choy JC, Brenner C, Kroemer G, van Breemen C, Margaron P, Hunt DW, McManus BM (2001) Mitochondrial release of apoptosis-inducing factor and cytochrome c during smooth muscle cell apoptosis. Am J Pathol 159:305–311

Guimond M, Balassy A, Barrette M, Brochu S, Perreault C, Roy DC (2002) P-glycoprotein targeting: a unique strategy to selectively eliminate immunoreactive T cells. Blood 100:375–382

Gupta S (1995) P-glycoprotein expression and regulation. Age-related changes and potential effects on drug therapy. Drugs Aging 7:19–29

Hadjantonakis AK, Nagy A (2001) The color of mice: in the light of GFP-variant reporters. Histochem Cell Biol 115:49–58

Hamblin MR, Tawakol A, Castano PA, Gad F, Zahra T, Ahmad A, Stern J, Ortel B, Chirico S, Shirazi A, Syed S, Muller JE (2003) Macrophage-targeted photodynamic detection of vulnerable atherosclerotic plaque. Proc SPIE (in press)

Hasan T, Lin CW, Lin A (1989) Laser-induced selective cytotoxicity using monoclonal antibody-chromophore conjugates. Prog Clin Biol Res 288: 471–477

Hasan T, Ortel B, Moor A, Pogue B (2003) Photodynamic therapy of cancer. In: Kufe DW, Pollack RE, Weichselbaum RR, et al. (eds) Cancer Medicine, 6th edn. B.C. Decker Hamilton, Ontario, pp 605–622

Hawrysz DJ, Sevick-Muraca EM (2000) Developments toward diagnostic breast cancer imaging using near-infrared optical measurements and fluorescent contrast agents. Neoplasia 2:388–417

Hunt DW, Chan AH (2000) Influence of photodynamic therapy on immunological aspects of disease – an update. Expert Opin Investig Drugs 9: 807–817

Iinuma S, Schomacker KT, Wagnieres G, Rajadhyaksha M, Bamberg M, Momma T, Hasan T (1999) In vivo fluence rate and fractionation effects on tumor response and photobleaching: photodynamic therapy with two photosensitizers in an orthotopic rat tumor model. Cancer Res 59:6164–6170

Jiang FN, Jiang S, Liu D, Richter A, Levy JG (1990) Development of technology for linking photosensitizers to a model monoclonal antibody. J Immunol Methods 134:139–149

Kennedy JC, Marcus SL, Pottier RH (1996) Photodynamic therapy (PDT) and photodiagnosis (PD) using endogenous photosensitization induced by 5-aminolevulinic acid (ALA): mechanisms and clinical results. J Clin Laser Med Surg 14:289–304

Kessel D (1992) The role of low-density lipoprotein in the biodistribution of photosensitizing agents. J Photochem Photobiol B 14:261–262

Kessel D, Luo Y (1998) Mitochondrial photodamage and PDT-induced apoptosis. J Photochem Photobiol B 42:89–95

Kessel D, Luo Y (1999) Photodynamic therapy: a mitochondrial inducer of apoptosis. Cell Death Differ 6:28–35

Kessel D, Woodburn K, Gomer CJ, Jagerovic N, Smith KM (1995 a) Photosensitization with derivatives of chlorin p6. J Photochem Photobiol B 28:13–18

Kessel D, Woodburn K, Henderson BW, Chang CK (1995 b) Sites of photodamage in vivo and in vitro by a cationic porphyrin. Photochem Photobiol 62:875–881

Konan YN, Gurny R, Allemann E (2002) State of the art in the delivery of photosensitizers for photodynamic therapy. J Photochem Photobiol B 66:89–106

Lee CC, Pogue BW, Burke GC, Hoopes PJ (2003) Spatial heterogeneity and temporal kinetics of photosensitizer (AlPcS2) concentration in murine tumors RIF-1 and MTG-B. Photochem Photobiol Sci 2:145–150

Lee CC, Pogue BW, Strawbridge RR, Moodie KL, Bartholomew LR, Burke GC, Hoopes PJ (2001) Comparison of photosensitizer (AlPcS2) quantification techniques: in situ fluorescence microsampling versus tissue chemical extraction. Photochem Photobiol 74:453–460

Leunig A, Betz CS, Mehlmann M, Stepp H, Arbogast S, Grevers G, Baumgartner R (2000) Detection of squamous cell carcinoma of the oral cavity by imaging 5-aminolevulinic acid-induced protoporphyrin IX fluorescence. Laryngoscope 110:78–83

Liang C, Sung KB, Richards-Kortum RR, Descour MR (2002) Design of a high-numerical-aperture miniature microscope objective for an endoscopic fiber confocal reflectance microscope. Appl Opt 41:4603–4610

Marcus SL, Sobel RS, Golub AL, Carroll RL, Lundahl S, Shulman DG (1996) Photodynamic therapy (PDT) and photodiagnosis (PD) using endogenous photosensitization induced by 5-aminolevulinic acid (ALA): current clinical and development status. J Clin Laser Med Surg 14:59–66

Marijnissen JP, Star WM, in't Zandt HJ, D'Hallewin MA, Baert L (1993) In situ light dosimetry during whole bladder wall photodynamic therapy: clinical results and experimental verification. Phys Med Biol 38:567–582

Marti A, Jichlinski P, Lange N, Ballini JP, Guillou L, Leisinger HJ, Kucera P (2003) Comparison of aminolevulinic acid and hexylester aminolevuli-

nate induced protoporphyrin IX distribution in human bladder cancer. J Urol 170:428–432

Mathupala SP, Rempel A, Pedersen PL (1997) Aberrant glycolytic metabolism of cancer cells: a remarkable coordination of genetic, transcriptional, post-translational, and mutational events that lead to a critical role for type II hexokinase. J Bioenerg Biomembr 29:339–343

Messmann H (2000) 5-Aminolevulinic acid-induced protoporphyrin IX for the detection of gastrointestinal dysplasia. Gastrointest Endosc Clin N Am 10:497–512

Moan J, Berg K (1991) The photodegradation of porphyrins in cells can be used to estimate the lifetime of singlet oxygen. Photochem Photobiol 53:549–553

Murray JM (1992) Neuropathology in depth: the role of confocal microscopy. J Neuropath Exp Neurol 51:475–487

Nelson JS, Liaw LH, Orenstein A, Roberts WG, Berns MW (1988) Mechanism of tumor destruction following photodynamic therapy with hematoporphyrin derivative, chlorin, and phthalocyanine. J Natl Cancer Inst 80:1599–1605

Ntziachristos V, Bremer C, Weissleder R (2003) Fluorescence imaging with near-infrared light: new technological advances that enable in vivo molecular imaging. Eur Radiol 13:195–208

Ntziachristos V, Tung CH, Bremer C, Weissleder R (2002) Fluorescence molecular tomography resolves protease activity in vivo. Nat Med 8:757–760

Oenbrink G, Jurgenlimke P, Gabel D (1988) Accumulation of porphyrins in cells: influence of hydrophobicity aggregation and protein binding. Photochem Photobiol 48:451–456

Patterson MS, Wilson BC, Graff R (1990a) In vivo tests of the concept of photodynamic threshold dose in normal rat liver photosensitized by aluminum chlorosulphonated phthalocyanine. Photochem Photobiol 51:343–349

Patterson MS, Wilson BC, Wyman DR (1990b) The propagation of optical radiation in tissue I. Models of radiation transport and their application. Lasers Med Sci 6:155–168

Patterson MS, Wilson BC, Wyman DR (1990c) The propagation of optical radiation in tissue II. Optical properties of tissues and resulting fluence distributions. Lasers Med Sci 6:379–390

Pogue BW, Hasan T (2003) Targeting in photodynamic therapy and photoimaging. OPN 14:36–43

Pogue BW, Burke GC (1998) Fiber optic bundle design for quantitative fluorescence measurement from tissue. Appl Opt 37:7429–7436

Pogue BW, Poplack SP, McBride TO, Wells WA, Osterman KS, Osterberg UL, Paulsen KD (2001) Quantitative hemoglobin tomography with diffuse near-infrared spectroscopy: pilot results in the breast. Radiology 218:261–266

Polo L, Valduga G, Jori G, Reddi E (2002) Low-density lipoprotein receptors in the uptake of tumour photosensitizers by human and rat transformed fibroblasts. Int J Biochem Cell Biol 34:10–23

Rahimipour S, Ben-Aroya N, Ziv K, Chen A, Fridkin M, Koch Y (2003) Receptor-mediated targeting of a photosensitizer by its conjugation to gonadotropin-releasing hormone analogues. J Med Chem 46:3965–3974

Richter AM, Waterfield E, Jain AK, Canaan AJ, Allison BA, Levy JG (1993) Liposomal delivery of a photosensitizer, benzoporphyrin derivative monoacid ring A (BPD), to tumor tissue in a mouse tumor model. Photochem Photobiol 57:1000–1006

Riedl CR, Daniltchenko D, Koenig F, Simak R, Loening SA, Pflueger H (2001) Fluorescence endoscopy with 5-aminolevulinic acid reduces early recurrence rate in superficial bladder cancer. J Urol 165:1121–1123

Riedl CR, Plas E, Pfluger H (1999) Fluorescence detection of bladder tumors with 5-amino-levulinic acid. J Endourol 13:755–759

Sakaeda T, Nakamura T, Okumura K (2003) Pharmacogenetics of MDR1 and its impact on the pharmacokinetics and pharmacodynamics of drugs. Pharmacogenomics 4:397–410

Schmidt-Erfurth U, Hasan T, Gragoudas E, Michaud N, Flotte TJ, Birngruber R (1994) Vascular targeting in photodynamic occlusion of subretinal vessels. Ophthalmology 101:1953–1961

Shin DM, Gimenez IB, Lee JS, Nishioka K, Wargovich MJ, Thacher S, Lotan R, Slaga TJ, Hong WK (1990) Expression of epidermal growth factor receptor, polyamine levels, ornithine decarboxylase activity, micronuclei, and transglutaminase I in a 7,12-dimethylbenz(a)anthracene-induced hamster buccal pouch carcinogenesis model. Cancer Res 50:2505–2510

Sitnik TM, Hampton JA, Henderson BW (1998) Reduction of tumour oxygenation during and after photodynamic therapy in vivo: effects of fluence rate. Br J Cancer 77:1386–1394

Sitnik TM, Henderson BW (1998) The effect of fluence rate on tumor and normal tissue responses to photodynamic therapy. Photochem Photobiol 67:462–466

Soukos NS, Hamblin MR, Keel S, Fabian RL, Deutsch TF, Hasan T (2001) Epidermal growth factor receptor-targeted immunophotodiagnosis and photoimmunotherapy of oral precancer in vivo. Cancer Res 61:4490–4496

Stolz B, Weckbecker G, Smith-Jones PM, Albert R, Raulf F, Bruns C (1998) The somatostatin receptor-targeted radiotherapeutic [^{90}Y-DOTA-DPhe1, Tyr3]octreotide (^{90}Y-SMT 487) eradicates experimental rat pancreatic CA 20948 tumours. Eur J Nucl Med 25:668–674

Taroni P, Pifferi A, Torricelli A, Comelli D, Cubeddu R (2003) In vivo absorption and scattering spectroscopy of biological tissues. Photochem Photobiol Sci 2:124–129

Utzinger U, Richards-Kortum RR (2003) Fiber optic probes for biomedical optical spectroscopy. J Biomed Optics 8:121–147

Vrouenraets MB, Visser GW, Loup C, Meunier B, Stigter M, Oppelaar H, Stewart FA, Snow GB, van Dongen GA (2000) Targeting of a hydrophilic photosensitizer by use of internalizing monoclonal antibodies: A new possibility for use in photodynamic therapy. Int J Cancer 88:108–114

Vrouenraets MB, Visser GW, Stigter M, Oppelaar H, Snow GB, van Dongen GA (2001) Targeting of aluminum (III) phthalocyanine tetrasulfonate by use of internalizing monoclonal antibodies: improved efficacy in photodynamic therapy. Cancer Res 61:1970–1975

Vulcan TG, Zhu TC, Rodriguez CE, Hsi A, Fraker DL, Baas P, Murrer LH, Star WM, Glatstein E, Yodh AG, Hahn SM (2000) Comparison between isotropic and nonisotropic dosimetry systems during intraperitoneal photodynamic therapy. Lasers Surg Med 26:292–301

Wagnieres GA, Star WM, Wilson BC (1998) In vivo fluorescence spectroscopy and imaging for oncological applications. Photochem Photobiol 68:603–632

Wilson BC, Patterson MS, Lilge L (1997) Implicit and explicit dosimetry in photodynamic therapy: a new paradigm. Lasers Med Sci 12:182–199

Wood SR, Holroyd JA, Brown SB (1997) The subcellular localization of Zn(II) phthalocyanines and their redistribution on exposure to light. Photochem Photobiol 65:397–402

Yarmush ML, Thorpe WP, Strong L, Rakestraw SL, Toner M, Tompkins RG (1993) Antibody targeted photolysis. Crit Rev Ther Drug Carrier Syst 10:197–252

Zhang M, Zhang Z, Blessington D, Li H, Busch TM, Madrak V, Miles J, Chance B, Glickson JD, Zheng G (2003) Pyropheophorbide 2-deoxyglucosamide: a new photosensitizer targeting glucose transporters. Bioconjug Chem 14:709–714

Ernst Schering Research Foundation Workshop

Editors: Günter Stock
Monika Lessl

Vol. 1 (1991): Bioscience ⇋ Societly Workshop Report
Editors: D.J. Roy, B.E. Wynne, R.W. Old

Vol. 2 (1991): Round Table Discussion on Bioscience ⇋ Society
Editor: J.J. Cherfas

Vol. 3 (1991): Excitatory Amino Acids and Second Messenger Systems
Editors: V.I. Teichberg, L. Turski

Vol. 4 (1992): Spermatogenesis – Fertilization – Contraception
Editors: E. Nieschlag, U.-F. Habenicht

Vol. 5 (1992): Sex Steroids and the Cardiovascular System
Editors: P. Ramwell, G. Rubanyi, E. Schillinger

Vol. 6 (1993): Transgenic Animals as Model Systems for Human Diseases
Editors: E.F. Wagner, F. Theuring

Vol. 7 (1993): Basic Mechanisms Controlling Term and Preterm Birth
Editors: K. Chwalisz, R.E. Garfield

Vol. 8 (1994): Health Care 2010
Editors: C. Bezold, K. Knabner

Vol. 9 (1994): Sex Steroids and Bone
Editors: R. Ziegler, J. Pfeilschifter, M. Bräutigam

Vol. 10 (1994): Nongenotoxic Carcinogenesis
Editors: A. Cockburn, L. Smith

Vol. 11 (1994): Cell Culture in Pharmaceutical Research
Editors: N.E. Fusenig, H. Graf

Vol. 12 (1994): Interactions Between Adjuvants, Agrochemical and Target Organisms
Editors: P.J. Holloway, R.T. Rees, D. Stock

Vol. 13 (1994): Assessment of the Use of Single Cytochrome P450 Enzymes in Drug Research
Editors: M.R. Waterman, M. Hildebrand

Vol. 14 (1995): Apoptosis in Hormone-Dependent Cancers
Editors: M. Tenniswood, H. Michna

Vol. 15 (1995): Computer Aided Drug Design in Industrial Research
Editors: E.C. Herrmann, R. Franke

Vol. 16 (1995): Organ-Selective Actions of Steroid Hormones
Editors: D.T. Baird, G. Schütz, R. Krattenmacher

Vol. 17 (1996): Alzheimer's Disease
Editors: J.D. Turner, K. Beyreuther, F. Theuring

Vol. 18 (1997): The Endometrium as a Target for Contraception
Editors: H.M. Beier, M.J.K. Harper, K. Chwalisz

Vol. 19 (1997): EGF Receptor in Tumor Growth and Progression
Editors: R.B. Lichtner, R.N. Harkins

Vol. 20 (1997): Cellular Therapy
Editors: H. Wekerle, H. Graf, J.D. Turner

Vol. 21 (1997): Nitric Oxide, Cytochromes P 450,
and Sexual Steroid Hormones
Editors: J.R. Lancaster, J.F. Parkinson

Vol. 22 (1997): Impact of Molecular Biology
and New Technical Developments in Diagnostic Imaging
Editors: W. Semmler, M. Schwaiger

Vol. 23 (1998): Excitatory Amino Acids
Editors: P.H. Seeburg, I. Bresink, L. Turski

Vol. 24 (1998): Molecular Basis of Sex Hormone Receptor Function
Editors: H. Gronemeyer, U. Fuhrmann, K. Parczyk

Vol. 25 (1998): Novel Approaches to Treatment of Osteoporosis
Editors: R.G.G. Russell, T.M. Skerry, U. Kollenkirchen

Vol. 26 (1998): Recent Trends in Molecular Recognition
Editors: F. Diederich, H. Künzer

Vol. 27 (1998): Gene Therapy
Editors: R.E. Sobol, K.J. Scanlon, E. Nestaas, T. Strohmeyer

Vol. 28 (1999): Therapeutic Angiogenesis
Editors: J.A. Dormandy, W.P. Dole, G.M. Rubanyi

Vol. 29 (2000): Of Fish, Fly, Worm and Man
Editors: C. Nüsslein-Volhard, J. Krätzschmar

Vol. 30 (2000): Therapeutic Vaccination Therapy
Editors: P. Walden, W. Sterry, H. Hennekes

Vol. 31 (2000): Advances in Eicosanoid Research
Editors: C.N. Serhan, H.D. Perez

Vol. 32 (2000): The Role of Natural Products in Drug Discovery
Editors: J. Mulzer, R. Bohlmann

Vol. 33 (2001): Stem Cells from Cord Blood, In Utero Stem Cell Development, and Transplantation-Inclusive Gene Therapy
Editors: W. Holzgreve, M. Lessl

Vol. 34 (2001): Data Mining in Structural Biology
Editors: I. Schlichting, U. Egner

Vol. 35 (2002): Stem Cell Transplantation and Tissue Engineering
Editors: A. Haverich, H. Graf

Vol. 36 (2002): The Human Genome
Editors: A. Rosenthal, L. Vakalopoulou

Vol. 37 (2002): Pharmacokinetic Challenges in Drug Discovery
Editors: O. Pelkonen, A. Baumann, A. Reichel

Vol. 38 (2002): Bioinformatics and Genome Analysis
Editors: H.-W. Mewes, B. Weiss, H. Seidel

Vol. 39 (2002): Neuroinflammation – From Bench to Bedside
Editors: H. Kettenmann, G. A. Burton, U. Moenning

Vol. 40 (2002): Recent Advances in Glucocorticoid Receptor Action
Editors: A. Cato, H. Schaecke, K. Asadullah

Vol. 41 (2002): The Future of the Oocyte
Editors: J. Eppig, C. Hegele-Hartung

Vol. 42 (2003): Small Molecule-Protein Interaction
Editors: H. Waldmann, M. Koppitz

Vol. 43 (2003): Human Gene Therapy:
Present Opportunities and Future Trends
Editors: G. M. Rubanyi, S. Ylä-Herttuala

Vol. 44 (2004): Leucocyte Trafficking:
The Role of Fucosyltransferases and Selectins
Editors: A. Hamann, K. Asadullah, A. Schottelius

Vol. 45 (2004): Chemokine Roles in Immunoregulation and Disease
Editors: P. M. Murphy, R. Horuk

Vol. 46 (2004): New Molecular Mechanisms of Estrogen Action and Their Impact on Future Perspectives in Estrogen Therapy
Editors: K. S. Korach, A. Hillisch, K. H. Fritzemeier

Vol. 47 (2004): Neuroinflammation in Stroke
Editors: U. Dirnagl, B. Elger

Vol. 48 (2004): From Morphological Imaging to Molecular Targeting
Editors: M. Schwaiger, L. Dinkelborg, H. Schweinfurth

Vol. 49 (2005): Molecular Imaging
Editors: A. A. Bogdanov, K. Licha

Supplement 1 (1994): Molecular and Cellular Endocrinology of the Testis
Editors: G. Verhoeven, U.-F. Habenicht

Supplement 2 (1997): Signal Transduction in Testicular Cells
Editors: V. Hansson, F.O. Levy, K. Taskén

Supplement 3 (1998): Testicular Function:
From Gene Expression to Genetic Manipulation
Editors: M. Stefanini, C. Boitani, M. Galdieri, R. Geremia,
F. Palombi

Supplement 4 (2000): Hormone Replacement Therapy
and Osteoporosis
Editors: J. Kato, H. Minaguchi, Y. Nishino

Supplement 5 (1999): Interferon: The Dawn of Recombinant
Protein Drugs
Editors: J. Lindenmann, W.D. Schleuning

Supplement 6 (2000): Testis, Epididymis and Technologies
in the Year 2000
Editors: B. Jégou, C. Pineau, J. Saez

Supplement 7 (2001): New Concepts in Pathology and
Treatment of Autoimmune Disorders
Editors: P. Pozzilli, C. Pozzilli, J.-F. Kapp

Supplement 8 (2001): New Pharmacological Approaches
to Reproductive Health and Healthy Ageing
Editors: W.-K. Raff, M.F. Fathalla, F. Saad

Supplement 9 (2002): Testicular Tangrams
Editors: F.F.G. Rommerts, K.J. Teerds

Supplement 10 (2002): Die Architektur des Lebens
Editors: G. Stock, M. Lessl